Transactions of the ASME®



**Transactions of the ASME, The Journal of Fluids Engineering** (ISSN 0098-2202) is published quarterly (Mar., June, Sept., Dec.) for $100 per year by The American Society of Mechanical Engineers, 345 East 47th Street, New York, NY 10017. Second class postage paid at New York, NY and additional mailing offices. POSTMASTER: Send address changes to The Journal of Fluids Engineering, c/o THE AMERICAN SOCIETY OF MECHANICAL ENGINEERS, 22 Law Drive, Box 2300, Fairfield, NJ 07007-2300.
**CHANGES OF ADDRESS** must be received at Society headquarters seven weeks before they are to be effective. Please send old label and new address.
**PRICES:** To members, $29.00, annually; to nonmembers, $100. Add $15.00 for postage to countries outside the United States and Canada.
**STATEMENT** from By-Laws. The Society shall not be responsible for statements or opinions advanced in papers or . . . printed in its publications (B7.1, Par. 3),

**INDEXED** by Applied Mechanics Reviews and Engineering Information, Inc.

# Journal of Fluids Engineering

Published Quarterly by The American Society of Mechanical Engineers

VOLUME 111 • NUMBER 1 • MARCH 1989

Journal of Fluids Engineering

# Editorial

Questions are not widely used in our literature. The typical paper in fluid mechanics, or in science and engineering generally, contains not a single question. It is possible that people wish, subconsciously, to appear knowlegeable, and that posing questions for which they have no answers produces a sense of uncomfortable vulnerability. There are success stories at both ends of the spectrum. Willard Gibb's seminal paper on Equilibrium, all 250 pages, has no questions. But the famous "Hilbert Problems," twenty-three questions posed in a 1900 paper by David Hilbert, have had a tremendous impact on the direction of mathematics, and on the careers of numerous mathematicians. To eschew questions is probably eminently inefficient.

While we all wish to be on the cutting edge of our respective research activities, very few of us have vision acute enough to choose the crucial issues to address, or the questions to ask, in the course of problem definition. Our dilemma is intensified because the thought processes by which the most prescient among us identify and select key questions is usually not described. We do not know the weight that chance and experience carry in those processes.

Collectively, the scientific community is quick to recognize a major area of worthwhile research in the wake of a significant breakthrough, for example the superconductivity discoveries of the last two years. It is easy to jump on a bandwagon, more difficult to predict the arrival of that bandwagon years in advance. What questions in Onnes's mind urged him to investigate superconductivity in the early years of this century? Whatever they were, those questions represented the initial condition that ultimately shaped a problem area currently of dominant importance.

Our papers rarely report on research-initiating questions in detail. Instead, they point to the importance of the problem area (generated from the questions) and report on answers. The question-asking stage is neglected, and germinal ideas recede into the background.

In a response to these concerns, the 1989 Winter Annual Meeting will include a session on "Unanswered Questions in Fluid Mechanics." Its Call for Papers is printed below. Readers are encouraged to join in this effort to define boundaries of our knowledge of fluid mechanics by suggesting questions that may provoke discussion and fruitful research.

**Joseph A. C. Humphrey** **Lloyd MacG. Trefethen**

# Computational Methods With Vortices—The 1988 Freeman Scholar Lecture

**Turgut Sarpkaya**
Distinguished Professor of Mechanical Engineering,
Naval Postgraduate School,
Monterey, CA 93943

*A comprehensive review is presented of the computational methods based upon Helmholtz's powerful concepts of vortex dynamics, making use of Lagrangian or mixed Lagrangian-Eulerian schemes, the Biot-Savart law or the Vortex-in-Cell methods. The ingenious approximations and smoothing schemes developed in search of predictive models, qualitative solutions, new insights, or just some inspiration in the simulation of often two-dimensional, occasionally three-dimensional, and almost always incompressible fluids are described in detail. One is forewarned at the onset that chaos awaits at the end of the road. The challenge is to produce results in the face of ever accumulating errors within a time scale appropriate for the investigation.*

*The review is organized around two major sections: Theoretical foundations and practical applications of vortex methods. The first covers topics such as vorticity and laws of transportation, evolution equations for a vortex sheet, real vortices and instabilities, Biot-Savart law, smoothing techniques (cutoff schemes, amalgamation of vortices, subvortex methods), cloud-in-cell or vortex-in-cell methods, body representation (Routh's rule, surface singularity distributions), operator splitting and the random walk method (description and convergence), and asymmetry introduction. The next section covers contra flowing streams, vortical flows in aerodynamics (vortex sheet roll-up; slender-body, two-vortex, multi-discrete vortex, and segment or panel methods; three-dimensional flow models, and vortex-lattice methods), separated flow about cylindrical bodies (circular cylinder, sharp-edged bodies, arbitrarily-shaped bodies), general three-dimensional flows (vortex rings, turbulent spots, temporally and spatially-growing shear layers, and other applications (vortex-blade interactions, combustion phenomena, acoustics, contour dynamics, interaction of line vortices, chaos, and turbulence). The review is concluded with a brief comparison of these methods with others used in computational fluid dynamics and a personal view of their future prospects.*

## 1 Introduction: User Beware

Helmholtz (1858) was the first to show, in what is now regarded as one of the most important contributions in fluid mechanics, that in an inviscid fluid vortex lines remain continually composed of the same fluid elements and flows with vorticity can be modeled with vortices of appropriate circulation and "infinitely small cross section" — quantum vortex lines. It is this realization that led to the discretization of the compact regions of vorticity into an assembly of vortices (with finite or infinite vorticity) embedded in an otherwise potential flow. The Lagrangian or the Lagrangian-Eulerian description of the evolution of the discretized vorticity field constitutes the essence of the computational methods with vortices. With few notable exceptions, applications have been limited to incompressible flow cases for which the Biot-Savart law or the Green's function method applies. Isolated line vortices, vorticity blobs, vortex balls or vortons, or toroidal vortices are introduced into the flow field and tracked numerically by a Lagrangian or a mixed Lagrangian-Eulerian scheme. In this process, the representation of the body, with the imposed boundary conditions, often becomes an integral part of the computation of the flow field. When geometrically simple solid boundaries are present, suitable image vortices are introduced to satisfy the zero normal velocity condition. For complex geometries, boundary integral or panel methods are used and the free vortex filaments, vortex rings, vortex sheets, or blobs are included in the potential flow model.

In spite of many elegant contributions (assisted by the computer of the day), the creation and tracking of mutually interacting parcels of vorticity, continue to pose great difficulties, often requiring numerous ad hoc assumptions to produce or reproduce the "best" or the "expected" solution with errors which are hard to estimate quantitatively and to minimize systematically. The applicability of most models is limited to cases that fit the simplifying assumptions. Most of

Contributed by the Fluids Engineering Division for publication in the JOURNAL OF FLUIDS ENGINEERING. Manuscript received by the Fluids Engineering Division September 28, 1988.

the models behave poorly beyond the parameter range for which they were developed, primarily because they violate may consistency conditions and moment inequalities. As noted by Dritschel (1988), "the nearly inevitable and incessant drive of an inviscid fluid to produce finer and finer scales of motion prevents any finite algorithm from accurately modelling even the largest scales of motion for arbitrarily long times."

Various schemes have been devised to reduce the computer time and to delay, limit, circumvent, or bound the instabilities or chaotic behavior which may result either from the singular behavior of the computational elements or from the ill-posed nature of the problem solved. Regardless of the particular details of the method used, arbitrarily small initial disturbances give rise to nonsmooth solutions in finite time. Of course, one does not know what the errors are (assuming that one can define them) in a given situation when there are no exact solutions. Depending on one's ultimate goal and the degree of sophistication, one may be satisfied with a reasonable-looking answer to a well-posed problem (in search of inspiration), or with only the overall similarity of the computed and photographed flow fields (e.g., vortex patterns, flame fronts), or with the agreement of the integrated quantities (e.g., lift and drag forces), or with the comparison of the instantaneous variation of the velocity and pressure fields.

There has been and perhaps there will always be some skepticism about the use of vortices for flow simulation. One can find convincing reasons to disappoint the pessimistic as well as the optimistic reader. Serious questions are now being raised as to whether a continuous region of vorticity (containing no vortices) may be discretized into an assembly of discrete vortices (with finite or infinite vorticity), whether one can insure that the solution of the discretized system actually approximates a solution of the continuous system, whether numerical instability can be distinguished from transition to turbulence, and whether two-dimensional hydrodynamics and monochromatic disturbances have a serious role to play in three-dimensional nature. However, the alternative methods deserve no less skepticism even though some have been around a longer time and developed more fully.

Much has been written about vortex methods since the pioneering works of von Karman (1911) and Rosenhead (1931). This was just about the time when Richardson (1922) attempted to integrate the finite-difference form of the meteorological equations (by hand, of course) in order to make the first numerical weather forecast. These works had an everlasting impact on the future studies. Richardson's failure pointed out the need for the development of numerical theories. Rosenhead's success revealed the seductive nature of the vortex methods and strengthened the belief that the vortices are an infinite source of inspiration and frustration. The present interest in these methods derives from the hope to simulate large scale structures that are complementary to experimental data and to predict flow characteristics which cannot be measured, at least without great difficulty.

During the course of about sixty years, the number of vortex elements increased from two to a hundred thousand while the desk calculators and moving fingers were replaced by super computers and line printers. Particularly exasperating is that almost every paper, at least in part, represents a new method. Furthermore, polarization, duplication, and "independent" discovery are beginning to set in. The production of information even in this highly specialized subject has exceeded anyone's ability to use it without devoting a large fraction of the research time to assimilate it. Review articles have become the only practical avenue of approach for newcomers to the subject partly to resist the tide of the papers generated with the help of parallel processors, partly to familiarize them with the ideas and pertinent references, and partly to minimize the rediscovery of the existing methods and ideas.

This paper is as much a review of these methods as it is a review of the ad-hoc assumptions, ingenious approximations, and smoothing techniques conceived and used during the past six decades. They could be better appreciated and tolerated if one judges them in the spirit best described by the great German poet and dramatist Johann Wolfgang von Goethe: "Man, instead of complaining about the thorns of a rose, should be thankful to God for having created a rose among so many thorns."

Many of the results which established our knowledge about vortex methods can be found in the reviews by Clements and Maull (1975), Fink and Soh (1974), Saffman and Baker (1979), Saffman (1981), Leonard (1980, 1985), and Aref (1983). These did an excellent job of reviewing either the early work in the field or the more recent contributions or some more specialized methods and problems. The present review is intended to be a comprehensive and even-handed account of computational methods with vortices. The objective was neither to provide a survey of the Art's instantaneous State nor to drive a procession of facts across the reader's attention span. Every attempt has been made to generalize the approaches and to explain the basic physical and mathematical ideas underlying the major methods and their applications. The reader is frequently reminded that the representation of a continuous distribution of vorticity by a finite number of discrete vortices is the major source of inaccuracy, the growth of the cost of computations with the square of the number of vortex elements is the greatest disadvantage, and the need to devise schemes to cope with the consequences of both is the fundamental weakness of the computational methods with vortices.

## 2 Theoretical Foundations and Numerical Schemes

**2.1 Vorticity and Laws of Transportation.** In homogeneous fluids, vorticity $\nabla x\mathbf{u}=\omega$ is produced only at the boundaries of fluid regions. Vorticity can also be generated in the interior of inhomogeneous fluids or at a free surface when gravity is acting. In fact, the creation of vorticity by advection of the mean gradient is a fundamental process in geophysical flows. However, the discussion here will be restricted to homogeneous incompressible fluids.

The vorticity transport equation for a fluid of uniform density $\rho$ and viscosity $\nu$ subjected only to irrotational body forces, is derived from the momentum equation in the form

$$\frac{D\omega}{Dt}=\frac{\partial\omega}{\partial t}+\mathbf{u}\cdot\nabla\omega=\omega\cdot\nabla\mathbf{u}+\nu\nabla^2\omega \tag{1}$$

in which use is made of the relations that the divergences of the velocity and the vorticity are zero. The term $\mathbf{u}\cdot\nabla\omega$ represents the rate of change due to convection of fluid. The term $\omega\cdot\nabla\mathbf{u}$ represents the rate of deformation of the vortex lines and exists only in a three-dimensional flow. The stretching of the vortex lines concentrates vorticity, increases velocity fluctuations and decreases the minimum length scale in the flow. The last term represents the rate of change due to molecular diffusion of vorticity (with suitable assumptions it may be made to represent both molecular and turbulent diffusion). The motion of an incompressible fluid can thus be represented as the creation and subsequent evolution of a self-interacting vorticity field. To know the vorticity field as a function of space and time is to understand the motion of fluids.

In an inviscid fluid, vorticity is a kinematic property of a given fluid particle and, like matter, it can neither be created nor destroyed, i.e., vortex lines are material lines. Thus, it can undergo only convection and deformation. Consequently,

tracking the evolution of vorticity leads immediately to a Lagrangian description.

In a viscous fluid, however, the vorticity produced at a boundary is carried away by convection and diffusion. This process determines the entire flow field which in turn controls the production of vorticity. The discretized representation (approximation) of these processes, particularly in flows where the distribution of vorticity is compact, constitutes the essence of the computational methods with vortices.

For two dimensional and unidirectional flows $(u,0,0)$, $\omega \cdot \nabla \mathbf{u} = 0$ and equation (1) reduces to

$$\frac{D\omega}{Dt} = \nu \nabla^2 \omega \tag{2}$$

and the vorticity is now a scalar quantity which is attached to and transported with the fluid. These equations are analogous to the kinematical behavior of magnetic field lines in a medium with finite electrical resistivity.

For a two-dimensional, incompressible and inviscid flow, equation (2) may be written in terms of the vorticity $\omega$ and the stream function $\Psi$ as,

$$\frac{D\omega}{Dt} = \frac{\partial \omega}{\partial t} + \mathbf{u} \cdot \nabla \omega = 0 \tag{3}$$

and

$$\nabla^2 \Psi = -\omega \tag{4}$$

Equation (4) is Poisson's equation and enables one to determine $\Psi$ from $\omega$. The stream function $\Psi$ is related to the velocity components through

$$u = \partial \Psi / \partial y \qquad \text{and} \qquad v = -\partial \Psi / \partial x \tag{5}$$

The computational methods with vortices owe their existence to that of the vorticity equation and to the fact that the distribution of vorticity in real flows is often sufficiently compact for its idealization in terms of singularities imbedded in an otherwise inviscid domain.

The higher the Reynolds number, the more compact the regions of vorticity. This is advantageous to dealing with the entire flow field through the use of grid-dependent differencing schemes and piecewise smooth interpolation functions [at least in theory, before one faces $O(N^2)$ vortex interactions, Kelvin-Helmholtz instability (short wavelength instability), turbulence, and the need for numerous ad hoc assumptions and disposable parameters!] The disappearance of the pressure does, in fact, introduce drawbacks into some methods (e.g., random walk method) as far as the calculation of the pressure distribution on the body is concerned. This is partly because the solution of the vorticity equation, with appropriate boundary conditions, produces results in terms of a nonmeasurable kinematic quantity: vorticity (for indirect methods see Agui and Jimenez, 1987; Imaichi and Ohmi, 1983; and Cantwell and Coles, 1983). Consequently, the results of numerical experiments can be compared with those of physical experiments only indirectly. Some numerical schemes (to be discussed in detail later) calculate the pressure distribution and the time-dependent integrated quantities (e.g., lift and drag forces) indirectly and approximately as quantities averaged over a sufficiently large number of time steps.

Lucid interpretations of vorticity and the equation governing its transport are given by Lighthill (1963), Batchelor (1967), and Morton (1984). Here we will describe only briefly some of the most important conclusions.

The generation of vorticity at rigid boundaries and its subsequent decay have been the subject of much discussion. Lighthill (1963) invoked the existence of vorticity sources in a region of falling pressure along the boundary and vorticity sinks (at which vorticity is abstracted at the surface) in a following region of rising pressure. This is based on the fact that the tangential-vorticity source strength is related to the pressure gradient, at least for flow over a stationary plane surface $(y = 0)$, by

$$-\nu \frac{\partial \omega_z}{\partial y} = \nu \frac{\partial}{\partial y}\left(\frac{\partial v}{\partial x} - \frac{\partial u}{\partial y}\right) = \nu \frac{\partial^2 u}{\partial y^2} = \frac{1}{\rho}\frac{\partial p}{\partial x} \tag{6}$$

Batchelor (1967) also noted that "vorticity cannot be created or destroyed in the interior of a homogeneous fluid under normal conditions, and is produced only at the boundaries," implying that the mechanism whereby vorticity is lost is by diffusion to the boundaries. Morton (1984), has finally clarified all prior concepts regarding the generation and decay of vorticity. His conclusions will be summarized here since the understanding of where and how the vorticity is lost is of central importance in the numerical schemes to be discussed later. According to Morton, "vorticity generation results from tangential acceleration of a boundary, from tangential initiation of boundary motion and from tangential pressure gradients acting along the boundary," "vorticity once generated cannot subsequently be lost by diffusion to boundaries," "reversal of the sense of acceleration or of the sense of pressure gradient results in reversal of the sense of vorticity generated" (which is interpreted by Lighthill as a vorticity sink), "walls play no direct role in the decay or loss of vorticity," and "vorticity decay results from cross-diffusion of two fluxes of opposite sense and takes place in the fluid interior."

The solution of real fluid flow problems with vortex models often forces one to think (at times to defend) simultaneously the behavior of vortices in terms of viscous and inviscid concepts. Thus, it is necessary to summarize briefly some of the major differences between the characteristics of vortices in viscous and inviscid fluids. In an *inviscid* incompressible fluid of uniform density, subjected to irrotational body forces, the circulation around any closed material curve is invariant (Kelvin's circulation theorem). This is a consequence of the fact that there is no diffusion and vorticity is transported solely by the convection of the fluid. In a *viscous* fluid, however, the circulation about a closed contour moving with the fluid depends on the contour of integration. The rate of change of vorticity in a material volume is due solely to diffusion across the boundary of the volume. The appreciation of this difference is of importance in the determination of the vorticity generated by a body, vorticity found in the wake, and the estimation of the circulation of a vortex. Sample calculations of the vorticity diffusion in the wake of a cylinder are given by Eaton (1987).

**2.2 Evolution Equations for a Vortex Sheet.** The conjugate complex velocity $\bar{q}(z)$ induced by a *two-dimensional vortex sheet* of strength $\gamma(s, t) = \partial \Gamma / \partial s$ situated on the contour $C$ is given by the Rott-Birkhoff nonlinear integro-differential equation (Rott, 1956; Birkhoff, 1962)

$$\bar{q}(z) = u - iv = \frac{1}{2i\pi}\int_C \frac{\gamma(s',t)ds'}{z - z(s',t)} + U_e - iV_e \tag{7a}$$

where $U_e$ and $V_e$ are the components of an external irrotational velocity field evaluated at $z$. *The Cauchy principal value is assumed for the integral to calculate the velocity at points on the sheet.* Equation (7*a*) has been generalized to the case of a vortex sheet with small thickness by Moore (1978). If the circulation $\Gamma$ is chosen as the Lagrangian variable to identify points on the sheet, equation (7*a*) may be written as (Birkhoff, 1962),

$$\frac{\partial \bar{z}}{\partial t}(\Gamma, t) = \frac{1}{2i\pi}\int_C \frac{d\Gamma'}{z(\Gamma,t) - z(\Gamma',t)} + U_e - iV_e \tag{7b}$$

Equations (7*a*) and (7*b*) ensure the continuity of pressure across the sheet and the conservation of circulation of segments lying between any two points moving with the sheet.

However, they do not ensure consistent and analytically tractable solutions; one must resort to numerical methods.

The standard and perhaps the crudest procedure is to identify the position of the sheet using a finite number of marker points. Then the motion of the sheet is approximated by calculating the trajectories of the marker points. For example, of the trailing-vortex sheet of a wing is represented by an array of $n$ line vortices per half wing, equation (7*a*) reduces an initial value problem, consisting of a set of $2n$, first order, ordinary differential equations whose solution requires suitable smoothing schemes. The next level of approximation is to replace the sheet by a large number of segments or panels through the use of piecewise polynomial representations for both $\gamma$ and $s$ and to simulate the highly rolled-up inner region either by an isolated line vortex or by a finite region of distributed vorticity. These and other methods such as the vortex-lattice and panel methods are discussed in Section 3.2.2.

**2.3 Real Vortices and Instabilities.** Real vortices are not concentrated singularities of infinite vorticity. The best known among these are the Rankine and Lamb (Oseen) models. The Rankine vortex rotates as a solid body within its core and is characterized by a potential flow outside, i.e., all of the vorticity is confined to the core region. The tangential velocity distribution for an isolated Rankine vortex has the form

$$v_\theta = \frac{\Gamma}{2\pi r} \quad (r > r_c) \qquad \text{and} \qquad v_\theta = \frac{\Gamma}{2\pi}\frac{r}{r_c^2} \quad (r < r_c) \tag{8}$$

with an artificial discontinuity ar $r = r_c$.

The Lamb (1932) model involves a Gaussian vorticity distribution and a circumferential velocity given by

$$\omega(r,t) = (\Gamma_0/4\pi\nu t)\exp(-r^2/4\nu t) \tag{9a}$$

and

$$v(r,t) = (\Gamma_0/2\pi r)[1 - \exp(-r^2/4\nu t] \tag{9b}$$

Equation (9) is an exact solution of the Navier-Stokes equations for *a single viscous vortex in an unbounded incompressible domain* and $\sqrt{2\nu t} = r_0$ is the standard deviation of the vorticity distribution. The radius at which the tangential velocity reaches a maximum is $r_m = 2.24\sqrt{\nu t} = 1.584 r_0$.

Obviously, even a single vortex with a compact support (e.g., Rankine vortex) is not an exact solution of the Navier-Stokes equations. A single Lamb vortex (which has an infinite support in an unbounded domain) is an exact solution. However, the velocity field of a multi-Lamb-vortex system is not strictly an exact solution because the nonlinearity of the Navier-Stokes equations does not permit the superposition of the vortex fields.

Rayleigh (1916) analyzed the stability of single vortices with general distributions of circulation, swirl velocity, and vorticity, but only for axisymmetric perturbations. He showed that stability against such perturbations is assured if $\Gamma^2$ nowhere decreases with $r$, i.e.,

$$d(\Gamma^2)/dr = 8\pi^2 r^2 \omega V_\theta > 0 \tag{10}$$

Otherwise the vortex is unstable to axisymmetric perturbations. A vortex with a $\Gamma^2$ that decreases somewhere is said to have a circulation overshoot (Govindaraju and Saffman, 1971). This phenomenon has not yet been observed experimentally, probably due to the fact that it is difficult to make measurements where it occurs. Clearly, a vortex is unstable if it has vorticity whose sign is opposite the swirl velocity. This, however, is not the only mechanism whereby a single laminar or turbulent vortex is dissipated. Vortex bursting or vortex breakdown has been shown experimentally to play a more dominant role in the demise of a vortex (see, e.g., Sarpkaya 1971, 1983). Axial flow (Bergman 1969; Widnall and Bliss 1971; Moore and Saffman 1972) and ambient turbulence (Sarpkaya and Daly 1987) are known to affect the stability of a vortex pair and the occurrence of vortex bursting.

The stability of vortex sheets and, in particular, the Helmholtz instability have been the subject of intense interest. It is a well-known fact that an infinitesimal disturbance of wavelength $\lambda$ on a plane sheet of strength $\kappa$ grows like $\exp(\pi\kappa t/\lambda)$, according to which the shorter waves grow faster. The stability of unsteady two-dimensional vortex sheets was discussed by Saffman (1974), Moore and Griffith-Jones (1974), and Moore (1976, 1981, 1984). Saffman and Baker (1979) suggested that the spiralling vortex sheets may be stable to Helmholtz instability because their strength decreases at a rate faster than that necessary to stabilize the sheets against a local Helmholtz instability. However, experiments show that the roll-up of both two-dimensional as well conical vortex sheets is accompanied by Helmholtz instability (Pierce, 1961; Tomassian, 1979; Gad-el-Hak and Blackwelder, 1985, 1987; Payne et al., 1967; Sarpkaya et al., 1988).

Trailing vortices are made of rolled-up vortex sheets. During their formation process, the tightly spiralled regions exhibit velocity jumps between the vortex sheets. They are then liable to helical instabilities, even to Helmholtz-type instability. The Helmholtz waves on the vortex sheet quickly degenerate into turbulence, which mixes the sheets and smoothens the vortex cores. The turbulence so generated encroaches upon the external potential flow, spinning it up at the expense of angular momentum in the core. There results a circulation overshoot and corresponding countersign vorticity in the region of circulation overshoot. The ensuing Rayleigh instability produces strong turbulence and further encroachment into the potential flow. The mathematical model used to date of concentrating vorticity onto a tightly wound spiral surface has, of course, no strict counterpart in real flows, although measurements of the velocity field in such cores have shown up to one to two of the outer turns of the spiral. Further inwards, viscous diffusion smears out any trace of such discontinuities and an approximately axisymmetric swirling flow with distributed vorticity appears. This, in fact, is the basis of the scheme of amalgamating the inner spirals into a finite core region to avoid sheet kinking and spurious interaction between spirals at or near the end of the sheet. The serendipitous consequence of this scheme is to delay the discrete form of the Helmholtz instability in the remainder of the sheet.

The three-dimensional instability of an initially parallel vortex pair has attracted great attention because of its importance in the understanding of the demise mechanisms of aircraft trailing vortices. Crow (1970) was the first to show that both symmetric and asymmetric modes of instability will develop on the vortices due to the mutual inductance of the sinusoidally perturbed pair. Crow has also shown that the instability grows exponentially and results either in a linking of the vortex pair into a series of crude vortex rings or in a highly disorganized intermingling of the vortices. Once again, vortex bursting may occur on one or both of the vortices. It is now agreed that sinusoidal instability, vortex breakdown, axial velocity in the vortices, ambient turbulence, and the stratification of the medium govern the demise of the trailing vortices and the evolution of internal waves in a stratified medium (Widnall et al., 1971; Moore, 1972; Moore and Saffman, 1972; Widnall, 1975; Sarpkaya, 1983; Sarpkaya and Daly, 1987).

Another form of three-dimensional instability concerns the vortices shed from bluff bodies. Even if the body is two-dimensional and even if the vortices are shed in a two-dimensional manner, three-dimensional vortex instabilities may distort the filament and affect the spanwise and chordwise correlation of pressure on the body. This raises questions

regarding the applicability of the two-dimensional models, the possible means with which the two-dimensional calculations may be corrected to adequately account for the three-dimensional distortions of the vortex filaments (artificial reduction of circulation), and the repesentation of a three-dimensional vorticty field (containing curved vortex filaments with core and finite self-induction) by two dimensional vortices (with or without a core and no self induction). Thus, one needs to know the source of the three-dimensionality in order to devise models either to replace the two-dimensional calculations or to correct them. Furthermore, one has to make sure that the mechanism of instability is the same for both the continuous and the discrete systems and that both lead to the same type of large and small scale structures.

In order to address some of these questions, Widnall (1985a, 1985b) analyzed the three-dimensional instability of two highly idealized cases: A single vortex separating from a cylinder as well as that of the Föppl vortices (two symmetrical stationary vortices behind a circular cylinder, see, e.g., Milne-Thomson, 1960 and Weihs and Boasson, 1979). Her calculations have shown that the most unstable mode of instability for the single vortex separating from a circular cylinder is three-dimensional. She reached similar conclusions for various modes (symmetric and asymmetric) for the Föppl vortices. This investigation as well as those of Crow (1970) and Widnall and Sullivan (1972) suggests that the neglect of three-dimensionality can lead to disagreements with experimental results. This is in addition to two-dimensional instabilities resulting from the discretization of a field of continuous vorticity which may not be representative of the behavior of the continuous system.

The instability of vortex rings has attracted much theoretical and experimental interest following the pioneering work of Krutzsch (1939). A detailed review of the subject is presented by Widnall (1975) (see also Saffman, 1970, and 1978 for a succinct critique of earlier stability calculations). The mutual interaction of vortex rings generated, for example, by a bluff body or by a round jet is of importance in the numerical simulation of three-dimensional flows. There is a strong interest in the understanding of the details of the vortex linking and the emergence of new vortex rings (i.e., the cross-linking or the cut-and-connect mechanism) and in the establishment of a possible relationship between these phenomena, noise and turbulence. According to Hussain (1986) "The cut-and-connect provides an alternative mechanism for energy cascade and a mechanism for generation of helicity (and thus perhaps coherent structures)." The vortex reconnection is prohibited in inviscid flows by Helmholtz's theorem. Thus, viscous effects are necessary for its occurrence (see also Ashurst and Meiron 1987). A direct numerical simulation of the phenomenon, starting with a closed knotted vortex tube, is given by Kida and Takaoka (1987) through the use of the full Navier-Stokes equations.

**2.4 Biot-Savart Law (The Direct Summation Method).** The velocity induced by the vorticity concentrated in a bounded region is given by the volume integral (see, e.g., Batchelor 1967)

$$\mathbf{u}(\mathbf{r},t) = -\frac{1}{4\pi}\int\int\int \frac{(\mathbf{r}-\mathbf{r}')x\omega(\mathbf{r}',t)}{|\mathbf{r}-\mathbf{r}'|^3}\, dv(\mathbf{r}') \qquad (11)$$

which was found experimentally by Biot and Savart in 1820 in connection with the determination of the magnetic field intensity (corresponding to $u$) induced by an element of electric current (corresponding to $\omega$) and was established analytically by Ampere in 1826.

If vorticity is concentrated at a single curved filament of circulation $\Gamma$ (*the thin filament approximation*), equation (11) reduces to

$$\mathbf{u}(\mathbf{r},t) = -\frac{\Gamma}{4\pi}\int_C \frac{[\mathbf{r}(s)-\mathbf{r}'(s')]x\dfrac{\partial \mathbf{r}'}{\partial s'}}{|\mathbf{r}(s)-\mathbf{r}'(s')|^3}\, ds' \qquad (12)$$

in which $r(s)$ describes the filament centerline in terms of the arclength $s$, and $\partial \mathbf{r}/\partial s'$. $ds'$ is the filament tangent vector. Equation (12) yields a logarithmically infinite self-induced velocity (Batchelor 1967) if the filament is curved, and zero self-induced velocity if it is straight, i.e., a *line vortex* (a straight vortex filament of non-zero circulation, vanishing cross-section, and infinite vorticity). There is no two-dimensional *point* vortex. The thin filament approximation is further simplified, to deal with the logarithmic singularity, through the use of the *Local* (or Self) *Induction Approximation*, LIA, (the local approximation that the core radius is very small and the dominant term in the motion is proportional to the local curvature and directed along the binormal), introduced by Da Rios (1906), Hama (1962, 1963), and Arms and Hama (1965), modified by Betchov (1965), and used, e.g., by Schwarz (1982) are Aref and Flinchem (1984). As noted by Buttke (1988), *LIA does not allow for stretching or compression of a vortex filament.* Only the (neglected) nonlocal terms allow one the desired three-dimensional realism.

There are two additional difficulties with the Biot Savart approach even for two-dimensional flow simulations with line vortices. First, the vortex filaments are singularities and, hence, create large velocities and/or critical velocity differences in their neighborhood. This causes instabilities and physically impossible sheet crossings along and near the edges of the sheet. This, in fact has been the case with most of the earlier works. Clearly, the propensity for mutual orbiting of the vortices and the meandering of the edge of the vortex sheet in an otherwise inviscid environment are at the heart of the problem.

The second difficulty with the Biot Savart method concerns the CPU per time step. The number of operations required for the velocity-field calculation is proportional to $N^2$ where $N$ is the number of vortices. Thus, the CPU time increases significantly as more vortices are added. These two difficulties gave rise to numerous smoothing schemes and hybrid methods to be discussed in the following sections.

**2.5 Smoothing Techniques.** As noted earlier, the Rott-Birkhoff equation does not ensure consistent solutions. Van der Vooren (1980, in report form in 1965) showed that the principal-value integral in equation (7) could be evaluated accurately through the regularization of the integrand with a cancellation function. Unfortunately, this did not appear to be the sole cause of the difficulty, as his calculations led to chaotic behavior.

Moore (1979, 1981, 1984) has shown that the discretization of the principal value integral in equation (7) is not the cause of the pathological instability and that the ill-posedness is introduced by the very step of replacing a thin shear layer by a vortex sheet. For the discretized vortex sheet, Moore identified the difficulties as a discrete form of the well-known Helmholtz instability and showed that the most unstable mode has a period equal to twice the spacing of the vortices. He has also shown that the fastest growth rates are for the smallest wavelengths (as with the continuous Helmholtz instability) and that increasing the number of vortices increases the growth rate of the disturbance. Meiron, et al. (1982), using a more general spectral method and initial disturbances of finite amplitude were able to identify singularities in the sheet curvature and to confirm Moore's (1979) asymptotic prediction of the critical time at which the singularities appeared.

When chaos pervades, suggestions for smoothing reign

supreme. The challenge to obtain a smooth roll-up through line-vortex discretization of a thin shear layer proved to be seductive and the rush was on to discover smoothing schemes or surgical techniques with the implicit assumption that they have a negligible effect on the dynamics of large-scale structures: Velocity cutoff or use of vortices with a core or compact support, amalgamation of a number of vortices into a single vortex, use of subvortices, rediscretization of the sheet, and other filtering and smoothing techniques.

*2.5.1 Cutoff Schemes.* Numerous cutoff schemes have been introduced to desingularize equation (7) (Rosenhead, 1930; Spreiter and Sacks, 1951; Hama, 1962, 1963; Arms and Hama, 1965; Crow, 1970; Widnall et al., 1971; Moore, 1972; Moore and Saffman, 1972; Kuwahara and Takami, 1973; Chorin and Bernard, 1973; de Bernardinis and Moore, 1985; Clements and Maull, 1973, 1975).

The first is Rosenhead's (1930) method, as modified by Moore (1972), according to which the evolution equation for the one-dimensional continua of space curves $r_i(\xi)(i=1, 2, \ldots, N)$ for N filaments is given by (see, e.g., Leonard 1985)

$$\frac{\partial \mathbf{r}_i}{\partial t} = -\sum_j \frac{\Gamma_j}{4\pi} \int \frac{[\mathbf{r}_i(\xi,t) - \mathbf{r}_j(\xi',t)] \times \frac{\partial \mathbf{r}_j}{\partial \xi'} d\xi'}{(|\mathbf{r}_i - \mathbf{r}_j|^2 + \alpha\sigma_j^2)^{3/2}} \tag{13a}$$

in which $\sigma$ is the core radius (specified by a vorticity distribution) and $\alpha$ is a parameter related to the fraction of circulation within the radius $r=\sigma$ (Moore 1972) [$\alpha=0.413$ for a Gaussian core (Leonard 1980a) and $\alpha=0.22$ for a uniform vorticity distribution (Ashurst and Meiron 1987)]. The assumed core radius is not expected to remain constant during the evolution of the toroidal vortex. It may depend on time and on the axial velocity within the filament (Widnall et al., 1971; Moore and Saffman, 1972; Leonard, 1985). The interaction of filaments with different core radii may be expressed by modifying equation (13*a*) as,

$$\frac{\partial \mathbf{r}_i}{\partial t} = -\sum_j \frac{\Gamma_j}{4\pi} \int \frac{[\mathbf{r}_i(\xi,t) - \mathbf{r}_j(\xi',t)] \times \frac{\partial \mathbf{r}_j}{\partial \xi'} d\xi'}{(|\mathbf{r}_i - \mathbf{r}_j|^2 + \alpha(\sigma_i^2 + \sigma_j^2)^{3/2}} \tag{13b}$$

where $\alpha=0.2065$ yields the correct speed of a ring vortex in the limit $\sigma_i \ll$ ring radius (Leonard 1980b). A lucid discussion of the asymptotic analysis leading to equation (13*b*) is given by Moore and Saffman (1972). The above cutoff scheme modifies the denominator of the term under the integral sign in equation (12) and mimics the thickening of the vortex sheet by viscosity. A similar scheme has been used by Meng (1978) in connection with the evolution of a vortex ring in a stratified and shearing environment. He replaced $r_{ij}^3$ in the denominator of equation (12) by $(r_{ij}^3 + r_c^3)$ for the three-dimensional case and $r_{ij}^2$ by $r_{ij}^2 + r_c^2$ for the two-dimensional case.

For an assembly of closed filaments, the energy

$$E = \frac{1}{2} \sum_{ij} \Gamma_i \Gamma_j \int \frac{\frac{\partial \mathbf{r}_i}{\partial \xi_i} \cdot \frac{\partial \mathbf{r}_j}{\partial \xi_j} d\xi_i d\xi_j}{\left(\left|\mathbf{r}_i - \mathbf{r}_j\right|^2 + \alpha(\sigma_i^2 + \sigma_j^2)\right)^{1/2}} \tag{14}$$

is conserved and positive definite only when $\sigma_i$ is independent of time. It approximates the volume integral of the kinetic energy when the cores do not overlap. If $\sigma$ is adjusted locally to conserve volume, the core size becomes $\xi$ and time dependent and the energy is no longer conserved. This is not surprising since axial flows are neglected and the energy in the swirling component of velocity is not accurately accounted for (see, e.g., Siggia, 1985 and Pumir and Siggia, 1987).

In the second and more commonly used cutoff scheme, proposed, apparently independently, by Spreiter and Sacks (1951), Roy (1957), Kuwahara and Takami (1973), and Chorin and Bernard (1973), the line vortex is replaced by a "blob": a vortex with an *invariable* core shape and size or "compact support." Spreiter and Sacks used a Rankine vortex. Kuwahara and Takami used the Lamb vortex on the grounds that it describes exactly the velocity field of a *single* viscous vortex. They have noted that the velocity field of a multi-Lamb-vortex system "is not strictly exact because they are incompatible with the Navier-Stokes equation, whose nonlinearity does not permit the superposition of the vortex fields." In fact, it is because of this realization that they called $\nu$ in equation (9*b*) "artificial viscosity." Kuwahara and Takami studied the rotation of vortex tubes of elliptic and circular section, comprised of numerous line vortices (with $\nu=0$) and obtained angular velocities comparable with those given by the exact solution. They have also studied the roll-up problem and have shown that the inclusion of "artificial viscosity" smoothens the roll-up but the degree of roll-up decreases with increasing $\nu$. Furthermore, the artificial viscosity does not prevent the eventual occurrence of strong irregularity in the region of high vortex concentration (see, e.g., Dalton and Wang, 1988).

Kuwahara and Takami's blob had a time-dependent core radius, and that of Chorin and Bernard a fixed radius (the first to be widely noted). Even though core expansion appears to simulate the viscous diffusion of the vortex, Greengard (1985) argued, without giving any error limits, that the core spreading scheme does not converge to the correct equation of motion except when the flow field outside the region $|\omega|>0$ is uniform. The rigid-blob idealization is not dynamically consistent either and violates Euler's equations and Helmholtz's laws! Nevertheless, both schemes have been used extensively (see, e.g., Ghoniem et al., 1987b).

In addition to its strength, position, axial symmetry, and nondeformability, a blob is specified by its cutoff radius and cutoff function (describing the shape of the core velocity distribution, e.g., a Rankine or Lamb vortex). The scalar vorticity field at time $n \cdot \Delta t$ is represented by

$$\omega^n(x) = \sum_{i=1}^{N} K_\sigma(x_i^n - x)\Gamma_i \tag{15}$$

where $x_i^n$ is the position of the $i$th blob, $\Gamma_i$ its strength, and $K_\sigma$ the cutoff function, with a cutoff radius $\sigma$ [see Chang (1988) for a fairly complete list of the commonly used cutoff functions]. The Chorin and Bernard blob had a stream function $\Psi$ such that

$$\psi = \begin{cases} (2\pi)^{-1}\Gamma \log r & (r > \sigma) \\ (2\pi)^{-1}\Gamma(r/\sigma) & (r \le \sigma) \end{cases} \tag{16a}$$

The corresponding cutoff function is given by

$$K\sigma(x) = \begin{cases} (2\pi\sigma|x|)^{-1} & |x| < \sigma \\ 0 & |x| \ge \sigma \end{cases} \tag{16b}$$

For $r<\sigma$, the velocity induced by such a vortex is that of rigidly rotating fluid core and for $r>\sigma$, it is identical to that of a line vortex.

The velocity field created by vortices with small but finite area is finite everywhere and quantitatively correct away from the core. Near the core, the velocity is only qualitatively correct since the vorticity distribution about each blob is not allowed to distort in the prevailing strain field. This imposes a

lower limit on the wavelength of the disturbances which can be used in stability calculations. This is in addition to the fact that *a linear sum of vortices with finite cores does not constitute an exact solution of the nonlinear equations of motion.* If the vortices are well separated, the use of blobs is not necessary. If two or more blobs are allowed to overlap, Helmholtz's law (vortex lines are material lines) and the law of conservation of total energy are violated. The amount of energy lost depends on the core size chosen. The larger the core size the greater the loss of energy. For a given core size, the energy remains nearly constant but lower than the strictly inviscid value. The limitations of the approach regarding the rapid distortion of the finite regions of vorticity have been brought out by the analyses of Dushane (1973) and Portnoy (1976, 1977).

The use of blobs (i) does not ensure smooth roll-up but, as pointed out by Moore (1984), provides damping of short waves; (ii) must be regarded as a mathematical artifice to limit the large velocities induced by vortices in their immediate neighborhood; and (iii) requires a judicious selection of the shape of the velocity distribution and the core size relative to the inter-vortex spacings (the degree of overlapping of the blobs). Note that the velocity and vorticity at a point in a region occupied by overlapping blobs are determined by the contributions of surrounding "layers" of blobs and not just by the core function of one blob.

In general the blob scheme modifies the *numerator* of the integral in equation (12) by introducing a smoothing function $g(c)$ which depends on the assumed structure of the vortex core (Leonard et al. 1985). Equation (12) then is written as

$$\frac{\partial \mathbf{r}_i}{\partial t} = -\sum_j \frac{\Gamma_j}{4\pi} \int \frac{\left[\mathbf{r}_i(\xi,t)-\mathbf{r}_j(\xi',t)\right] x \frac{\partial \mathbf{r}_j}{\partial \xi'}\, g\left(\left|\mathbf{r}_i-\mathbf{r}_j\right|/\sigma_j\right)}{|\mathbf{r}_i-\mathbf{r}_j|^3}\, d\xi' \tag{17}$$

where $g(c)$ is arbitrary within certain constraints. Leonard et al. (1985) used

$$g(c) = c^3/(c^2+\alpha)^{3/2} \tag{18}$$

where $\alpha = 0.413$ corresponds to a Gaussian core and $\alpha = 0.22$ to a uniform vorticity distribution in the ring core, as noted earlier.

Equation (17) yields the velocity field evaluated at the center of the vortex. It satisfies the conditions of conservation of total circulation and linear and angular impulse either if $\sigma_i = \sigma$ or if $g(c)$ is slightly modified so that

$$\frac{\partial \mathbf{r}_i}{\partial t} = -\sum_j \frac{\Gamma_j}{4\pi} \int \frac{\left[\mathbf{r}_i(\xi,t)-\mathbf{r}_j(\xi',t)\right] x \frac{\partial \mathbf{r}_j}{\partial \xi'}\, g\left\{\left|\mathbf{r}_i-\mathbf{r}_j\right|/[(\sigma_i^2+\sigma_j^2)/2]^{1/2}\right\}}{|\mathbf{r}_i-\mathbf{r}_j|^3}\, d\xi' \tag{19}$$

Equation (17) may be made to satisfy the conservation of total kinetic energy by using the vorticity-weighted average of the velocity over the blob (Leonard's schemes B and D). Such refinements are not deemed commensurate with all the other approximations inherent to the analysis. However, the overlap of the filament cores provides a smoother distribution of the vorticity and, as shown by Ashurst and Meiburg (1988), is necessary for convergence to Euler equations (see also Meiburg and Lasheras, 1988). However, vortex filaments may be quickly depleted by large strains, making their overlap impossible without special treatments which, in turn, distort the velocity field.

The geometry of each space curve is approximated by a sequence of linear segments between successive nodes. In an improved version of this method, Leonard et al. (1985) used a trapezoidal rule to integrate along each curve with parametric cubic splines to estimate the derivatives $\partial \mathbf{r}/\partial \xi$ at each node. He claimed that the new method requires only half the number of arithmetic operations per node point and only half the number of node points for equivalent accuracy. Ashurst and Meiburg (1988) used continuous filaments described by cubic splines with second-order integration in space and time in simulating the evolution of three-dimensional shear layers.

An alternative to the continuous-vortex-filaments representation of vorticity in three-dimensional flow is the use of *vortex balls* (vortons according to Saffman and Meiron 1986, or vortex arrows according to Leonard 1975) and the volume integral given by equation (11). The vorticity field is discretized into a number of vortex balls, each with an assigned vorticity. Each ball is characterized by a core radius, a core function, a circulation, and a material vector element that describes the distribution of vorticity along the axis of the element. The core radius and the core function remain invariant with time. Circulation of an element is constant but the vorticity changes with stretch of the material element. The accurate representation of the continuous vorticity field and the local vorticity intensification requires that the core functions associated with neighboring elements must highly overlap and the elements experiencing severe stretch must be split into two in the local direction of the vorticity, i.e., sub-vortons must be created as in Maskew's (1977) sub-vortex model (note that the velocity field in the vicinity of the sub-vortons is not identical to that of the original vorton field). The use of vortex balls allows substantial deformation of the core of a toroidal vortex at different radial stations (see e.g., Ghoniem et al., 1987a, Knio and Ghoniem, 1988, Shirayama et al., 1985, and Section 3.4).

For the two-dimensional case, a simple modification is needed to equations (12) and (17). For example, equation (12) reduces to

$$\frac{\partial \mathbf{x}_k}{\partial t} = -\frac{1}{2\pi} \sum_{\substack{j=1 \\ j\neq k}}^{N} \frac{(\mathbf{x}_k-\mathbf{x}_j) x \hat{e}_z \Gamma_j}{|\mathbf{x}_k-\mathbf{x}_j|^2} \tag{20}$$

and equation (17) becomes

$$\frac{\partial \mathbf{x}_k}{\partial t} = -\frac{1}{2\pi} \sum_{\substack{j=1 \\ j\neq k}}^{N} \frac{(\mathbf{x}_k-\mathbf{x}_j) x \hat{e}_z \Gamma_j g(|\mathbf{x}_k-\mathbf{x}_j|/\sigma_j)}{|\mathbf{x}_k-\mathbf{x}_j|^2} \tag{21}$$

where $\mathbf{x}_k(x_k, y_k)$.

In terms of complex variables, equation (20) may be written as

$$u_k + iv_k = \dot{z}_k = \frac{i}{2\pi} \sum \Gamma_j \frac{z_k - z_j}{|z_k - z_j|^2} \tag{22a}$$

or as

$$u_k - iv_k = \dot{\bar{z}}_k = \frac{1}{2i\pi} \sum \frac{\Gamma_j}{z_k - z_j} \tag{22b}$$

The effect of an assumed core (e.g., a Rankine vortex), can easily be incorporated into the above equations by rewriting equation (22*a*) as

$$u_k + iv_k = \dot{z}_k = \frac{i}{2\pi} \sum \Gamma_j \frac{z_k - z_j}{r_{jk}^2} \tag{23a}$$

for $r_{jk} = |z_j - z_k| > \sigma$ and as

$$u_k + iv_k = \frac{i}{2\pi\sigma^2}\sum \Gamma_j (z_k - z_j) \tag{23b}$$

for $r_{jk} < \sigma$, (counterclockwise $\Gamma$ is considered positive). The velocity induced at $z_k$ by the underlying irrotational flow (e.g., uniform flow, doublet, etc.) will have to be added to that induced by the vortices.

One may desingularize equation (22*a*) or equation (23*a*), for example, by replacing $r_{ij}^2$ by $r_{ij}^2 + r_c^2$, where $r_c$ is a measure of the core radius (Meng (1978). For $r_{jk} \ll r_c$, and therefore in the core, the velocity grows linearly with respect to the radial distance but falls off as $1/r_{jk}$ if $r_{jk} \gg r_c$. This is the method originally proposed by Rosenhead (1930), as noted earlier in connection with equation (13).

Krasny (1987), in computing the roll-up of a vortex sheet in the Trefftz plane, desingularized equation (22*b*) by multiplying the right-hand side with what he called "an artificial smoothing parameter" to obtain

$$u_k - iv_k = \dot{\bar{z}}_k = \frac{1}{2i\pi}\sum_j \frac{\Gamma_j}{z_k - z_j}\frac{|z_k - z_j|^2}{|z_k - z_j|^2 + \delta^2} \tag{24}$$

Equation (24) is identical to Meng's (1978) modification of equation (22*b*) to include a core radius as

$$u_k - iv_k = \dot{\bar{z}}_k = \frac{1}{2i\pi}\sum_j \Gamma_j \frac{z_k - z_j}{r_{jk}^2 + r_c^2} \tag{25}$$

which, in turn, is the two-dimensional version of the desingularization scheme proposed by Rosenhead (1930). Equation (25) has been rediscovered by Inoue (1985a) also in connection with his vortex simulation of a turbulent mixing layer.

The use of an Oseen or Lamb vortex [equation (9*b*)] to simulate an expanding vortex core is not identical to the use of Rosenhead's smoothing scheme. The two methods yield nearly the same tangential velocity distributions as a function of $r/\delta$ for $1.44 < 4\nu t/\delta^2 < 1.63$ (see Fig. 1). The viscous-diffusion solution of Lamb for an isolated line vortex corresponds to an ever increasing $\delta$ in equation (24) for $4\nu t/\delta^2 > 1.63$. It is because of this reason that Rosenhead's scheme ($\delta$ = constant) leads to the roll-up of tighter spirals, relative to other schemes using either the Lamb model (see, e.g., Dalton and Wang 1988) or the Fink and Soh (1978) model, (rediscretization with a growing central line vortex). The asymptotic form of the spiral and the growth rate of the Kelvin-Helmholtz instability depend on the initial amplitude and type of disturbance and $\delta$ (Pozrikidis and Higdon 1985, Krasny 1987). Krasny's (1987) roll-up calculations suggest that the large-scale dynamics become independent of $\delta$ as $\delta \to 0$. Clearly, Rosenhead's (1930) desingularization scheme is akin to, but not identical to, the use of a blob, even though in the most recent literature they are both being called the blob-method.

Other ad hoc cutoff schemes exist and undoubtedly new ones will be introduced. For example, Clements and Maull (1973) used equistrength discrete vortices to investigate the effect of different wing loading distributions on the roll-up. In order to deal with the very large velocities induced on the final vortex in the sheet, they have placed an upper bound on the initial velocity of the vortices near the tip and amalgamated those responsible (never more than two) whose mutually-induced velocity exceeded the imposed bound.

*2.5.2 Amalgamation of Vortices.* Two or more vortices have been amalgamated into a central line vortex in numerous ways and for a number of reasons: to limit the unrealistically large velocities induced in each other, to minimize their propensity to orbit about each other, to simulate more closely some naturally occurring merging, and to reduce the computer

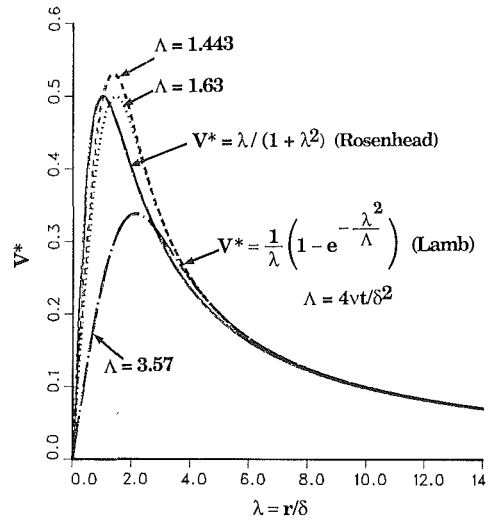


**Fig. 1 Comparison of the Lamb and Rosenhead (1930) velocity profiles**

time. Apparently, Ham (1968) (who credited S. Widnall for the suggestion) was the first to use this scheme.

Amalgamation is an approximation and there is no "correct" or "guaranteed" way to perform it. One should use it with care and, if possible, verify that it did not introduce unacceptably large errors. Unfortunately, it is often difficult to assess the more elusive effects of merging on the numerical predictions since the problem is highly nonlinear and since its consequences are intermingled with those of many other parameters and ad hoc assumptions.

It has been customary to amalgamate two or more vortices into a single vortex of strength $\Gamma_j$, placed at their center of vorticity, given by

$$z = \Sigma\Gamma_j z_j / \Sigma\Gamma_j \tag{26}$$

This process conserves only total circulation and linear momentum. With merging of likesign vortices, ($\Gamma_i\Gamma_j > 0$), the second moment of vorticity distribution decreases and the velocity fields before and after the amalgamation are not identical. Consequently, discontinuities occur in the calculated force acting on a body if either the generalized Blasius theorem or the time-rate of change of impulse is used. Thus, it is not advisable to merge vortices close to a boundary. In unidirectional flow past bluff bodies, the vortex clusters beyond a given distance from the body have been merged into a single equivalent vortex, primarily to reduce the CPU time (note that the velocity field in the vicinity of the merged vortex is not identical to that prior to merging). For oscillating flows, the merging is not advisable even if it takes place away from the body at the time of its execution. The merged vortex may subsequently be convected back across the body and give rise to velocities and pressures vastly different from those which would have been created by the original cluster (the wake return is an important phenomenon in periodic flow about bluff bodies) (see, e.g., Sarpkaya 1986a, 1986b).

The oppositely signed vortices are often combined, when their separation distance is less than a prescribed value, to mimic the cancellation of oppositely signed vorticity (thought to be the major mechanism of enhanced energy dissipation in turbulent flow). The removal of a vortex from the field, when it is closer than a prescribed distance to a boundary, (or to its image), is based on the same idea.

Merging of vortices into a single vortex to represent the innermost part of a rolled-up shear layer is based on the realization that a spiral with infinite number of turns cannot be represented by a finite number of vortices (J.H.B. Smith, 1968; Moore, 1974). Such a merging helps (i) to avoid the effects of the erratic motion of the tip vortices (sheet crossing,

hooks, kinks, etc.) stemming from the sparsity of the vortices in the tip region or from the inadequate (or inappropriate) representation of the compressive parts of the sheet, (ii) to smoothen the rest of the sheet by eliminating the attendant consequences of propagation of the tip perturbations along the feeding sheet, and more importantly, (iii) to recognize the natural fact that the viscous diffusion smears out the velocity discontinuities, leading to an approximately axisymmetric swirling flow with distributed vorticity, as discussed in Section 2.3. Furthermore, this merging technique in consort with other techniques (e.g., rediscretization) allows the calculation to be taken beyond time limits of the basic discrete vortex calculations (Moore, 1981).

The merging technique has been used extensively in a variety of applications. For example, it has been used by Fink and Soh (1974) to deal with the singular behavior at the tips of the sheet; by Rom and Almosnino (1978) to calculate the nonlinear lift on canard configurations where merging resulted in twice as much lift relative to that without merging by Deffenbaugh and Marshall (1976) to simulate the flow about a cylinder where merging affected the transverse force in the early stages of the flow development (showing that amalgamation on the one side and in the vicinity of the cylinder causes large changes in the pressure distribution in the neighborhood of the merged vortex, as expected); by Sarpkaya and Shoaff (1979b) to calculate the evolution of flow about stationary and transversely oscillating circular cylinders; by Longuet-Higgins (1981) in connection with his model of oscillating flow over steep sand ripples; by Bromilow and Clements (1982) to simulate the roll-up of vortex sheets where clusters of vortices in the region of roll-up were amalgamated into a single equivalent vortex; by Spalart (1982) to reduce the computer time in the simulation of separated flows where a manually adjusted error limit on the difference of the velocity fields before and after the emerging was introduced to keep the total number of vortices near a chosen number.

The merging processes described above are irreversible, i.e., the merged vortex does not become unmerged at a later time and its strength remains constant. In the case of the tip-vortex, however, the strength of the merged vortex grows at each time step (a black hole from which no vorticity escapes). Clearly, remerging and/or merging of vortices with large circulations, large inter-vortex spacings, and small distances from the body have incalculable consequences and are strongly discouraged.

Another type of merging, which we will call "pseudo-merging," is used to split the Biot-Savart interaction between N vortices into long- and short-range effects in order to decrease the $N^2$-dependence of the calculations and hence the CPU time. The merging is temporary and fictitious, i.e., the distant vortex cluster retains its original form at the end of the time step. Only short-range effects involving nearby vortices are computed directly. Various versions of such a scheme have been used by Hockney et al. (1974), Hockney and Eastwood (1981), Spalart (1982), Tiemroth (1986a, 1986b), Ghoniem et al. (1986), Anderson (1986, *the method of local corrections*), Baden and Puckett (1988), and Greengard and Rokhlin (1987, *the fast multipole method*).

Tiemroth (1986a) introduced what he called the "discrete vortex in cell algorithm (DVIC)." Aside from the apparent similarity of the names, the DVIC scheme, has nothing in common with the VIC (vortex-in-cell) scheme to be discussed in Section 2.6. In the DVIC scheme, a potentially large collection of line vortices or blobs are temporarily replaced (at each time step) by a single vortex. The basic idea is that a group of vortices or blobs behaves as a single vortex if one is far enough away that the leading term in a series expansion of the complex velocity is dominant, and that one can approximate the velocity field at any point in the domain of convergence with arbitrarily high accuracy by using enough terms in the series. For this purpose, (i) a temporary grid of suitable cell size is introduced to group the vortices, (ii) "$p$" Laurent series terms (the number of terms being retained in the Laurent expansions) are calculated from the series expansion of the complex velocity for each cell that contains more than "$p$" vortex blobs, and (iii) the velocity of each blob is calculated by using the Biot-Savart law for the blobs within a given cell and within the "$q$" adjacent cells, and, using the first "$p$" terms of the series for all other cells. The accuracy of the method, the cost of the overhead and the actual computer time saved depend on the cell size, the choice of "$p$," the use of real or complex variables, the distribution, number, and the core size of the blobs, judicious selection of the "mass center" of the blobs in a cell, the existence of single sign or both signs of circulation in a cell (blobs are grouped according to the sign of the circulation and treated separately to avoid more complex centroid problems), and the time invested in coding. Tiemroth carried out a series of sample calculations to ascertain the relative error for the DVIC algorithm and the CPU time. It appears that the advantages of the DVIC scheme are only marginal. However, it does preserve the grid-free character of the vortex model. Spalart's (1982) scheme is essentially the same as that described above.

The "dipole-in-cell" (DIC) method, developed by Ghoniem et al. (1986), is another effort to reduce the CPU time in dealing with a large number of vortices or blobs. The flow field is divided into a number of square cells M. As in the DVIC scheme, blobs in a given cell are temporarily combined into two blobs, according to the sign of their circulation, and each is placed at the "center of mass" of their like-sign counterparts through the use of the conservation of the first moment of the vorticity field. The vortex blobs in a cell are replaced by a dipole located at the centroid of the original vorticity and used to update the induced velocity in the far field. The name "dipole-in-cell" is a misnomer since the strengths of the like-sign vortices in a cell are not necessarily identical. In fact, they may all be the same sign.

Anderson's (1986) *method of local corrections* approximates the far-field interactions by solving a discrete Poisson equation through the use of a finite difference mesh, with spacing $h$, superimposed on the domain. Greengard and Rokhlin's (1987) *fast multipole method* uses multipole and Taylor series expansions together with a hierarchical refinement of the computational domain in order to carry out $N$-vortex interactions in an amount of time proportional to $N$. In both methods, the interactions with near neighbors are computed directly.

It is clear from the foregoing that merging is used partly to overcome the pathological problems of the vortex methods, partly to decouple the local and far field interactions in order to reduce the computer time, and partly, and justifiably, to simulate the behavior of nature. Its use requires many numerical experiments, interactive computing, and a "feel" for the flow simulated.

*2.5.3 Subvortex Method.* Maskew (1973, 1977), concerned with the problems associated with the vortex-sheet roll-up in two dimensions, noted that the "core models" are applied without reference to neighboring vortices and are not satisfactory for both components of velocity. The "spread models," where vorticity associated with each vortex is distributed on the two straight segments joining the vortices (e.g., in a triangular fashion), require information about the neighboring vortices, and its three-dimensional form is cumbersome to apply. Maskew proposed a discretized form of the spread model, the so-called "subvortex technique," where the subvortices with a Rankine-vortex core are distributed evenly along the sheet joining the vortex to its two immediate neighbors. He has shown that the discretization of a vortex sheet introduces significant velocity errors only within a

distance from the sheet equal to the vortex spacing in the lattice. His technique enhances the versatility of vortex-lattice-based methods by providing the effect of a much finer discretization (i.e., preventing the "holes" in the lattice from being "seen"). The subvortex technique increases the computation time and is not expected to prevent the occurrence of instabilities in the roll-up of vortex sheets. It has been rediscovered by Ghoniem et al. (1987a, 1987b, 1988) for the simulation of reacting shear layers and by Mook et al. (1987) for the simulation of unsteady wake behind an airfoil.

Meng and Thomson (1978) repacked the vortices either by adding a new one or deleting an old one when the separation distance between neighboring vortices exceeded or fell below a preset limit. They have also proposed (but not actually used) to impose an equal-separation-distance scheme according to which the vortices and the physical variables are rearranged at each time step. A scheme similar to those of Maskew (1977) and Meng and Thomson (1978) was used by Siddiqi (1987) in connection with the Trefftz problem. Starting at the tip and using the slope information, he fitted, at each time step, a cubic spline to the sheet and redistributed each line vortex into two equal vortices when the sheet segment representing the vortex stretched beyond a prescribed amount. The basic aim of the redistribution (at the expense of increasing the number of vortices) is to try to keep the sheet segment length per vortex approximately constant so as to ensure that each roll-up turn is represented by an adequate number of vortices. Siddiqi was able to obtain three turns at a time when 90 percent of the circulation has rolled up.

*2.5.4 Rediscretization Method.* Fink and Soh (1974, 1978) compared the multi-vortex model with the original Cauchy principal-value integral [equation (7)] and concluded that the late time randomness is a consequence of the representation of the continuously evolving vortex sheet by an ever-increasing population of discrete vortices, i. e., the integration errors are the cause of the chaotic motion. They have shown that the Cauchy principal value evaluation of the Biot-Savart integral for the induced velocity of a segmented continuous vortex sheet includes a term, proportional to the logarithm of the ratio of the distances between adjacent vortices, which is not accounted for in the line vortex repesentation of the sheet. Their major conclusion was that the logarithmic term may be eliminated and thereby the errors could be significantly reduced if the vortices were equally spaced along the sheet (rediscretization or regridding). At each time step, the vorticity density is represented by an entirely new set of equidistant vortices whose strengths are adjusted to give a good representation of that density. This is the essence of the rediscretizaton method. Evidently, this procedure does not resolve all of the computational errors particularly in regions where the curvature of the sheet is small, e.g., the region close to the center of the vortex spiral. Furthermore, the curve-fitting errors incurred in the process of interpolation at every time step may accumulate as time increases. Fink and Soh's (1974) sample calculations, including the roll-up of a vortex sheet (where the tip vortices are allowed to amalgamate into a growing central line vortex), showed smooth roll-up for much longer periods of time than had been previously reported, but the details of their rediscretizaiton scheme are lacking.

Fink and Soh's (1974, 1978) method and other rediscretization, regridding, or redistribution techniques (e.g., Siddiqi 1987) can slow down the effects of the discrete form of the Helmholtz instability (Moore, 1979, 1981, 1984) but do not make the vortex-sheet methods convergent. Furthermore, they introduce some diffusion of vorticity, either along or away from the sheet, and, hence, errors into the calculations at all wavelengths. Sarpkaya (1975a) found no special substantial improvement when using Fink and Soh's method instead of the method of line vortices for the roll-up of vortex sheets shed from an inclined plate in a uniform ambient flow started impulsively from rest (Sarpkaya 1975b). Sarpkaya and Shoaff (1979a, 1979b) have further explored the strengths and weaknesses of the rediscretization scheme in connection with an impulsively-started flow about a circular cylinder (Sarpkaya 1966, 1978b).

Baker (1976, 1977, 1980) has shown that (i) the smoothing achieved by Fink and Soh is a consequence of keeping the point closest to the spiral center fixed during the process of rediscretization, assigning to that fixed point the vorticity necessary to conserve circulation, and the strong flow induced by the amalgamated vortex (see also Faltinsen and Pettersen 1982), (ii) the accumulation of vorticity at the tip in an ad hoc manner is an approximation to the innermost turns of the spiral, (iii) the method is unreliable and eventually leads to the sheet kinking and crossing (becoming increasingly severe as the number of vortices is increased), (iv) the method is not suitable for treating a general class of flows, and (v) the Fink and Soh method ignores the sheet curvature (equal spacing in chordlength instead of arclength was used) and hence it is only first order accurate in the roll-up region. Baker (1980) has further shown that the application of Fink and Soh's method to a ring wing (the circular vortex sheet with sinusoidal vorticity distribution for which there is an exact solution) failed to prevent the sheet from crossing itself (see Fig. 2).

Moore (1981) discussed the effects of Fink and Soh's smoothing technique and Longuet-Higgins and Cokelet's (1976) five-point filtering technique, [$z_i = (-z_{i-2} + 4z_{i-1} + 10z_i + 4z_{i+1} - z_{i+2})/16$] (originally designed to suppress a "sawtooth" instability in the computed free surface) and found that both techniques improved the results, but still led to the sheet crossing. Roberts (1983) showed that the five-point scheme of Longuet-Higgins and Cokelet may lead to hopelessly large errors in some applications. He used Fourier spectral representations for the position and potential of a free shear layer and was able to remove the numerical instability by a simple modification of the highest (even) Fourier mode.

Higdon and Pozrikidis (1985) used a higher-order rediscretization scheme replacing the continuous vortex sheet with a collection of circular arcs and the circulation distribution with piecewise trigonometric polynomials. The time step was continually adjusted, such that the maximum angle subtended by the arcs did not exceed a specified limit during the time step. The concept is quite similar to that of Mangler and Smith (1959) who used a single arc to model the inner portion of the vortex sheet shed from a delta wing, and to that of Hoeijmakers and Vaatstra (1983), who used an adaptive curvature-dependent-segment scheme and piecewise polynomial representations of arc shape and vorticity to

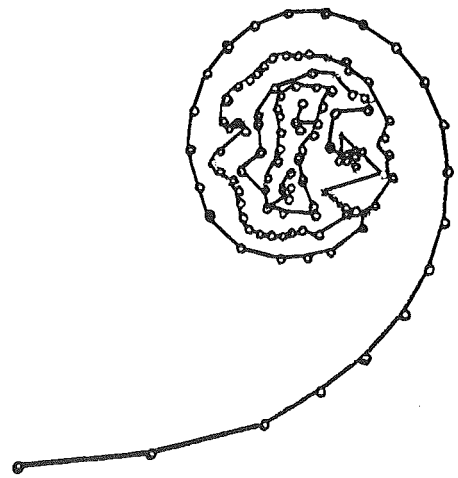

**Fig. 2 Chaotic motion of vortices in the spiralling region of a vortex sheet**

simulate the roll-up of a vortex into an amalgamated core. Higdon and Pozrikidis studied the evolution of two special sheets: a circular vortex sheet with sinusoidal circulation distribution (representing a vortex sheet shed by a thin circular rim or wing at small angles of attack), (see also Baker 1980), and an infinite plane vortex sheet subjected to periodic disturbances (see also Meiron et al. 1982). They have concluded that their calculations provide a good description of the roll-up, but cannot give an exact result for the shape of the sheet at *the critical time: the time at which a singularity forms in the vortex sheet* (Moore, 1979, Meiron, et al., 1982, Krasny, 1986a, 1986b). The appearance of singularity or the onset of the breakdown of predictability at a finite time is attributed to the combination of increasing velocity, decreasing lengthscale, and hence the diminishing timescale. In the case of the Fink and Soh model, the use of equally-spaced points prevents a resolution fine enough to analyze the singularity. The potential loss of resolution, which is usually provided by more closely spaced Lagrangian points in areas of large gradients, is a serious disadvantage. However, compared with other numerical smoothing schemes, rediscretization can potentially remove less energy from the system, especially in the limit of very small vortex spacings (but see Section 2.6).

Krasny's (1986a) scheme is based on a filtering technique through the use of fast Fourier transforms in order to inhibit the destructive effects of round-off errors. The amplitudes that have magnitudes less than the floating-point precision of the calculation are set to zero at each time step. Krasny applied this technique to a periodically perturbed vortex sheet and obtained convergent results up to the estimated time that the curvature singularity appears. Beyond that time, one has to use one of the other smoothing techniques to stabilize the calculations.

To sum up, rediscretization of line vortices or vortex segments delays, but does not prevent, the occurrence of an instability at a finite time. Apparently, the vortex sheet method is not convergent after this time. There is a potential loss of resolution in areas of large gradients. Part of the reason for the smoothness of the results obtained with rediscretization is attributable to the strong flow induced by, and the stabilizing effect of, the amalgamated vortex. The combination of these two schemes delays but does not inhibit the instabilities in the roll-up process. To be sure, the instability is not limited to vortex methods. It is also an inherent characteristic of the space discretization methods.

**2.6 Cloud-in-Cell (CIC) or Vortex-in-Cell (VIC) Method.** The use of the Biot-Savart law to calculate the velocities of a large number of vortices (as many as 100,000) stretches the capacity of even the fastest computers of the day and requires methods to reduce the CPU time (the community of super computer users is relatively small, but is growing rapidly). A similar requirement, not related to the use of the Biot-Savart law, had existed in the early 1950's in connection with the solution of complex flow problems. It is in response to that need that the particle-in-cell (PIC) or marker-in-cell (MIC) method was developed at Los Alamos in 1955 (Harlow, 1964), These methods combined some of the best features of both the Lagrangian and Eulerian approaches. The Lagrangian particles representing the elements of fluid move through a fixed Eulerian mesh which, in turn, is used to characterize the field variables.

The PIC method has subsequently been used in plasma simulation where it acquired the new name of the "cloud-in-cell" (CIC) method (Birdsall and Fuss, 1969; Langdon, 1970; Eastwood and Hockney, 1974; Eastwood, 1975). Christiansen (1973) used it to study the interaction of vortices (see also Christiansen and Zabusky, 1973; Baker, 1976, 1977; Meng and Thomson, 1978; Baker, 1979; Leonard, 1980a; Murman and Stremel, 1982). The method is now known as the CIC or the VIC (the vortex-in-cell) method as far as computational methods with vortices are concerned.

The key to the execution of this grid-dependent hybrid scheme is to bypass the Biot-Savart law and to use sequentially the Lagrangian frame to track the vortices, and the Eulerian frame to calculate the velocity field through the use of Poisson's equation. This requires a fine-enough grid (often with several levels of mesh), the assumption that the vortices in a given cell temporarily become cell-shaped blobs with a prescribed vorticity distribution (often uniform), a vorticity-allotment scheme which allocates vorticity to the surrounding mesh points (i.e., from the location of the vortices to the nearest node points of the mesh), a numerical solution of Poisson's equation by a "fast Poisson solver" (these generally require fairly simple boundary conditions, see, e.g., Burridge and Temperton 1979; Schumann and Sweet, 1988), and an interpolation scheme which determines the velocities at the location of the original vortices (or at any other point) from the node point values. The last step couples with a Lagrangian description of vortex convection, completing a cycle of the VIC scheme. Normally, a simple bilinear interpolation provides satisfactory results for both the vorticity-allotment and velocity-interpolation schemes. Both the stream function (Christiansen, 1973; Baker, 1979) and velocity potential (Murman and Stremel, 1982) have been used as the dependent field variable. The former is limited to two-dimensional flows. The latter is designed for nonlinear vortex wake modeling in three-dimensional compressible potential flow calculations.

The method is implemented as follows. In its simplest form, vorticity of the $n$th vortex in a given cell is allocated to the four surrounding meshpoints according to the area-weighting scheme,

$$\omega_i = \Gamma_n A_i / A^2 \quad i = 1, 2, 3, 4 \tag{27}$$

where $\Psi_n$ is the circulation of the vortex and $A$ is the area of the cell (see Fig. 3). When the vorticity allotment to the surrounding meshpoints is completed for all vortices in all cells, Poisson's equation ($\nabla^2 \Psi = -\omega$) is solved to obtain $\Psi_{i,j}$ at all mesh points $(i,j)$. Then the velocity components are calculated at $(i,j)$ through a simple differencing scheme,

$$u_{i,j} = (\Psi_{i,j+1} - \Psi_{i,j-1})/2M \tag{28a}$$

$$v_{i,j} = -(\Psi_{i+1,j} - \Psi_{i-1,j})/2M \tag{28b}$$

where $M$ is the cell dimension. The velocity of the $n$th vortex in the cell is then found from

$$u_n = \Sigma u_i A_i / A \quad , \quad v_n = \Sigma v_i A_i / A \tag{29}$$

These equations form a consistent set of interpolation functions in the sense that a single line vortex will not move in its own velocity field. The computing time used to implement the

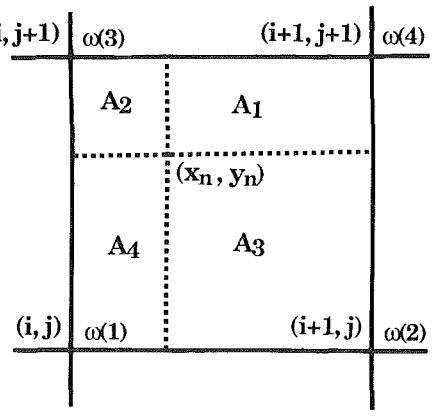


**Fig. 3 Area weighting scheme for the distribution of vorticity on the mesh (cloud-in-cell method)**

solution depends on the configuration of the overlapping meshes, the complexity of the allotment and interpolation schemes, and the boundary conditions.

The method also extends to the three-dimensional discrete Poisson equation, which can be solved by performing a two-dimensional FFT on each plane, solving tridiagonal systems in the third direction, and then performing a two-dimensional inverse FFT on each plane (Christiansen, 1973; Burridge and Temperton, 1979).

The basic advantages of the VIC technique are as follows. The number of velocity calculations does not increase as $N^2$ as in Biot-Savart approach. For incompressible flows, Poisson solvers require order $M \log_2 M$ operations where $M$ is the number of grid points. Thus, the VIC technique requires less computing time (linear in $N$) compared with the direct summation method and enables one to track a larger number of vortices (several thousand) compared with several hundred with the direct summation. One must, however, be warned that in some cases the time saved may be disappointingly small because of the Eulerian-step overhead. The velocity field calculation is effectively desingularized by smearing the vorticity over a cell area, i.e., a singular problem is desingularized by an artificial viscosity. However, the vortex wake remains well defined throughout the computational domain because of the Lagrangian treatment of the vorticity field. This is unlike the Eulerian treatments which lead to the rapid dissipation of the dependent field variable in compact regions of vorticity, unless multiple scale grids or an adaptive mesh are used to exhibit features which vary rapidly over a wide range of spatial and temporal scales (see, e.g., Erlebacher and Eiseman, 1987). Finally, the Lagrangian part of the hybrid scheme enables the vortical structures to "float" over the fixed Eulerian mesh of the velocity field (Harlow 1964; Murman and Stremel, 1982).

The disadvantages of the VIC scheme may be summarized as follows. It makes an otherwise grid-free method once again grid-dependent. Thus, the minimizing of the blockage effects in bluff-body flows may require a prohibitively large number of cells. The use of overlapping meshes may alleviate the problem but it may also introduce errors hard to assess. The VIC scheme introduces a pseudo-viscosity into the flow (some may regard it as an advantage for it stabilizes the velocity field calculations) and gives a finite width to the vortex sheet because vorticity is spread over a mesh cell area. The Eulerian step smoothens the conceptual diffusion of vorticity but the Lagrangian step preserves the singular character of the line vortex. Both the Eulerian and Lagrangian steps create numerical errors and lead to some anisotropy on the smallest scales. Consequently, the method and its fine-scale behavior are sensitive to the size of the mesh, the surface boundary conditions, the number of vortices and the time-step, as noted by Murman and Stremel (1982) and Rottman et al. (1987). The flow features of scale smaller than the grid cannot be accurately resolved. Thus, the CIC simulation (e.g., of a "turbulent" mixing layer) may not reproduce the actual flow as faithfully as the direct summation simulation. On the other hand, vortex models do not and should not pretend to deal with fine-scale structures. This is a disadvantage also shared by finite difference calculations which do not predict eddies smaller than the mesh spacing and unsteady phenomena faster than the scale of the time step used (Braza et al., 1986). It is generally assumed that the behavior of large scale vortex structures is relatively insensitive to the fine-scale instabilities (which is not rigorously true in a turbulent flow, Kourta et al., 1987) and to the precise details of the initial perturbations.

Christiansen (1973) investigated the motion and the stability of line vortices arranged to simulate Rankine's combined vortex. He has conducted seven numerical experiments on the test model and found that the most significant numerical error arises from the anisotropic CIC-interpolation of velocities given by equation (29). He has concluded that the only way to remove the truncation errors associated with the finite difference forms is to adopt either a more complex interpolation algorithm or to employ a different mesh structure (for example a hexagonal or triangular mesh). Interpolation algorithms, much more costly than the CIC method, have been developed by Hockney et al. (1974) for applications in plasma simulations where isotropic force fields from single particles are required (see also Christiansen and Zabusky, 1973).

An interpolation function, smoother than the original four-point weighting, was suggested by Peskin (1977), in a slightly different context, and subsequently used by Tryggvason (1988a) in connection with the numerical simulation of the Rayleigh-Taylor instability and the vortical structures arising out of it (see also Kerr 1988). Wang (1977) used cubic splines for interpolation (i.e., referring to the nearest 16 grid points rather than the nearest 4 for each vortex node) and a Gaussian shape factor or "filter" in wave vector space. In their generalization of the CIC scheme to the analysis of a vortex-sheet interface, separating two fluids of slightly different densities, Meng, and Thomson (1978) used the bilinear interpolation scheme and a vorticity distribution for each vortex which approximated a Gaussian distribution.

In a careful study of vortex wake roll-up, Baker (1979) applied the CIC method to the simulation of two-dimensional vortex sheets generated by a wing and by a wing-flap configuration (see Fig. 4). He demonstrated that the redistribution and interpolation errors introduce instabilities in the vortex sheet on the order of the mesh spacing. Murman and Stremel (1982) developed an algorithm to compute vortex wake features in two dimensional time-dependent potential flows. The approach is a modification of Baker's (1979) method for the stream function-vorticity equations. Other applications of the VIC scheme are described in Section 3.3.

**2.7 Body Representation.** Analysis of flow through the use of vortex methods requires exact or approximate methods to satisfy the condition that the resulting flow is parallel to the body surface, or that the body is a streamline, or that the normal velocity relative to the body is zero, if possible, everywhere on the body contour, if not, at a number of collocation points. The zero slip-velocity condition and vorticity generation will be discussed later.

For three-dimensional bodies, the use of the vortex or doublet sheets to satisfy the zero normal velocity condition is quite common. Two-dimensional flows have more alternatives. The very special, and yet the most studied, case of flow about a circle needs nothing more than the simple circle theorem which yields an image per vortex at the inverse point (no image is needed at the center for it would violate the conditions at infinity, unless flow symmetry is imposed with respect to the $x$-axis). In placing a cylinder of arbitrary cross-section into a two-dimensional flow, one could use, if possible, an exact conformal transformation (e.g., the Shwartz-Christoffel transformation) (see, e.g., Sarpkaya, 1975; Clements and Maull, 1975; Nagano et al., 1981) or an approximate numerical transformation through the use of a truncated Laurent series (von Kerczek and Tuck, 1969; Shoaff and Franks, 1981; Dawson and Marcus, 1970) or isolated or distributed singularities or panels (sources, sinks, vortices, or vortex or doublet sheets) (see, e.g., Hess and Smith, 1964; Hess, 1975; Hess and Friedman, 1981; Lewis, 1981; Porthouse and Lewis, 1981; Chorin, 1978; Hoeijmakers 1983; Inamuro et al., 1984; Sarpkaya and Ihrig, 1986). The last two methods require an assessment of the leakage through the boundary.

The use of a conformal transformation for a two-dimensional flow requires a special rule (Routh's rule, as described below) to calculate correctly the velocities in the physical plane.

*2.7.1 Routh's Rule.* In computing the complex velocity at the position of a line vortex in the physical $z$-plane through the

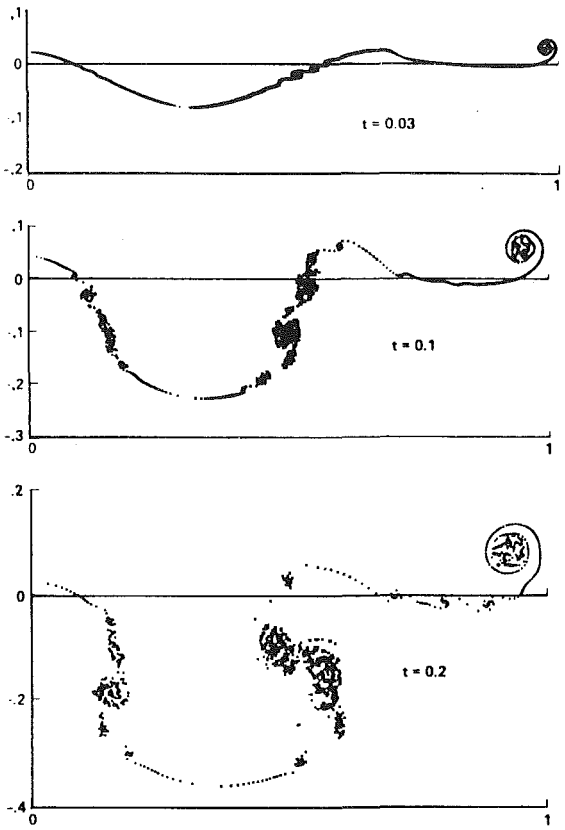


**Fig. 4(*a*) Vorticity distribution behind a wing-body with deployed flap at different times (Baker, 1977)**

use of that in the transformed λ-plane, $[z=f(\lambda)]$, the straightforward differentiation of the complex velocity potential $F(\lambda)$ as,

$$\frac{d}{d\lambda}\left[F(\lambda)-\frac{i\Gamma_k}{2\pi}\log(\lambda-\lambda_k)\right]\frac{1}{f'(\lambda)}\Big|_{\lambda_k} \tag{30}$$

is not sufficient. *The velocity of a vortex in one plane does not give the correct velocity when transformed to another plane.* As first noted by Routh (see, e.g., Milne-Thomson, 1969), the transformation gives rise to an additional term, often referred to as Routh's correction. The corrected velocity in the physical plane then becomes

$$u_k-iv_k=\frac{d}{d\lambda}\left[F(\lambda)-\frac{i\Gamma_k}{2\pi}\log(\lambda-\lambda_k)\right]\frac{1}{f'(\lambda)}\Big|_{\lambda_k} - \frac{i\Gamma_k}{4\pi}\frac{f''(\lambda_k)}{[f'(\lambda_k)]^2} \tag{31}$$

where the vortex position $\lambda_k$ in the transformed plane corresponds to that at $z_k$ in the physical plane. The last term in equation (31) is Routh's correction and results from the fact that the determination of the velocity at $z_k$ requires the subtraction of $(i\Gamma_k/2\pi)\log(z-z_k)$ from $F(\lambda)$ or, in terms of λ, the terms

$$\frac{i\Gamma_k}{2\pi}\log(\lambda-\lambda_k)+\frac{i\Gamma_k}{2\pi}\log\left(1-\frac{c^2}{\lambda\lambda_k}\right) \tag{32}$$

in which $c$ is the radius of the circle in the λ plane and the last term is the source of Routh's correction. The various versions and applications of equation (31) have been given by Sarpkaya (1968a), Clements (1973a, 1973b, 1977), Sarpkaya (1975b), Conlisk and Rockwell (1981), and Panaras (1985).

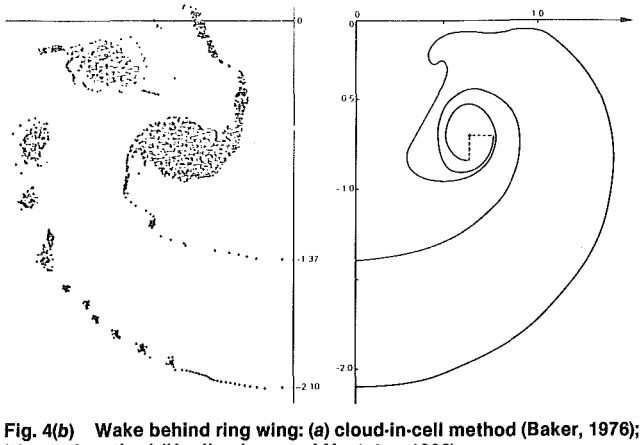

**Fig. 4(*b*) Wake behind ring wing: (*a*) cloud-in-cell method (Baker, 1976); (*b*) panel method (Hoeijmakers and Vaatstra, 1983)**

*2.7.2 Surface Singularity Distributions.* The use of surface singularity distributions for two- and three-dimensional attached flows is well advanced and has been extensively described in the past (Hess and Smith, 1964; Hess and Friedman, 1981; Webster, 1975; Pien 1964; Chang and Pien, 1975; Johnson and Rubbert, 1975; Asfar et al., 1979; Noblesse, 1983; Nagati et al., 1987).

In its most general form, the surface is represented by source and doublet sheets (or equivalently vortex sheets). Either the Neumann condition ($\partial\phi/\partial n$ specified) or the Dirichlet condition ($\phi$ specified) is used. Green's theorem is invoked to express the fact that any solution $\phi$ can be expressed as the sum of the influences of source and doublet sheets on the boundary surface. The resulting integral equation is discretized into a set of algebraic equations and solved numerically for the strengths of a finite number of discrete singularities on or near the body surface by enforcing the boundary condition (typically, a Neumann boundary condition) at collocation points. However, because this can lead to numerical difficulties, the Neumann condition is transformed into a internal Dirichlet condition using Green's theorem to obtain a Fredholm integral of the second kind. Here the discussion is limited to two-dimensional flows. An in depth account of the mathematical details of the boundary integral method is given by Hunt (1980).

It is a well-known fact that across a vortex sheet the normal component of velocity is continuous and the tangential velocity jumps by an amount $\gamma$ (the strength of the vortex sheet). One half of this jump is on the external side of the sheet and an equal but opposite amount is on the internal side of the sheet (as in the case of two counter-flowing streams with velocities $\gamma/2$). Thus, the condition that the body contour is a closed streamline may be satisfied by rendering the sum of the velocities *just inside the contour* equal to zero everywhere. The resulting integral equation can be discretized in a straightforward manner using a panel method with straight line or curved segments along which the vorticity is either piecewise constant (a first order scheme) or varying linearly with matching end point values (or even a higher-order scheme). In practice, the body contour is represented by $M$ straightline segments along each of which $\gamma$ is constant. Then the condition of zero internal tangential velocity at the $i$th collocation point (in the middle of the $i$th segment) is given by

$$U_e^t(i)+\sum_{j=1}^{M}\gamma(j)K(i,j)=0 \tag{33}$$

where $U_e^t(i)$ is the tangential velocity at the $i$th collocation point due to the ambient flow plus all other singularities in the flow, (calculated before the introduction of the vortex sheet), $\gamma(j)$ is the strength of the $j$th segment, and $K(i,j)$ is the cou-

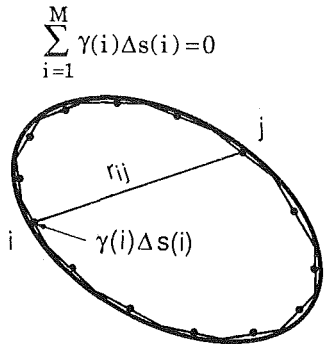


**Fig. 5 Discretization of a two-dimensional contour**

pling coefficient or the influence matrix, dependent strictly on the geometry of the body. It can be evaluated and stored once and for all through the use of

$$K(i,j) = \frac{1}{2}\delta_{i,j} + \frac{1}{2\pi}\int_{s_m}^{s_n} \frac{[\mathbf{r}(s)x\mathbf{e}_z]\cdot t_i ds}{|\mathbf{r}(s)|^2} \tag{34}$$

when $\delta_{i,j}$ is the Kronecker delta, $r(s)$ is the position vector of the $i$th collocation point from the point $s$ on the $j$th segment, and $\mathbf{t}_i$ is the tangential unit vector at the $i$th collocation point. In matrix form, equation (33) may be written as

$$[K][\gamma] = [b] \quad \text{with} \quad b(i) = -U_e^t(i) \tag{35}$$

Further simplification may be achieved by representing the body by $M$ line vortices of strengths $\Gamma(j) = \gamma(j)\Delta s(j)$, located at the center of each segment, rather than by sheet segments (see Fig. 5). Then the coupling coefficient $K(i,j)$ reduces to (Martensen 1959)

$$K(i,j) = \frac{1}{2}\delta_{i,j} + \frac{1}{2\pi}\frac{(x_i - x_j)\left[\frac{dy}{ds}\right]_i - (y_i - y_j)\left[\frac{dx}{ds}\right]_i}{[(x_i - x_j)^2 + (y_i - y_j)^2]} \tag{36}$$

Note that the tangential velocity $U_e^t(i)$ also may be expressed in terms of a coupling coefficient, very similar to $K(i,j)$, and the gradient of the velocity potential representing the ambient flow plus all other singularities in the flow field.

Equations (33) and (35) do not yield a unique vorticity distribution due to the nearly singular nature of the matrix **K**. However, one may regularize the matrix **K** and render the vorticity distribution unique by assuring the continuity of the pressure gradient on the body (see Section 2.1 and Morton, 1984), i.e., by enforcing the necessary condition that

$$\oint \gamma(s)ds = 0 \quad \text{or} \quad \sum_{i=1}^{M} \gamma(i)\Delta s(i) = 0 \tag{37}$$

If there are additional bodies in the flow, equation (37) must be satisfied for each for exactly the same reasons. The use of $M$ collocation points (e.g., the midpoints of the segments) leads to $(M+1)$ equations [including equation (37)] and $M$ unknowns ($\gamma_i$). The ambiguity may be resolved, for example, by ignoring one of the collocation points (Stansby and Dixon 1983). However, the fact remains that the $\Psi = 0$ condition is satisfied only at the collocation points, i.e., the body is represented only approximately at points other than the control points. One can minimize the error by using, for example, a least squares technique to minimize the residues of equation (33) at as many control point as possible rather than rendering equation (33) exactly zero at a few number of points (Sarpkaya and Ihrig 1986). One may also use the Lagrangian multiplier ($\lambda$) method to minimize an appropriate functional with respect to $\gamma$ and $\lambda$ (Tiemroth 1986a).

A body may also be represented by a set of discrete vortices whose positions are fixed but the strengths are calculated at each time step to satisfy the *zero normal velocity* condition either exactly at $(M-1)$ points or approximately at a larger number of points through the use of the least squares technique. The condition that the total circulation of all the vortices (on the body and in the wake) must be zero is used as the $M$th equation (Inamuro et al., 1983, 1984, Sarpkaya and Ihrig, 1986).

**2.8 Shedding of Discrete Vortices From the Separation Points.** Discrete vortex or *discrete vorticity models* (DVM) have been applied extensively to separated flow about bluff bodies with the added predicaments, repeated almost *ad nauseum*: how is separation to be defined, where are the separation lines, what is the rate of shedding of vorticity, how does the separating stream surface leave the body, what conditions should be satisfied at the separation lines (s), what is the relationship between the Kutta condition and separation from a smooth surface (both for steady and unsteady flows about interacting or non-interacting bodies), and what are the effects of the numerical and facility-related parameters on separation and asymmetry inception? These questions still remain essentially unresolved (see, e.g., Peake and Rainbird, 1975).

Vorticity may be shed either from the separation points (which must be known a priori) or from the entire surface of the body or partly from the separation points and partly from a prescribed segment of the body surface (using the no-slip condition to determine their strength and the core radius to determine their position). This section deals only with the shedding of nascent vortices from the separation points. It will be assumed that the separation points are either fixed, as in the case of sharp-edged bodies, or known through experiments, or by a boundary-layer calculation coupled with the inviscid solution. This is where the vortex methods exhibit their greatest weakness for a number of reasons, particularly for unsteady flows.

The methods used in the past for the determination of the rate of vorticity may be roughly classified into two broad categories. The first of these involves the use of variable nascent vortex positions (Sarpkaya, 1968b, 1975) and the second, the use of fixed nascent vortex positions (see, e.g., Clements, 1973b; Clements and Maull, 1975; Kiya and Arie, 1977a).

The method of fixed positions involves the selection of a suitable point in the flow near the separation point and the use of the velocity $U_s$ at that point to calculate the rate at which vorticity is shed into the wake from

$$\frac{\partial \Gamma}{\partial t} = \frac{1}{2}U_s^2 \tag{38}$$

with some inspiration from the seminal works of Fage and Johansen (1927, 1928). The previous applications of this method did not examine the effect of the position of the nascent vortices on the velocity distribution in the neighborhood of the separation point. Only the distance of the fixed point to be body was varied and bracketed between two subjective limits by comparing the calculated results with those obtained experimentally (Kiya and Arie, 1977a). In this method, no interaction is allowed between the shed vortices and the amplitude of oscillation of the point or the time of appearance of the nascent vortices. Furthermore, the time interval is chosen more or less arbitrarily (Kiya and Arie, 1977a, 1977b) (repeating a few calculations with a single program with only the time step changed and also by referring to the results of the previous investigations). Thus, the velocities at the outer edges of the shear layers are only indirectly related to the strength of the nascent vortices and the fixed time interval. Evidently, the velocities in the inner and outer edges of the shear layers, the time interval, the strength and position of the nascent vortices, and the Kutta condition are interdependent. Thus, the position of the nascent vortices and the time interval cannot be chosen arbitrarily, even if they are chosen judiciously on the basis of previous experience and trial calculations.

Sarpkaya (1975b) used the method of variable nascent vortex positions and determined the rate of shedding of vorticity from the relation

$$\frac{\partial \Gamma}{\partial t} = \frac{1}{2} U_{sh}^2 \tag{39}$$

where $U_{sh}$ is interpreted as the velocity in the shear layers calculated by using the average of the transport velocities of the first four vortices in each shear layer. The positions of the nascent vortices are chosen so as to satisfy the Kutta condition at the edges of the body and thus they can move slightly with time. Thus, this method simulates in a satisfactory manner the mechanism of feedback from wake fluctuations to the fluctuations in the rate of circulation. The number of disposable parameters is reduced to a minimum and in this sense this method is superior to the method of fixed positions. However, the use of the average of the transport velocities of the first four vortices remained questionable.

Sachs et al., (1967) placed, in the plane of a wing, a sheet of vorticity of strength $\gamma$ (per unit length) and length $\Delta s = V_t \Delta t$, $V_t$ being the velocity induced at the tip by the vortices in the field. The value of $\gamma$ was determined from the Kutta condition that the flow leaves the plate smoothly. The sheet was then replaced by a single vortex or strength $\gamma \Delta s$ at a point in the wing plane which again satisfied the Kutta condition. The nascent vortex was moved with the velocity induced at that point (see also Piziali, 1966; and Duffy, et al., 1984). Evans and Bloor (1977) studied the flow past a flat plate of height $h$ in a channel. The nascent vortex was placed at a point $z = i(h + \epsilon/2)$, in the plane of the plate, and the vortex strength was taken to be $0.5U^2\Delta t$, $U$ being the velocity at $z = i(h + \epsilon)$. The value of $\epsilon$ and hence $\Delta\Gamma$ were found from the Kutta condition (see also Kiya et al., 1982 for a slightly improved version of this scheme).

In applications to sharp-edged bodies, it was often assumed that the vorticity flux could not be calculated through the use of the mathematically finite velocity occurring at the sharp edges of the body. This assumption was based on the fact that the separation points are singularities of the transformation used and the numerical procedures may not be stable. Mostafa (1987) has shown that the tip velocity can be calculated accurately and that the nascent vortex does not necessarily lie in the plane of the plate.

In the case of the circular cylinder, the nascent vortex was usually placed at a distance $\epsilon$ from the cylinder surface (with its image at the inverse point) along the radial line passing through the separation point. Assuming zero slip velocity at the separation point and a suitable $\Delta t$, *the values of* $\epsilon$ and $\Delta\Gamma = 0.5\ U_s^2 \Delta t$ were calculated. The velocity $U_s$ was either taken as the velocity at the separation point prior to the introduction of the nascent vortex (Deffenbaugh and Marshall, 1976; Sarpkaya and Shoaff, 1979a), or found by iteration (Stansby, 1977).

The foregoing is only a small sample of the schemes used to introduce nascent vortices. Evidently, letting a body give birth to vorticity in discrete steps, in an otherwise continuous process, is not a simple matter. None of the method cited above related $\Delta t$ to both $\epsilon$ and $\Delta\Gamma$, nor dealt with the breakaway angle of the separation streamline, nor with the velocity distribution in the vicinity of the separation point after the introduction of the nascent vortex.

Often the question arises regarding the angle which the separation streamline makes with the body. Oswatitsch (1957) has shown that the said angle for a viscous flow is given by

$$\tan\theta_s = -3(d\tau_w/dx)/(dp/dx) \tag{40}$$

Sychev (1972), Messiter and Enlow (1973), and Messiter (1975, 1983) have shown that the triple-deck equations describe finite Reynolds number effects in the neighborhood of the separation point where the free streamline leaves the wall. This is in agreement with Prandtl's suggestion that a large-scale breaking away of the boundary layer (separation) occurs in steady flow when the wall shear stress vanishes. The separation streamline becomes tangent to the body in the limit as $\nu \to 0$. This is not in conflict with the Oswatitsch relationship. The flow that is being modeled here is viscous (meaning finite Reynolds number) and it is perfectly permissible to have a separation at non-zero angle with respect to the wall, regardless of the character of the singularities used to construct the model.

Figure 6(*a*) shows the velocity distribution near the separation point of a cylinder. The vortex was placed at $\epsilon = 0.04$ and was given a small core to eliminate the discountinuity in the velocity profile near the vortex position. Clearly, the no-slip condition is satisfied but there is a back flow slightly above the cylinder surface. It is the occurrence of such a back flow that pushes the separation point further and further upstream at

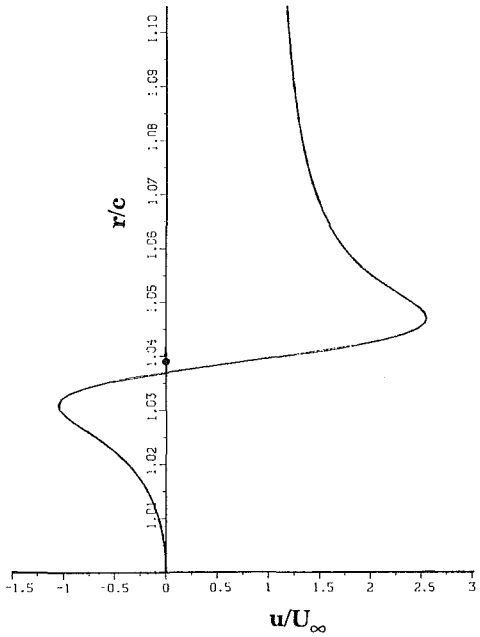


**Fig. 6(*a*) Velocity profile along the radial line passing through the separation point (nascent vortex on the radial line)**

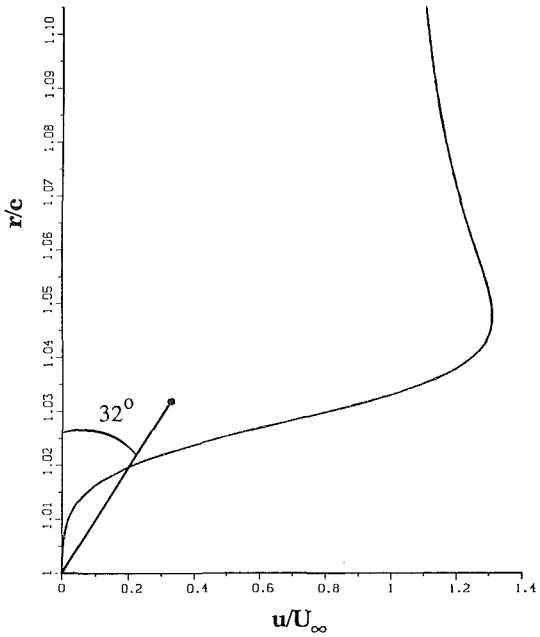


**Fig. 6(*b*) Velocity profile along the radial line passing through the separation point (nascent vortex on the 32°-line)**

each time step. The vortex has to be placed at a point such that both the *no-slip* condition and the *no-back-flow* condition are satisfied. A systematic study shows that the nascent vortex must be placed on a 32-degree line, passing through the separation point (see Fig. 6(*b*)). This result is not dependent on the number of vortices shed in the previous cycles since the velocity distribution in the vicinity of the separation point is dictated by the nascent vortex and by the separation velocity $U_s$, which includes the effect of all the elements characterizing the flow prior to the introduction of the nascent vortex. The calculations may be performed as follows. Assume a vortex position along the radial line; find the vortex strength from the no-slip condition; calculate $\Delta t$ from $\Delta\Gamma/(0.5U_s^2)$; and convect all vortices with the velocity induced on them for a time interval $\Delta t$. The time interval varies from cycle to cycle. If $\Delta t$ is too large or too small (depending on the convection scheme used: simple Eulerian or higher order scheme), one may choose the initial fixed position of the vortex closer to or further away from the surface along the 32-degree line. The second alternative is to use a fixed $\Delta t$ and to find the position of the vortex along the said line by iteration so that the no-slip condition is satisfied. The time step should be chosen carefully enough to make sure that the displacement of the vortices in the regions of largest convection is sufficiently small to minimize curvature effects. The method described above eliminates most of the ambiguities associated with the earlier methods of nascent vortex introduction. Furthermore, it is not restricted to cylinders with mobile separation points. Mostafa (1987) and Munz (1987), working with Sarpkaya, on the simulation of decelerating flow about cambered plates, representative of a two-dimensional non-porous parachute, have described in detail the use of fixed and variable time-step methods (see also Sarpkaya et al., 1987 and Mostafa et al., 1987).

The importance of the correctness of the position and strength of the nascent vortices stems from the fact that the position of the mobile separation points and the calculated forces (particularly the lift force) and pressures strongly depend on the strength and position of both the vortices in the immediate vicinity of the body, and the vortex clusters in the wake. The Strouhal number does not seem to be overly sensitive to the type of nascent vortex introduction.

Another reason for the proper introduction of the vortices is the determination of the "correct" amount of the artificial circulation reduction to be applied in an effort to account for the differences between the numerical simulation and the flow simulated. Practically all applications of vortex models to unsteady separated flows past two-dimensional bluff bodies have shown that the circulation of the vortices should be reduced as a function of time and space in an ad hoc manner in order to bring the calculated forces, pressures, and circulations into closer agreement with those measured (for approximate measurements of apparent circulation, see Schmidt and Tilmann 1972). Such a circulation-reduction mechanism was first proposed and used by Sarpkaya and Shoaff (1979a, 1979b). Subsequently, it has been used by other researchers in a variety of applications. The reduction in circulation is justified as accounting for the three-dimensional deformation of vortex filaments in physical and numerical experiments (for the latter, see Widnall 1985a, 1985b), assuming that the predictions of the numerical model are "correct" for the idealized two-dimensional flow.

The preceding discussion has more or less settled everything required for the construction of a relatively simple model, except the most important question of where separation occurs. The determination of the separation points or lines would in principle require calculation of the boundary layer at each time step. Even in *steady* two-dimensional flow, separation points can only be predicted approximately and with difficulty for laminar flows and hardly at all for turbulent flows. In unsteady flow, the mobile separation points (when they are not fixed by sharp edges), may undergo large excursions. This experimental fact renders the treatment of boundary layers on bluff bodies subjected to periodic wake return extremely difficult, particularly when the state of the boundary layer changes during a given cycle.

A definition of separation that is meaningful for all kinds of *unsteady flows* has not yet been established. As pointed out by Simpson (1981), "it is too narrow a view to use vanishing surface shearing stress or flow reversal as the criterion for separation. Only in steady freestream two-dimensional flow do these conditions usually accompany separation. In unsteady two-dimensional flow, the surface shear stress can change sign with flow reversal, but without breakaway. Conversely, the breakdown of the boundary layer concept can occur before any flow reversal is encountered (Sears and Telionis, 1975, Telionis, 1979)." (see also McCroskey, 1982; Van Dommelen and Shen, 1983; Telionis and Mathioulakis, 1984; Geissler, 1985; Poling and Telionis, 1986). According to the MRS criterion (Moore, 1957, Rott, 1956, and Sears, 1956, 1976), it is the simultaneous vanishing of the shear and the velocity at a point within the boundary layer that determines the separation point. However, even this definition is not without ambiguities. Taneda (1977, 1980) has shown experimentally that (i) the shedding of fluid particles from the wall is the most meaningful definition of separation for most time-dependent flows, (ii) this definition coincides with the Prandtl criterion in the case of steady two-dimensional flow over a fixed wall, and (iii) flow separation can be detected only by observing the integrated streaksheet.

An extension of the Kutta condition to unsteady flow has been suggested by Giesing (1968a, 1968b, 1969) and Maskell (1971), in connection with airfoils with sharp trailing edges: *For a changing bound circulation, the stagnation streamline is parallel to the surface on the side of high total head.* A lucid discussion of this proposal is given by Basu and Hancock (1978) (see also Archibald, 1975; Ho and Chen, 1981; McCroskey, 1982; and Crighton 1985). The Giesing-Maskell condition does not reduce to the classical steady Kutta condition that the stagnation streamline in the aft of the airfoil is attached to the trailing edge. Two of the several consequences of the steady Kutta condition are that the pressure is continuous across the vortex sheet (the sheet is force free) and the velocities at the top and bottom at the trailing edge are equal, i.e., the stagnation streamline bisects the wedge angle of the airfoil. There is sufficient experimental evidence (see Krause et al., 1985 and Poling and Telionis, 1986) to show that the steady Kutta condition is violated in rapidly varying unsteady flows about airfoils. The method of Basu and Hancock (1978) for airfoils with one shedding edge was extended by Stansby (1985) to sharp-edged cylinders with two shedding edges, using an iterative procedure, some ad hoc assumptions and the VIC scheme. His attempts to apply the method to base edges and secondary separation of rectangular bodies were unsuccessful due to the extreme unsteadiness of the flow. The flow about sharp-edged bodies is discussed in greater detail in Section 3.3.2.

It appears that the question of separation will have to be settled empirically or experimentally. The finding of separation points, and the determination or specification of the boundary, should be regarded as separate problems as far as the discrete vortex models are concerned. Nevertheless, they tend to interact and whether one should attempt to solve them as part of the numerical model is another question.

As far as vortex methods are concerned, the importance of the time history of the position of the separation point comes not only from the determination of the point introduction of new vorticity but also from the determination of the strength and the velocity of convection of the nascent vortices. In unsteady flow, the time rate of change of circulation is no longer given by $d\Gamma/dt = 0.5U_s^2$, as in steady flow, where $U_s$ is

the outer flow velocity at separation, but by $(0.5U_s^2 - U_sU_\theta)$ where $U_\theta$ is the speed of the separation point (Sears, 1976).

### 2.9 Operator Splitting and Random Walk Methods

*2.9.1 Description of the Method.* The sequential rather than simultaneous convection and diffusion of vorticity is known as the operator splitting or fractional-step or time-splitting method. It was proposed by Chorin (1973) in connection with his work on the flow of a "slightly" viscous flow over a circular cylinder in two dimensions. In this method, the vorticity equation is divided into a convective and diffusive part and the two equations are solved sequentially. Thus, instead of equation (2), one solves

$$\frac{\partial \omega}{\partial t} + \mathbf{u} \cdot \nabla \omega = 0 \tag{41}$$

and

$$\frac{\partial \omega}{\partial t} = \nu \nabla^2 \omega \tag{42a}$$

or its suitably non-dimensionalized form

$$\frac{\partial \omega}{\partial t} = \frac{1}{\mathrm{Re}} \nabla^2 \omega \tag{42b}$$

Thre Green function Gr of the one-dimensional form of equation (42*a*)

$$\mathrm{Gr}(y,t) = \sqrt{\mathrm{Re}/4\pi t}\, \exp\left(-\frac{\mathrm{Re}}{4t} y^2\right) \tag{43}$$

is identical to the probability density function $P$ of a Gaussian random variable $\eta_y$ with a zero mean and a standard deviation $\sigma$

$$P(\eta_y;t) = \sqrt{1/2\pi\sigma^2}\, \exp\left(-\frac{1}{2\sigma^2} \eta_y^2\right) \tag{44}$$

if $\sigma = \sqrt{2t/\mathrm{Re}}$. In two dimensions, one has: $\mathrm{Gr}(x,y,t) = \mathrm{Gr}(x,t)\mathrm{Gr}(y,t)$ and $P(\eta_x,\eta_y;t) = P(\eta_x;t)P(\eta_y;t)$. Thus, the solution of equation (42*a*) is simulated stochastically by a two-dimensional displacement of the vortex elements in two orthogonal directions using two independent sets of Gaussian random numbers, each having a zero mean and a standard deviation $\sigma = \sqrt{2\Delta t/\mathrm{Re}}$. This is an adaptation to hydrodynamics of Glimm's (1965) random choice method.

Briefly, a typical application of the operator-splitting scheme proceeds as follows. The body surface is discretized into a number of sheet generation panels. The "zero normal velocity" condition is satisfied either exactly through the use of conformal transformation (if one exists) or approximately through the solution of Poisson's equation ($\nabla^2\Psi = -\omega$ with $u = \Psi_y$ and $v = -\Psi_x$). The tangential velocity at the center of each panel is calculated as described in Section 2.7.2 and vortex-sheet segments (Chorin (1978) (or blobs as originally done by Chorin 1973) are generated in such a way that the slip velocity is nullified and no normal flow is introduced. This is the basis of the creation of new vorticity. At time $t = n\Delta t$ the vorticity is approximated by a sum of linear concentrations of vorticity so that

$$\gamma^n(x,y) = \sum_i \gamma_i S_f(x - x_i^n)\, \delta(y_i^n - y) \tag{45a}$$

where $\gamma_i$ is the strength of the $i$th vortex sheet, $(x_i^n, y_i^n)$ is its center, $\delta$ is the Dirac delta function, and $S_f$ is a smoothing function. Originally, Chorin (1978) used a "hat" or "tent" function defined as

$$S_f(x) = \begin{cases} 1 - |x/\lambda| & |x| \le \lambda \\ 0 & \text{otherwise} \end{cases} \tag{45b}$$

where $\lambda$ is half the sheet length. $S_f$ varies from unity at the center of the sheet to zero at each end. If the vorticity field is not accurately discretized (with vortex elements with sufficiently small circulation), parasitic vortex elements may emerge and the induced velocity field may be contaminated with large errors. Finding the "not to exceed" value of $\Gamma_m$ which will make the results independent of $\Gamma_m$ is not a simple matter. In fact, the number of elements used in the simulation appears to have the strongest influence on accuracy (Ghoniem and Cagnon, 1987). Furthermore, extreme caution is needed near the separation points (if known where!) and sharp corners (Baden and Puckett, 1988) since the validity of the vortex-sheet algorithm is dependent on the boundary layer approximation, which ceases to apply where the flow detaches from the wall.

Once the discretization is complete, a random walk with Gaussian probability distribution and zero mean and standard deviation $\sqrt{2\nu\Delta t}$ or $\sigma = \sqrt{2\Delta t/\mathrm{Re}}$ is given to each computational element (the vortex sheets diffuse perpendicular to the wall only and the sheets that penetrate the body are reflected back into the flow). The sheets are transformed into blobs and vice versa at the edge of a constant thickness *sheet layer* (a numerical artifice, not a boundary layer). Each computational element is convected using a simple or modified Eulerian scheme, the latter often with negligible gain in accuracy, except possibly in the regions where the convection velocities and the time-integration diffusion are large. For example, Ng and Ghoniem (1986) had to use a higher-order scheme (Heun's method) to minimize the smearing of the structures in a shear layer and to numerically realize the experimentally-observed vortex-pairing (Eulerian convection did inhibit pairing). The velocities of blobs are determined either through the use of the Biot-Savart law (or its modified forms, as described in Section 2.5.2) or through the use of the VIC scheme or a variationally-optimized grid-insensitive vortex-tracing scheme (Buneman, 1974; van der Vegt and Huijsmans, 1984). The velocity field for the sheets is calculated by adding the velocity on the body surface (just below the particular sheet) due to all other elements, except the sheets, to that induced by the sheets within the sheet layer. Normally, a second random walk is given to each element and the above process is repeated. The plots of velocity, pressure, force, etc. are averaged or smoothened over several time-steps to remove the random component associated with the method.

The steps outlined above are certainly not unique and many different versions exist. Some authors have dispensed with the sheet-blob metamorphosis and discretized the vortex sheet into a set of new discrete vortices (e.g., P. A. Smith 1986) and applied a random walk for a time interval of $\Delta t$ or $\Delta t/2$. Van der Vegt and Huijsmans (1984) removed the vortices which diffuse into the body in the time step immediately after their creation. The vortices from the previous time steps which diffuse into the body are replaced at the surface. Paul A. Smith (1986) simply reflected the discrete vortices lying inside the body. Tiemroth (1986) and Teng (1982) used highly complex sheet-blob-metamorphosis schemes through the use of various ad hoc assumptions. Van Dommelen (1987) simply placed the blobs on a circle of $r = (c + 0.675\sqrt{2\nu\Delta t}$ and annihilated those which remained in the region $c < r < (c + 1.27\sqrt{2\nu\Delta t})$ following the convection and diffusion steps. Baden and Puckett (1988) discarded the blobs that end up outside the image of the sheet layer. Also, all their sheets had the same magnitude of $\gamma_{\max}$ (maximum sheet strength). No sheets were created when $|u_i| < \gamma_{\max}$. Hence, the no-slip boundary condition is satisfied at a point only up to order $\gamma_{\max}$. Others (e.g., Chorin 1978) created sheets at the $i$th gridpoint whenever $|u_i| > \gamma_{\min}$ for some $\gamma_{\min} < \gamma_{\max}$ such that the sum of the strengths of these sheets exactly cancels $u_i$. According to Puckett (1987), the two foregoing sheet-creation algorithms show no increase in accuracy when the latter, more costly sheet-creation algorithm is used.

Various accuracy and stability constraints have been proposed or imposed on some of the parameters entering into the computation (time step $\Delta t$, sheet length $2\lambda$, minimum and maximum sheet strengths $\gamma_{min}$ and $\gamma_{max}$, shapes of the smoothing and core functions, cutoff distance, etc.). Usually $\Delta t$ times the maximum $U_\infty$ is made smaller than the sheet length (the so-called "CFL" accuracy condition) in order to ensure that sheets move downstream at a rate of no more than on grid point per time step. There are a number of additional accuracy and stability conditions (see e.g., Puckett, 1987) whose "constants" cannot be predicted from a theory but have to be chosen to fit in with experiments.

Hybrid versions of the time-splitting method have been developed through the use of the VIC scheme (Stansby and Dixon, 1983; Van der Vegt and Huijsmans, 1984; Van der Vegt and de Boom, 1985; Vada and Skomedal, 1986; Skomedal and Vada, 1987, Van der Vegt, 1988). The diffusion introduced by the convection scheme and augmented by the random walk is further enhanced by the vortex-in-cell algorithm.

Other users of the random-walk method have introduced a set of new discrete vortices at each time step at a distance $\epsilon = ds/\pi$, with strengths $\Delta\Gamma = v_s ds$. This method approximately nullifies the slip velocity $v_s$ at each $\Delta t$, provided that $ds$ is chosen sufficiently small (e.g., $ds = \pi\sigma$, $\sigma =$ the core radius). The vortices are then convected or both convected and diffused sequentially. The vortices which penetrate the body have either been reflected or ignored. Yet others have introduced vortices in the manner described above only over a segment of the body (downstream face of the body between the separation points). Clearly, the combinations of schemes are limited only by one's imagination and ultimate goal: acquisition of predictive power, an approximate solution, or a new insight.

Most or all of the foregoing schemes share the following facts. The number of vortices increases rapidly, the computation of the convection velocity becomes prohibitively expensive, the evolution of large local strains increases the blob spacing relative to the core radius (local blob population depletion) and can lead to large errors in the resolution of the vorticity and the velocity field, and the calculations may be carried out only for relatively small fluid displacements. The use of Maskew's (1973, 1977) "subvortex" (sub-blob, subvorton, or reblobbing) technique or its variations to repopulate the depleted areas causes a further blob-population explosion. The implementation of the sub-blob scheme, requiring another step in the calculations, and the increase of the number of blobs, further increase the CPU time. Note that the velocity fields before and after reblobbing are not the same in the vicinity of the new blobs. In this process, the use of higher order core representations (e.g., a fourth order Gaussian core) to achieve better accuracy becomes debatable. The calculation of forces and pressures requires either special averaging techniques or special schemes (e.g., that of Quartapelle and Napolitano, 1983) or the use of the simple rate of change of impulse expression (see equation (47*b*)). The number of physical parameters, ad hoc schemes, programming tricks, and convection "fixes" becomes very large, making a parametric analysis of their separate as well combined nonlinear effects on the predicted results practically impossible, notwithstanding the arguments regarding the "robustness" of the algorithms devised. Even the methods using most elaborate schemes and as many as 100,000 blobs require the use of an artificial circulation reduction (circulation decay) in order to bring the numerical results into closer agreement with those measured (similarity of flow kinematics gives only a zeroth order satisfaction). Evidently, vortex models became more, not less, cumbersome with the passage of time and the increase of computer power. The disciples of vortex methods have not yet arrived at simplicity and reliability in spite of their best efforts.

*2.9.2 On the Convergence of the Operator Splitting Methods.* Chorin (1973) was the first to point out that "the crucial problem is to assess the effect of the interaction between the random and deterministic parts of the convection"; "We do not expect valid solutions at low Re," and "At the other extreme, some difficulty may be expected at very high Reynolds numbers. This is so because the boundary layers formed by the algorithm are made up of a few bouncing vortices and are thus noisy; turbulence effects should therefore appear at too small a value of Re, as they do, for example, in noisy wind tunnels around rough bodies." All applications of the operator-splitting method(s) have confronted these valid concerns and attempted to overcome them through numerous schemes regarding the blob core size (cutoff), vorticity distribution (cutoff function), number of overlapping blobs, number of random walks per integration step, initial distribution of the blobs, blob depletion in large strain fields, and turbulent diffusion.

Convergence proofs for the method are given by Hald and Del Prete (1978), Hald (1979, 1985) and Beale and Majda (1982a,b). Roberts (1985) tested the accuracy of the method in highly idealized conditions (blobs of equal strength and uniform distribution in an unbounded fluid) and concluded that the accuracy of the method depends heavily on the initial distribution and strength of the blobs. Marchioro and Pulvirenti (1982) showed that the method approximates the Navier-Stokes equations in a weak sense, as the initial grid size and cutoff approach zero in an appropriate way. Goodman (1987) showed that the method will, with high probability, produce good approximations to the true velocities. Beale and Majda (1981, 1985), Anderson and Greengard (1985) and Anderson (1986) also discussed errors introduced in time-splitting, in the approximate solution in Euler equations, in the smoothing and in sampling. Anderson and Greengard (1985) described two schemes for use in three-dimensional vortex modelling; (i) *connected-filaments* scheme where the vortex stretching is determined from the change in filament length, and (ii) *disconnected-discrete-vortices* scheme where the change of magnitude of vorticity requires the determination of the local strain. Greengard (1986) gave a convergence proof of the connected-filament scheme and Beale (1986), of the disconnected-vortices scheme.

All of the foregoing proofs dealt with *laminar flows in the absence of boundaries*. As noted by Ashurst and Meiburg (1988), "The style of these proofs is to bound the errors in the discrete velocity versus the exact velocity from a known vorticity distribution." "A sufficiently smooth initial distribution is assumed, the smoothness determines the time interval in which the error estimates are valid." "Stability is shown in the sense that sufficiently small errors in the computed motion yield bounded errors in velocity." As far as the bluff-body flows are concerned, there does not seem to be any proof that the random walk method will correctly simulate the behavior of flow either in the vicinity of the separation points or in the regions depopulated by large strains, or in the regions where the flow is turbulent (e.g., the wake of a cylinder at Reynolds numbers larger than about 400). None of the proofs dealt with the question of what does random walk mean or represent in a turbulent wake even though all proofs allude to high-Reynolds-number flows. In subcritical bluff-body flows, the motion is laminar in only a small region, i.e., molecular diffusion is confined to the laminar boundary layers near the wall from which the whole of the vorticity originally diffuses. The region of vorticity generation is the region where the laminar diffusion is the predominant process. In regions (the wake of body) of varying intensities and scales of turbulence, viscous diffusion is unimportant. Consequently, the use of random walk throughout the flow does not make sense.

Most of the convergence proofs are related to specific flow examples where the simulations of known solutions and

phenomena, e.g., Kelvin-Helmhotz instability of a shear layer, wall-driven flow in a rectangular enclosure (Choi et al., 1988), flow over a backward-facing step (Ghoniem and Sethian, 1987; Ghoniem and Cagnon 1987; Sethian and Ghoniem, 1988) for which there is a wealth of experimental data, are used to refine the numerical parameters (a minimum of six disposable parameters) and to calibrate the numerical scheme. Often, calculations are performed at relatively low Reynolds numbers in the laminar regime. Even though only the *viscous diffusion* via random walk is simulated, it is often claimed (or implied) that the method is applicable to high Reynolds number turbulent flows. The word "turbulent" is taken to mean "the instability of small-scale flow and the resulting coagulation of vorticity into large fluid structures that comes with increasing Reynolds number" (Sethian and Ghoniem, 1988). According to Simpson (1987), "Most methods do not incorporate the correct physics for the backflow region: namely, that turbulence diffusion and dissipation control the backflow behavior and that the backflow mean velocity profile is determined by the large-scale fluctuations which scale on the maximum shear stress." [See Amano and Goel (1985, 1987) for computations of turbulent flow beyond backward-facing steps using Reynolds-Stress closure models].

This is not the proper forum to offer a critical assessment of the numerous "convergence proofs." Instead, we will offer two quotations which, in our opinion, fairly accurately summarize the state of the random walk method. Perlman (1985) noted that "The accuracy of the vortex method depends on the choice of the cutoff function and of the cutoff length $\sigma$ and on the initialization of the vorticity distribution. The best value of $\sigma$ is larger than $h$, the initial distance between the vortices; it is time-dependent in the sense that longer time integration requires a larger $\sigma$" (i.e., stronger diffusion, in a manner similiar to that naturally provided by the Lamb-vortex model). "In addition, the optimal choice of $\sigma$ is insensitive to the smoothness of the flow. If $\sigma$ is close to $h$, then the accuracy is lost in a relatively short time. This loss of accuracy is caused by the growth of the discretization error." Perlman (1985) investigated the practical effect of these choices on the vortex method for inviscid flows in the absence of boundaries. As noted earlier, $\sigma$ does not remain larger than $h$ everywhere at all times even if it were so at the start of the calculation. Large strains and blob depopulation are an integral part of the vortex dynamics. Hald (1986) noted that ". . . if the time step is small and if we use a large number of particles, then the error in the computed solution is small—with high probability. This does not mean that the error is small in any particular "numerical" experiment—only that it is unlikely to be large." He also emphasized that "On the other hand, by repeating the experiments an increasing number of times, we can construct a probability space such that the method diverges almost surely (if anything can go wrong, it will eventually)." "The proper concept for numerical work is therefore convergence in probability and not convergence almost everywhere." Earlier, Milinazzo and Saffman (1977) critically examined the consequences of replacing a continuous distribution of vorticity by a finite number of discrete vortices of compact support and, using a random walk component to simulate the effects of viscous diffusion, arrived at essentially the same conclusions. They have also shown that the VIC scheme produced comparable error at a much reduced CPU time. Roberts' (1985) revisit of the "circular vortex" problem of Milinazzo and Saffman (1977) and Chang's 1988) use of a uniform grid (with only 856 vortices), and a variance reduction technique to reduce the sampling errors, did not refute or allay the criticisms regarding the accuracy of the random vortex schemes.

Notwithstanding the foregoing idealized proofs and arguments, Ng and Choniem (1986) were "surprised to discover," in connection with their work on a confined spatially-developing shear layer, "the fact that nonoverlapping cores produce accurate results" "since most theoretical studies (e.g., Beale and Majda, 1982) indicate that $\delta$ (core radius) should be larger than $h$ (the initial distance between the vortices)." Ng and Ghoniem's explanation of this finding that "the vorticity field in this simulation changes in time and may not conform identically with the assumptions of the theory" is contrary to Ghoniem and Sherman's (1985) earlier work where "vorticity is continuously generated inside the field by the action of the baroclinic torque, and at the wall by the satisfaction of the no-slip condition" and contrary to the proof by Hald (1986), establishing the convergence of random methods with creation of vorticity and showing that the error is independent of viscosity!

A few additional facts must be noted. The overlapping blobs must be regarded as mathematical artifices (many souls in one body!) since vorticity carrying non-deforming fluid particles cannot occupy the same space at the same time (the exclusion principle). If the blobs are well separated, the technique is not really necessary since it does not make any difference whether they are blobs or line vortices (of infinite vorticity). The simulation of viscous diffusion by random walk is based on numerical convenience and it has nothing whatever to do with the physical process being simulated. As noted by Peters and Thies (1982), "In using the random vortex method *to simulate large coherent structures* there has been uncertainty about how to interpret the nature of the diffusion process. If the diffusion of vorticity corresponds to the molecular transport process, as Chorin (1973) suggests, then a nonstationary two-dimensional laminar flow field is calculated. The number of vortices would then need to be very large—representing individual molecules of the system. In fact, it has been shown that a very large number of particles is needed to solve even the one-dimensional heat conduction problem (Peters 1975). If, on the other hand, the diffusion process is to be considered turbulent, then the choice of the turbulent diffusion coefficient and the turbulent length scale distribution are unknown input parameters." This brings one back to square one: turbulence modelling. It is also clear that the random-walk method does not and cannot prescribe a specific Reynolds number. In fact, the Reynolds number mimicked in all vortex models is that of the experiments to which the numerical predictions are retrofitted or with which the numerical schemes are calibrated. Finally, quantities such as forces and pressures, important for comparison with experiments, can only be obtained by averaging or smoothing over several time steps. Instantaneous values may and often do exhibit unrealistically large variations.

As noted above, in order for the random walk method to work for the cases to which it may logically be applied, one should have many blobs close to each other with overlapping cores. It is this requirement that minimizes the effect of nonlinearity of the convective acceleration terms (neither a single blob nor a linear sum of blobs with compact support is an exact solution of the Navier-Stokes equations). It is the same requirement that makes the use of the Biot-Savart law prohibitively expensive. The schemes devised to overcome this difficulty have been described in Sections 2.5.2 (DVIC and DIC schemes) and 2.6 (CIC or VIC technique). Note that the VIC method does not really require a blob and as noted by Chorin (1973) "the alternative methods of solution employ a grid, which would destroy the principle of our method." Nevertheless, the random walk and the VIC technique have been combined in recent years (e.g., Stansby and Dixon 1983) to reduce the CPU time. In some applications (e.g., Sethian and Ghoniem 1988; Tiemroth 1986) higher order time integration schemes, in lieu of Euler's scheme, have been used, hoping that a better solution will result. Puckett (1987) pointed out that "one may be doing twice as much work for a negligible gain in accuracy." Since each random step puts into further disorder the existing state of the vortex jungle, it does not

seem to be reasonable to attempt to refine the accuracy of the deterministic step even in the regions of high convective velocity (but see Ng and Ghoniem, 1986).

**2.10 Asymmetry Introduction.** In classical vortex methods, the asymmetry of flow about symmetric bluff bodies is induced by means of an artificial perturbation (see, e.g., Sarpkaya and Shoaff, 1979a). This is often criticized as a shortcoming of these methods, particularly by those using random-walk methods (e.g., Spalart, 1982; Spalart and Leonard, 1981; Spalart et al., 1983; Tiemroth 1986). It is not generally appreciated that in physical experiments the symmetry is destroyed by the presence of multiple perturbation sources and that the numerical experiments with or without random walks cannot model the perturbations of nature yielding the final asymmetry. The initial conditions are never given and are never the same. As noted by Braza et al. (1986), "It is beyond the experimental ability of the researcher to control or even recognize all possible contingencies that may arise in an experiment designed to study the evolution of the asymmetry. When the flow is in a critical state to become asymmetrical, a very small cause can have a very great effect." The random walk cannot simulate a given state of disturbances in a given experimental situation. In fact, in all classical vortex models, random walk could have been used (for a short time) as one of the "artificial perturbation schemes," to induce asymmetry, in lieu of others too numerous to describe here. This does not settle the question of when will the first Karman vortex shed from a circular cylinder. The fact that the "artificial disturbances" of short duration vice permanent random perturbations lead to the same flow pattern indicates that "the periodic character of the flow appearing beyond a critical value of the Reynolds number is an intrinsic property of the Navier-Stokes equations and does not depend on the nature of the perturbations" (Braza et al. 1986). Moreover, the perturbations seem only to be responsible for the change of the regime from steady to periodic flow, but they are not necessary as a source of energy to sustain the periodic flow. In short, in praise of automatic asymmetry, the random walk is no virtue. The perturbation that provides the shortest establishment phase should be chosen to save computer time.

It is clear from the foregoing that even though some subjective decisions and ad-hoc assumptions are required in the selection of the proper values and procedures (the method of approximation is what distinguishes the various approaches), it is important that the numerical procedure used to implement the method is stable, and that the results do not critically depend on the magnitude of the disposable parameters introduced. The ultimate objective of the simulation via vortex dynamics is the acquisition of new insights rather than accurate predictions. The flow simulated by the numerical model may not be physically realizable even under controlled laboratory conditions.

## 3 Evolution and Applications of Vortex Methods

**3.1 Contra Flowing Streams.** The interface between two parallel incompressible streams in shear, i.e., the vortex sheet across which the tangential component of velocity is discontinuous, has been studied analytically, experimentally, and numerically (see, e.g., Ho and Huerre, 1984). The results have shown that it is linearly unstable and does degenerate into a series of vorticity concentrations (Kelvin-Helmholtz instability) when exposed to a small disturbance. As noted by Rizzi and Engquist (1987), the crests and the troughs of the disturbance waves constrict the streamlines ahead of them and diverge those behind them. This makes the pressure inside a crest or trough larger than that outside. The resulting pressure gradients (which are in opposite directions), and moment, amplify and twist the initial disturbance waves (see Fig. 7).

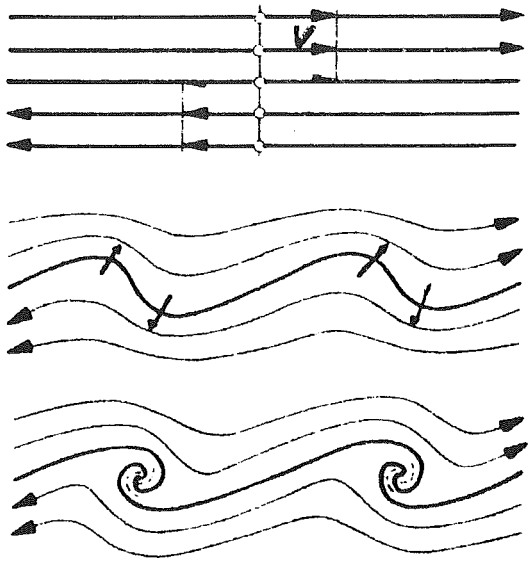

**Fig. 7 Onset of the Kelvin-Helmholtz instability for two parallel incompressible streams in shear (Rizzi and Engquist, 1987)**

Rosenhead (1931), in his pioneering work, introduced a discrete vortex approximation to investigate the evolution of a sinusoidally perturbed two-dimensional vortex sheet, separating two streams of equal density and opposite but equal velocity $U$. He replaced the continuous sheet of vorticity by twelve line vortices of strength $(U\lambda/6)$, distributed uniformly along one wavelength of the sinusoidal perturbation at intervals of $x=\lambda/12$. The initial distribution of vorticity along the sinusoidally-perturbed sheet was not uniform. His hand calculations (over four time steps) clearly demonstrated the roll-up process, at least in the initial stages of motion. The unavailability of a computer was partly responsible for the encouraging results.

Birkhoff and Fisher (1959) repeated Rosenhead's calculations with a computer using twenty-two vortices per wavelength and smaller time steps in their Runge-Kutta integration routine. They have demonstrated that the energy invariance of a set of line vortices prevents any two vortices from getting arbitrarily close to each other. They have concluded that the self-induced motion of an array of line vortices will ultimately produce randomness of position (i.e., no true roll-up is possible) and that viscosity is essential to the smooth roll-up of real vortex sheets. This criticism of the vortex model underscored the problems to be resolved and gave rise to the smoothing schemes discussed earlier.

Hama and Burke (1960) also repeated Rosenhead's calculations using twelve vortices over a wavelength and sixteen time steps instead of the four used by Rosenhead. They arrived at essentially the same conclusions as Birkhoff and Fisher's that the vortex sheet concentrates into clusters of vorticity in a most contorted fashion. Then they spaced the vortices unevenly along the disturbed sheet, so as to represent the sheet with vortices of equal strength, and obtained smooth roll-up.

Abernathy and Kronauer (1962) investigated the stability of two shear layers (of constant initial strength), between a central stream of thickness $h$ and velocity $+U$ and two outer streams of infinite extent and velocity $-U$. After showing that the said shear layers have two growing and two decaying modes, they replaced each layer by discrete vortices and examined their evolution in time for a range of values of $\lambda/h$ between 0.12 and 0.34 where $\lambda$ is the wavelength of the initial disturbance (consisting of two asymmetric modes). They showed that (i) the vortices form asymmetric clouds, resembling a vortex street, (ii) the Karman spacing $\lambda/h=0.28$ is the smallest ratio for which only two clouds form per wavelength,

and (iii) the cloud spacing broadens as in the case of real vortex wakes behind bluff-bodies. For $Ut/\lambda$ larger than about 0.7, the motion of vortices became random and "there was no longer sufficient evidence to suggest the existence of vortex sheets." Nevertheless, they were able to demonstrate that the net vorticity in each cloud is "diminished by the vorticity swept into the cloud by the opposite vortex row." This work, while adding further credibility to the use of the discrete vortices and elucidating the roll-up mechanism of the shear layers, did not deal with a body and the generation of vorticity. Thus, the investigation was unable to deal with the consequences of nonuniform distribution of vorticity along a growing shear layer.

Michalke (1963–1965) investigated the instability of a thick shear layer, represented by a linear velocity distribution (i.e., constant vorticity). Using three and four parallel rows of line vortices and different wavenumbers, he was able to show that the entire shear layer as well as the individual rows roll up into concentrated vortices (tightest for the most unstable perturbation).

Beavers and Wilson (1970), in an effort to understand the vortex growth in a two-dimensional jet, studied the rate at which local disturbances (as opposed to periodic ones in earlier studies) would propagate upstream on two initially parallel, oppositely signed, *finite* length shear layers (finite, because of computational constraints). They have, in fact, shown that both symmetric and non-symmetric small disturbances move upstream relative to the shear layers.

Zaroodny and Greenberg (1973) analyzed the non-breaking, but arbitrarily large amplitude, shallow water waves by representing the water surface and the sea bed by continuous vortex sheets. Zalosh (1976) used the discrete vortex method to study the behavior of an interfacial vortex sheet (e.g., oil/water interface) in the presence of gravity and surface tension effects. He calculated the early time-disturbance growth rates and the overall form of the interface for disturbance amplitudes outside the realm of linear Kelvin-Helmholtz stability theory. At late times, the chaotic motion of the individual vortices caused the calculations to break down in the sense that the line vortices no longer simulated a continuous vortex sheet. Baker et al. (1982) investigated the motion of free surfaces in incompressible, irrotational, inviscid layered flows through the use of the evolution equations for the position of the free surfaces and appropriate dipole (vortex) and source strengths. The resulting Fredholm integral equations of the second kind were solved by iteration in both two and three dimensions. The nonlinear interaction between a rising vortex pair and a free surface has been investigated by Sarpkaya (1986c), Sarpkaya et al. (1988), Tryggvason (1988b), and Marcus and Berger (1989).

The growing awareness of the significance of large scale coherent structures in turbulent flows (Brown and Roshko, 1974; Winant and Browand, 1974; Roshko, 1976; Hussain, 1986) has led to the suggestion that these structures might play a role in the mechanisms responsible for the hydrodynamic sound generated in shear flows. However, this is a subject of much controversy (Crow and Champagne, 1971; Moore, 1977; Lau and Fisher, 1975; Crighton, 1975; Hussain, 1986). According to Hussain (1986), most of the noise is produced by the breakdown of the initial toroidal structures into substructures, via the cut-and-connect mechanism, and their subsequent interactions.

Acton (1976) modeled a thick shear layer with several parallel rows of discrete vortices, as was done earlier by Michalke (1963), but with rigidly-rotating cores such that a single coherent structure consisted of a set of many discrete vortices. Initially, vortices in each of the waves roll up into rotating concentrations which subsequently revolve about each other until they coalesce. The behavior reported by Acton is in good qualitative agreement with the pairing description of Winant and Browand (1974). Grabowski and Telste (1977) represented the shear layer occurring at the interface of two streams of different velocity by a large number of discrete vortices and obtained results which are in excellent agreement with the calculations of Acton (1976) and, as far as the large scale evolution of the shear layer is concerned, in qualitative agreement with the experimental observations of Winant and Browand (1974) (see also Damms and Kuchemann 1974). They have also concluded that the small-scale motion (regarded to be insignificant in the discrete vortex models) has overwhelming effects on the acoustic predictions and that the role of large scale behavior in the generation of hydrodynamic noise cannot be elucidated. The last conclusion called for a careful scrutiny of the similar hydrodynamic noise predictions by Davies et al. (1975), Hardin (1973), and by Hardin and Mason (1977). Aref and Siggia (1980) calculated the roll-up of the two-dimensional shear layer through the use of the VIC method to obtain rms velocities and Reynolds shear stresses, which are much larger than the experimental results. Meng and Thomson (1978) conducted numerical studies on Rayleigh-Taylor instability, the Saffman-Taylor instability, trailing vortices in a wind shear, and the gravity currents through the use of discrete vortices and compared the results obtained with the Biot-Savart law and Rosenhead's (1930) smoothing scheme [see equations (24) and (25)] with those obtained with the VIC method.

In the foregoing, the mixing layer was replaced by a time-developing shear layer. Another approach is to simulate directly the spatial growth in a real shear layer (e.g., the turbulent mixing layer produced by a splitter plate). Observations of such a mixing layer by Brown and Roshko (1974) and by Winant and Browand (1974) clearly showed that the mixing layer consists of a row of quasi two-dimensional coherent structures. The behavior of perturbed free shear layers from the coherent-structures point of view is reviewed in detail by Ho and Huerre (1984). The two- and three-dimensional instability of a temporally growing mixing layer has recently been studied by direct numerical integration of the Navier-Stokes equations by Metcalfe et al. (1987) (see Claus 1986 for a pseudospectral approach and Canuto et al. 1987 for a full treatment of the spectral methods in fluid dynamics). The imperfect nature of the analogy between the temporal growth of periodic disturbances (often a single monochromatic disturbance) and the spatial growth in a real shear layer has been discussed by many workers (see, e.g., Aref and Siggia, 1980; Aref 1983; Corcos and Sherman 1984). As noted by Pozrikidis and Higdon (1985), the restriction of the disturbances to a single wavelength explicitly eliminates one of the most important growth mechanisms, i.e., the possibility of vortex pairing.

Ashurst (1979) used blobs and the random walk technique to simulate the mixing layer. His calculations with blobs of constant core radius were not satisfactory. However, his use of an exponentially spreading (aging) blob (Lamb vortex) showed "dramatically different" results and produced good agreement between the measured and calculated Reynolds stresses and RMS velocity fluctuations. Ashurst concluded that *pairing* is the primary growth mechanism (see Fig. 8). As noted by Saffman and Baker (1979), the effect of diffusion is invoked twice and as argued by Greengard (1985), the core spreading approximates the wrong equation. It appears that Ashurst's model called for an artificial reduction of circulation. It would have been interesting to see what would have happened without the random walk. Inoue (1985a) has done just that by using the Biot-Savart law and Rosenhead's desingularization scheme [equation (24)], without citing the latter and calling it the vortex blob method (to which it is akin, but not identical). Even though he claimed "reasonably good agreement with experiments, at least for a small time step," his calculated values are about twice those measured (same as Ashurst's fixed core results). Inoue attributed the differences

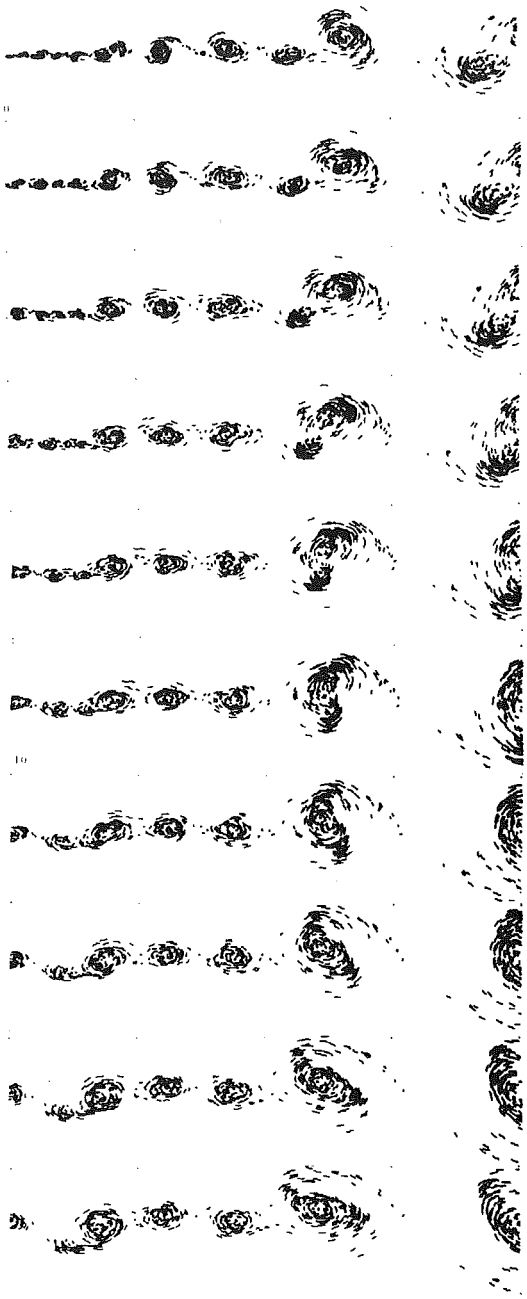

**Fig. 8 Simulation of the mixing layer: streakline plots of each discrete vortex for a unit time ($L/\Delta U$) with respect to the average velocity ($L\Delta U/\nu = 1000$) (Ashurst 1979)**

to the "non-negligible three-dimensionality" of the flow and to the effect of time step. Furthermore, he concluded that *entrainment* is the main mechanism for the growth of the shear layer. Subsequently, Inoue and Leonard (1987) presented an improved version of Inoue's earlier work on forced/unforced mixing layers. Additional numerical simulations of the shear layer are reported by Leonard (1980a), McInville et al. (1965), Mansour (1985), Ng and Ghoniem (1986) and Ghoniem and Ng (1987). Leonard used blobs without random walk; McInville et al. used a compact finite-difference algorithm; and Mansour used the VIC scheme. Ghoniem and Ng used both blobs and random walk and concluded, among other things, that pairing occurs without entrainment and the individual vortices grow by entrainment, i.e., the shear layer grows by both mechanisms (agreeing with both Ashurst 1979 and Inoue, 1985a). The ability of the random walk methods to reproduce the intermittent structure of the flow is primarily due to the fact that *the turbulent viscosity in such flows is more likely to be constant* (Peters and Thies 1982). According to Townsend (1956) the "effective" Reynolds number in free turbulent flows is rather invariant and not very high. In other words, the flow simulated corresponds to a laminar flow when $\mathrm{Re} \to \infty$ or to a turbulent flow with a constant eddy viscosity (a large laminar viscosity coefficient). As noted earlier, the Reynolds number mimicked in all vortex models is that of the experiments to which the numerical predictions are retrofitted or with which the numerical scheme is calibrated. Attempts made to simulate turbulent boundary layers over bluff bodies through the use of a turbulence model (e.g., the zero-equation model of Baldwin and Lomax 1978) will be taken up later. Suffice it to note that the viscous diffusion through a noisy numerical scheme does not represent turbulence but, as noted by Chorin (1973), the rough representation of the boundary layer (say over a circular cylinder) could trigger a premature onset of the drag crisis analogous to the effect of a rough boundary or a noisy flow. In any case, one has to remember that turbulence is a three-dimensional phenomenon. As noted by Cantwell (1981), "Generally, the simulations reproduce the large-scale motions in these flows (vortex-sheet roll-up, mixing layers, wakes, turbulent spots) remarkably well. However, they tend to do less well at simulating the associated stresses. At least part of the reason for this appears to be due to the neglect of small-scale three-dimensional motions, which contribute significantly to the stress." Apparently, the modelling of vortical flows by essentially inviscid approaches can provide us with insight into the physics of gross flow structures for only relatively simple cases and for the duration of the calculations.

A finite difference calculation of the asymmetric mixing through the use of a flux-corrected transport scheme is given by Grinstein et al. (1986). Three-dimensional flows are discussed in Section 3.4.

**3.2 Vortical Flows in Aerodynamics.** Vortex sheets, vortices and vortex interactions are the predominant aerodynamic features of steady or unsteady, compressible or incompressible, separated or unseparated flow about wings, bodies, or their complex and often unconventional configurations. The vortex sheet created by and left in the wake of a lifting surface of finite span at cruise conditions gives rise to familiar trailing vortices. Highly swept wings with sharp leading edges, slender bodies, and more complex aircraft configurations at relatively high angles of attack lead to extensive regions of vortical flow both over and in the wake of the body (known as the high-$\alpha$ problem). The flow may be symmetrical or asymmetrical and may be accompanied by large scale instabilities (vortex merging, vortex breakdown, multi-cell vortices). The impingement of vortices on control surfaces may give rise to severe control problems.

In the course of time, numerous methods of numerical simulation of the vortical flows have emerged. These have been extensively reviewed during the past ten years by Kandil (1979), Polhamus (1979), J. H. B. Smith (1980, 1986), Hoeijmakers (1983, 1985), and Newsome and Kandil (1987) [see also Hussaini and Salas (1985) and the AGARD publications: CP-247 1979; AG-252 1980; LS-121 1982; and CP-342 1983]. The increasing power of the computer has simplified and improved the adaptation and the nature of the models. The sharp-edged delta wings and slender bodies have attracted most attention, both theoretically and experimentally, primarily because of their relative generality and obvious practical importance. A relatively small but important class of these flows concerns the *wake roll-up structure and the rolled-up vortices.* It is for historical reasons that this problem will be discussed here first. Subsequently, a relatively brief summary of the basic methods will be described.

*3.2.1 Vortex Sheet Roll-up and Trailing Vortices.* Trailing vortices are made of rolled-up vortex sheets. The ultimate objective of the numerical methods discussed in this section is to predict the structure of the vortical flow from its inception to its final demise. This is still an unsolved problem for it involves not only the rolling-up of the vortex sheets but also two large scale instabilities (sinusoidal instability and vortex bursting) in an environment whose characteristics are difficult to quantify. An excellent review of past work on vortex core structure is given by Widnall (1975).

Prandtl (1919) and Betz (1932) predicted that vortex sheets behind wings will roll-up towards their tips. Kaden (1931), neglecting the mutual interaction between the two tip vortices, considered a *semi-infinite sheet* of vorticity produced by the parabolic lift variation that approximates the elliptic variation at the edge. He has presented the leading term of an asymptotic expansion describing the roll-up as a tightly wound spiral of infinite length. This spiral is always wound up even at $t=0^+$. Further terms have been calculated by Moore (1975) and Guiraud and Zeytounian (1977, 1979). The asymptotic expansion contains unknown parameters which are determined by the flow outside the spiral. In particular, the location of the spiral is unknown (an advance knowledge of the topology of the vortex structure turns out to be an important requirement in many cases involving massive separation). Thus, a numerical procedure, coupled with some iteration and intuitive "feel," is required to fully determine the motion.

Betz (1932) developed a theory of vortex-sheet roll-up by assuming that the flow in the cores is circular, with circulation increasing radially outward from the core centroid. Following the introduction of an ad hoc assumption regarding the moment of impulse of the vortex sheet, he obtained the core circulation distribution for any given span loading. The Betz velocity distribution rises to infinity as $r/b_o \to 0$, but Moore and Saffman (1973) have shown that viscosity removes the singularity. They have also pointed out that the Betz model does not conserve kinetic energy.

Spreiter and Sacks (1951) pioneered one approach to the problem by postulating a core vorticity distribution (Rankine vortex) with a radial scale as a free parameter, then solving for the core radius by equating induced drag to kinetic energy per unit length of track after roll-up. This resulted in a core radius of $r_c = 0.0982\ b_o$ with $b_o$ as the initial separation between the two columnar trailing vortices. Unlike that of Betz, the Spreiter and Sacks model conserves kinetic energy.

Donaldson et al. (1974) has emphasized that the Rankine and Lamb models are drastically in disagreement with the vortex core velocities measured behind large aircraft. The reason for this is partly due to the fact that the predicted core radius is extremely sensitive to the assumption that all the vorticity is concentrated in the cores (see also Staufenbiel 1984, Higuchi et al. 1987, Arakeri et al. 1988).

The models of Betz (1932), Kaden (1931), Spreiter and Sacks (1951), and the subsequent contributions of Jordan (1973), Bilanin and Donaldson (1975), and Rossow (1977), which extended the Betz model to determine the maximum tangential velocity, do not predict the details of the roll-up such as the shape of the sheet, or the circulation contained in the tip roll-up region. Furthermore, and even more significantly, the modification of the potential flow by viscosity or turbulent mixing and axial velocity is not taken into consideration. This modification was first discussed by Squire (1954) with the assumptions of an initially concentrated line vortex and a constant eddy viscosity (see also Hoffman and Joubert 1963; and Phillips, 1981 regarding the effect of turbulence). Batchelor (1964) elucidated the role of axial velocity in a laminar, initially concentrated line vortex. The effect of wing span loading, wing tip shape, angle of attack, axial velocities and their direction, ambient turbulence, among other variables, are now known to affect the evolution and longevity of rolled-up vortex sheets behind a lifting surface (see, e.g., Donaldson and Sullivan, 1971; Govindaraju and Saffman, 1971; Brown, 1973; Corsiglia et al. 1973; 1976; Donaldson and Blanin, 1975; Iversen, 1975; El-Ramly and Rainbird, 1977; Saffman, 1974; Moore and Saffman, 1973; Shamroth, 1979; Sarpkaya, 1983; Sarpkaya and Daly, 1987).

*3.2.2 Numerical Models.* Leaving aside the co-called $1/2\alpha$-method of Bollay (1939) and the leading-edge suction analogy of Polhamus (1966) [see Hardy and Fiddes (1988) for its latest application to non-planar wings], the existing "fitted" vortex models (as opposed to "captured vortex" methods that solve the Euler and Navier-Stokes equations) may be classified as the "cross-flow or slender-body" models and the "three-dimensional flow" models. Their basic features are discussed in the following.

*3.2.2.1 Cross-Flow or Slender-Body Models:* The difficulties offered by the full treatment of the three-dimensional flow may be circumvented by reducing the problem to a two-dimensional one in successive cross-flow planes. The number of the cross-flow planes may even be reduced to one by assuming the flow field to be *geometrically conical.* Methods in this category ignore the upstream effect of the trailing edge (for subsonic flow), large variations in streamwise direction on slender bodies, and the interaction of vortices generated from various components of the body. Furthermore, a conical geometry does not make a conical flow. The limits of applicability of the slender-body assumption are determined from a comparison of the predicted and measured flow characteristics with full awareness of the fact that not only the limitations noted above but also the facility-related phenomena such as freestream turbulence, surface roughness, vibration, and tunnel blockage may cause gross differences in the flow pattern and large scatter among different measurements of the force and moment coefficients and pressure distributions. Gad-el-Hak and Blackwelder (1985) presented photographic evidence that the vortices on delta wings originate as a series of smaller vortices shed from the leading edge of the wing. These vortices rotate around each other and pair to form larger vortices while simultaneously moving downstream. In their experiments (Re ranged from $1.3\times10^4$ to $3.5\times10^5$), the vortices paired at least three times before reaching the trailing edge of the wing. What role the tip shape, dye introduction scheme and the towing conditions played in these observations is unknown (see also Brennenstuhl and Hummel 1987). The different types of flow that can occur on the lee-surface of delta wings at supersonic speeds is described in great detail by Seshadri and Narayan (1988).

The numerical methods in the category of *slender-body models* consist of simple two-vortex models, first- and higher-order panel methods with various treatment of the vortex core, and the discrete vortex models.

*Two-Vortex Models:* The representation of the spiralling of the vortex sheets by an inviscid model within the framework of the slender-body (quasi-two-dimensional flow) theory was first presented by Legendre (1953), Edwards (1954) and Brown and Michael (1954) in the problem of a delta wing of conical planform, exhibiting leading-edge separation.

The model consists of two symmetrical concentrated vortices connected to the separation points by two feeding sheets of vanishingly small vorticity. The net force on the total vortex system is rendered globally zero, separately on each side. There is then a force on the concentrated vortex [Joukowski force $= i\rho\Gamma(W_1 - \dot{\zeta}_1)$] which is balanced by an equal and opposite force $[i\rho\dot{\Gamma}(\zeta_1 - \zeta_0]$ on the idealized feeding sheet [see Fig. 9 for definitions and Rott (1956) and Bryson (1959) for a derivation]. This means that the concentrated vortex does not lie along a streamline, or in the cross flow, i.e., its velocity is

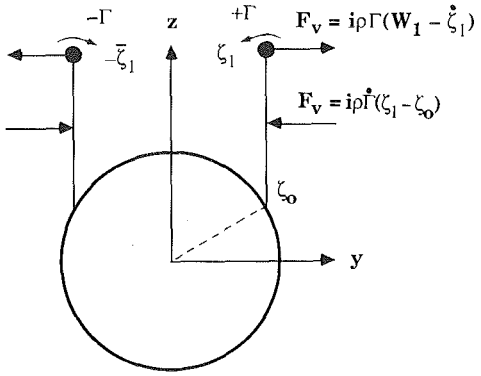


Fig. 9 Definition of the force-free feeding sheet (Bryson, 1959)

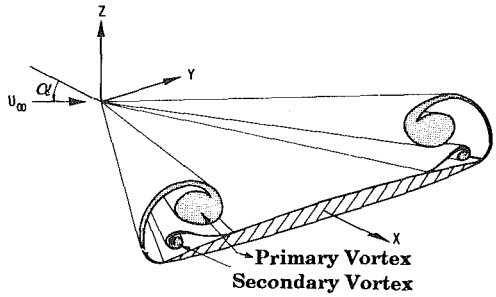


Fig. 10(a) Primary and secondary separations over a delta wing (from Hoeijmakers, 1983)

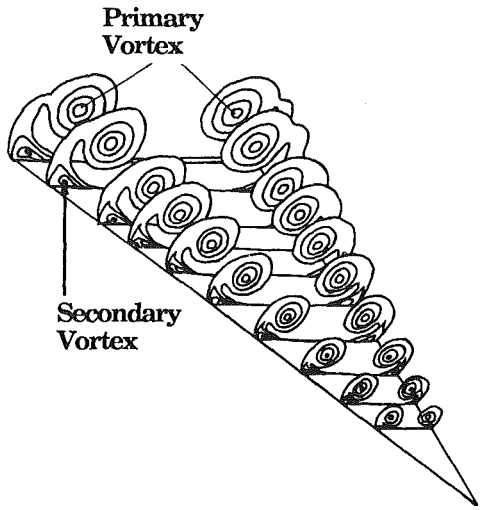


Fig. 10(b) Total pressure contours and secondary separation (Delta wing, $AR = 1$, $M_\infty = 0.3$, $Re_L = 0.95 \times 10^6$) (Thomas et al., 1987)

not equal to the local fluid velocity. The relative velocity of the vortex with respect to the fluid is directed towards the point of origin of the vorticity feeding it. Note that the moment acting on each vortex and its feeding sheet is not zero $[M = \rho\dot{\Gamma}(\zeta_1 - \zeta_0)^2/2]$. Furthermore, the two-vortex model ignores the effect of the secondary separation (a universal feature of real flow over slender wings, see Fig. 10), resulting from the adverse pressure gradient in the spanwise direction in the region just outboard of the lateral position of the center of the primary vortex. Bergeson and Porter (1960) have shown that the strength of the secondary vortices relative to that of the primary vortices is not negligible and "no mathematical treatment which fails to include the effect of secondary vortices on the flow field can accurately predict the lift force." Experiments show that the extent of the effect of secondary separation on pressure distribution is largest for the laminar boundary layer and increases with decreasing angle of attack and decreasing leading-edge sweep (Hummel 1979, Kjelgaard and Sellers III, 1988). Thus, for the two-vortex model to apply, the sweep angle should be sufficiently large and the angle of incidence should be large enough to minimize the neglect of the secondary (and often tertiary) separation and small enough to prevent vortex breakdown. Furthermore, the numerical results should be compared with experimental data corresponding to a turbulent boundary layer flow (J. H. B. Smith, 1968). Recent finite-difference calculations through the use of the Euler and Navier-Stokes equations by Rizzi and Muller (1988) (see also Rizzi and Purcell, 1987) have shown that rounding of the leading edges of a swept delta wing can have profound effects on the position and number of separation points and on the occurrence of multiple vortices (see, e.g., DeMeis, 1988). Euler equations, even with higher order dissipation functions, cannot handle smooth surface separation (see, e.g., Kandil and Chuang, 1988) and require a more precise numerical implementation of the surface boundary conditions (Raj and Brennan, 1987). The use of artificial viscosity in the Euler codes and the physical viscosity in the Navier-Stokes equations [including the inevitable artificial diffusion of the flow features due to numerical dissipation, particularly with low-order integration schemes (Nakamura et al., 1982)] do not necessarily lead to similar results, suggesting the action of different mechanisms for primary and even secondary separation points. The fact that the two types of viscosity do not necessarily lead to the same separation points over curved surfaces must be kept in mind using the vortex methods.

Vortex characteristics of isolated *bodies of revolution* have been studied extensively, again in the framework of slender body theory, with the added predicaments, noted earlier: where are the separation lines, what is the rate of shedding of vorticity, how does the separating stream surface leave the body, what conditions should be satisfied at the separation lines(s), what is the relationship between the Kutta condition and separation from a smooth surface, etc.

Bryson (1959) used the two-vortex model to obtain a solution for the nonlinear forces on circular cones (represented by a source of increasing strength, i.e., the so-called transpiration technique) and cylinders at high angles of attack in the subsonic to moderately supersonic velocity range. The assumption is that the strength of the primary vortices grows with increasing distance downstream in a manner analogous to the growth, in time, of the vortices behind a two-dimensional cylinder in crossflow, impulsively started from rest. In reality, there must be some interaction between axial and cross flows. The impulsive flow analogy which assumes independence of these components must therefore be regarded as a convenient way of approximating the evolution of flow.

Bryson forced the separation line and the positions of the line vortices to be *symmetric* about the incidence plane. Each vortex was connected to the fixed and prescribed separation points with a cut of vanishingly small vorticity. A Kutta type condition (the tangential component of the cross-flow is zero on the body) was invoked at the separation points. The direction of the separation line was thereby calculated to be 30 degrees from the downstream tangent to the cylinder. In spite of its remarkable simplicity, Bryson's analysis predicted the normal force at the early stages of motion fairly accurately (see Sarpkaya 1966). At later times, vorticity flows back from the vortex to the generation point (an unacceptable result) and the force drops sharply and unrealistically. However, the most remarkable feature of Bryson's model is that it owes its limited success to the *forced symmetry* of the vortices. Davis (1969), working with Sarpkaya, recast Bryson's model to remove the forced symmetry. The use of initial values (including symmetric separation points) identical to those of Bryson failed to

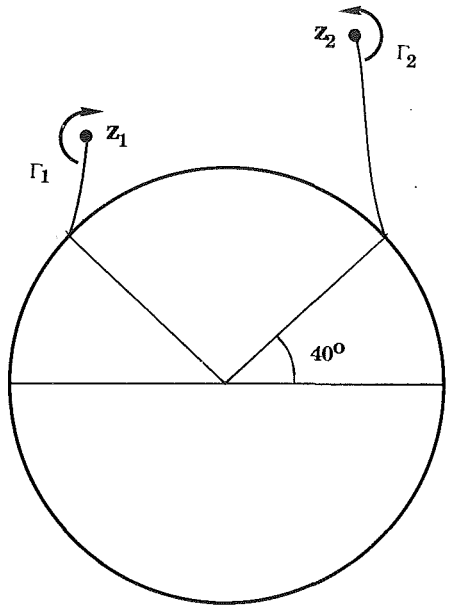


**Fig. 11 Consequences of the removal of the lateral symmetry in Bryson's (1959) problem: asymmetric vortex formation (Davis, 1969)**

produce symmetric vortex positions (Fig. 11 is a plot of the tabulated data given in Davis's thesis). It was discovered that the matrix yielding the rates of change of the strengths and positions of the vortices is ill-conditioned and the slightest truncation error leads to abnormally large values for $\Gamma_1$, $\Gamma_2$, $z_1$, and $z_2$. The unexpected and surprising asymmetry of the vortices was not interpreted as an explanation of the sectional side force which has since become an important problem (see, e.g., Thompson and Morrison 1971; Hall 1987). Rather, it was discovered that the two force-balance equations for the vortex-cut are the source of the ill-conditioned behavior of the matrix yielding the strengths and positions of the two vortices. This, in turn, is due to the fact that the moment acting on a vortex and its connecting sheet is not zero. In fact, all vortex models using the no-force condition on the connecting sheet or on the vortex-cut may exhibit similar behavior if formulated without forcing artificial symmetry. In other words, imposed symmetry can hide computational instability. However, it was then (1969), and it is still now, this writer's opinion that the vortex asymmetry resulting from the ill-conditioned nature of the governing set of equations explains neither the existence nor the non-deterministic behavior of the side forces. This is not to say that the side force is not a consequence of vortex asymmetry, but rather to emphasize that the source of asymmetry resides upstream of the separation points, not in the ill-conditioned behavior of the approximate equations.

Kuhn et al. (1971), Dyer et al. (1982) and Fiddes (1985) have independently repeated Davis's (1969) calculations, removing the assumption of lateral asymmetry but retaining the no-force condition on the vortex-cut and obtained asymmetric vortices. Kuhn et al. found the vortex positions and forces to be quite sensitive to the initial asymmetry. Dyer et al. and Fiddes have concluded that the bifurcation of the asymmetric positions from the symmetric vortex positions is the explanation of the large levels of side force. As noted above, this is not believed to be the proper explanation. In fact, a careful multi-vortex analysis of the impulsively-started flow by Sarpkaya and Shoaff (1979a), without resorting to the vortex-cut and no-force assumption, did not yield a bifurcation to asymmetric state, at least without introducing an asymmetry in the separation points and/or in the shear layers. A similar conclusion has been reached by Almosnino (1985) using a non-linear vortex-lattice method. A thorough discussion of the forebody and missile side forces and the time analogy is given by Hall (1987).

Wardlaw (1974, 1975) extended Bryson's model to the calculation of the flow field surrounding an ogive cylinder at high angles of attack. In doing so, he relaxed the symmetry condition and determined the free parameters inherent to the model by a comparison to drag coefficient data on an impulsively-started cylinder in cross flow. This model required the empirical input of many different parameters.

The two vortex model has been later extended to apply to bodies of elliptic cross section and of cambered longitudinal axis by Schindel and Chamberlain (1967) and by Schindel (1969). The location of the separation points (lines) are estimated independently through the use of experimental results, empiricism, or boundary-layer approximation.

*Multi-Discrete-Vortex Models:* They have been used to simulate the evolution of vortex sheets emanating from the leading- or trailing edges of lifting surfaces and from the separation lines of axisymmetric bodies (within the framework of the slender body assumption). Historically, however, the calculation of a smooth vortex sheet roll-up in the wake of a finite-span lifting surface (with attached flow at cruise conditions) has become a major test case particularly for discrete vortex models and a magnificent obsession for the aerodynamicist and numerical analyst alike. These investigations dealt primarily with the two-dimensional self-induced motion of the vortex sheet in a plane (the so-called "Trefftz-plane" in wing theory) so far downstream from the lifting surface that the bound vorticity produces negligible effect, i.e., the three-dimensional steady vortex sheet is considered to be two-dimensional and unsteady (see Moore and Saffman 1973 for a formal justification).

Westwater (1935) pioneered the application of discrete vortex modelling of the motion of a vortex sheet of finite span with the variation of vorticity

$$\omega(x) = 2Ux(a^2 - x^2)^{-1/2} \tag{46}$$

produced by an elliptically loaded wing. The vortex sheet intersects the $x$-$y$ plane in the strip $y=0$, $-a \le x \le a$, at time $t=0$. He used ten equistrength line vortices, distributed along a semi-span, and obtained an orderly roll up starting at the edges. The assumptions inherent to the analysis are valid only for lightly loaded wings since the bound vorticity, the effect of the semi-infinite array in the direction of upstream infinity, and the interaction of the shear layer with the flow around the tip are neglected.

Takami (1964) and Moore (1971) were unable to reproduce Westwater's results even though they have used a multi-vortex approximation with the help of a computer. The results exhibited chaotic motion in the region of the spiral even at the early stages of motion due to the propensity of closely spaced vortices for rapid mutual orbiting. The amplification of the chaotic motion in spite of the increase of the number of vortices and the use of more accurate time-integration schemes was most disconcerting. Takami also found (through the use of other vorticity distributions, including the one produced by a wing with cusped tips) that the region of irregular motion is not confined to the vicinity of the tips but extends over much of the sheet.

Sacks et al. (1967) simulated the flow about a wing-body combination using conformal transformation for the configuration geometry and discrete vortices for the leading-edge vortex sheet. This did not require a vortex core nor the assumption of conical flow. Each new vortex (nascent vortex) was placed in the plane of the wing. The predicted forces were in reasonable agreement with the measurements even though the vortex sheet was quite chaotic. Xieyuan (1985) used a similar technique to simulate the flow about double-delta wings. The position of the large scale vortex motion agreed

with that found experimentally but the motion of the individual vortices was quite disorderly. As it is often the case in computational vortex dynamics, the reasonableness of the results depends on the criteria of credibility.

Schwartz (1981) considered the roll-up of the trailing vortex sheet produced by a wing of finite span and cusped tips through the use of a series expansion in time and found that the sheet remains analytic for some time but ultimately develops a singularity in the form of an exponential spiral at the tips. This problem differs significantly from those discussed above, because the circulation is singular at the tips starting from the initial instant.

Bromilow and Clements (1982) amalgamated clusters of vortices in the region of roll-up into a single equivalent vortex (an extension of Moore's technique 1974) and subjected the remaining part of the vortex sheet to repeated rediscretization [an extension of Fink and Soh's method (1974), but using the cubic spline and a four-point Lagrangian interpolation routine to account for the curvature effect]. This prevented vortices on the evolving parts of the sheet from becoming too close or too distant. They have shown, as did Moore (1974) and Baker (1980), that the technique of central vortex amalgamation alleviates the effects of the erratic motion of the vortices in the compressive parts of the sheet and eliminates the attendant problem of propagation of these perturbations along the feeding sheets until the time when too few vortices are representing the sheet. The combined technique allowed the calculation to be taken beyond time limits of the basic discrete vortex calculations, as noted earlier by Fink and Soh (1974).

Clements and Maull (1973) used equistrength discrete vortices to investigate the effect of different wing loading distributions on the roll-up, hoping that some non-elliptic distributions might lead to weaker tip vortices with relatively small drag penalties. Their results have shown that minimizing, as much as possible, the high rate of change of $\Gamma$ near the wing tips would decrease the strength and the rate of roll up of the tip vortices with relatively small drag penalties. Chorin and Bernard's (1973) calculations with blobs showed that the form of the roll-up at the tips matched Kaden's spiral well.

Siddiqi (1987) used a slightly different smoothing scheme without amalgamation in calculating the roll-up of a vortex sheet for an elliptically loaded wing. Starting at the tip and using the slope information, he fitted, at each time step, a cubic spline to the sheet and redistributed each line vortex into two equal vortices when the sheet segment representing the vortex stretched beyond a prescribed amount. The basic aim of the redistribution (at the expense of increasing the number of vortices) was to try to keep the sheet-segment length per line vortex approximately constant so as to ensure that each roll-up turn is represented by an adequate number of vortices even as it stretches. He was able to obtain three turns at a time when 90 percent of the circulation has rolled up. Cheng et al. (1985, 1988) used discrete vortices to calculate the vortical flow over a slender delta wing with leading edge flaps. The algorithms were similar to those of Sarpkaya (1975) with the exception that the strength and location of the nascent vortices were determined from the "no-net-force condition" (Edwards 1954, Bryson 1959). Cheng et al. found that, apart from the flap-generated vortices, the secondary eddies produced at the hinge also contribute noticeably to the vortex lift even at moderate angles of attack.

Two-dimensional multi-vortex models were also applied to separated flow over axisymmetric and arbitrary cross sectional bodies at angle of attack. Angelucci (1971, 1973) extended Sacks et al.'s (1967) model through the use of numerous ad hoc assumptions. Separation lines were assumed to be known and only symmetrical separation was treated through the use of the impulsive flow analogy. The multi-vortex model was extended and considerably improved by Marshall and Deffenbaugh (1975), Wardlaw (1975), Deffenbaugh and Koerner (1977), and Shivananda and Oberkampf (1981). Peace (1983) used the multi-vortex model to calculate the leading edge vortex flows on slender wings with lengthwise camber or with a strake. He used the amalgamated line vortex, vortex-cut, and no-force assumptions together and imposed symmetry. Flow about general slender planforms and wings with thickness was calculated by Maskew and Rao (1982) and by Nathman (1984) using a low-order panel method to represent the solid surface and an improved discrete vortex method to simulate the vortex sheet.

Clearly, an infinite sheet comprised of equisign, equistrength, and equispaced vortices remains stationary. However, a sheet of finite length, comprised of the same type of vortices, cannot remain stationary because the velocity induced in the vortices, particularly in the one at the edge of the sheet, is no longer balanced out. The singular nature of the vorticity distribution at the tip gives rise to a small "hook" at the very tip of the sheet at small times. At later times this initial irregularity is strained by the velocity field into a larger reverse hook in the vortex core. The *propensity for mutual orbiting* of the vortices is dependent on the relative strengths, positions, and core shapes of the vortices situated on either side of any given vortex in the sheet. Thus, the mutual orbiting of the vortices and the meandering of the edge of the vortex sheet in an otherwise inviscid environment are at the heart of the problem. These facts may well have discouraged, if not put an end to, the further use of the discrete vortex modeling of the vortex sheets. But the challenge to obtain a smooth roll-up through line-vortex discretization of a thin shear layer proved to be seductive and the rush was on to discover or rediscover suitable smoothing techniques, discussed in Section 2.5. As far as the Trefftz-plane problem is concerned, Krasny's (1987) use of Rosenhead's (1930) smoothing technique produced some of the best roll-up result to date, (see Fig. 12).

*Segment or Panel Methods.* The purpose of these methods is to account for the finite vorticity in the outer feeding sheet, connected to an isolated potential vortex representing the inner part (Mangler and Smith 1959). The vortex sheet is divided into a number of straight or curved segments and the vorticity or doublet distribution on them is approximated by piecewise polynomial representations. The tightly rolled-up inner region of the spiral is represented by an isolated vortex. It is connected to the remainder of the sheet with a force-free cut. Often the sheet is resegmented through the use of a suitable scheme to keep the segment length below a prescribed value . J. H. B. Smith (1966, 1968) used a large number of small concentrated vortices at arbitrarily chosen points on in (the unknowns being the polar distances of the sheet segments, the values representing the sheet strengths, and the strength of the isolated vortex and its two coordinates). He used the Kutta-Joukowski condition of finite velocity at the leading edge, the no-force condition on the vortex-cut combination, the no-pressure difference condition across the sheet, and the conical normal velocity condition on the sheet and solved the resulting equations through an iterative approach. The predicted pressure distributions compared quite well with those obtained experimentally, except near the trailing edge where the flow must eventually return to the freestream pressure. The comparison of the results of the Brown and Michael model with those of Mangler and Smith (1959), Smith (1968), and Barsby (1972, 1973) shows the importance of the correct representation of the outer sheet as far as the position of the concentrated vortex, the fraction of the circulation in the sheet (about 50 percent), and the total circulation are concerned. However, Smith's model overpredicts, by a considerable amount, the load distribution towards the trailing edge, for the Kutta condition cannot be satisfied there by the conical theory.

The use of a line vortex to represent the core gives rise to a logarithmic singularity in all the models cited above. Roy

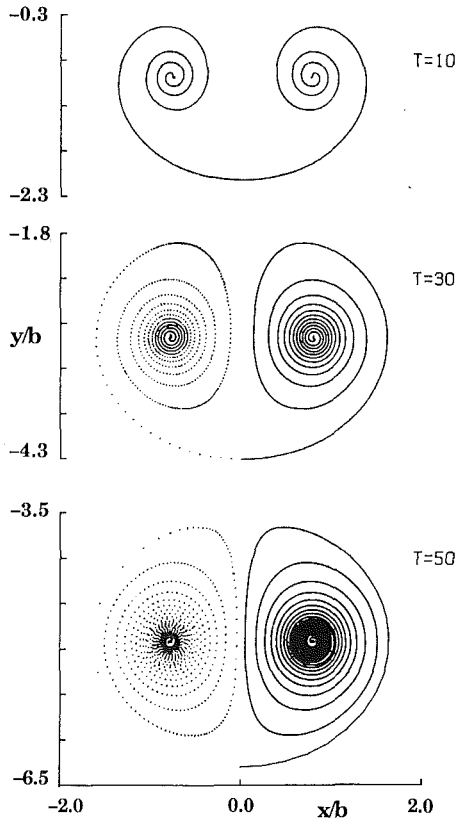


**Fig. 12 Vortex sheet roll-up in the Trefftz plane at different times ($\delta = 0.2$) (Krasny, 1987). The vortex blob positions are plotted on the left and an interpolating curve is plotted on the right.**

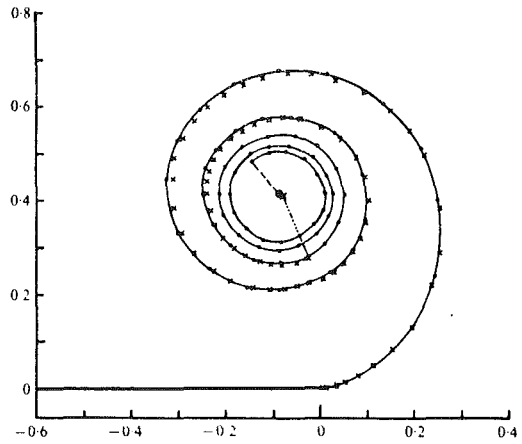


**Fig. 13 An example of unsteady self-similar roll-up of a vortex sheet (Pullin, 1978)**

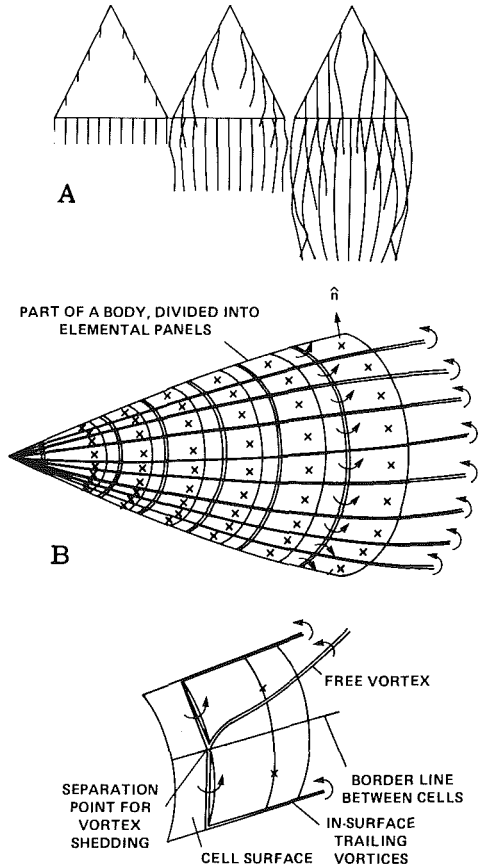


**Fig. 14 Vortex-lattice method: (*a*) vortex-wake shedding and roll-up sequence over a delta wing (Katz, 1984); (*b*) subsonic flow on a slender body (Almosnino, 1985)**

(1957) suggested, as did Spreiter and Sacks (1951) earlier, that a finite core of vorticity be used to replace the end of the spiral sheet in order to limit the velocity (this idea has later been independently discovered by several others and used successfully to achieve a smooth roll-up). The Mangler and Smith model has been extended to non-conical planforms by Clark (1976).

Pullin (1973, 1978–1979) and Pullin and Perry (1980) used a method similar to that of Smith (1968). The difference is in the treatment of the governing integro-differential equation, the specification of the percent of vorticity in the sheet (instead of the extent of the sheet), and the initial approximation to commence the iteration (see Fig. 13).

A complete description of the panel method is presented by Maskew (1980). The perturbation potential is expressed as a sum of the potentials induced by singularity distributions on the surface of the body. The surface is discretized into a set of planar panels, each associated with a prescribed form of source and doublet singularity distribution. The resulting set of linear equations for the unknown singularity strengths are solved by the application of suitable boundary conditions.

Higher-order panel methods based on the slender-body approximation were developed by Hoeijmakers et al. (1983) and by Hoeijmakers (1984) for conical and quasiconical flow (see also Nagati et al. 1987). In general, the panel methods produce smoother vortex sheets than the discrete vortex models of Maskew and Rao (1982) and Fink and Soh (1974). Boundary-layer calculations have been incorporated into the analysis through an iterative inviscid-viscid procedure in order to account for the effect of secondary separation on the upper surface pressure distribution (De Bruin 1984; Wai et al. 1985; DeJarnette and Woodson 1984).

The numerical simulation of the formation and roll-up of the tip vortex in both subsonic and transonic flows through the use of a multi-block zonal algorithm which solves the thin-layer Navier-Stokes and the Euler equations is presented by Srinivasan et al. (1986).

*3.2.2.2 Three-Dimensional Aerodynamic Flow Models.* A number of fully three-dimensional flow models have been developed for the prediction of wake roll-up to overcome the limitations of the slender body models. These consist of non-linear vortex lattice methods and panel methods.

*Vortex-Lattice Models:* Belotserkovskii (1968) introduced the idea of approximating the bound-vortex sheet by a bound-vortex lattice and the free-vortex sheets by a set of segmented free-vortex lines (in the case of steady flow) or by a growing

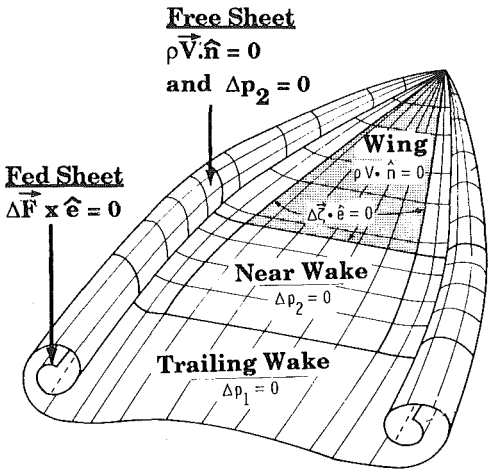


Fig. 15 Boeing free-vortex-sheet model (Johnson et al., 1980)

free-vortex lattice (in the case of unsteady flow). Each element is associated with a horse-shoe vortex. Discrete line vortices trail to infinity downstream along the trailing and side edges (see Fig. 14). Their alignment with the local flow direction provides the necessary boundary conditions on the vortex sheets. The strengths of the vortices are determined through the use of an iterative technique by imposing the zero normal velocity condition at the midpoint of the 3/4-chord line of the elements. The model has been considerably improved and extensively used since its inception (Rehbach 1973, 1977, 1978; Kandil 1979, 1985; Aparinov et al. 1976; Kandil et al., 1976a, 1976b, 1984; Belotserkovskii and Nisht 1974; Asfar et al. 1979; Rom et al. 1981; Almosnino and Rom 1983; Katz 1981, 1984; Thrasher 1982; Almosnino 1985). The results have shown that the model is rather crude and exhibits undesirable singular behavior (see, e.g., Schroder 1980). Even though overall forces are predicted reasonably well, the local velocity or pressure distribution on the body and the vortex-sheet geometry are not sufficiently accurate. This is an inherent limitation of the vortex lattice method. Increasing the number of vortices makes the matters worse (Rusak et al. 1983). The results strongly suggest that great care must be taken in deciding the position of separation lines, panel arrangement and control point placement (see, e.g., Van Tuyl 1988). The separation line must be known a priori either through experiment, correlation, or by a boundary-layer solution coupled with the inviscid solution.

*Panel Methods.* The model consists of the wing surface, the leading-edge vortex sheet, the feeding sheet, the near wake, and the trailing wake. Vortex sheets consisting of small panels or vortex elements are inserted into the flow and allowed to roll up under their own influence for several turns. The remaining core is modeled by an isolated line vortex. The position and strength of the vortex sheets and isolated vortices are determined as part of the solution. The vortex sheets are modelled by piecewise continuous doublet distributions, eliminating the consequences of the singular behavior of the line vortices (see Fig. 15). The most prominent among the higher-order panel methods are the Boeing LEV-Model by Johnson et al. (1980); the VORSEP-Model of NLR (National Aerospace Lab of The Netherlands) by Hoeijmakers and Bennekers (1979), Hoeijmakers et al. (1983), and Hoeijmakers (1985); and the Hybrid vortex model of Kandil (1980). The LEV and VORSEP models are quite similar, differing only in their numerical implemenation. Their predictions compare favorably well, differing only in detail. The comparison with experiments is good to encouraging as far as the overall accuracy of the position of the vortices is concerned. The local accuracy depends on the shape of the wing, the angle of attack, the number of panels, the order of accuracy of the finite difference expressions used to calculate the derivatives, and the smoothing applied. The calculated pressure distributions compare reasonably well with those measured (Hummel and Redeker 1972) on wings with turbulent boundary layers, for which the effect of the secondary separation is relatively small.

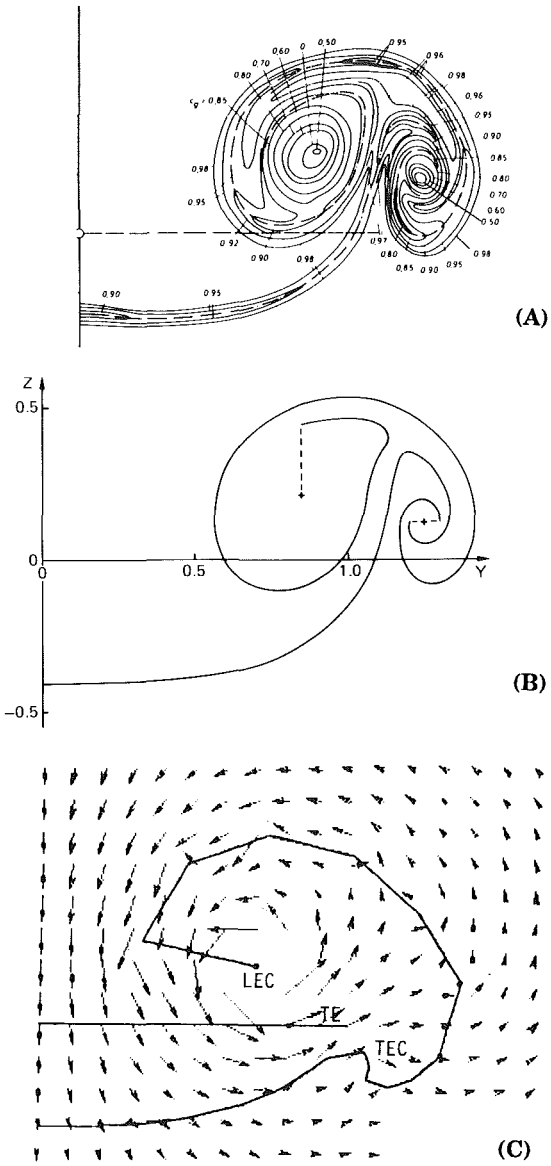


Fig. 16 Examples of double-branched vortex wake at 1.067 half spans behind a delta wing with $AR = 1$ at $\alpha = 20$ deg. (A): (Hummel, 1979); (B): Hoeijmakers, 1983); and (C): (Kandil, 1980).

In the nonlinear Hybrid model of Kandil et al. (1984), vortex panels (triangular panels in the wake) with a first-order vorticity distribution are used in the near -field calculations. In the far-field calculations, the distributed vorticity over each far-field panel is lumped into equivalent concentrated vortex lines. This method has been modified by Yeh and Plotkin (1986) and applied to large aspect ratio wings with a closer look at the trailing wake roll-up.

Experiments (Hummel 1979, Elle and Jones 1961, Hummel and Redeker 1972, Hummel 1979) have shown that the sense of roll of the shear layer emanating from the trailing edge of a wing, with highly swept-back leading edge, is opposite to that of the primary shear layer, i.e., they form a double-branched vortex (see Fig. 16). Even though the downstream development of the interaction of these two shear layers remains to be

resolved, the panel methods cited above predict, with varying degrees of detail, the form of the double-branched vortex.

None of the methods is capable of predicting the occurrence of vortex breakdown or dealing with high-enough angles of attack at which vortex breakdown occurs. It is equally important to note that the models discussed so far deal only with steady or quasi-steady situations. The vortex breakdown is quite sensitive to the sweep angle of the wing and is responsible for aerodynamic hysteresis effects. These lead to a double-valued behavior of the steady-state aerodynamic response to variations in one of the motion variables such as angle of attack (Orlik-Ruckemann 1982). In summary, the high-$\alpha$ aerodynamics involves, by its very nature, highly complex unsteady phenomena and the existing vortex methods, however elegant, cannot yet deal with them. Their refinement will require additional physics to deal with the interaction of vortices with other components of the aircraft and with the transient behavior of vortices in adverse pressure gradients. In recent years, finite-difference analysis of Euler and Navier-Stokes equations (see, e.g., Eriksson and Rizzi 1981), Rizzi and Eriksson 1985, Rizzetta and Shang 1986, and Rizzi and Muller 1988) has made great strides towards the analysis of separated flow about lifting bodies. However, neither the Euler nor the Navier-Stokes codes can capture a sharp vorticity discontinuity without smearing it over a number of computational cells in spite of the successive stepwise refinement of the numerical parameters. In this case the mismatch between model-based prediction and actual behavior is wholly attributable to numerical diffusion (the *bete noire* of the grid-dependent computational approaches). Thus, the computed vortical-flow region occupies a larger volume than that enclosed by the actual vortex sheet. Even though the details of the smeared flow are not correct, the centroids of vorticity remain reasonably unaffected (Rizzi 1988) because of the radial nature of the diffusion. Nevertheless, the Euler programs are not likely to supplant the vortex methods on the grounds of either the physical realism or the economy of computation as far as subsonic flows with sharp vorticity discontinuities are involved. The emerging fact is that the vortex methods are not better equipped to deal with stability, smoothing, dissipation, dispersion, and turbulence than finite-difference and finite-volume methods. Arguments to the contrary are presented by Hitzel (1988).

**3.3 Separated Flow About Cylindrical Bluff Bodies.** Observations, as well as numerical experiments, show that the wake of a bluff body is comprised of an alternating vortex street (ignoring for the time being the effect of splitter plates and the proximity of other bodies or boundaries). The character of the vortices immediately behind the body and in the wake further downstream depend on the Reynold number, condition of the body surface (smooth or rough), and the intensity and length-scale of the turbulence in the ambient flow. For a time-dependent flow, the instantaneous state as well as the past history of the flow play significant roles and it is not possible to give a general set of normalized parameters. Not only the numerical experiments but also the physical experiments with time-dependent flows are extremely difficult. In this sense, the purpose of computational methods with vortices is to provide numerical simulations whose predicitions can either be confirmed with physical experiments yet to be conducted or relied upon as physically realizable even when the experimentation is nearly impossible. The said purpose certainly is not the retrofitting of the predictions to the existing data through the manipulation of a number of disposable parameters, and the use of ad hoc assumptions, even though this is often done to calibrate the numerical scheme to perform numerical experiments within a narrow range of the governing and influencing parameters.

*3.3.1 Flow About a Circular Cylinder.* A great deal of theoretical, experimental and numerical research has been devoted to the understanding of the near and far wake of bluff bodies, in general, and of a circular cylinder in particular. The impetus for this research comes partly from practical needs and partly from a desire to understand phenomena such as separation, transition, shear layer evolution, wake instabilities, and fluid-structure interactions. Exciting new phenomenological and structural discoveries continue to be made both numerically and experimentally (see, e.g., Cantwell 1976; Schewe 1986; Braza et al. 1986; Sreenivasan et al. 1987).

Much interest has been given to the unsteady boundary layer development around an impulsively started cylinder. Telionis (1979) found that the unsteady classical boundary-layer solution develops a singularity within a finite time, implying the nonexistence of a steady classical solution (see also Van Dommelen 1981). The formation of this singularity has been confirmed by Cowley (1983), Van Dommelen and Shen (1983), Ingham (1984), and Henkes and Veldman (1987).

Sarpkaya (1963) was the first to derive general expressions for the lift and drag coefficients for a circular cylinder immersed in a time-dependent flow comprised of the ambient flow, a doublet, any number of discrete vortices and their images. He included an image at the center of the circle which was later omitted (Sarpkaya 1968b, 1969) because of the fact that the shed vortices leave a circulation opposite to their own on the body, as pointed out by Gerrard (1967). The complex force is given by

$$D+iL=2\pi\rho c^2\dot{U}-i\rho\sum_{j=1}^{n}\Gamma_j[(u_j+iv_j)-(u_{ji}+iv_{ji})] \qquad (47a)$$

or by

$$D+iL=2\pi\rho c^2\dot{U}-i\rho\frac{\partial}{\partial t}\sum_{j=1}^{n}\Gamma_j\left(z_j-\frac{c^2}{z_j}\right) \qquad (47b)$$

in which $\Gamma_j$ is taken positive in the clockwise direction. $(u_j+iv_j)$ is the complex velocity of the $j$th real vortex, $(u_{ji}+iv_{ji})$ is the complex velocity of the $j$th image vortex, and $c$ is the radius of the circle. Equations (47*a*) and (47*b*) may be easily generalized to cylinders of arbitrary shape. Since 1963, they have been rederived numerous times (see, e.g., Tiemroth 1986a).

Gerrard (1967) was the first to apply the discrete vortex model to the flow about a circular cylinder. He noted that "A particularly important part of the vortex model of the flow and the most difficult aspect of the design of the model, is the positioning of the points of appearance of the elementary vortices representing the vortex sheets and the determination of their strength." Gerrard also recognized the importance of simulating the effect of Reynolds number. In fact, even after twenty years of work with ever-increasing computer power, the problem of relating the creation and diffusion of vorticity to a Reynolds number without an abundant dose of disposable parameters still remains unresolved. Gerrard used the width of the formation region at a control surface (a surface at $x=R$ at which the nascent vortices are introduced into the flow) as the major scale effect. The strength of the nascent vortices was determined from the velocity at the point of introduction. In doing so, however, he introduced a disposable time parameter characterizing the oscillations of the wake width and ignored the effect of the shear layer upstream of the control surface. He obtained a relatively crude vortex street and lift and drag force traces. Nevertheless, Gerrard's work has pointed out all of the major difficulties to be faced by future investigators.

The cylinder problem was taken up by Sarpkaya (1968b) and by Bellamy-Knights (1967), working with Sarpkaya. The vortices were introduced half-way between the points at which the absolute velocity reached a maximum on the front and rear faces of the cylinder. The nascent vortices were introduced at

the separation points and a small distance from the cylinder surface. The strength of the nascent vortices was made equal to $0.5(V_f^2 - V_r^2)\,\Delta t$ to account for the oppositely-signed vorticity contributed to the shear layer by the reverse flow on the rear face of the cylinder. This was the first time that *the effect of rear separation or secondary separation* was incorporated into a discrete vortex model. The flow was forced to remain symmetric and represented by vortices fewer than 100. In spite of these limitations, the results showed the rolling-up of the vortices, the development of the Helmholtz instability [as experimentally observed by Pierce (1961), and by many others since then], and the rise of the drag coefficient to a maximum at the early stages of the flow due to the rapid accumulation of vorticity in the growing vortices.

Sarpkaya's work was extended by Davis (1969), working with Sarpkaya, to include the evolution of asymmetric flow. He developed two models: the two-vortex model (discussed earlier) and the multi-vortex model. The second model showed periodic vortex shedding behavior and the computed drag exhibited realistic behavior in reaching a maximum soon after the impulsive start, then decreasing somewhat, and oscillating about a mean level. The computer of the day limited the calculations to short times and the Strouhal number was not predicted. However, Davis's work clearly pointed out the need for the use of a boundary layer, the importance of a systematic sensitivity analysis, and the critical importance of the strength and position of the nascent vortices. Exploratory models were described by Laird (1971) and Chaplin (1973). Both authors fixed the separation points and the strength of the nascent vortices. Chaplin's work, even though quite approximate, had two novel features which are worth emphasizing in light of the more recent developments: the representation of the forebody boundary layer by a number of vortices (placed on an arc of fixed radius) and the use of Rankine vortices (with a core radius of 0.1), a method independently discovered by others since Spreiter and Sacks (1951). Yang and Bar-Lev (1976) used two symmetrically situated vortices (Bryson's model 1959) to study the initial phase of the impulsively-started flow about a cylinder. Even though some of their assumptions are untenable, they were the first to use a boundary layer expansion in powers of elapsed time, valid for small time, to determine the position of the separation points.

Chorin (1973) applied his time-splitting method to flow past a circular cylinder. His *time-averaged* drag coefficients (with expected substantial variance in the instantaneous values) were close to the experimental values. At $\mathrm{Re} = 10^5$, the drag coefficient was $C_d = 0.29$. He conjectured "that the rough representation of the boundary layer triggers a premature onset of the drag crisis, analogous to the effect of a rough boundary or a noisy flow." No Strouhal number was reported.

Kuwahara (1978) divided the boundary into 64 partitions to start the calculations and replaced each with a line vortex with the same circulation as the corresponding partition. The vortices were introduced at a small distance from the surface (approximately half the boundary layer thickness, not sheet layer as in random walk methods). In subsequent steps, only two nascent vortices were placed at fixed separation points. His calculated drag coefficient for $\mathrm{Re} = 10{,}000$ and nascent vortex angle of $\pm 90$ degrees was about half that found experimentally. He then claimed that the position of the nascent vortex is not essential.

Marshall and Deffenbaugh (1975) developed a model to determine the forces and moment on a body of revolution in separated flow. The model is based on cross flow analogy, an expanding (or contracting) cylinder with a time-varying radius, a vortex core with fixed cut off distance, the unsteady Navier-Stokes equations for the position of the primary separation points, and rear shear layer separation with an ad hoc assumption. Their calculated forces, moments, and separation regions compared well with those obtained experimentally for moderate angles of attack [see also Deffenbaugh and Koerner (1977), where Stratford's (1957, 1959) separation criterion is used].

Sarpkaya and Shoaff (1979a, 1979b) have presented a method for determining the flow over a stationary and transversely-oscillating circular cylinder using the method of Fink and Soh (1974) to rediscretize the vortices along a vortex sheet at each time. The attachment points of the sheets to the cylinder are the separation points as determined through boundary layer calculations. They have introduced the idea of *circulation reduction* to account for the effects of three-dimensionality of the flow and were able to obtain results in good agreement with experiments through the use of a suitable circulation-reduction scheme. The calculated forces without the circulation reduction were about 25 percent larger. The Strouhal number was essentially unaffected by the circulation reduction. Surprisingly enough, ten years later, more sophisticated and elaborate methods, based on random walk and cloud-in-cell schemes, using as many as 32,000 vortices and super computers were unable to reproduce the early stages of the drag force with equal accuracy (see Fig. 17).

Vortex calculations based on the assumption of two-dimensional flow do not accurately predict the dynamics of the flow (in particular, the lift and drag forces, and the pressure distribution). This is in part due to the fact that they lack the ability to capture small-scale turbulence structures which arise due to vortex stretching and tilting with respect to the main flow plane. This is true whether one uses a traditional vortex model or one with random walks, blobs, etc. Again as noted, an artificial reduction in circulation is introduced to account for the three-dimensionality effects, assuming that the discrepancy between the calculated and measured quantities is due to the neglect of three-dimensional effects alone. Obvious-

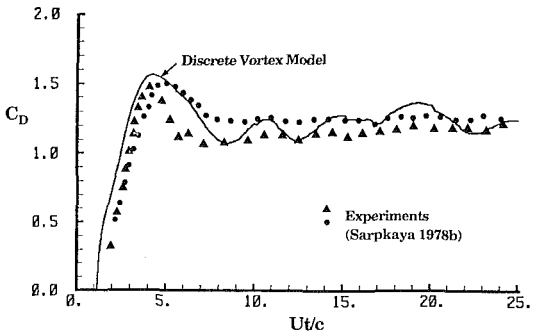


**Fig. 17(a) Evolution of drag on a circular cylinder immersed in an impulsively-started steady flow (Sarpkaya and Shoaff, 1979a) (discrete vortex model with circulation reduction)**

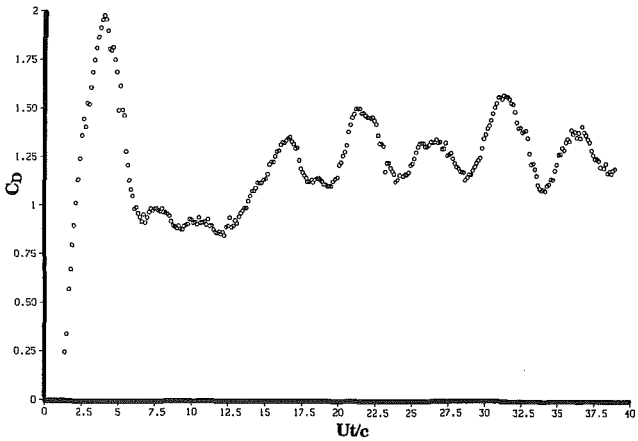


**Fig. 17(b) Same as Fig. 17(a) except that the numerical model has no circulation reduction**

ly, it tends to account for all other ad hoc assumptions regardless of the method used.

Deffenbaugh and Shivananda (1980) carried out two distinct studies. First, they extended their previous work (Marshall and Deffenbaugh, 1974) to flow about an impulsively started cylinder in a slightly compressible flow. Second, they reconsidered the earlier impulsive flow case in an incompressible fluid with the addition of random walk component to velocity of the vortices. Their use of the random walk differs from that of Chorin (1973) and Cheer (1979) in the form of the core velocity distribution and in the introduction of the vortices. The nascent vortices were placed near the separation points, calculated either through the solution of the unsteady boundary-layer equations using an integral momentum approach or by approximating the steady solution using Stratford's (1957) method. Rear shear layer separation is determined by an ad hoc algorithm based on the assumption that the rear shear layers remain attached over the same fraction of a region of adverse pressure gradient as the forward boundary layers (for details see Deffenbaugh and Marshall 1976 and Deffenbaugh 1979). The separation angles for the turbulent case were determined using Stratford's (1959) (see also Takada 1975) turbulent separation citeria immediately after separation occurred at the rear stagnation point. The lift and drag coefficients were calculated using a form of the generalized Blasius theorem (Sarpkaya 1963, 1968b). Their results have shown that the effect of including a random walk component of velocity to the motion of the discrete vortices is difficult to discern. The predicted lift and drag coefficients were considerably higher than the corresponding experimental values (Sarpkaya, 1978b) and continued to increase with time. They have also concluded that the circulation must be reduced to achieve results which agree with experiment and the reduction mechanisms must be more accurately modeled.

Cheer (1983a) applied the combined sheet-blob algorithm first to flow over a circular cylinder and over airfoils at various angles of attack (with incorrect circulation at infinity) and then correctly to the initial stages of impulsively-started flow over a cylinder (Cheer, 1983b). Her flow structures for very small times were quite similar to those photographed by Bouard and Coutanceau (1980). This is not too surprising since the classical multi-vortex models with rear separation yield similar flow patterns (Mostafa, 1987).

Faltinsen and Pettersen (1982, 1987) and Pettersen and Faltinsen (1983) used a vortex tracking scheme in which sources and dipoles were distributed over boundaries and free shear layers. The boundary value problem (Fredholm's integral equation of the second kind and the constraint on the velocity jump at the separation points) for the velocity potential was solved at each time step. For the flow about bluff bodies, a boundary layer calculation (based on an assumed eddy-viscosity formulation) was performed to predict the separation points. The shear layers were fed at the separation points and rediscretized, after every Eulerian-convection step, using Fink and Soh's method. The potential jump at the new segment ends were found by a linear interpolation. Faltinsen and Pettersen (1987) encountered considerable difficulties with the prediction of the primary and secondary separation points and with the vorticity returning to the body in oscillating flows and had to introduce various ad hoc schemes (e.g., reduction of vorticity in the primary and secondary shear layers by 10 percent. They have applied their method to impulsively-started flow about a smooth cylinder and obtained satisfactory drag coefficients and Strouhal numbers for both subcritical and transcritical flow. They have also applied the vortex tracking method to flow past a ship section and to sinusoidally oscillating flow about a normal plate and a circular cylinder (separation points fixed at $\theta_s = \pm 90$ deg). However, only the kinematics of these flows were calculated for short times. In treating the problem of vortex-sheet roll-up, Faltinsen and Pettersen (1982) again used Fink and Soh's (1974) rediscretization technique and Moore's (1975) core amalgamation scheme. As noted earlier, the combination of these two schemes delays the instabilities in the roll-up process.

Stansby and Dixon (1982) used the CIC scheme to emphasize the importance of secondary shedding in two dimensional wake formation at high-Reynolds-number flow about a cylinder. They placed the primary separation point at downstream of the velocity maximum, at the point where $U = 0.95 U_{\max}$ for the subcritical flow and at $0.82\ U_{\max}$ for the supercritical flow. These brought the measured and calculated separation angles into closer agreement. The secondary separation points were placed at points where the maximum velocity occurred on the afterbody. They concluded that the inclusion of the secondary separation brings the pressure distributions and vorticity structures as subcritical and supercritical Reynolds numbers into good agreement with experiment. Evidently, the agreement achieved is strongly dependent on the particular velocity ratios used to calculate the separation points. Furthermore, the importance of the secondary separation depends on the shape of the afterbody. In some cases the downstream vorticity production is quite small due to the nearly flat pressure distribution there (Achenbach 1972).

Smith (1986) and Smith and Stansby (1985, 1987) calculated a number of flows (laminar boundary layer above an infinite plane surface, induced by sinusoidal onset flow and by linear waves; separated laminar flow induced by sinusoidal waves over a rippled bed; and steady flow over cylinders of arbitrary shape for Re = 1,000) using vortex sheets, random walk, and the VIC scheme. Attached flows were simulated successfully. However, the separated flow cases required the use of a "suitably chosen decay factor" (circulation reduction) to bring the results into agreement with experiment, even under conditions in which the flow was purely laminar. As usual, the three-dimensionality effects have been invoked to justify the use of a circulation decay law.

Rottman et al. (1987) studied the two-dimensional motion of a *fluid cylinder* released from rest into a uniform ambient flow. The inviscid case was considered first, using analytical methods for small and large times and three numerical methods (Vortex-sheet, vortex blob, and the VIC method), followed by the viscous case, using the VIC method with random walks (Re = 484). Among other things, they have found that the drag of the cylinder is overestimated by about 15 percent (the base pressure is underpredicted), and that the results computed with Re = 250 nd 484 are virtually identical, while the experiments (Thom 1933) show significant differences. Apparently, the random walk method (with or without the VIC scheme) failed to correctly represent the effect of the molecular diffusion, particularly at such low Reynolds numbers.

Kimura and Tsutahara (1987) calculated the flow about a rotating circular cylinder using discrete vortices with experimentally-determined fixed separation points. They were primarily interested with the reverse Magnus effect.

Applications of discrete vortex models to *oscillating* flow ($U = U_m \sin 2\pi t/T$) about bluff bodies have had either gross simplifications, or have met with various difficulties. Ward and Dalton (1969) considered only symmetric flow situations with fixed separation points. Stansby (1977, 1979, 1981) either determined the separation points through an ad hoc scheme (steady flow calculations) or fixed them at $\pm 90$ degrees (oscillating ambient flow) and used the velocity of the nascent vortex rather than the velocity at the separation point to calculate the vortex strengths. This resulted in significantly less vorticity input and prevented the returning vortices from interacting freely with the boundary layers and separation points. As in previous methods, he amalgamated the vortices

and ignored those which crossed the boundary. No detailed comparison of the measured and calculated flow kinematics was offered.

Iwagaki et al. (1976) and Sawaragi and Nakamura (1979) determined the separation points using Schlichting's (1932) periodic boundary layer theory (valid only for Keulegan-Carpenter (1958) numbers $K(=U_m T/D=2\pi A/D)\ll 1$). They have not used the Kutta condition and incorrectly included an image vortex at the center of the cylinder. Finally, the calculations were performed for only three-quarters of a cycle, hardly enough time for the transient flow to develop into quasi-steady state. Kudo (1979, 1981) investigated the sinusoidally oscillating flow about a flat plate normal to the flow. The wake was assumed to remain symmetrical. Kudo's model used a Kutta condition, combined with a highly complicated force- and momentum-free nascent-vortex-placement scheme. Ikeda and Himeno (1981) studied the oscillating flow about a cylinder and a Lewis form. Separation points were assumed to be given by Schlichting's (1932) solution. As with Sawaragi and Nakamura (1979), they incorrectly retained the image vortices at the center of the cylinder. A relatively crude application of the multi-vortex model, with gross simplifications, to oscillating flow about two circular cylinders in tandem was attempted by Ikeda (1984a, 1984b).

Stansby and Dixon (1983) presented a two-dimensional method for calculating laminar flows around cylinders of arbitrary shape, in which the vorticity created at the surface at each time step was calculated using a boundary integral technique. Molecular diffusion even in the highly turbulent wake was simulated by random walks and the convection was performed with the VIC method. They have obtained reasonable agreement with experimental force coefficients and shedding frequencies in their simulation of steady and oscillatory flow about a circular cylinder. The details of the flow were not investigated and emphasis was placed on efficiency of computation. However, their calculations for $K=10$ failed to predict the transverse vortex street observed experimentally (see, e.g., Sarpkaya 1985, 1986a, 1986b). Obviously, it is necessary to match the flow patterns, not just the force coefficents. Tiemroth (1986a) criticized Stansby and Dixon (1983) for their failure to use an optimal method to satisfy the circulation condition and to give rigorously correct arguments in their derivation.

Van der Vegt and Huijsmans (1984), Van der Vegt and de Boom (1985), and Van der Vegt (1988) represented the body with straightline segments and constant source and vortex distributions, and used the random walk scheme with a variationally-optimized, grid-insensitive, blob-tracing algorithm, with as many as 20,000 blobs, to calculate the impulsively-started flow about a cylinder ($\mathrm{Re}=26{,}000$). They have amalgamated, "with the greatest care," the blob clusters "sufficiently away" from the cylinder and discarded those beyond a downstream boundary. Their results were strongly influenced by the choice of the time step. An optimum step of 0.045 yielded $C_d=1.34$ (mean), 1.66 (max), 0.99 (min), and 0.11 (RMS). With a time step of 0.15, "the calculated forces were considerably worse, despite the fact that the computed vortex structures looked reasonable." The separation points in Van der Vegt's (1988) optimized calculations are too large (see Fig. 18) and nearly correspond to those for a supercritical flow *even though the Reynolds number is only 26,000.* This is undoubtedly because of the pseudo-turbulence effects and premature transition produced by the algorithm (the noise due to bouncing blobs), as anticipated by Chorin (1973). It is rather surprising that Van der Vegt was able to obtain subcritical-flow drag coefficients for what appears to be a supercritical flow. Van der Vegt's (1988) calculations, with as many as 51,000 blobs, for the sinusoidally oscillating flow about a cylinder ($K=13.7$) failed to show a transverse vortex street but produced interesting flow patterns. Unfortunately,

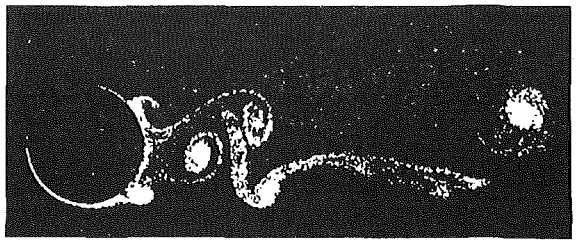

**Fig. 18(a) Computed vorticity field of the flow around a cylinder in uniform flow at Re = 21,000 (Van der Vegt, 1988)**

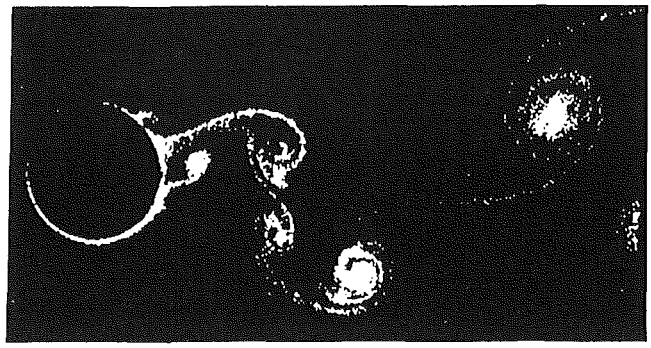

**Fig. 18(b) Same as Fig. 18(a) (at a different time)**

no in-line force traces were presented. The differences between the calculated (tabulated) statistical data (max, min, mean, and rms) for the force-transfer coefficients and those obtained experimentally (Sarpkaya 1976, 1987) are too large to be attributed either to cycle-to-cycle variations in the measured forces or to three-dimensional flow effects, as is often done in an attempt to account for the differences between the measured and predicted values and/or to justify the use of an artificial circulation reduction. In any case, Van der Vegt's simulations are restricted, for obvious reasons, to rather short times to draw any meaningful conclusions.

Skomedal and Vada (1985, 1987) and Vada and Skomedal (1986) used a slightly modified version of the code developed by Stansby and Dixon (1983) and P. A. Smith (1986) to calculate steady flow about a single circular cylinder in laminar and turbulent flow, supercritical flow around two cylinders in various configurations (see also Stansby, Smith, and Penoyre 1987), and the vortex-induced oscillations of a cylinder (see Sarpkaya 1978a, 1979). They used 15,000 to 100,000 discrete vortices and an eddy-viscosity model with constant mixing length (a combination of vortex methods and small-scale modeling to simulate turbulent diffusion in the wake) and found that even the smallest mixing length made the matters worse compared with the no-turbulent diffusion case. Moreover, they had to apply a circulation reduction to bring the measured and calculated results into closer agreement. As noted earlier, a decay law accounts not only for the three-dimensionality effects but also for the shortcomings of the numerical model and the nonlinear effects of other ad-hoc assumptions. These papers are marred with numerous misstatements and ad hoc assumptions and are motivated primarily by a desire to develop a computer code to calculate force-transfer coefficients for use in the design of offshore structures. The results are chiefly interesting in the particular context in which they were obtained, and detailed review would be out of place here.

Tiemroth (1986a) used a modified version of the random walk method together with the DVIC scheme (see Section 2.5.2) to calculate the impulsively started flow about a circular cylinder and to simulate the flow around a cylinder subjected

to regular free surface waves. He introduced a number of submerged singularity panels to satisfy the boundary conditions at the collocation points on the body. Futhermore, he modeled the vortex sheet as a "tent" function (a triangular distribution of vorticity), reflected the sheets about the wall when they passed through the wall, and used the Rankine vortex as the blob core function, a suitable metamorphosis between the sheets and blobs, two random walks and a modified Eulerian convection scheme with suitable "fixes."

Tiemroth (1986a), unlike Cheer (1983b), gave rigorously correct arguments in the derivation of his equations and numerical procedures whenever possible. As such, his work represents one of the more comprehensive descriptions of the random walk method, coupled with a clear understanding of the basic fluid mechanics. He was unable to calculate the shear stress and the pressure distribution because the interpolation functions used by him were not sufficiently smooth. The singular nature of the vortex sheets precluded the direct evaluation of the pressure from equation (6). He resigned to calculate the force through the use of the rate change of impulse, equation (47*b*), *ignoring the contribution of the vortex sheets* in the sheet layer.

Tiemroth had to choose eight free parameters (the sheet layer height, the length of the sheet generation panel, the cell size (all relative to $D$), the maximum sheet strength relative to $U_\infty$, the normalized time step $U\Delta t/D$, the number of Laurent series terms retained in the DVIC algorithm, the number of singularity panels, and the maximum slip relative to the maximum sheet strength (for which no sheet is generated), in addition to the Reynolds number. Thus, a complete parametric analysis was prohibitively laborious.

In spite of the enormous effort which went into the numerical experiment, Tiemroth's results were quite disappointing and mostly qualitative. He calculated the flow about the cylinder at Reynolds numbers of Re = 4,000, 9,500, and 95,000 at very small times (maximum $Ut/D = 3$ for Re = 9,500) and found that the force coefficients were insensitive to the variations in Re. Neither the drag coefficients nor the lift coefficents show any resemblance to those measured (Sarpkaya 1966, 1978b) or calculated (Thoman and Szewczyk 1969; Sarpkaya and Shoaff 1979). Tiemroth was unable to calculate a Strouhal number since the calculations could be carried out only for short times. Also, it was nearly impossible to determine the location of the separation points because the velocity field was quite irregular near the boundary. He assumed that "separation occurs near the point at which one first observes significant amounts of vorticity of opposite sign to that of the upstream boundary layer because the generation of vorticity reflects back flow." Using this subjective criteria, he obtained separation angles between 75 and 80 degrees (measured from the front stagnation point). His wave flow calculations were limited to very low Keulegan-Carpenter numbers ($K < 3$) at which inertia ($\pi\rho D^2 \dot{U}/2$) dominates the in-line force and the effect of separation is relatively small (Sarpkaya (1986b, Sarpkaya and Isaacson 1981).

The works of Van der Vegt (1988), Tiemroth (1986a), and others cast serious doubt on the ability of the random-walk method to deal with bluff-body flows. The major drawbacks of the scheme are the inability of the noisy blobs to represent the boundary layer for the intended Reynolds number, the very large CPU times, and the sensitivity of the results to numerous assumptions (e.g., blob characteristics, sheet layer thickness, and time-interval).

A finite-difference analysis of the Navier-Stokes equations for a sinusoidally-oscillating ambient flow about a circular cylinder at $K = 5$ (Re = 1000) and $K = 7$ (Re = 700) by Baba and Miyata (1987) shows that the calculations can be carried out only for short times (less than two cycles of flow oscillation) with a non-super computer.

Mostafa (1987), working with Sarpkaya and using multi-

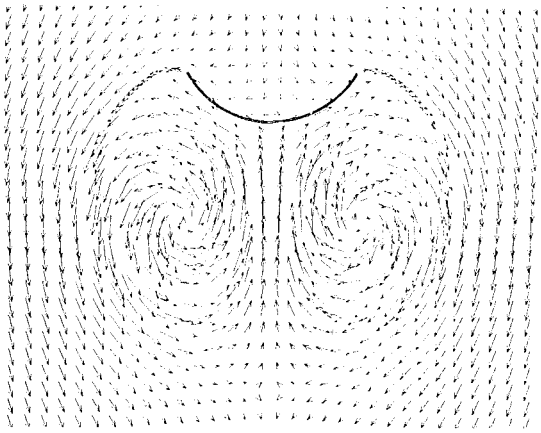

**Fig. 19(*a*) Unsteady flow past a 120-deg cambered plate (Mostafa, 1987; Mostafa et al., 1989)**

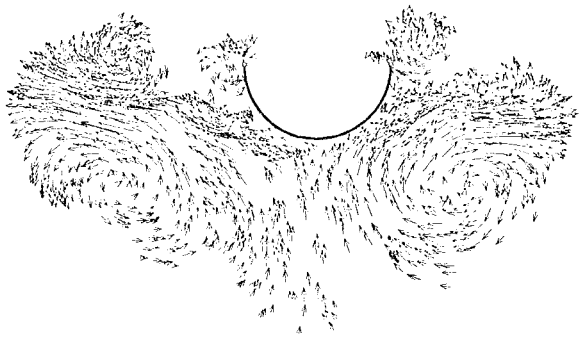

**Fig. 19(*b*) Same as Fig. 19(*a*) (a later stage of the decelerating flow)**

discrete vortices (with core), simulated accurately the sinusoidally oscillating flow about a circular cylinder and the decelerating flow about cambered plates (see Fig. 19). His calculations for $K = 12$ have reproduced correctly and for the first time the transverse vortex street observed experimentally (see, e.g., Sarpkaya 1985, 1986b). However, the calculated forces were somewhat larger than those measured (Sarpkaya 1976). No circulation reduction was used in the model (see also Sarpkaya et al. 1987).

The numerical simulation of steady flow past a circular cylinder undergoing in-line and/or transverse oscillations through the use of two-dimensional unsteady Navier-Stokes equations was undertaken by Lecointe et al. (1987) for relatively small amplitudes ($a/D = 0.13$). The results look very promising. During the past few years, the researchers at the Kuwahara Institute of Space and Astronautical Science (Tokyo) have obtained very impressive finite-difference simulations of unsteady flow about stationary and vibrating cylinders (see Fig. 20) (Tamura et al., 1988; Tsuboi et al., 1989; Kawamura et al., 1985, 1986; Himeno et al., 1985; Shirayama and Kuwahara, 1987; Obayashi and Kuwahara, 1987; Shirayama et al., 1987; Obayashi and Fujii, 1985, just to name a few) using super computers with vector processors with capabilities approaching 1 Gflops. Similar results at corresponding Reynolds numbers have not been achieved by vortex methods and are not likely to be achieved soon.

**3.3.2 Flow About Sharp-Edged and Arbitrarily-Shaped Bodies.** For sharp-edged bodies, various methods of determining the rate of circulation shedding may be made to produce indistinguishable results through judicious specification of the disposable parameters. As noted earlier, Giesing (1969) has shown that the flow must leave the edge tangentially to the windward side provided that the sheet is modelled by a continuous sheet of vorticity in the vicinity of the edge. Similar nascent-vortex introduction schemes were used by Soh and

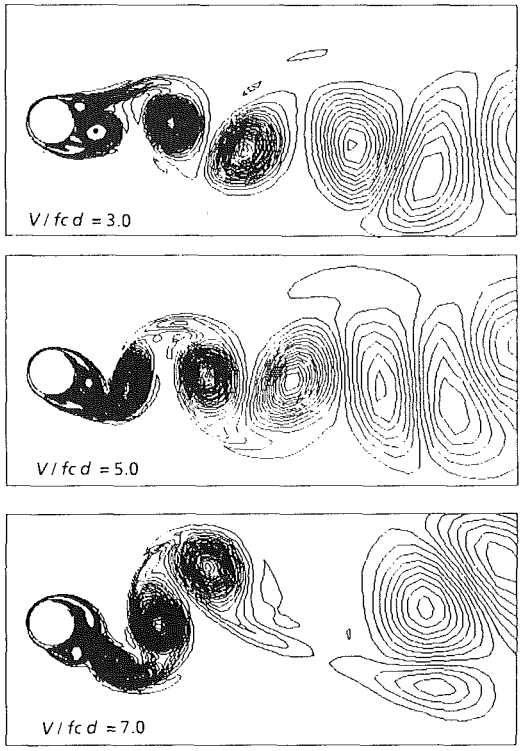


**Fig. 20 Forced vibration of a circular cylinder. Finite-difference solution of the Navier-Stokes equations (Tamura et al., 1988).**

Fink (1971), in their study of flow about bilge keels. However, when discrete vortices are used to introduce vorticity, the correct position of the nascent vortex does not necessarily lie on the tangent. Only the unique positions of the nascent vortex yield separation-velocity profiles that are compatible with the condition that in an inviscid flow the velocity and acceleration extrema occur on the body (Mostafa 1987). It turns out that the time step used, the separation point velocity, and the point of nascent vortex introduction are interrelated and none can be assigned arbitrarily or on the basis of trial calculations.

One of the earliest applications of the discrete vortex methods to sharp-edged bodied was made by Ham (1968) in connection with the aerodynamic loading of a two-dimensional airfoil during dynamic stall. His paper contains a number of original ideas, including the use of the amalgamation of vortices to avoid erratic motion.

Clements (1973b) used the Schwartz-Christoffel transformation to map the exterior region of a two-dimensional, square-based, half-infinite body into an upper half plane. The discrete vortices were superimposed on a steady parallel ambient flow. The Kutta condition was not invoked in this version of the model. Instead, the strengths of the nascent vortices were determined from $0.5\ U_s^2\ \Delta t$ where $U_s$ is the velocity in the plane of the rear face of the body a short distance out from the separation points. Subsequently, the model was modified (Clements 1973b, Clements and Maull 1975) and the nascent vortices were introduced a short distance $\epsilon$ downstream of the separation points, in the planes of the body sides, with strengths determined from the Kutta condition. The range of the disposable parameter $\epsilon$ was determined by trial computations using the stability of the Strouhal number and the form of the vortex cluster as criteria. The calculations gave reasonable Strouhal numbers and vortical structures. However, the model was unable to yield a usable base pressure coefficient. Standard values for the disposable parameters were determined and the model was applied to flow behind a blunt-based body with low velocity base bleed, to the cross-stream oscillations of the same body, to the flow behind a blunt-based section with a base cavity, and to flow down a step. The results of the first two cases correlated well with experiments but those of the last two (base-cavity and step flows) did not. Once again, calculations have shown that the use of vortex models requires an advance knowledge of the flow topology (such as the existence and possibly the position of the additional separation points). Deterministic means must be devised for the creation, placement and convection of vortices so as to reduce the disposable parameters. These will, in turn, help to distinquish the shortcomings of the model from the behavior of the actual flow and show which particular phenomenon controls or influences the observed differences between the experiments and predictions.

Kuwahara (1973) studied the impulsively started flow about an inclined plate for various angles of attack (30, 45, 60, 75, and 89 degrees) using a conformal mapping to transform the plate to a circle. The nascent vortices were introduced at fixed points along the edges of the plate and made to satisfy the Kutta condition. The calculated drag coefficient had a mean value about twice that found experimentally. Periodic vortex shedding was predicted but no Strouhal numbers were given.

Belotserkovskii and Nisht (1973) used discrete vortices to study the separated flow over a flat plate at angles of attack from 0 to 90 deg. They have used the Kutta condition (their Chaplygin-Zhukovskii condition) at the two edges of the plate. Other details were not presented. The calculated normal force coefficient was far in excess of that measured at the corresponding angles, save for the range of angles of attack from 30 to 45 degrees (see also Belotserkovskii and Nisht, 1974, 1978).

Sarpkaya (1975b) and Kiya and Arie (1977a, 1977b, 1980) have investigated the vortex shedding behind a flat plate at incidence to the flow. The former determined the strength of the nascent vortices from $d\Gamma/dt = 0.5U_s^2$ ($U_s$ being taken as the mean of the velocities of the four most-recently-shed vortices) and the position of the nascent vortices through the use of the Kutta condition. The calculated normal force coefficient was about 25 percent larger than the experimental values. Kiya and Arie fixed the position of the nascent vortices. The wake axis was not aligned with the ambient flow, indicating that equal amounts of vorticity were not shed from the two edges of the plate over many cycles of vortex shedding. Sheen (1986) simulated the vortical flow around a Joukowski airflow in unsteady motion, the dynamical effects on an oscillating airfoil with a free vortex in its vicinity, and the vortex shedding from an inclined flat plate. In the case of the flat plate, no forces were calculated and the comparison with experiments were confined to the kinematics of the flow. Basuki and Graham (1987) used the VIC method to calculate the impulsively started flow past a 11 percent-thick Joukowski airfoil at 30-degree incidence and concluded that the method predicts too strong a roll-up, an unrealistic suction peak, and excessively large fluctuations in lift. More realistic results were achieved through the use of a vortex decay technique, "provided the circulation removed is transferred so as not to affect the bound circulation." Shigemi (1987) used a relatively simple discrete vortex model to study the separated flow around airfoils. He calculated the effect of the total pressure loss on the lift and drag forces. The problem of the recirculating flow in a square cavity with one edge moving was simulated by Shestakov (1979) using the blob algorithm and an ADI finite-difference algorithm which solves block-tridiagonal matrices along each coordinate direction (Beam and Warming 1976).

Shoaff and Franks (1981) applied the model developed by Sarpkaya and Shoaff (1979b) to the analysis of flow about noncircular cylinders. Considerable difficulties were encountered with the determination of the separation points and the model was found to be very sensitive to the difference between the starting times of the shear layers (Franks, 1983). The

comparison of the measured and predicted drag forces (Sarpkaya and Kline, 1982) was only fair even after circulation reduction.

Nagano et al. (1982) analyzed the two-dimensional flow past a rectangular prism of height $h$ and depth $d$ through the use of an appropriate conformal mapping and the discrete vortex model. Suitable assumptions were made regarding the strength and position of the nascent vortices and the circulation reduciton. Their calculations have, in general, correctly predicted the trends in experimental results. However, the numerical model has failed to predict the large increase in the drag coefficient in the vicinity of $d/h = 0.62$. Inamuro et al. (1983, 1984) used the surface-singularity (discrete vortex) distribution model to calculate the flow around a square prism. They have found good agreement between the calculated and measured lift and drag coefficients over a range of incidences $\alpha = 0$ to 45 deg. However, the Strouhal numbers were too high. It appears that they were unaware of the earlier applications of this type of body and flow modelling. Their method does not satisfy the Kutta condition and the boundary vortices are allowed to shed downstream from the separation points (two front corners only). A random vortex simulation of wind-flow over a building is given by Summers et al. (1985).

Ribaut (1983) used vortex sheets and sources together with an ad hoc vorticity dissipation scheme to calculate the flow about a flat plate and a blunt trailing-edge section. Computed results compared quite well with those measured through proper selection of dissipation.

Sarpkaya and Ihrig (1986) investigated both experimentally and numerically the impulsively-started flow about rectangular prisms. The body and the shear layers were represented by discrete vortices. The condition of zero normal velocity on the body was satisfied by minimizing the error in normal velocity through the use of the method of least squares. The Kutta condition was used to determine the position of the nascent vortices and the Kelvin condition of zero total circulation is satisfied exactly. The vortices were assumed to be represented by a Lamb (1954) vortex. The force exerted on the body was calculated through the use of the generalized Blasius theorem. Comparison of the predicted and measured forces showed reasonably good agreement with respect to the frequency of the oscillations, i.e., the Strouhal number is correctly predicted. However, the amplitudes of the predicted forces are somewhat larger. A numerical solution of this problem at Reynolds numbers less than about 1000 (through the use of special finite differencing schemes for time and convection) is given by Davis and Moore (1982) and Davis et al. (1984).

Vortex shedding from sharp-edged cylinders and plates in steady and oscillating flow was investigated by Graham (1977, 1980, 1985) and by Naylor (1982), working with Graham, through the use of three methods (Brown and Michael model 1954, multi-discrete-vortex model, and the CIC method). Their results have shown that oscillatory flow at low Keulegan-Carpenter numbers can be represented quite accurately. At higher $K$, the two-dimensional vortex models tend to overestimate the vortex shedding and induced forces without modelling of secondary separation or three-dimensional effects (through the use of an exponential circulation decay "law"). The application of the vortex methods to the prediction of the hydrodynamic damping and the nonlinearities in the responses of barge-like bodies in still water is made by a number of investigators (see, e.g., Brown and Patel 1981), Faltinsen and Sortland, 1987, Ikeda and Himeno, 1981, Patel and Brown, 1986, Downie et al., 1988).

Spalart (1982) and Spalart et al. (1981, 1983) described several codes to calculate separated flow about various bluff bodies (squares, airfoils, tilt-rotor wing). The flow is divided into two regions: an inviscid outer flow and a viscous inner region. The inner layer is represented by a piecewise-linear vortex sheet of zero thickness. The outer region is represented by discrete vortices of constant core radius. The flow in the inner region is solved by finite difference discretization in space and an implicit method in time. In addition, the Baldwin-Lomax (1978) algebraic turbulence model ("zero-equation" model) is used with some modifications. Spalart (1982) had to introduce numerous ad-hoc assumptions (filtering and truncating of the radial position of the vortex sheet, artificial dissipation, thickness of the inner layer, core radius, coupling algorithm, just to name a few). He used vortex merging, when some conditions were satisfied (the original version of the DVIC scheme). The codes developed were not able to produce satisfactory results, as judged by experiments, even with the most judiciously selected values of the arbitrary parameters. No rolling-up of the vortex sheets were discernable, and the drag coefficents were relatively low. For the circular cylinder, the drag coefficient decreased steadily as the Reynolds number increased from $10^4$ to $10^7$. No drag crisis was observed. Spalart attributed the shortcomings of his models to the "transition" of the separating shear layers, the difficulty of handling the flow around sharp corners (square body), the delicate nature of the coupling algorithm, the three-dimensional character of the real flow, the interference with the wind-tunnel walls, etc. The real difficulty with this or similar schemes is that it purports to solve the viscous flow problem near the boundary of high-Reynolds number flow by sidestepping the enormous difficulties encountered with the finite difference schemes and through the use of various artifices which, in turn, require numerous ad-hoc assumptions. It may work for one or two problems but there is no assurance that it will work for a broader class of separated flow problems. It appears that there are no simple detours around the difficulties encountered by the finite difference schemes, at least not with strongly singular vortex sheets and sensitive coupling schemes.

Mostafa (1987) and Munz (1987) analyzed decelerating flow about cambered plates through the use of discrete vortices. Nascent vortices were introduced in such a manner that the conditions of Kutta and the occurrence of velocity and acceleration extrema on the body were satisfied at each time step. No circulation reduction was used in the calculations. The measured and predicted forces were found to be in reasonable agreement, primarily because the calculations were limited to the early stages of the decelerating flow.

**3.4 General Three-Dimensional Flows.** A number of three-dimensional flow examples are described by Leonard (1980a, 1980b, 1985) and by Leonard et al. (1985). These include the interaction of vortex rings (Parekh et al. 1983), interaction of solitons on a rectilinear vortex (Aref and Flinchem, 1984), instability of vortex rings (Ashurst, 1981), and the evolution of the time-developing round jet (Ashurst, 1983). These examples show the underdeveloped state of the three-dimensional vortex methods, the extra cost for carrying out the calculations, and the great difficulty in comprehending the results (without three-dimensional multi-color graphics).

The growth of a turbulent spot in a laminar boundary layer, as the spot evolves from a localized disturbance in the layer, was simulated numerically by Leonard (1980b) using a vortex filament discription of the vorticity field. Each filament is represented by space curve $x_i(\xi,t)$, where $\xi$ is a parameter along the curve, by a circulation $\Gamma_i$, and by an effective core radius $\sigma_i$, which parametrizes the assumed Gaussian vorticity distribution within the filament. The generation of new vorticity at the wall due to the "no slip condition" is ignored. Equation (13*b*) suitably modified to account for the laminar base flow and the contributions of the images, is used to calculate the motion of the space curves. Leonard found that the gross properties of the spot *away from the wall*, including the velocities of the leading and trailing edges and the velocity

perturbations, are in good agreement with experiment. Leonard's work should be contrasted with the direct numerical simulation of turbulent spots in plane Poiseuille and boundary layer flow by Henningson et al. (1987).

DeBernardinis et al. (1981) studied the unbounded oscillatory flow around a disk and the bounded oscillatory flow through a sharp-edged orifice. The shed vortex sheet is represented by a sequence of discrete vortex rings and the solid bodies by a distribution of bound discrete vortex rings whose strengths are chosen to satisfy the Neumann or zero normal velocity boundary condition. In general, the gross properties of the flows are predicted accurately.

Ashurst and Meiburg (1988) presented a numerical study of the evolution of the two- and three-dimensional instabilities in a *temporally growing* plane shear layer. They included two signs of vorticity to account for the effect of the weaker boundary layer leaving the splitter plate and used continuous filaments described by cubic splines with second-order integration in space and time. The calculations through the use of equation (13*b*) have only been carried out until the initial filament arclength doubled because of the diminishing timestep and the increasing number of node points. These bounds resulted from the need to deal with *node depletion due to large strain effects*, i.e., from the repeated remeshing of the filaments so as to keep the arclength between the nodes always less than the filament core diameter but more than half of the initial core radius. Ashurst and Meiburg demonstrated the formation of concentrated streamwise vortices in the braids (the two sleeves connecting neighboring spanwize rollers) as observed in the experiments of Lasheras and Choi (1988) with *spatially-growing* mixing layer with similar perturbations. Meiburg, and Lasheras (1988) carried out an experimental and numerical investigation of the three-dimensional transition in plane wakes and demonstrated, among other things, that important features of the development of the three-dimensional evolution can be reproduced by vortex methods (identical in most respects to the one used by Ashurst and Meiburg 1988) even at Reynolds numbers as low as 100. Ghoniem et al. (1987a) and Knio and Ghoniem (1988) applied the *vortex-ball* version of the three dimensional scheme to the numerical simulation of vortex rings with finite and deformable cores (see Fig. 21) and to the simulation of streamwise vorticity in a periodically excited planar shear layer of finite thickness. An interesting three-dimensional flow visualization and numerical analysis [through the use of equation (12)] of a coflowing jet is given by Agui and Hesselink (1988), with an eddy captured in a hologram for the reader! The method appears to be a useful tool for topological analysis of complex structures.

**3.5 Other Applications.** There are numerous other applications of vortex methods which do not fit conveniently into any of a few broad categories. Inoue (1985b) used the multi-discrete-vortex model to simulate the flow past a porous plate (e.g., a rigid flat parachute). The nascent vortices were introduced at two fixed points near the edges of the plate $[at \pm (1+0.1)i]$ and the strength of the vortices was determined from the Kutta condition. A variable time step was used to limit the amount of convection of the vortices. No asymmetry was introduced and no amalgamation was employed. Consequently, the calculations were restricted to relatively small times. The predicted flow kinematics were in good qualitative agreement with those obtained from flow visualization.

McCracken and Peskin (1980) combined a finite-difference method with the vortex blob algorithm to study the flow of a viscous fluid through the mitral valve of the human heart (see also Peskin, 1972, 1977, 1982, and Peskin and Wolfe, 1978).

Special unsteady vortical flows have been investigated in connection with dynamic stall around an oscillating wing (McAlister and Carr, 1979; Sheen, 1986) and in connection

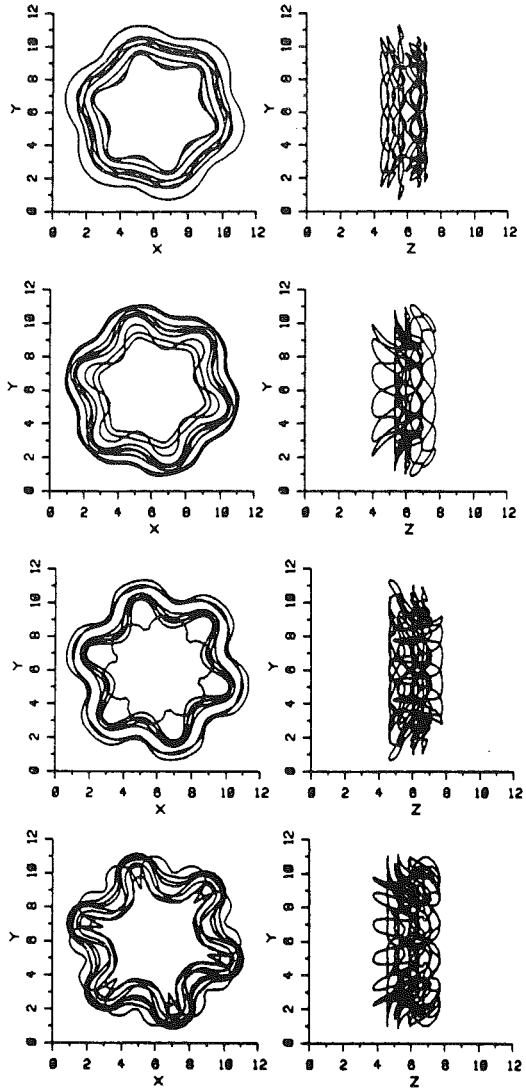

**Fig. 21 Evolution of the unstable mode of a vortex torus with $\sigma/R = 0.35$, perturbed at $t = 0$ with $\epsilon/R = 0.02$ and $n = 6$ (Ghoniem et al., 1987a)**

with the explanation of extra lift generated by some fish and cetaceans in propulsive movements (Savage, 1979, Maxworthy, 1981). Strickland et al. (1979) used a vortex lattice method to study the aerodynamic performance of the Darrieus turbine and obtained satisfactory agreement between the measured and calculated normal force.

Panaras (1985, 1987) and Poling et al. (1987) used a conformal transformation and discrete vortices to simulate the interaction of a blade and a foil with vortices drifting with the free stream. Their results have shown that forcing frequencies higher than the frequency of vortex passage can be anticipated (see also Dickinson, 1988 who used blobs). Mathioulakis and Telionis (1983) used a combination of conformal mapping, a cut-off length to limit the velocities, and distribution of bound vortices to model the flow through a cascade of blades. The results illustrated how the developing wake of one blade influences the flow over the next blade and eventually induces stall. Recently, Hsu and Wu (1988) developed a vortex flow model for the two-dimensional blade-vortex interaction, introduced a new trailing-edge flow model (unsteady Kutta condition), and developed closed-form solutions for the vortex-induced unsteady force.

Random vortex models have been applied in recent years to "turbulent" combustion in open and closed vessels (Sethian, 1984), to the formation and inflammation of *planar* turbulent

jets (Cattolica et al., 1987; Ghoniem et al., 1986 who used the so-called dipole-in-cell scheme), and to turbulence-combustion interactions (Ghoniem et al., 1987b) in a reacting *two-dimensional* shear layer through the use of a new transport element method (a generalized Lagrangian particle scheme which is constructed to compute solutions of convective-diffusive-reactive scalar transport equation). The work of Cattolica et al. is particularly interesting for it deals with an axisymmetric flame development and offers a comparison of the predicted flame shapes with those obtained through laser-schlieren visualization. In general, it is assumed that stochastic methods can be used to model the fluid mechanics with the reactive flame front viewed as a flame sheet with infinitely fast chemistry. Even if a connection between the random vortex scheme and turbulence were to be established, it is not applicable to unsteady combustion problems that require a deterministic approach, as noted by Cattolica et al. (1987). Turbulent flow is inherently three-dimensional and the flame speed in such an environment depends strongly on flame stretch. There are a number of other factors which limit the utilization of the vortex methods to study combustion problems. In this connection, the experimental findings of Broadwell and Dimotakis (1986) regarding the modeling of reactions in turbulent flows and the informative review of Spalding (1986) on the application of the two-fluid model of turbulence to combustion phenomena are worth noting.

The application of vortex methods to sound generation by nominally steady, low Mach number, mean flow over a cavity has attracted some attention (see, e.g., Hardin and Block, 1979, Hardin and Mason, 1977, and Breit et al., 1988). The last investigators have found that the Strouhal number at the peak of the broadband noise spectrum is in the range of the lowest-order edge tones rather than being well above the edge-tone Strouhal numbers as predicted by Hardin and Mason (1977).

*3.5.1 Contour Dynamics.* Zabusky et al. (1979) presented a *contour dynamics* algorithm for the Euler equations in two dimensions as a generalization of the so-called "water-bag" model used to study plasma dynamics. By truncating the accessible range of spatial scales, it is applied to the two-dimensional, nonlinear evolution of *piecewise-constant* vorticity distributions, within deformable finite-area-vortex regions (bounded by contours of vorticity discontinuity), in an inviscid, incompressible and unbounded fluid. Thus, it is a method to deal with the interaction of closed contours (two-dimensional, homogeneous, deformable, jelly-like creatures) rather than with the interaction of the individual vortices within a contour. Nodes are added or deleted as contours elongate, merge, and even undergo "surgery" (to systematically eliminate small scales of motion and thus, to minimize scale-resolution requirements and the CPU time, Dritschel 1988b). The motion of a fluid particle depends only on the instantaneous positions of the contours of vorticity discontinuity (see Fig. 22) and is given by the following sum of contour integrals (Deem and Zabusky, 1978, Dritschel, 1986, 1988a, 1988b)

$$\frac{d\mathbf{x}}{dt}=\mathbf{u}(\mathbf{x})=-\frac{1}{2\pi}\sum_{k}\tilde{\omega}_k\oint_{C_k}\log\left|\mathbf{x}-\mathbf{x}_k\right|d\mathbf{x}_k \qquad (48)$$

It has been shown that when two or more deformable vortex regions come sufficiently close, self- and mutual interactions cause vortex pulsation, temporary-and-permanent coalescence, and the ejection of vortex arms. The stability calculations of Saffman and Schatzman (1981, 1982a, 1982b) support Zabusky et al.'s (1979) conjecture that an asymmetric Karman vortex street with $b/a=0.281$ is stable or has at least a slow instability, because of the damping provided by self-consistent wavelike deformations of the finite area vortex

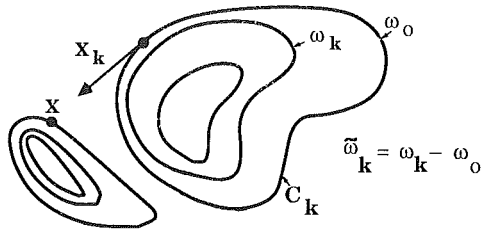


**Fig. 22 Definition sketch for the contour integrals in contour dynamics (Dritschel, 1988)**

regions. For detailed discussions and application of the contour dynamics algorithm and its motivations, the reader is referred to Christiansen and Zabusky (1973), Zabusky (1980, 1981), Dritschel (1986, 1988a, 1988b), and, in particular, to Melander et al. (1987) to find out which vortex is "victorious".

**3.5.2 Chaos With Few Singularities.** The mutual interaction of a number of line vortices in two-dimensions has attracted some attention due to its direct connection with "chaos." (see, e.g., Aref, 1983, 1984, Aref and Kambe, 1988). As noted by Keller (1984), "The extensive verbal and graphical descriptions of chaotic solutions have not yet been condensed into a few general principles."

The existing state of knowledge may be summarized as follows. The equations describing the motion of line-vortices in an arbitrary domain are a Hamiltonian dynamical system, i.e., equation (20) may be written as (see, e.g., Aref 1984)

$$\Gamma_k u_k=\frac{\partial H}{\partial y_k}\quad,\quad \Gamma_k v_k=\frac{\partial H}{\partial x_k} \qquad (49a)$$

where

$$H=-\frac{1}{2\pi}\sum_{1\le k\le j\le N}\Gamma_k\Gamma_j\log|z_k-z_j| \qquad (49b)$$

For a general flow geometry, the motion of $N$ vortices beyond a maximum number $N^*$ is chaotic, i.e., sufficient uncertainty in the values of the initial conditions leads to an unpredictable, unknowable, or uncertain state (but not to a hierarchy of scales). It has been generally agreed that an accurate enough knowledge of the past may enable one to make reliable predictions about the future. It turns out that this is not necessarily true. In laboratory experiments, as in astronomy, the initial conditions are never given or precisely definable. Mathematically, it was possible to avoid this question and speak of *given initial conditions*. It is now realized (as anticipated by Poincare, 1893), through analysis and numerical experiments with idealized singularities (vortices, sources and sinks, never mind the fact that an inviscid vortex cannot be turned on and off at will!), that there are systems where any finite-precision information about the initial conditions does not necessarily lead to finite-precision information about the later stages of the motion. Such systems are said to be nonintegrable.

Chaos is not difficult to arrive at by numerical simulation. In fact, in the case of vortices in an unbounded domain, the calculations are almost trivial. One only needs equation (20), a sufficient number of vortices, an integration scheme, and a computer (preferably a super one). The motion of $N^*=3$ vortices in an unbounded domain is integrable. For $N\ge 4$, the motion is nonintegrable. Rigid boundaries lead to a reduction in the number of real (as opposed to image) vortices sufficient for chaotic behavior (a simple example with $N=1$ is given by Sarpkaya, 1986a). Note that this has nothing to do with body-vortex interactions which tend to cause a faster transition to three-dimensionality. For circulation-driven chaos, integrability or nonintegrability is dependent not only on the number of vortices and the presence or absence of rigid

boundaries but also on the background potential flow into which the vortices and their images are imbedded. Chaotic advection is a kinematical feature independent of the momentum equations governing the flow and can take place *without circulation about any fluid contour*, i.e., one does not have to have a vortex system; a pulsed source-sink system will do just as well (Jones and Aref, 1988).

The dynamics of a few potential line vortices or other singularities cannot deal with the effects of viscosity, finite vorticity, self-induction, spanwise mutual induction instability, and vortex stretching. Thus, it does not deal with turbulence. As noted by Aref (1984) "chaotic few-vortex systems are essentially laminar flows with stochastic properties. Organized vortex structures, on the other hand, are regular flow patterns in otherwise stochastic velocity fields. Neither fits comfortably into the inherited hierarchy of laminar versus turbulent."

There are some fundamental questions regarding the type of flow simulated by vortex methods which have not yet been adequately dealt with by any researcher. These questions stem partly from the use of such concepts as chaos (often meaning turbulence) and large-scale coherent and small-scale incoherent structures (implying that there is nothing in between), and partly from the application of personalized criteria of credibility to the various numerical simulations. The opinions (too many to reproduce here) run from noncommittal prologues to highly exaggerated claims. However, it is generally agreed that (i) the behavior of a "*many-vortex system*" (exhibiting large coherent structures rather than chaotic dynamics with many degrees of freedom) is not an extrapolation of the behavior of a "*few vortex system*" (structureless chaos, uniform disorder), (ii) with suitable refinement of the relevant numerical parameters and ad hoc "theories," vortex models may be made to predict (often qualitatively) the dynamics of large scale coherent structures which in turn determine all the dynamics of the flow, assuming that there are essentially two scales (large and small) and the effect of interactions between small-scales (surely chaotic, three-dimensional and significant contributors to stresses) and large-scale structures (sometimes periodic) is negligible (it is a well-known fact that the various scales of turbulence interact), (iii) the large scale structures are superimposed on a background of turbulence or, perhaps more accurately, *vice versa* (Roshko, 1976), and (iv) what is calculated is neither a laminar nor a turbulent flow with correct physics throughout the flow. It is often a noisy, "laminar-like," flow at a reduced Reynolds number or a "turbulent-like" flow with a constant eddy viscosity, (see Section 3.1 and Peters and Thies, 1982). What is missing from the two-dimensional simulations is the three-dimensionality of the flow, enormous range of scales (a factor of about $10^5$ between the largest and smallest eddies), and the excitation of many degrees of freedom which constitute the very essence of turbulence (see, e.g., Aref, 1983, 1984).

## 4 Conclusions

A numerical model must accurately reproduce a large class of experimental observations and measurements with only a few disposable parameters, and it must make definite prediction about the results of future physical experiments. How well did the computational models with vortices fare? To try to answer this question we have given a nearly full account of the theoretical foundations and practical applications of various methods, models, and schemes. Based on this background, partial answers, undoubtedly to be refined in future years, may be provided as follows.

The numerical realization of Helmholtz's powerful concept, that flows with vorticity could be modeled with line vortices of "infinitely small cross section" (quantum vortex lines), turned out to be anything but simple and revealed the complex nature of the problems to be resolved in dealing with real fluids. These problems are subtle, and difficult to assess unambiguously, as evidenced from the following digest: (i) Kelvin-Helmholtz instability, sheet crossings, and chaotic motion of vortices (distinct from that of a few vortex systems) gave rise to various smoothing schemes (e.g., velocity cut-off, rediscretization). (ii) Body representation, creation of vorticity, specification of the strength and position of the nascent vortices, determination of separation points, and the asymmetry introduction led to the use of the approximate boundary-layer equations and the Kutta condition in steady and unsteady flows. (iii) Inability to deal with three-dimensional flow effects, vortex stretching, and the annihilation of vorticity in the overlapping regions of oppositely-signed vorticity led to the use of ad-hoc vorticity-reduction schemes. (iv) Lack of a meaningful definition of the scale effects (Reynolds number) confined calculations to unknown "high Reynolds number Flows," and the comparisons with experiments to cases where such comparisons appeared to be "reasonable" (not an uncommon occurrence in science). (v) Computer time and storage demands, though not too excessive relative to those for the operator-splitting methods, forced the development of numerous time-saving schemes (e.g., the VIC scheme, merging of vortices, fast algorithms). Contrary to common belief, however, the long CPU time is not the greatest impediment to the effectiveness of vortex methods. Rather, it is the necessity to introduce and to deal with a large number of disposable parameters that constitutes the most serious drawback. (vi) The difficulties associated with the assessment of validity or the range of the validity of the numerous, non-linearly related, ad hoc schemes and attempts to imitate the high Reynods number "two-dimensional" flow experiments, by suitably adjusting disposable parameters until some features of the observed phenomena are mimicked, turned each application into a new model. Consequently, no single line-vortex model emerged that can be applied to a wide variety of flows. However, practically all well-disciplined and well-documented multi-line vortex models predicted results which are neither too far from those of the "nearly-two-dimensional" experiments nor sufficiently free from ad hoc assumptions (even if some disposable parameters spanned only over a narrow range). Nevertheless, these models do not, in the strictest sense, fulfill our stated requirements for a satisfactory numerical model. It is entirely possible that vorticity does not like to be discretized.

The introduction of vortices with non-deformable finite cores (blobs and vortons) reduced the propensity of the vortices to sprint and to orbit about each other, but created a whole host of new problems. Finite-cored vortices violate Helmholtz's law that vorticity is a material quantity, i.e., the rigid-blob idealization is not dynamically consistent. If the vortices are created, convected, and diffused in a viscous fluid (where vorticity is not a material quantity), then one encounters another kind of problem: The nonlinearity of the Navier-Stokes equations does not permit the superposition of finite-cored vortices, not even the sum of two Lamb vortices in an unbounded medium.

The foregoing confronted the researchers with a choice between Helmholtz's infinitesimal vortices and finite-cored rigid blobs, and their respective undesirable features and incalculable consequences. It seemed that on could minimize the nonlinear effects of the Navier-Stokes equations by significantly increasing the number of blobs, by forcing them to overlap, and by judiciously choosing the cut-off radius and the shape of the velocity cut-off function. The use of the Navier-Stokes equations and the creation and diffusion of vorticity in real fluids gave rise to the operator-splitting and random-walk methods. It seemed, at least when it was first introduced by Chorin (1973), that the vortex methods finally arrived at a level which could let vorticity convect and diffuse

itself according to the laws of motion and take care of the scale effects. However, closer scrutiny during the past fifteen years has consistently revealed serious problems and, indeed, the promise of the method outweighed the results presented since its inception. The implied explicit link between the blobs, the operator-splitting scheme and the Navier-Stokes equations became as much obscured as that between the line vortices of Helmholtz and the classical discrete vortex models because of a number of complex problems. These are nonlinear, subtle, and difficult to assess unambigously, as shown by the following brief summary: (i) None of the applications of the operator-splitting method managed to produce quantitative results, in good agreement with analytical solutions or physical experiments, without the use of an ample doze of disposable parameters subjected to successive stepwise refinements (e.g., the size, spacing, number, and the maximum circulation of blobs). (ii) The demands for computer storage and time increased by one or two orders of magnitude, confining the calculations to large computers or to shorter times (early stages of flow) or to smaller Reynolds numbers and requiring fast algorithms or the vortex-in-cell techniques. The use of the VIC scheme brought back the grid and, along with it, diffusion and the confinement effects. (iii) The statistical nature of the results required the averaging or smoothing of the velocity and pressure distributions and integrated quantities (e.g., lift and drag forces whose instantaneous values often do exhibit unrealistically large variations). (iv) The number of physical parameters, ad hoc schemes, and convection fixes became very large, making a parametric analysis of their separate as well as combined effects on the predicted results practically impossible, notwithstanding the convergence proofs and arguments regarding the robustness of the algorithms devised. (v) All of the convergence proofs dealt with laminar flows in the absence of boundaries, assuming a sufficiently smooth initial blob distribution. Excluded from the proofs is the fact that the diffusion of vorticity is affected by the wall proximity and by the boundary layer where the vorticity is not smoothly or uniformly distributed, initially or at any other time, (particularly near the separation points). *The noise of the bouncing blobs causes premature transition in the boundary layers.* In fact, the works of Van der Vegt (1988), Tiemroth (1986a), and others cast serious doubt on the ability of the random-walk method to deal with bluff-body flows. (vi) In regions of turbulent flow (wake and/or boundary layer), random walk does not make sense since viscous diffusion relative to turbulent diffusion is negligible. (vii) Turbulent flows require turbulence models to simulate small scale structures since random walk (without the use of a turbulence model) does not simulate turbulent diffusion or its consequences. There is, in fact, no proof that random walk at any Reynolds number produces anything other than viscous diffusion (except, of course near the boundary where vortex sheets and blobs, like a swarm of vorticity-flies, create a great deal of unwanted noise, and symptomatic transition). Thus, operator-splitting methods solve only laminar flow problems at small Reynolds numbers in a relatively more crude fashion than finite-difference methods. "If the diffusion process is to be considered turbulent, then the choice of the turbulent diffusion coefficient and the turbulent length scale distribution are unknown input parameters." (viii) The blob must be regarded as mathematical artifices to limit velocity since vorticity carrying, non-deforming, fluid elements cannot occupy the same space at the same time. (ix) The evolution of large local strains increases the blob spacing relative to the core radius (local blob population depletion) and can lead to large errors in the resolution of the vorticity and the velocity field, and the calculations may be carried out only for relatively small fluid displacements. The use of sub-blobs to repopulate the areas depleted by large strains causes a further blob-population explosion. The velocity fields before and after reblobbing are not the same in the vicinity of the new blobs.

The mismatch between model-based predictions and experimental results is not entirely due, or always attributable, to deficiencies in the model, but also lies in the three-dimensional nature of "two-dimensional" experiments. All vortex calculations show that the three-dimensional nature of the flow cannot be ignored. Clearly, flows known to be highly three-dimensional cannot be modelled with two-dimensional vortex dynamics. However, the application of vortex methods to three-dimensional flows is limited to relatively simple cases, yielding only qualitative information, often in unbounded domains, and requiring a healthy doze of approximations and a great deal of case-specific ingenuity. According to Ashurst (1987), the existing three-dimensional vortex methods suffer either from short wavelength instability of the connected vortex filaments or from the lack of spatial resolution when disconnected vortons or vortex sticks are used. As far as the three-dimensional bluff-body flows are concerned, again, we do not expect more than qualitative simulations in the laminar flow regime, requiring a large number of ad hoc "theories." These pessimistic remarks are tempered by the fact that the most significant results are often qualitative judgements which provide insights into the real physics of the phenomenon. This is in conformity with the more modest objectives of vortex models: identification of large-scale structures and acquisition of new insights. There seems to be general consensus that large scale structures rising above (or floating over) the small scale turbulence can be calculated qualitatively (and sometimes quantitatively, if the disposable parameters are carefully tuned); if the large-scale structures do not become quickly three-dimensional (or do not have the propensity to become three-dimensional as in the case of turbulent wall-bounded flows); if the large structures do not reside too long in a nearly confined region (e.g., in a recirculation zone), so as not to suffer excessive diffusion; and if the flow is in an equilibrium or weakly out-of-equilibrium state. Thus, the early stages of two- and three-dimensional flows without walls (free shear layers, vortex rings and their interaction, two-dimensional combustion based on scalar mixing), the early stages of two-dimensional and axisymmetric flows about bluff bodies (preferably with sharp corners), and the transient flow over airfoils and control surfaces can be simulated with relatively greater confidence and fewer assumptions than the subsequent nonlinear regimes. Some sort of "surgery" on the flow structures is needed to systematically eliminate small scales of motion in order to continue the calculations (e.g., filtering of filaments to remove sections where the radius of curvature is less than the core radius) (see Ashurst and Meiburg, 1988, Dritschel, 1988b).

The relative advantages and disadvantages of the Lagrangian and finite difference techniques have been pointed out by many investigators (see, e.g., Rizzi, 1987, Ashurst and Meiburg, 1988) and remains a subject for future study and, no doubt, vigorous debate. Often cited among these are the grid-free nature of the vortex methods and the exact treatment of the boundary conditions at infinity, (without the use of the VIC scheme); the need to deal only with vorticity, where it exists, rather than with velocities and pressure at every node point on a finite grid (i.e, concentration of the computational resources in a limited spatial domain); the better suitability (with proper smoothing!) of the Lagrangian method to deal with transient problems where vorticity regions have large deformation with steep gradients (which is hardest for finite difference methods); the advantages of vortex methods when vorticity fills the computational volume, more or less uniformly; the large CPU times for both methods (Biot-Savart law versus finite differencing over a large number of grid points); the need for a number of ad hoc assumptions in each method, particularly in vortex methods; the artificial diffusion in grid con-

vection schemes versus convection errors in the Lagrangian trajectories; inability of either technique to deal with turbulence without the use of turbulent diffusion or a sub-grid model (e.g., a sub-grid-scale eddy-viscosity model); the ability of the discrete vortex models to deal with flows of unknown topology (through the use of various smoothing schemes); the advantages of panel methods in dealing with wing vortices when the overall topology is known; and other advantages and disadvantages presented and discussed in this review. It must be emphasized that such a comparative listing is somewhat artificial and does not do justice to the subtleties of either method. Only the challenging problems and expectations bring out the best and the worst in them. The problem and what one expects and wants to do with the answer, rather than the exaggerated claims made on behalf of each method, will determine to a large extent whether one wants to follow the vorticity field or the velocity field. In either case, the code solves only an idealized mathematical problem and the results must be interpreted in view of the real physics.

In the midst of the remarkable progress made so far, it is rather difficult, if not dangerous, to speculate as to what is likely to happen in the future. Nevertheless, we expect that the territory of small-scale structures will remain impenetrable in the foreseeable future by any method or computer. The temptation to appeal to turbulence effects to justify the use of rather arbitrary parameters will not diminish. Some of the ad hoc assumptions will move into the "well-established facts" column as the congregational empathy and sample calculations and predictions with a given code increase. Demarcation of the areas of application of the various methods will be further blurred and there will be greater joint use of both methods (Eulerian and Lagrangian) on a given problem (e.g., treating the boundary regions by finite-difference techniques and convecting vorticity away by Lagrangian techniques), so that methods of the future may be hybrids. The Eulerian and Navier-Stokes finite-difference methods will benefit more from the progress to be made on computers (hyper-computers?), numerical theories (reduction of truncation errors and artificial dissipation), and simulations (e.g., computation of flow about geometrically complex configurations, hydro- and aeroelastic response of bodies, various compressible and incompressible unsteady flow phenomena, dynamic response of lifting bodied, combustion, and better assessment of the turbulence models). However, the finite-difference methods will not replace computational methods with vortices as a research tool, but they will complement and supplement them invaluably. The classical vortex methods, *preferably for bluff body flows* (using separation points, line vortices or blobs, no forced viscous diffusion), the operator-splitting method, *preferably for shear layers, laminar flames, and combustion* (using blobs, random walk, and the VIC scheme, and the spectral algorithms), and the panel methods, *preferably for vortical flows in aerodynamics* (in competition with Euler and Navier-Stokes codes) will continue to exist and flourish through complimentary numerical and physical experiments as long as they maintain demonstrable advantages over other methods. They may even be able to make definite predictions about the results of future experiments if they are tuned to the physics of the flow. In any case, the enigmatic smile of computational methods with vortices will continue to attract new admirers who, like the others before them, will try to minimize the existing deficiencies of these methods, bring new insights, pose new questions, and rediscover the power of the rich and remarkable concepts set forth 130 years ago by Helmholtz.

## Acknowledgments

This review was made possible by the Freeman Scholar Program in Fluids Engineering of the ASME. The author is grateful to the Program and the the Standing Committee of Professor A. J. Acosta, Dr. J. L. Dussourd, and Professor R. E. A. Arndt, for their encouragement and confidence.

The author wishes to express his sincere thanks to all those on whose work he has so extensively drawn to produce this review. Many people have responded generously to the author's requests for advice, references, advance copies of papers, reports, and theses, and/or the originals of some figures. The author is particularly indebted to (in alphabetical order): Professor H. Aref, Dr. Wm. T. Ashurst, The Honorable Judge Avni Ataisik, Dr. G. R. Baker, Professor S. A. Berger, Professor A. Cheer, Professor A. J. Chorin, Professor C. Y. Chow, Professor C. Dalton, Professor A. F. Ghoniem, Professor H. Hasimoto, Professor O. A. Kandil, Professor R. Krasny, Professor A. Leonard, Professor C. C. Mei, Professor P. G. Saffman, Professor P. K. Stansby, Professor D. P. Telionis, Dr. E. Tiemroth, and Dr. J. J. W. Van der Vegt for making his task a little easier during the past fifteen months. Professors A. J. Healey and P. J. Marto, author's friends and colleagues at the Naval Postgraduate School, read and commented on earlier drafts of this paper. The author has been fortunate to be associated with students whose work is referenced here: CAPT N. J. Collins, LT J. J. Daly, CAPT M. D. Davis, LCDR J. E. Elnitsky, Professor G. L. Hiriart, CDR C. J. Ihrig, CDR H. K. Kline, LCDR R. E. Leeker, Dr. S. I. M. Mostafa, LCDR P. D. Munz, and Dr. R. L. Shoaff. Author's and his students' projects referred to herein were supported by the National Science Foundation, the Office of Naval Research, and Defense Advanced Research Projects Agency.

## References

Abernathy, F. H., and Kronauer, R. E., 1962, "The Formation of Vortex Streets," *J. Fluid Mech.*, Vol. 13, pp. 1–20.

Achenbach, E., 1972, "Experiments on the Flow Past Spheres at Very High Reynolds Numbers," *J. Fluid Mech.*, Vol. 54, pp. 565–575.

Acton, E., 1976, "The Modelling of Large Eddies in a Two-Dimensional Shear Layer," *J. Fluid Mech.*, Vol. 76, pp. 561–592.

AGARD Publications: CP-247 (1979), AG-252 (1980), and LS-121 (1982), NATO.

Agui, J. C., and Jimenez, J., 1987, "On the Performance of Particle Tracking," *J. Fluid Mech.*, Vol. 185, pp. 447–468.

Agui, J. C., and Hesselink, L., 1988, "Flow Visualization and Numerical Analysis of a Coflowing Jet: A Three-Dimensional Approach," *J. Fluid Mech.*, Vol. 191, pp. 19–45.

Almosnino, D., 1985, "High Angle-of-Attack Calculations of the Subsonic Vortex Flow on Slender Bodies," *AIAA J.*, Vol. 23, No. 8, pp. 1150–1156.

Almosnino, D., and Rom, J., 1983, "Calculation of Symmetric Vortex Separation Affecting Subsonic Bodies at High Incidence," *AIAA J.*, Vol. 21, pp. 398-406.

Amano, R. S., and Goel, P., 1985, "Computations of Turbulent Flow Beyond Backward-Facing Steps Using Reynolds-Stress Closure," *AIAA J.*, Vol. 23, No. 9, pp. 1356–1361.

Amano, R. S., and Goel, P., 1987, "Investigation of Third-Order Closure Model of Turbulence for the Computation of Incompressible Flows in a Channel with a Backward-Facing Step," ASME JOURNAL OF FLUIDS ENGINEERING, Vol. 109, pp. 424–428.

Anderson, C. R., 1986, "A Method of Local Corrections for Computing the Velocity Field Due to a Distribution of Vortex Blobs," *J. Comput. Phys.*, Vol. 62, pp. 111-123.

Anderson, C. R., and Greengard, C., 1985, "On Vortex Methods," *SIAM J. Numer. Anal.*, Vol. 22, No. 3, pp. 413-440.

Angelucci, S. B., 1971, "A Multivortex Method for Axisymmetric Bodies at Angle of Attack," *J. of Aircraft*, Vol. 8, pp. 959–966.

Angelucci, S. B., 1973, "Multi Vortex Model for Bodies of Arbitrary Cross Sectional Shapes," AIAA-73-104.

Aparinov, V. A., Belotserkovskii, S. M., Nisht, M. I., and Sokolova, O. N., 1976, "On the Mathematical Simulation in an Ideal Fluid of Separated Flow Past a Wing and the Destruction of the Vortex Sheet," *Dokl. Ak. Nauk SSSR*, Vol. 227, pp. 820-823; Transl. as *Sov. Phys. Dokl.*, Vol. 21, No. 4, pp. 181–183.

Arakeri, V. H., Higuchi, H., and Arndt, R. E. A., 1988, "A Model for Predicting Tip Vortex Cavitation Characteristics," ASME JOURNAL OF FLUIDS ENGINEERING., Vol. 110, pp. 190–193.

Archibald, F. S., 1975, "Unsteady Kutta Condition at High Values of the Reduced Frequency Parameter," *J. Aircraft*, Vol. 12, pp. 545–550.

Aref, H., 1983, "Integrable, Chaotic and Turbulent Vortex Motion in Two-Dimensional Flows," *Ann. Rev. Fluid Mech.*, Vol. 15, pp. 345–389.

Aref, H., 1984, "Chaos in the Dynamics of a Few Vortices - Fundamentals and Applications," *Proc. XVIth Int. Cong. Theor. Appl. Mech.*, pp. 43–68.

Aref, H., and Flinchem, E. P., 1984, "Dynamics of a Vortex Filament in a Shear Flow, *J. Fluid Mech.*, Vol. 148, pp. 477–497.

Aref, H., and Kambe, T., 1988, "Report on the IUTAM Symposium: Fundamental Aspects of Vortex Motion," *J. Fluid Mech.*, Vol. 190, pp. 571–595.

Aref, H., and Siggia, E. D., 1980, "Vortex Dynamics of the Two-Dimensional Turbulent Shear Layer," *J. Fluid Mech.*, Vol. 100, pp. 705–737.

Arms, R. J., and Hama, F. R., 1965, "Localized-Induction Concept on a Curved Vortex and Motion of an Elliptic Vortex Ring," *Phys. Fluids*, Vol. 8, pp. 553–559.

Asfar, K. R., Mook, D. T., and Nayfeh, A. H., 1979, "Application of the Vortex-Lattice Technique to Arbitrary Bodies," *J. Aircraft*, Vol. 16, No. 7, pp. 421–424.

Ashurst, W. T., 1979, "Numerical Simulation of Turbulent Mixing Layers via Vortex Dynamics," *Turbulent Shear Flows I.*, (Eds. F. Durst et al.), Springer, pp. 402–413. (Also SAND 77-8612, Sandia Labs., Livermore).

Ashurst, W. T., 1981, "Vortex Ring Instability," *Bull. Am. Phys. Soc.*, Vol. 26, p. 1267.

Ashurst, W. T., 1983, "Large Eddy Simulation via Vortex Dynamics," AIAA-83-1879-CP.

Ashurst, W. T., 1987, "Vortex Simulation of Unsteady Wrinkled Laminar Flames," *Combust. Sci. and Tech.*, Vol. 52, pp. 325–351.

Ashurst, W. T., and Meiburg, E., 1988, "Three-Dimensional Shear Layers via Vortex Dynamics," *J. Fluid Mech.*, Vol. 189, pp. 87–110.

Ashurst, W. T., and Meiron, D. I., 1987, "Numerical Study of Vortex Reconnection," *Physical Review Letters*, Vol. 58, No. 16, pp. 1632–1635.

Baba, N., and Miyata, H., 1987, "Higher-Order Accurate Difference Solutions of Vortex Generation from a Circular Cylinder in an Oscillatory Flow," *J. Comput. Phys.*, Vol. 69, pp. 362–396.

Baden, S. B., and Puckett, E. G., 1988, "A Fast Vortex Code for Computing 2-D Flow in a Box," AIAA-88-3605-CP (in Proc. 1st Natl. Fluid Dyn. Cong., 1988, pp. 185-192).

Baker, G. R., 1976, "Studies of Vortex Motion," Ph. D. thesis, Cal. Inst. of Tech., Pasadena, CA.

Baker, G. R., 1977, "Roll Up of a Vortex Sheet Using the 'Cloud-in-Cell' Technique," in *Proc. Aircraft Wake Vortices Conference* (Ed. J. N. Hallock), Report No. FAA-RD-77-68, National Tech. Info. Center, Springfield, VA, pp. 124–135.

Baker, G. R., 1979, "The 'Cloud in Cell' Technique Applied to the Roll-up of Vortex Sheets," *J. Comput. Phys.*, Vol. 31, pp. 76-95.

Baker, G. R., 1980, "A Test of the Method of Fink and Soh for Following Vortex Sheet Motion," *J. Fluid Mech.*, Vol. 100, pp. 209–220.

Baker, G. R., Meiron, D. I., and Orszag, S. A., 1982, "Generalized Vortex Methods for Free-Surface Flow Problems," *J. Fluid Mech.*, Vol. 123, pp. 477–501.

Baldwin, B. S., and Lomax, H., 1978, "Thin Layer Approximation and Algebraic Model for Separated Turbulent Flows," AIAA-78-257.

Barsby, J. E., 1972, "Flow Past Conically Cambered Slender Delta Wings with Leading-Edge Separation," ARC R&M 3748.

Barsby, J. E., 1973, "Separated Flow Past a Slender Delta Wing at Low Incidence," *Aeronaut. Quart.*, Vol. 24, pp. 120-128.

Basu, B. C., and Hancock, G. J., 1978, "The Unsteady Motion of a Two-Dimensional Aerofoil in Incompressible Inviscid Flow," *J. Fluid Mech.*, Vol. 87, pp. 159–178.

Basuki, J., and Graham, J. M. R., 1987, "Discrete Vortex Computation of Separated Airfoil Flow," *AIAA J.*, Vol. 25, No. 11, pp. 1409–1410.

Batchelor, G. K., 1964, "Axial Flow in Trailing Vortices," *J. Fluid Mech.*, Vol. 20, pp. 645–658.

Batchelor, G. K., 1967, *An Introduction to Fluid Dynamics*, Cambridge University Press.

Beale, J. T., 1986, "A Convergent 3-D Vortex Method with Grid-Free Stretching," *Math. of Computation*, Vol. 46, pp. 401–424 and S15–S20.

Beale, J. T., and Majda, A., 1981, "Rates of Convergence for Viscous Splitting of the Navier-Stokes Equations," *Math. of Computation*, Vol. 37, No. 156, pp. 243–259.

Beale, J. T., and Majda, A., 1982a, "Vortex Method I: Convergence in Three Dimensions," *Math. of Computation*, Vol. 39, No. 159, pp. 1–27.

Beale, J. T., and Majda, A., 1982b, "Vortex Methods II: Higher Order Accuracy in Two and Three Dimensions," *Math. of Computation*, Vol. 39, No. 159, pp. 29–52.

Beale, J. T., and Majda, A., 1984, "Vortex Methods for Fluid Flow in Two or Three Dimensions," *Contemp. Math.*, Vol. 28, pp. 221–229.

Beale, J. T., and Majda, A., 1985, "High Order Accurate Vortex Methods with Explicit Velocity Kernels," *J. Comput. Phys.*, Vol. 58, pp. 188–208.

Beam, R., and Warming R. F., 1976, "An Implicit Finite Difference Algorithm for Hyperbolic Systems in Conservation Law Form," *J. Comput. Phys.*, Vol. 22, pp. 87–110.

Beavers, G. S., and Wilson, T. A., 1970, "Vortex Growth in Jets," *J. Fluid Mech.*, Vol. 44, pp. 97–112.

Bellamy-Knights, P. G., 1967, "Analytical Study of Symmetrical Separated Flow about a Circular Cylinder," M. S. thesis, Univ. of Manchester.

Belotserkovskii, S. M., 1968, "Calculation of the Flow About Wings of Arbitrary Planform at a Wide Range of Angles of Attack," *Izv. Ak. Nauk, Mekh. Zhid. Gaza*, No. 4, pp. 32-44; (RAE Library Translation 1433, 1970).

Belotserkovskii, S. M., and Nisht, M. I., 1973, "Investigation of Special Features of Flow Over a Flat Plate at Large Angles of Attack," *Izv. Ak. Nauk, Mekh. Zhid. Gaza*, No. 5, pp. 110–116; Translation as *Fluid Dynamics*, Vol. 8, 1975, pp. 772–777.

Belotserkovskii, S. M., and Nisht, M. I., 1974, "Unsteady Nonlinear Theory for a Thin Wing of Arbitrary Planform," *Izv. Ak. Nauk. Mekh. Zhid. Gaza*, No. 4, pp. 100–108; Translation as *Fluid Dynamics*, Vol. 9, 1974, pp. 583–589.

Belotserkovskii, S. M., and Nisht, M. I., 1978, "Modeling of Turbulent Wakes in Ideal Fluids (Separated Flow Over Bluff Bodies)," *Fluid Mech.-Soviet Research*, Vol. 7, No. 1, pp. 102–115.

Bergeson, A. J., and Porter, J. D., 1960, "An Investigation of the Flow Around Slender Delta Wings with Leading Edge Separation," Report No. 510, Princeton Univ.

Bergman, K. H., 1969, "On the Dynamic Stability of Convected Atmospheric Vortices," Ph. D. thesis, Univ. of Washington, Seattle.

Betchov, R., 1965, "On the Curvature and Torsion of an Isolated Vortex Filament," *J. Fluid Mech.*, Vol. 22, pp. 471–479.

Betz, A., 1932, "Verhalten von Wirbelsystemen," *Z. Angew. Math. Mech.*, Vol. 12, pp. 164–174. (Also NACA TM 713, June 1933).

Bilanin, A. J., and Donaldson, C. duP., 1975, "Estimation of Velocities and Roll-up in Aircraft Vortex Wakes," *J. Aircraft*, Vol. 12, pp. 578–585.

Birdsall, C. K., and Fuss, D., 1969, "Clouds-in-Clouds, Clouds-in Cells, Physics for Many-Body Plasma Stimulation," *J. Comput. Phys.*, Vol. 3, pp. 494–511.

Birkhoff, G., 1962, "Helmholtz and Taylor Instability," *Proc. Symp. on Appl. Math. Am. Math. Soc.*, Vol. 13, pp. 55-76.

Birkhoff, G. D., and Fisher, J., 1959, "Do Vortex Sheets Roll up?," *Rc. Circ. Mat. Palermo*, Ser. 2, Vol. 8, pp. 77–90.

Bollay, W., 1939, "A Nonlinear Wing Theory and Its Application to Rectangular Wings of Small Aspect Ratio," *Zeit. Angew. Math. Mech.*, Vol. 19, pp. 21–35.

Bouard, R., and Coutanceau, M., 1980, "The Early Stage of Development of the Wake Behind an Impulsively Started Circular Cylinder for $40 < Re < 10^4$," *J. Fluid Mech.*, Vol. 101, pp. 583–607.

Braza, M., Chassaing, P., and Ha Minh, H., 1986, "Numerical Study and Physical Analysis of the Pressure and Velocity Fields in the Near Wake of a Circular Cylinder," *J. Fluid Mech.*, Vol. 165, pp. 79–130.

Breit, S. R., Dickinson, A. L., and Howe, M. S., 1988, "Sound Generation by Flow Over a Cavity in a Duct: Discrete Vortex Simulation on a Parallel Processor," *Proc. Symp. on Hydrodynamic Performance Enhancement for Marine Applications* (to appear), Newport, R.I.

Brennenstuhl, U., and Hummel, D., 1987, "Experimentelle and Theoretische Untersuchungen uber die Wirbelbildung an Doppeldeltaflugeln," *Z. Flugwiss. Weltraumforsch.*, Vol. 11, pp. 37–49.

Broadwell, J. E., and Dimotakis, P. E., 1986, "Implications of Recent Experimental Results for Modeling Reactions in Turbulent Flows," *AIAA J.*, Vol. 24, No. 6, pp. 885–889.

Bromilow, I. G., and Clements, R. R., 1982, "Some Techniques for Extending the Application of the Discrete Vortex Method of Flow Simulation," *Aeronaut. Quarterly*, Vol. 33, pp. 73–89.

Bromilow, I. G., and Clements, R. R., 1983, "A Discrete Vortex Simulation of Kelvin-Helmholtz Instability," *AIAA J.*, Vol. 21, No. 9, pp. 1345–1347.

Brown, C. E., 1973, "Aerodynamics of Wake Vortices," *AIAA J.*, Vol. 11, No. 4, pp. 531–536.

Brown, C. E., and Michael, W. H., 1954, "Effect of Leading-edge Separation on the Lift of a Delta Wing," *J. Aero. Sci.*, Vol. 21, pp. 690–694 and 706. (Also NACA TN 3430, 1954).

Brown, D. T., and Patel, M. H., 1981, "The Calculation of Vorticity Effects on the Motion Response of a Flat Bottomed Barge to Waves," *Proc. Intl. Symp. Hyd. in Ocean Engng.*, Norwegian Inst. Tech.

Brown, G. L., and Roshko, A., 1974, "On Density Effects and Large Structure in Turbulent Mixing Layers," *J. Fluid Mech.*, Vol. 64, pp. 775–816.

Bryson, A. E., 1959, "Symmetric Vortex Separation on Circular Cylinders and Cones," ASME *Journal of Applied Mechanics*, Vol. 81, Ser. E., pp. 643–648.

Buneman, O., 1974, "Variationally Optimized, Grid-Insensitive Vortex Tracing," *Lecture Notes in Phys.*, No. 35, Springer-Verlag, pp. 111–115.

Burridge, D. M., and Temperton, C., 1979, "A Fast Poisson-Solver for Large Grids," *J. Comput. Phys.*, Vol. 30, pp. 145–148.

Buttke, T. F., 1988, "A Numerical Study of Superfluid Turbulence in the Self-Induction Approximation," *J. Comput. Phys.*, Vol. 76, pp. 301–326.

Cantwell, B. J., 1976, "A Flying Hot Wire Study of the Turbulent Near Wake of a Circular Cylinder at a Reynolds Number of 140,000," Ph. D. thesis, Calif. Inst. Tech.

Cantwell, B. J., 1981, "Organized Motion in Turbulent Flow," *Ann. Rev. Fluid Mech.*, Vol. 13, pp. 457–515.

Cantwell, B., and Coles, D., 1983, "An Experimental Study of Entrainment and Transport in the Turbulent Near Wake of a Circular Cylinder," *J. Fluid Mech.*, Vol. 136, pp. 321–374.

Canuto, C., Hussaini, M. Y., Quarteroni, A., and Zang, T. A., 1987, *Spectral Methods in Fluid Dynamics*, Springer-Verlag.

Cattolica, R. J., Barr, P. K., and Mansour, N. N., 1987, "Propagation of a Premixed Flame in a Divided-Chamber Combustor," AIAA-87-0222.

Chang, C.-C., 1988, "Random Vortex Methods for the Navier-Stokes Equations," *J. Comput. Phys.*, Vol. 76, pp. 281-300.

Chang, M. S., and Pien, P. C., 1975, "Hydrodynamic Forces on a Body Moving Beneath a Free Surface," *Proc. First Inter. Conf. on Numer. Ship Hydrodynamics*, DTNSRDC, Bethesda, MD, pp. 539–559.

Chaplin, J. R., 1973, "Computer Model of Vortex Shedding from a Cylinder," *Proc. ASCE, J. Hyd. Div.*, HY1, pp. 155–165.

Cheer, A., 1979, "A Study of Incompressible 2-D Vortex Flow Past Smooth Surfaces," Lawrence Berkeley Lab. Rep. LBL 9950.

Cheer, A. Y., 1983a, "A Study of Incompressible 2-D Vortex Flow Past a Circular Cylinder," *SIAM J., Sci. Statist. Comput.*, Vol. 4, pp. 685–705.

Cheer, A. Y., 1983b, "Numerical Analysis of Time-Dependent Flow Structures Generated by an Impulsively Started Circular Cylinder in a Slightly Viscous Incompressible Fluid," PAM-145l, Pure Appl. Math. Ctr., Univ. of CA, Berkeley.

Cheng, H. K., Edwards, R. H., and Jia, Z. X., 1985, "Simulation Studies of Vortex Dynamics of a Leading Edge Flap," *Studies of Vortex Dominated Flows* (Eds. M. Y. Hussaini and M. D. Salas), Springer-Verlag, pp. 195–222.

Cheng, H. K., Edwards, R. H., and Jia, Z. X., and Lee, C. J., 1988, "Vortex-Dominated Slender-Wing Problems: Studies by a Point-Vortex Method," AIAA-88-3744-CP, (in Proc. 1st Natl. Fluid Dyn. Cong., 1988, pp. 512-522).

Choi, Y., Humphrey, J. A. C., and Sherman, F. S., 1988, "Random-Vortex Simulation of Transient Wall-Driven Flow in a Rectangular Enclosure," *J. Comput. Phys.*, Vol. 75, pp. 359–381.

Chorin, A. J., 1973, "Numerical Study of Slightly Viscous Flow," *J. Fluid Mech.*, Vol. 57, pp. 785–796.

Chorin, A. J., 1978, "Vortex Sheet Approximation of Boundary Layers," *J. Comput. Phys.*, Vol. 27, pp. 428–442.

Chorin, A. J., and Bernard, P. S., 1973, "Discretization of a Vortex Sheet with an Example of Roll-up," *J. Comput. Phys.*, Vol. 13, pp. 423–429.

Christiansen, J. P., 1973, "Numerical Simulation of Hydromechanics by the Method of Point Vortices," *J. Comput. Phys.*, Vol. 13, pp. 363–379.

Christiansen, J. P., and Zabusky, N. J., 1973, "Instability, Coalescence and Fission of Finite Area Vortex Structures," *J. Fluid Mech.*, Vol. 61, pp. 219-243.

Clark, R. W., 1976, "Non-conical Flow Past Slender Wings with Leading-edge Vortex Sheets," Euromech 41, 1973, Norwich. (Also ARC R&M 3814 and RAE-TR-76037, 1976).

Claus, R. W., 1986, "Direct Numerical Simulations of a Temporally Evolving Mixing Layer Subject to Forcing," NASA TM 88896, (see also Proc. 10th Symp. on Turbulence, Univ. Missouri, Rolla).

Clements, R. R., 1973a, "Computer Models of Separated Flows Behind Two-Dimensional Bluff Bodies," Ph.D. thesis, Cambridge Univ.

Clements, R. R., 1973b, "An Inviscid Model of Two-Dimensional Vortex Shedding," *J. Fluid Mech.*, Vol. 57, pp. 321–336.

Clements, R. R., 1977, "Flow Representation, Including Separated Regions, Using Discrete Vortices," AGARD LS-86 on Computational Fluid Dynamics, Paper No. 5.

Clements, R. R., and Maull, D. J., 1973, "The Rolling-up of a Trailing Vortex Sheet," *Aeronaut. J.*, Vol. 77, pp. 46–51.

Clements, R. R., and Maull, D. J., 1975, "The Representation of Sheets of Vorticity by Discrete Vortices," *Prog. Aerospace Sci.*, Vol. 16, pp. 129–146.

Conlisk, T., and Rockwell, D., 1981, "Modelling of Vortex-Corner Interaction Using Point Vortices," *Phys. Fluids*, Vol. 24, pp. 2133-2142.

Corcos, G. M., and Sherman, F. S., 1976, "Vorticity Concentration and the Dynamics of Unstable Shear Layers," *J. Fluid Mech.*, Vol. 73, pp. 241–264.

Corsiglia, V. R., Schwind, R. K., and Chigier, N. A., 1973, "Rapid Scanning Three Dimensional Hot Wire Anemometer Surveys of Wing-Tip Vortices," *J. Aircraft*, Vol. 10, No. 12, pp. 752–757.

Corsiglia, V. R., Rossow, V. J., and Ciffone, D. L., 1976, "Experimental Study of the Effect of Span Loading on Aircraft Wakes," *J. Aircraft*, Vol. 13, No. 12, pp. 968–973.

Cowley, S. J., 1983, "Computer Extension and Analytic Continuation of Blasius' Expansion for Impulsive Flow Past a Circular Cylinder," *J. Fluid Mech.*, Vol. 135, pp. 389–405.

Crighton, D. G., 1975, "Basic Principles of Aerodynamic Noise Generation," *Prog. Aerospace Sci.*, Vol. 16, pp. 397–413.

Crighton, D. G., 1985, "The Kutta Condition in Unsteady Flow," *Ann. Rev. Fluid Mech.*, Vol. 17, pp. 411–445.

Crow, S. C., 1970, "Stability Theory for a Pair of Trailing Vortices," *AIAA J.*, Vol. 8, pp. 2172–2179.

Dalton, C., and Wang, X., 1988, "The Vortex Rollup Problem Using Lamb Vortices for the Elliptically Loaded Wing," AIAA-88-3746-CP (*Proc. 1st Natl. Fluid Dyn. Cong.*, 1988, pp. 531–538).

Damms, S. M., and Kuchemann, D., 1974, "On a Vortex-sheet Model for the Mixing Between Two Parallel Streams," *Proc. Roy. Soc. A*, Vol. 339, pp. 451–461.

Da Rios, L. S., 1906, "Sul Moto d'un Liquido Indefinito con un Filetto di Forma Qualunque," *Rend. Circ. Mat. Palermo*, Vol. 22, pp. 117–135.

Davies, P. O. A. L., Hardin, J. C., Edwards, A. V. J., and Mason, J. P., 1975, "A Potential Flow Model for Calculation of Jet Noise," AIAA-75-441.

Davis, M. D., 1969, "An Analytical Study of Separated Flow about a Circular Cylinder," M. Sc. thesis, Naval Postgraduate School, Monterey, CA.

Davis, R. W., and Moore, E. F., 1982, "A Numerical Study of Vortex Shedding from Rectangles," *J. Fluid Mech.*, Vol. 116, pp. 475–506.

Davis, R. W., Moore, E. F., and Purtell, L. P., 1984, "A Numerical-Experimental Study of Confined Flow around Rectangular Cylinders," *Phys. Fluids*, Vol. 27, pp. 46–59.

Dawson, C., and Marcus, M., 1970, "DMC—A Computer Code to Simulate Viscous Flow about Arbitrarily Shaped Bodies," *Proc. 1970 Heat Transfer and Fluid Mechanics Inst.*, (Ed. T. Sarpkaya), pp. 323–338.

Downie, M. J., Bearman, P. W., and Graham, J. M. R., 1988, "Effect of Vortex Shedding on the Coupled Roll Response of Bodies in Waves," *J. Fluid Mech.*, Vol. 189, pp. 243–264.

de Bernardinis, B., Graham, J. M. R., and Parker, K. H., 1981, "Oscillatory Flow Around Disks and Through Orifices," *J. Fluid Mech.*, Vol. 102, pp. 279–299.

de Bernardinis, B., and Moore, D. W., 1985, "A Ring-Vortex Representation of an Axi-Symmetric Vortex Sheet," *Studies of Vortex Dominated Flows* (Eds. M. Y. Hussaini and M. D. Salas), Springer-Verlag, pp. 33–43.

De Bruin, A. C., 1984, "Laminar and Turbulent Boundary-Layer Calculations on the Leeward Surface of a Slender Delta Wing at Incidence," NLR MP 84040 U. Amsterdam, The Netherlands.

Deffenbaugh, F. D., 1979, "Evaluation of the Discrete Vortex Wake Cross-Flow Model Using Vector Computers," TRW Rep. No. 30584-60001-RU-00.

Deffenbaugh, F. D., and Koerner, W. G., 1977, "Asymmetric Vortex Wake Development on Missiles at High Angles of Attack," *J. Spacecraft*, Vol. 14, No. 3, pp. 155–162.

Deffenbaugh, F. D., and Marshall, F. J., 1976, "Time Development of the Flow About an Impulsively Started Cylinder," *AIAA J.*, Vol. 14, pp. 908-913,

Deffenbaugh, F. D., and Shivananda, T. P., 1980, "Discrete Vortex Wake Modeling of Separated Flow Phenomena," TRW Report No. 33945-6001-UT-00.

DeJarnette, F. R., and Woodson, S. H., 1984, "Numerical and Experimental Determination of Secondary Separation on Delta Wings in Subsonic Flow," AIAA-84-2175.

DeMeis, R., 1988, "Tracking Vorticity in Flight," *Aerospace America* (AIAA), June, pp. 42–43.

Dickinson, A. L., 1988, "Computation of the Forces and Far-Field Sound Radiation from an Unsteady Two-Dimensional Airfoil Using the Vortex Method," MS Thesis in ME, MIT, Camb. MA.

Donaldson, C. duP., and Blanin, A. J., 1975, "Vortex Wakes of Conventional Aircraft," *AGARDograph* AGARD-AG-204.

Donaldson, C. duP., Snedeker, R. S., and Sullivan, R. D., 1974, "Calculation of Aircraft Wake Velocity Profiles and Comparison with Experimental Measurements," *J. Aircraft*, Vol. 11, pp. 547–555.

Donaldson, C. duP., and Sullivan, R. D., 1971, "Decay of an Isolated Vortex," *Aircraft Wake Turbulence and Its Detection* (Eds. J. Olson et al.), Plenum Press, pp. 389–412.

Donnelly, R. J., and Swanson, C. E., 1986, "Quantum Turbulence," *J. Fluid Mech.*, Vol. 173, pp. 387–429.

Dritschel, D. G., 1986, "The Nonlinear Evolution of Rotating Configurations of Uniform Vorticity," *J. Fluid Mech.*, Vol. 172, pp. 157–182.

Dritschel, D. G., 1988a, "Nonlinear Stability Bounds for Inviscid, Two-Dimensional, Parallel or Circular Flows with Monotonic Vorticity, and the Analogous Three-Dimensional, Quasi-Geostrophic Flows," *J. Fluid Mech.*, Vol. 191, pp. 575–581.

Dritschel, D. G., 1988b, "Contour Surgery: A Topological Reconnection Scheme for Extended Integrations Using Contour Dynamics," *J. Comput. Phys.*, Vol. 77, pp. 240–266.

Duffy, R. E., Czajkowski, E., and Jaran, C., 1984, "Finite Element Approximation to Theodorsen's Solution for Non-steady Aerodynamics of an Airfoil Section," AIAA-84-1640.

Dushane, T. E., 1973, "Convergence for a Vortex Method for Solving Euler's Equation," *Math. Comp.*, Vol. 27, pp. 719–728.

Dyer, D. E., Fiddes, S. P., and Smith J. H. B., 1982, "Asymmetric Vortex Formation from Cones at Incidence—A Simple Inviscid Model," *Aeronaut. Quart.*, Vol. 33, pp. 293–312.

Eastwood, J. W., 1975, "Optimal Particle-Mesh Algorithms," *J. Comput. Phys.*, Vol. 18, pp. 1–20.

Eastwood, J. W., and Hockney, R. W., 1974, "Shaping the Force Law in Two-Dimensional Particle Mesh Models," *J. Comput. Phys.*, Vol. 16, pp. 342–359.

Eaton, B. E., 1987, "Analysis of Laminar Vortex Shedding Behind Circular Cylinder by Computer-Aided Flow Visualization," *J. Fluid Mech.*, Vol. 180, pp. 117–145.

Edwards, R. H., 1954, "Leading-Edge Separation from Delta Wings," *J. Aero. Sci.*, Vol. 21, pp. 134–135.

El-Ramly, Z., and Rainbird, W. J., 1977, "Flow Survey of the Vortex Wake Behind Wings," *J. Aircraft*, Vol. 14, No. 11, pp. 1102–1109.

Elle, B. J., and Jones, J. P., 1961, "A Note on the Vorticity Distribution on the Surface of Slender Delta Wings with Leading-Edge Separation," *J. Roy. Aero. Soc.*, Vol. 65, pp. 195–198.

Eriksson, L-E., and Rizzi, A., 1981, "Computation of Vortex Flow Around Wings Using the Euler Equations," *Proc. 4th GAMM Conf. on Num Meth. in Fluid Mech.* (Ed. H. Viviand), Vieweg Verlag, Paris, pp. 87–105.

Erlebacher, G., and Eiseman, P. R., 1987, "Adaptive Triangular Mesh Generation," *AIAA J.*, Vol. 55, No. 10, pp. 1356–1364.

Evans, R. A., and Bloor, M. I. G., 1977, "The Starting Mechanism of Wave-Induced Flow Through a Sharp-Edged Orifice," *J. Fluid Mech.*, Vol. 82, pp. 115–128.

Fage, A., and Johansen, F. C., 1927, "On the Flow of Air Behind an Inclined Plate of Infinite Span," *Proc. Roy. Soc. A.*, Vol. 116, pp. 170–197.

Fage, A., and Johansen, F. C., 1928, "The Structure of Vortex Sheets," *Phil. Mag.*, Series 7, Vol. 5, pp. 417–441.

Faltinsen, O. M., and Pettersen, B., 1982, "Vortex Shedding Around Two-Dimensional Bodies at High Reynolds Numbers," *Proc. of the 14th Symp. Naval Hydro.*, Ann Arbor, pp. 1171–1213.

Flatinsen, O. M., and Pettersen, B., 1987, "Application of a Vortex Tracking Method to Separated Flow Around Marine Structures," *J. Fluids and Structures*, Vol. 1, pp. 217–237.

Faltinsen, O. M., and Sortland, B., 1987, "Slow Drift Eddy Making Damping of a Ship," *Appl. Ocean Res.*, Vol. 9, pp. 37–46.

Fiddes, S. P., 1985, "Separated Flow about Cones at Incidence-Theory and Experiment," *Studies of Vortex Dominated Flows* (Eds. M. Y. Hussaini and M. D. Salas), Springer-Verlag, pp. 285–310.

Fink, P. T., and Soh, W. K., 1974, "Calculation of Vortex Sheets in Unsteady Flow and Applications in Ship Hydrodynamics," *Proc. of the 10th Symp. on Naval Hydro.*, Cambridge, Mass., pp. 463–488. (Also, Univ. New South Wales Rep. Nav/Arch 74/1).

Fink, P. T., and Soh, W. K., 1978, "A New Approach to Roll-up Calculations of Vortex Sheets," *Proc. Roy. Soc. London A*, Vol. 362, pp. 195–209.

Franks, C. B., 1983, "Sensitivity Studies of Methods for Predicting Separation in Discrete Vortex Models," DTNSRDC-83/093, Bethesda, MD.

Gad-el-Hak, M., and Blackwelder, R. F., 1985, "The Discrete Vortices from a Delta Wing," *AIAA J.*, Vol. 23, No. 6, pp. 961–962.

Gad-el-Hak, M., and Blackwelder, R. F., 1987, "Control of Discrete Vortices from a Delta Wing," *AIAA J.*, Vol. 25, No. 8, pp. 1042–1049.

Geissler, W., 1985, "Unsteady Laminar Boundary-Layer Separation on Oscillating Configurations," *AIAA J.*, Vol. 23, No. 4, pp. 577–582.

Gerrard, J. H., 1967, "Numerical Computation of the Magnitude and Frequency of the Lift on a Circular Cylinder," *Phil. Trans. Roy. Soc.*, Vol. 261, No. 1118, pp. 137–162.

Ghoniem, A. F., Aly, H. M., and Knio, O. M., 1987a, "Three-Dimensional Vortex Simulation with Application to Axisymmetric Shear Layer," AIAA-87-0379.

Ghoniem, A. F., and Cagnon, Y., 1987, "Vortex Simulation of Laminar Recirculating Flow," *J. Comput. Phys.*, Vol. 68, pp. 346–377.

Ghoniem, A. F., Chen, D. Y., and Oppenheim, A. K., 1986, "Formation and Inflammation of a Turbulent Jet," *AIAA J.*, Vol. 24, No. 2, pp. 224–229.

Ghoniem, A. F., Heidarinejad, G., and Krishnan, A., 1987b, "Numerical Simulation of a Reacting Shear Layer Using the Transport Element Method," AIAA-87-1718.

Ghoniem, A. F., Heidarinejad, G., and Krishnan, A., 1988, "On Mixing, Baroclinicity and the Effect of Strain in a Chemically-Reacting Shear Layer," AIAA-88--0729.

Ghoniem, A. F., and Ng, K. K., 1987, "Numerical Study of a Forced Shear Layer," *Phys.* Fluids, Vol. 30, pp. 706–721.

Ghoniem, A. F., and Sethian, J. A., 1987, "Effect of Reynolds Number on the Structure of Recirculating Flow," *AIAA J.*, Vol. 25, No. 1, pp. 168–171.

Ghoniem, A. F., and Sherman, F. S., 1985, "Grid-Free Simulation of Diffusion Using Random Walk Methods," *J. Comput. Phys.*, Vol. 61, pp. 1–37.

Giesing, J. P., 1968a, "Nonlinear Interaction of Two Lifting Bodies in Arbitrary Unsteady Motion," ASME *Journal of Basic Engineering*, Vol. 90, pp. 387–394.

Giesing, J. P., 1968b, "Nonlinear Two-Dimensional Unsteady Potential Flow with Lift," *J. Aircraft*, Vol. 5, pp. 135–143.

Giesing, J. P., 1969, "Vorticity and Kutta Condition for Unsteady Multienergy Flows," ASME *Journal of Applied Mechanics*, Vol. 36, pp. 608–613.

Glimm, J., 1965, "Solutions in the Large for Nonlinear Hyperbolic Systems of Conservation Laws," *Comm. Pure Appl. Math.*, Vol. 18, pp. 697–716.

Goodman, J., 1987, "Convergence of the Random Vortex Method," *Comm. Pure Appl. Math.*, Vol. XL, pp. 189–220.

Govindaraju, S., and Saffman, P., 1971, "Flow in a Turbulent Trailing Vortex," *Phys. Fluids*, Vol. 14, No. 10, pp. 2074–2080.

Grabowski, W. J., and Telste, J. G., 1978, "A Discrete Vortex Simulation of a Two-Dimensional Shear Layer with Prediction of the Hydrodynamic Noise," DTNSRDC-78/050, Bethesda, MD.

Graham, J. M. R., 1977, "Vortex Shedding from Sharp Edges," Imp. Coll. London, Aero. Rep., 77-06, ISSN 0308 7247.

Graham, J. M. R., 1980, "The Forces on Sharp-Edged Cylinders in Oscillatory Flow at Low Keulegan-Carpenter Numbers," *J. Fluid Mech.*, Vol. 97, pp. 331–346.

Graham, J. M. R., 1985, "Numerical Simulation of Steady and Unsteady Flow about Sharp-Edged Bodies," *Separated Flow Around Marine Structures*, Norwegian Inst. of Tech., Trondheim, pp. 347–373.

Greengard, C., 1985, "The Core Spreading Vortex Method Approximates the Wrong Equation," *J. Comput. Phys.*, Vol. 61, pp. 345–348.

Greengard, C., 1986, "Convergence of the Vortex Filament Method," *Math. of Computation*, Vol. 47, pp. 387–398.

Greengard, L., and Rokhlin, V., 1987, "A Fast Algorithm for Particle Simulations," *J. Comput. Physics*, Vol. 73, pp. 325-348.

Grinstein, F. F., Oran, E. S., and Boris, J. P., 1986, "Numerical Simulations of Asymmetric Mixing in Planar Shear Flows," *J. Fluid Mech.*, Vol. 165, pp. 201-220.

Guiraud, J. P., and Zeytounian, R. Kh., 1977, "A Double Scale Investigation of the Asymptotic Structure of Rolled-up Vortex Sheets," *J. Fluid Mech.*, Vol. 79, pp. 93–112.

Guiraud, J. P., and Zeytounian, R. Kh., 1979, "A Note on the Viscous Diffusion of Rolled Vortex Sheets," *J. Fluid Mech.*, Vol. 90, pp. 197–201.

Hald, O. H., 1979, "Convergence of Vortex Methods for Euler's Equations: II.," *SIAM J. Numer. Anal.*, Vol. 16, pp. 726–755.

Hald, O. H., 1985, "Convergence of Vortex Methods for Euler's Equations: III.," PAM-270, Pure and Appl. Math. Ctr., Univ. CA, Berkeley.

Hald, O. H., 1986, "Convergence of a Random Method with Creation of Vorticity," *SIAM J. Sci. Stat. Comput.*, Vol. 7, No. 4, pp. 1373–1386.

Hald, O. H., and Del Prete, M. V., 1978, "Convergence of Vortex Methods for Euler's Equations," *Math. of Computation*, Vol. 32 (143), pp. 791–809.

Hall, R. M., 1987, "Forebody and Missile Side Forces and the Time Analogy," AIAA-87-0327.

Ham, N. D., 1968, "Aerodynamic Loading on a Two-Dimensional Airfoil During Dynamic Stall," *AIAA J.*, Vol. 6, No. 10, pp. 1927–1934.

Hama, F. R., 1962, "Progressive Deformation of a Curved Vortex Filament by its Own Induction," *Phys. Fluids*, Vol. 5, pp. 1156–1162.

Hama, F. R., 1963, "Progressive Deformation of a Perturbed Line Vortex Filament," *Phys. Fluids*, Vol. 6, pp. 526–534.

Hama, F. R., and Burke, E. R., 1960, "On the Rolling up of a Vortex Sheet," Univ. of Maryland TN No. BN-220. Also AFOSR, SUDAER No. 202.

Hardin, J. C., 1973, "Analysis of Noise Produced by an Orderly Structure of Turbulent Jets," NASA TN D-7242.

Hardin, J. C., and Mason, J. P., 1977, "Broadband Noise Generation by a Vortex Model of Cavity Flow," *AIAA J.*, Vol. 15, pp. 632–637.

Hardin, J. C., and Block, P. J., 1979, "Evaluation of a Vortex Model of Turbulent Cavity Flow," NASA TN-1505.

Hardy, B. C., and Fiddes, S. P., 1988, "Prediction of Vortex Lift of Non-Planar Wings by the Leading-Edge Suction Analogy," *Aeronautical J.*, pp. 154–164.

Harlow, F. H., 1964, "The Particle-in-Cell Computing Method for Fluid Dynamics," *Methods in Computational Phys.*, (Eds. B. Adler et al.), Vol. 3, pp. 319–343, Academic Press.

Helmholtz, H., 1858, "Uber Integrale der hydrodynamischen Gleichungen, welche den Wirbelbewegungen entsprechen," *Crelle-Borchardt*, Journal fur die reine und angewandte Mathematik, Berlin, Vol. LV, pp. 25-55. See also "On Integrals of the Hydrodynamical Equations which Express Vortex-Motion," Transl., P. G., Tait, in *Phil. Mag.* (4), 1867, Vol. 33, pp. 485–512.

Henkes, R. A. W. M., and Veldman, A. E. P., 1987, "On the Breakdown of the Steady and Unsteady Interacting Boundary-Layer Description," *J. Fluid Mechs.*, Vol. 179, pp. 513–529.

Henningson, D., Spalart, P., and Kim J., 1987, "Numerical Simulations of Turbulent Spots in Plane Poiseuille and Boundary Layer Flow," *Phys. Fluids*, Vol. 30, No. 10, pp. 2914–2917.

Hess, J. L., 1975, "The use of Higher-Order Surface Singularity Distributions to Obtain Improved Potential Flow Solutions for Two-Dimensional Lifting Airfoils," *Computer Methods in Appl. Mechs. & Engng.*, No. 5, pp. 11–35.

Hess, J. L., and Friedman, D. M., 1981, "An Improved Higher Order Panel Method for Three-Dimensional Lifting Potential Flow," NADC 79277-60, Naval Air Development Center.

Hess, J. L., and Smith A. M. O., 1964, "Calculation of Nonlifting Potential Flow about Arbitrary Three-Dimensional Bodies," *J. Ship Res.*, Vol. 8, No. 2, pp. 22–42.

Higdon, J. J. L., and Pozrikidis, C., 1985, "The Self-Induced Motion of Vortex Sheets," *J. Fluid Mech.*, Vol. 150, pp. 203–231.

Higuchi, H., Quadrell, J. C., and Farell, C., 1987, "Vortex Roll-up from an Elliptic Wing at Moderately Low Reynolds Numbers," *AIAA J.*, Vol. 25, No. 12, pp. 1537–1542.

Himeno, R., Shirayama, S., Kamo, K., Kuwahara, K., 1985, "Computational Study of Three-Dimensional Wake Structure," AIAA-85-1617.

Hitzel, S. M., 1988, "Wing Vortex Flows up into Vortex Breakdown," AIAA 88-2518.

Ho, C.-M., and Chen, S. H., 1981, "Unsteady Kutta Condition of a Plunging Airfoil," *Unsteady Turbulent Shear Flows* (Eds. R. Michel et al.), Springer, Berlin, pp. 197–206.

Ho, C.-M., and Huerre, P., 1984, "Perturbed Free Shear Layers," *Ann. Rev. Fluid Mech.*, Vol. 16, pp. 365–424.

Hockney, R. W., and Eastwood, J. W., 1981, *Computer Simulation Using Particles*, McGraw-Hill, New York.

Hockney, R. W., Goel, S. P., and Eastwood, J. W., 1974, "Quiet High-Resolution Computer Models of a Plasma," *J. Comput. Phys.*, Vol. 14, pp. 148–158.

Hoeijmakers, H. W. M., 1983, "Computational Vortex Flow Aerodynamics," AGARD CP-342, Paper No. 18.

Hoeijmakers, H. W. M., 1984, "Numerical Computation of Vortical Flow about Wings," von Karman Inst. Lect. Ser. on Computational Fluid Dynamics. Also NLR MP 83073 U, 1983.

Hoeijmakers, H. W. M., 1985, "Methods for Numerical Simulation of Leading Edge Vortex Flow," *Studies of Vortex Dominated Flows* (Eds. M. Y. Hussaini and M. D. Salas), Springer-Verlag, pp. 223-269.

Hoeijmakers, H. W. M., and Bennekers, B., 1979, "A Computational Model for the Calculation of the Flow about Wings with Leading-Edge Vortices," AGARD CP-247, Paper No. 25.

Hoeijmakers, H. W. M., and Vaatstra, W., 1983, "A Higher-Order Panel Method Applied to Vortex Sheet Roll-up," *AIAA J.*, Vol. 21, pp. 516–523.

Hoeijmakers, H. W. M., and Vaatstra, W., and Verhaagen, N. G., 1983, "On the Vortex Flow over Delta and Double-Delta Wings," *J. Aircraft*, Vol. 20, No. 9, pp. 825–832.

Hoffman, E. R., and Joubert, P. N., 1963, "Turbulent Line Vortices," *J. Fluid Mech.*, Vol. 16, pp. 395–411.

Hsu, A. T., and Wu, J. C., 1988, "Vortex Flow Model for the Blade-Vortex Interaction Problem," *AIAA J.*, Vol. 26, No. 5, pp. 621–623.

Hummel, D., 1979, "On the Vortex Formation over a Slender Wing at Large Incidence," AGARD-CP-247, Paper No. 15.

Hummel, D., and Redeker, G., 1972, "Experimentelle Bestimmung der gebundene Wirbellinien sowie des Stromungs-Verlaufs in der Umgebung der

Hinterkante eines Schlanken Deltaflugels," *Abh. Braunschweig, Wiss. Ges.*, Vol. 22, pp. 273–290.

Hunt, B., 1980, "The Mathematical Basis and Numerical Principles of the Boundary Integral Method for Incompressible and Potential Flow over 3-D Aerodynamic Configurations," *Numerical Methods in Applied Fluid Dynamics* (Ed. B. Hunt), Academic Press, pp. 49–135.

Hussain, A. K. M. F., 1986, "Coherent Structures and Turbulence," *J. Fluid Mech.*, Vol. 173, pp. 303–356.

Hussaini, M. Y., and Salas, M. D., 1985, *Studies in Vortex Dominated Flows* (Eds.), Springer-Verlag.

Ikeda, Y., 1984a, "Calculation of Lift Force Acting on Circular Cylinder in Oscillating Flow," TUB/ISM-Report No. 84/12, Tech. of Berlin, Institute fur Schiffs—und Meertechnik.

Ikeda, Y., 1984b, "Calculation of Viscous Interference Effect Between Two Circular Cylinders in Tandem Arrangement in Harmonically Oscillating Flow," TUB/ISm Report No. 84/11, Tech., Univ. Berlin, Institute fur Schiffs—und Meertechnik.

Ikeda, Y., and Himeno, Y., 1981, "Calculation of Vortex-Shedding Flow Around Oscillating Circular and Lewis-Form Cylinder," *Proc. 13th Int. Conf. on Numerical Ship Hydrodynamics*, pp. 335–346, Paris: Bassin d'Essais des Carenes.

Imaichi, K., and Ohmi, K., 1983, "Numerical Processing of Flow-Visualization Pictures: Measurement of Two-Dimensional Vortex Flow," *J. Fluid Mech.*, Vol. 129, pp. 283–311.

Inamuro, T., Adachi, T., and Sakata, H., 1983, "A Numerical Analysis of Unsteady Separated Flow by Vortex Shedding Model," *Bulletin of JSME*, Vol. 26, No. 222, pp. 2106–2112.

Inamuro, T., Saito, T., and Adachi, T., 1984, "A Numerical Analysis of Unsteady Separated Flow by the Discrete Vortex Method Combined with the Singularity Method," *Computers and Structures*, Vol. 19, No. 1-2, pp. 75–84.

Ingham, D. B., 1984, "Unsteady Separation," *J. Comput. Phys.*, Vol. 53, pp. 90–99.

Inoue, O., 1985a, "Vortex Simulation of a Turbulent Mixing Layer," *AIAA J.*, Vol. 23, pp. 367–372.

Inoue, O., 1985b, "A New Approach to Flow Problems Past a Porous Plate," *AIAA J.*, Vol. 23, No. 12, pp. 1916–1921.

Inoue, O., and Leonard, A., 1987, "Vortex Simulation of Forced/Unforced Mixing Layers," *AIAA J.*, Vol. 25, No. 11, pp. 1417–1418.

Iversen, J. D., 1975, "Correlation of Turbulent Trailing Vortex Data," *J. Aircraft*, Vol. 13, No. 5, pp. 338–342.

Iwagaki, Y., and Ishida, H., 1976, "Flow Separation, Wake Vortices and Pressure Distribution Around a Circular Cylinder Under Oscillatory Waves," *Proc. 15th Conf. on Coastal Engng.*, ASCE, Vol. 3, pp. 2341–2356.

Johnson, F. T., and Rubbert, P. E., 1975, "Advanced Panel-Type Influence Coefficient Methods Applied to Subsonic Flows," AIAA-75-50.

Johnson, F. T., Tinoco, E. N., Lu, P., and Epton, M. A., 1980, "Three-Dimensional Flow over Wings with Leading-Edge Vortex Separation," *AIAA J.*, Vol. 18, No. 4, pp. 367–380.

Jones, A. W., and Aref, H., 1988, "Chaotic Advection in Pulsed Source-Sink Systems," *Phys. Fluids*, Vol. 31, No. 3, pp. 469–485.

Jordan, P. F., 1973, "Structure of Betz Vortex Cores," *J. Aircraft*, Vol. 10, pp. 691–693.

Kaden, H., 1931, "Aufwicklung einer Unstabilen Unstetigkeits Flache," *Ingen. Arch.*, Vol. 2, 1931, pp. 140–168. (Also R.A.E. Library Trans. No. 43).

Kandil, O. A., 1979, "State of the Art of Nonlinear Discrete-Vortex Methods for Steady and Unsteady High Angle of Attack Aerodynamics," AGARD CP-247, Paper No. 5.

Kandil, O. A., 1980, "Numerical Prediction of Vortex Cores from Leading and Trailing Edges of Delta Wings," *Proc. 12th Congr. Int. Council of Aeronaut. Sci.*, ICAS Paper No. 14.2.

Kandil, O. A., 1985, "Computational Technique for Compressible Vortex Flows Past Wings at Large Incidence," *J. Aircraft*, Vol. 22, No. 9, pp. 750–755.

Kandil, O. A., Chu, L., and Tureaud, T., 1984, "A Nonlinear Hybrid Vortex Method for Wings at Large Angles of Attack," *AIAA J.*, Vol. 22, pp. 329–336.

Kandil, O. A., and Chuang, H. A., 1988, "Unsteady Transonic Airfoil Computation Using Implicit Euler Scheme on Body-Fixed Grid," *Proceedings of the Southeastern Conf. on Theo. and Appl. Mech.*, SCTAM XIV, pp. 1–18.

Kandil, O. A., Mook, D. T., and Nayfeh, A. H., 1976a, "Nonlinear Prediction of the Aerodynamic Loads on Lifting Surfaces," *J. Aircraft*, Vol. 13, pp. 22–28. (Also as AIAA-74-503).

Kandil, O. A., Mook, D. T., and Nayfeh, A. H., 1976b, "A New Convergence Criterion for the Vortex-Lattice Models of Leading-Edge and Wing-Tip Separation," NASA SP-405, pp. 285–300.

Katz, J., 1981, "A Discrete Vortex Method for the Non-Steady Separated Flow over an Airfoil," *J. Fluid Mech.*, Vol. 102, pp. 315–328.

Katz, J., 1984, "Lateral Aerodynamics of Delta Wings with Leading-Edge Separation," *AIAA J.*, Vol. 22, No. 3, pp. 323–328.

Kawamura, T., and Kuwahara, K., 1984, "Computation of High Reynolds Number Flow Around a Circular Cylinder with Surface Roughness," AIAA-84-0340.

Kawamura, T., and Kuwahara, K., 1985, "Direct Simulation of a Turbulent Inner Flow by Finite-Difference Method," AIAA-85-0376.

Keller, J. B., 1984, "Computers and Chaos in Mechanics," *Theoretical and Applied Mechanics* (Eds. F. I. Niordson and N. Olhoff), North-Holland, pp. 31–41.

Kerr, R. M., 1988, "Simulation of Rayleigh-Taylor Flows Using Vortex Blobs," *J. Comput. Phys.*, Vol. 76, pp. 48–84.

Keulegan, G. H., and Carpenter, L. H., 1958, "Forces on Cylinders and Plates in an Oscillating Fluid," *J. of Research*, National Bureau of Standards, Paper No. 2857, Vol. 60, No. 5, pp. 423–440.

Kida, S., and Takaoka, M., 1987, "Bridging in Vortex Reconnection," *Phys. Fluids*, Vol. 30, pp. 2911–2914.

Kimura, T., and Tsutahara, M., 1987, "Flows about a Rotating Circular Cylinder by the Discrete-Vortex Method," *AIAA J.*, Vol. 25, No. 1, pp. 182–184.

Kiya, M., and Arie, M., 1977a, "A Contribution to an Inviscid Vortex-Shedding Model for an Inclined Flat Plate in Uniform Flow," *J. Fluid Mech.*, Vol. 82, pp. 223–240.

Kiya, M., and Arie, M., 1977b, "An Inviscid Numerical Simulation of Vortex Shedding from an Inclined Flat Plate in Shear Flow," *J. Fluid Mech.*, Vol. 82, pp. 241–253.

Kiya, M., and Arie, M., 1980, "Discrete-Vortex Simulation of Unsteady Separated Flow Behind a Nearly Normal Plate," *Bulletin of JSME*, Vol. 23, No. 183, pp. 1451–1458.

Kiya, M., Arie, M., and Harigane, K., 1980, "Numerical Simulation of Gross Structure of Turbulent Plane Mixing Layer by Discrete-Vortex Model," *Bulletin of the JSME*, Vol. 23, pp. 1959–1966.

Kiya, M., Sasaki, K., and Arie, M., 1982, "Discrete-Vortex Simulation of a Turbulent Separation Bubble," *J. Fluid Mech.*, Vol. 120, pp. 219–244.

Kjelgaard, S. O., and Sellers III, W. L., 1988, "Detailed Flowfield Measurements Over a 75° Swept Delta Wing for Code Validation," *Proc. AGARD Symp. on Validation of Computational Fluid Dynamics*, Lisbon, pp. 1–14.

Knio, O. M., and Ghoniem, A. F., 1988, "On the Formation of Streamwise Vorticity in Turbulent Shear Flows," AIAA-88-0728.

Kourta, A., Boisson, H. C., Chassaing, P., and Ha Minh, H., 1987, "Nonlinear Interaction and the Transition to Turbulence in the Wake of a Circular Cylinder," *J. Fluid Mech.*, Vol. 181, pp. 141–161.

Krasny, R., 1986a, "A Study of Singularity Formation in a Vortex Sheet by the Point Vortex Approximation," *J. Fluid Mech.*, Vol. 167, pp. 65–93.

Krasny, R., 1986b, "Desingularization of Periodic Vortex Sheet Roll-up," *J. Comput. Phys.*, Vol. 65, pp. 292–313.

Krasny, R., 1987, "Computation of Vortex Sheet Roll-Up in the Trefftz Plane," *J. Fluid Mech.*, Vol. 184, pp. 123–155.

Krause, E., Ehrhardt, G., and Schweitzer, 1985, "Experiments on Unsteady Flows about Wing Sections," *Proc. Conf. on Low Reynolds Number Airfoil Aerodynamics* (Ed. T. J. Mueller), The Univ. of Notre Dame, UNDAS-CP-77B123, pp. 255–266.

Krutzsch, C. H., 1939, "Uber eine Experimentell Beobachtete Erscheinung an Wirbelringen bei Wirklichen Flussigkeiten," *Ann. Phys.*, Vol. 35, pp. 497–523.

Kudo, K., 1979, "An Inviscid Model of Discrete-Vortex Shedding For Two-Dimensional Oscillating Flow Around a Flat Plate," *J. Soc. Naval Arch. of Japan*, Vol. 145, pp. 54–62.

Kudo, K., 1981, "Hydrodynamic Forces of the Oscillating Flat Plate," *Proc. 3rd Int. Conf. on Numerical Ship Hydrodynamics*, Paris, pp. 347–358.

Kuhn, G. D., Spangler, S. B., and Nielsen, J. N., 1971, "Theoretical Analysis of Vortex Shedding from Bodies of Revolution in Coning Motion," *AIAA J.*, Vol. 9, No. 5, pp. 784–790.

Kuwahara, K., 1973, "Numerical Study of Flow Past an Inclined Flat Plate by an Inviscid Model," *J. Physical Soc. Japan*, Vol. 35, pp. 1545–1551.

Kuwahara, K., 1978, "Study of Flow Past a Circular Cylinder by an Inviscid Model," *J. Physical Soc. Japan*, Vol. 45, pp. 292–297.

Kuwahara, K., and Takami, H., 1973, "Numerical Studies of Two-Dimensional Vortex Motion by a System of Point Vortices," *J. Phys. Soc. Japan*, Vol. 34, pp. 247–253.

Laird, A. D. K., 1971, "Eddy Formation Behind Circular Cylinders," *J. Hyd. Div.*, ASCE, Vol. HY6, pp. 763–775.

Lamb, H., 1932, *Hydrodynamics*, Cambridge Univ. Press, 6th ed.

Langdon, A. B., 1970, "Effects of the Spatial Grid in Simulation Plasmas," *J. Comput. Phys.*, Vol. 6, pp. 247–267.

Lasheras, J. C., and Choi, H., 1988, "Three-Dimensional Instability of a Plane, Free Shear Layer: An Experimental Study of the Formation and Evolution of Streamwise Vortices," *J. Fluid Mech.*, Vol. 189, pp. 53–86.

Lau, J. C., and Fisher, M. J., 1975, "The Vortex-Street Structure of 'Turbulent' Jet, Part I, *J. Fluid Mech.*, Vol. 67, pp. 299–337.

Lecointe, Y., Piquet, J., and Plantec, J., 1987, "Flow Structure in the Wake of an Oscillating Cylinder," *Forum on Unsteady Flow Separation* (Ed. K. N. Ghia), ASME FED-Vol. 52, pp. 147–157.

Legendre, R., 1953, "Ecoulement au Voisinage de la Pointe Avant d'une Aile a Forte Fleche aux Incidences Moyennes," *Recherche Aeronautique*, Vol. 35.

Leonard, A., 1980a, "Vortex Methods for Flow Simulation," *J. Comput. Phys.*, Vol. 37, pp. 289–335.

Leonard, A., 1980b, "Vortex Simulation of Three-Dimensional Spotlike Disturbances in a Laminar Boundary Layer," *Turbulent Shear Flows*-2 (Eds. L. J. S. Bradbury et al.), Springer-Verlag, pp. 67–77.

Leonard, A., 1985, "Computing Three-Dimensional Incompressible Flows with Vortex Elements," *Ann. Rev. Fluid Mech.*, Vol. 17, pp. 523–559.

Leonard, A., Couet, B., and Parekh, D. E., 1985, "Two Studies in Three-Dimensional Vortex Dynamics: A Perturbed Round Jet and an Inhomogeneous Mixing Layer," *Separated Flow Around Marine Structures*, pp. 289–307, The Norwegian Inst. of Tech., Trondheim.

Lewis, R. I., 1981, "Surface Vorticity Modeling of Separated Flows from

Two-Dimensional Bluff Bodies of Arbitrary Shape," *J. of Mech. Engng. Sci.*, Vol. 23, No. 1, pp. 1–12.

Lighthill, M. J., 1963, "Introduction: Boundary Layer Theory," Chapter 2 in *Laminar Boundary Layers* (Ed. L. Rosenhead), Oxford Univ. Press, pp. 72–82.

Longuet-Higgins, M. S., 1981, "Oscillating Flow over Steep Sand Ripples," *J. Fluid Mech.*, Vol. 107, pp. 1–35.

Longuet-Higgins, M. S., and Cokelet, E. L., 1976, "The Deformation of Steep Surface Waves on Water. I. A Numerical Method of Computation," *Proc. Roy. Soc. London*, Series A, Vol. 350, pp. 1–26.

Mangler, K. W., and Smith, J. H. B., 1959, "A Theory of the Separated Flow Past a Slender Delta Wing with Leading-Edge Separation," *Proc. Roy. Soc. London*, Vol. 251A, pp. 200–217.

Mangler, K. W., and Smith, J. H. B., 1959, "A Theory of the Flow Past a Slender Delta Wing with Leading-Edge Separation," *Proc. Roy. Soc.*, Vol. 251A, pp. 200–217.

Mansour, N. N., 1985, "A Hybrid Vortex-in-Cell Finite-Difference Method for Shear Layer Computation," AIAA Paper 85-0372.

Marchioro, C., and Pulvirenti, M., 1984, "Vortex Methods in Two-Dimensional Fluid Mechanics," *Lecture Notes in Phys.*, No. 206, Springer, New York. (See also *Comm. Math. Phys.*, Vol. 84, 1982, pp. 483–503).

Marcus, D. L., and Berger, S. A., 1989, "The Inviscid Interaction Between a Rising Vortex Pair and a Free Surface," (to appear in *Phys. of Fluids*).

Marshall, F. J., and Deffenbaugh, F. D., 1975, "Separated Flow over a Body of Revolution," *J. Aircraft*, Vol. 12, No. 2, pp. 78–85.

Martensen, E., 1959, "Calculation of the Pressure Distribution over Profile in Cascade in Two-Dimensional Potential Flow by Means of a Fredholm Integral Equation," *Zweiter Art. Arch. Rat. Mech. Anal.*, Vol. 3, No. 3, pp. 253–270.

Maskell, E. C., 1971, "On the Kutta-Joukowski Condition in Two-Dimensional Unsteady Flow," Unpublished note, Royal Aircraft Establishment, Farnborough, England.

Maskew, B., 1973, "A Subvortex Technique for the Close Approach to a Discretized Vortex Sheet," *J. Aircraft*, Vol. 14, pp. 188–193. (Also NASA TM-X-62.487, 1973).

Maskew, B., 1977, "Subvortex Technique for the Close Approach to a Discretized Vortex Sheet," *J. Aircraft*, Vol. 14, No. 2, pp. 188–193.

Maskew, B., 1980, "Calculations of Two-Dimensional Vortex-Surface Interference Using Panel Methods," NASA CR-159334.

Maskew, B., and Rao, B. M., 1982, "Calculation of Vortex Flows on Complex Configurations," ICAS Paper 82-6.2.3. See Also "Flows with Leading-Edge Vortex Separation," NASA CR 165858.

Mathioulakis, D., Telionis, D. P., 1983, "Modeling Rotating Stall by Vortex Dynamics," AIAA-83-0002.

Maull, D. J., 1979, "An Introduction to the Discrete Vortex Method," IUTAM/IAHR, Karlsruhe.

Maxworthy, T., 1981, "The Fluid Dynamics of Insect Flight," *Ann. Rev. Fluid Mech.*, Vol. 13, pp. 329–350.

McAlister, K. W., and Carr, L. W., 1979, "Water Tunnel Visualizations on Dynamic Stall," ASME JOURNAL OF FLUIDS ENGINEERING, Vol. 101, pp. 376–380.

McCracken, M. F., and Peskin, C. S., 1980, "A Vortex Method for Blood Flow Through Heart Valves," *J. Comput. Phys.*, Vol. 35, pp. 183–205.

McCroskey, W. J., 1982, "Unsteady Airfoils." *Ann. Rev. Fluid Mech.*, Vol. 14, pp. 285–311.

McInville, R. M., Gatski, T. B., and Hassan, H. A., 1985, "Analysis of Large Vortical Structures in Shear Layers," *AIAA J.*, Vol. 23, No. 8, pp. 1165–1171.

Meiburg, E., and Lasheras, J. C., 1988, "Experimental and Numerical Investigation of the Three-Dimensional Transition in Plane Wakes," *J. Fluid Mech.*, Vol. 190, pp. 1–37.

Meiron, D. I., Baker, G. R., and Orszag, S. A., 1982, "Analytic Structure of Vortex Sheet Dynamics. Part I. Kelvin-Helmholtz Instability," *J. Fluid Mech.*, Vol. 114, pp. 283–298.

Melander, M. V., Zabusky, N. J., and McWilliams, J. C., 1987, "Asymmetric Vortex Merger in Two Dimensions: Which Vortex is 'Victorious'?" *Phys. Fluids*, Vol. 30, No. 9, pp. 2610–2612.

Meng, J. C. S., 1978, "The Physics of Vortex-Ring Evolution in a Stratified and Shearing Environment," *J. Fluid Mech.*, Vol. 84, pp. 455–469.

Meng, J. C. S., and Thomson, J. A. L., 1978, "Numerical Studies of Some Nonlinear Hydrodynamic Problems by Discrete Vortex Element Methods," *J. Fluid Mech.*, Vol. 84, pp. 433–453.

Messiter, A. F., and Enlow, R. E., 1973, "A Model for Laminar Boundary-Layer Flow near a Separation Point," *SIAM J. Appl. Math.*, Vol. 25, pp. 655–670.

Messiter, A. F., 1975, "Laminar Separation—A Local Asymptotic Flow Description," AGARD Conf. Proc. No. 168, Paper No. 4.

Messiter, A. F., 1983, "Boundary-Layer Interaction Theory," ASME *Journal of Applied Mechanics*, Vol. 50, pp. 1104–1113.

Metcalfe, R. W., Orszag, S. A., Brachet, M. E., Menon, S., and Riley, J. J., 1987, "Secondary Instability of a Temporally Growing Mixing Layer," *J. Fluid Mech.*, Vol. 184, pp. 207–243.

Michalke, A., 1963, "On the Instability and Nonlinear Development of a Disturbed Shear Layer," Hermann Fottinger Inst. fur Stromungstechnik, Univ. Berlin, TN No. 2, 1963.

Michalke, A., 1964, "Zur Instabilitat und Nichtlinearen Entwicklung einer Gestorten Scherschicht," *Ing. Arch.*, Vol. 33, pp. 264–276.

Michalke, A., 1965, "Vortex Formation in a Free Boundary Layer According to Stability Theory," *J. Fluid Mech.*, Vol. 22, Part 2, pp. 371–383.

Milinazzo, F., and Saffman, P. G., 1977, "The Calculation of Large Reynolds Number Two-Dimensional Flow Using Discrete Vortices with Random Walk," *J. Comput. Phys.*, Vol. 23, pp. 380–392.

Milne-Thomson, L. M., 1960, *Theoretical Hydrodynamics*, 4th ed., The MacMillan Co., New York.

Mook, D. T., Roy, S., Choksi, G., and Alexander, D. M., 1987, "On the Numerical Simulation of the Unsteady Wake Behind an Airfoil," AIAA-87-0190.

Moore, C. J., 1977, "The Role of Shear-Layer Instability Waves in Jet Exhaust Noise," *J. Fluid Mech.*, Vol. 80, pp. 321–368.

Moore, D. W., 1971, "The Discrete Vortex Approximation of a Finite Vortex Sheet," Cal. Inst. Tech. Rep. AFOSR-1804-69.

Moore, D. W., 1972, "Finite Amplitude Waves on Aircraft Trailing Vortices," *Aeronaut. Quart.*, Vol. 23, pp. 307–314.

Moore, D. W., 1974, "A Numerical Study of the Roll-up of a Finite Vortex Sheet," *J. Fluid Mech.*, Vol. 63, pp. 225–235.

Moore, D. W., 1975, "The Rolling up of a Semi-Infinite Vortex Sheet," *Proc. Roy. Soc.*, London, Ser. A, Vol. 345, pp. 417–430.

Moore, D. W., 1976, "The Stability of an Evolving Two-Dimensional Vortex Sheet," *Mathematika*, Vol. 23, pp. 35–44.

Moore, D. W., 1978, "The Equation of Motion of a Vortex Layer of Small Thickness," *Stud. Appl. Math.*, Vol. 58, pp. 119-140.

Moore, D. W., 1979, "The Spontaneous Appearance of a Singularity in the Shape of an Evolving Vortex Sheet," *Proc. Roy. Soc.* Series A, Vol. 365, pp. 105–119.

Moore, D. W., 1981, "On the Point Vortex Method," *SIAM J. Sci. Stat. Comput.*, Vol. 2, No. 1, pp. 65–84.

Moore, D. W., 1984, "Numerical and Analytical Aspects of Helmholtz Instability," in *Theoretical and Applied Mechanics*, IUTAM (Eds. F. I. Niordson and N. Olhoff), North-Holland, pp. 263–274.

Moore, D. W., and Griffith-Jones, R., 1974, "The Stability of an Expanding Circular Vortex Sheet," *Mathematika*, Vol. 21, pp. 128–133.

Moore, D. W., and Saffman, P. G., 1972, "The Motion of a Vortex Filament with Axial Flow," *Phil. Trans. Roy. Soc.*, Vol. 272, pp. 403–429. (Also AFOSR-TR-72-2384, 1972).

Moore, D. W., and Saffman, P. G., 1973, "Axial Flow in Laminar Trailing Vortices," *Proc. Roy. Soc.* A, Vol. 333, pp. 491–508.

Moore, D. W., and Saffman, P. G., 1975, "The Density of Organized Vortices in a Turbulent Mixing Layer," *J. Fluid Mech.*, Vol. 69, pp. 465–473.

Moore, F. K., 1957, "On the Separation of the Unsteady Laminar Boundary Layer," IUTAM-Symposium (Berlin). *Boundary Layers*, Freiburg, pp. 296–311.

Morikawa, G. K., and Swenson, E. V., 1971, "Interacting Motion of Rectilinear Geostrophic Vortices," *Phys. Fluids*, Vol. 14, pp.1058–1073.

Morison, J. R., O'Brien, M. P., Johnson, J. W., and Schaaf, S. A., 1950, "The Force Exerted by Surface Waves on Piles," *AIME Pet. Trans.*, Vol. 189, pp. 149–154.

Morton, B. R., 1984, "The Generation and Decay of Vorticity," *Geophys. Astrophys. Fluid Dynamics*, Vol. 28, pp. 277–308, Gordon and Breach Science Publishers, Inc., England.

Mostafa, S. I. M., 1987, "Numerical Simulation of Unsteady Separated Flows," Ph.D. thesis, Naval Postgraduate School, Monterey, CA.

Mostafa, S. I. M., Sarpkaya, T., and Munz, P., 1989, "Numerical Simulation of Unsteady Flow About Cambered Plates," AIAA-89-0290.

Munz, P., 1987, "Unsteady Flow About Cambered Plates," M.S. thesis, Naval Postgraduate School, Monterey, CA.

Murman, E. M., and Stremel, P. M., 1982, "A Vortex Wake Capturing Method for Potential Flow Calculations, AIAA Paper No. AIAA-82-0947.

Nagano, S., Naito, M., and Takata, H., 1982, "A Numerical Analysis of Two-Dimensional Flow Past a Rectangular Prism by a Discrete Vortex Model," *Computer and Fluids*, Vol. 10, No. 4, pp. 243–259.

Nagati, M. G., Iversen, J. D., and Vogel, J. M., 1987, "Vortex Sheet Modeling with Curved Higher-Order Panels," *J. Aircraft*, Vol. 24, No. 11, pp. 776–782.

Nakamura, Y., Leonard, A., and Spalart, P., 1982, "Vortex Simulation of an Inviscid Shear Layer," AIAA-82-948.

Nathman, J. K., 1984, "Estimation of Wake Roll-up over Swept Wings," AIAA Paper 84-2174.

Naylor, P. J., 1982, "A Discrete Vortex Model for Bluff Bodies in Oscillatory Flow," Ph. D. thesis, Univ. of London.

Newsome, R. W., and Kandil, O. A., 1987, "Vortex Flow Aerodynamics—Physical Aspects and Numerical Simulations," AIAA-87-0205.

Ng, and Ghoniem, A. F., 1986, "Numerical Simulation of a Confined Shear Layer," *Dynamics of Reactive Systems Part II: Modeling and Heterogeneous Combustion* (Eds. J. R. Bowen et al.), Published by AIAA, pp. 18–49.

Noblesse, F., 1983, "A Slender-Ship Theory of Wave Resistance," *J. Ship Res.*, Vol. 27, No. 1, pp. 13–33.

Obayashi, S., and Fujii, 1985, "Computation of Three-Dimensional Viscous Transonic Flows with the LU Factored Scheme," AIAA-85-1510.

Obayashi, S., and Kuwahara, K., 1987, "Navier-Stokes Simulation of Side Wall Effect of Two-Dimensional Transonic Wind Tunnel," AIAA-87-0037.

Orlik-Ruckemann, K. J., 1982, "Unsteady Aerodynamics and Dynamic Stability at High Angles of Attack," AGARD-LS-121, Paper No. 8.

Oswatitsch, K., 1957, "Die Ablosungsbedingung von Grenzschichten,"

*Grenzschichtforschung* (Ed. H. Gortler), Springer Verlag, Berlin, pp. 357–367.

Panaras, A. G., 1985, "Pressure Pulses Generated by the Interaction of a Discrete Vortex with an Edge," *J. Fluid Mech.*, Vol. 154, pp. 445–462 (see also AGARD-CP-386, 1985, pp. S3.1–S3.16).

Panaras, A. G., 1987, "Numerical Modeling of the Vortex/Airfoil Interaction," *AIAA J.*, Vol. 25, No. 1, pp.5–11.

Parekh, D. E., Leonard, A., Reynolds W. C., 1983, A Vortex Filament Simulation of a Bifurcating Jet," *Bull. Am. Phys. Soc.*, Vol. 28, p. 1353.

Patel, M. H., and Brown, D. T., 1986, "On Predictions of Resonant Roll Motions for Flat-Bottomed Barges," *Roy. Inst. Naval Arch., Supplementary Papers*, Vol. 128.

Payne, F. M., Ng, T. T., and Nelson, R. C., 1986, "Visualization and Flow Surveys of the Leading Edge Vortex Structure on Delta Wing Planforms," AIAA-86-0330.

Peace, A. J., 1983, "A Multi-Vortex Model of Leading-Edge Vortex Flows," *Int. J. for Numer. Meth. in Fluids*, Vol. 3, pp. 543–565.

Peake, D. J., and Rainbird, W. J., "Technical Evaluation Report on the Fluid Dynamics Panel Symposium on Flow Separation," AGARD-AR-98, 1975, pp. 1–12.

Perlman, M., 1985, "On the Accuracy of Vortex Methods," *J. Comp. Phys.*, Vol. 59, pp. 200–223.

Peskin, C. S., 1972, "Flow Patterns Around Heart Valves: A Numerical Method," *J. Comput. Phys.*, Vol. 10, pp. 252–271.

Peskin, C. S., 1977, "Numerical Analysis of Blood Flow in the Heart," *J. Comput. Phys.*, Vol. 25, pp. 220–252.

Peskin, C. S., 1982, "The Fluid Dynamics of Heart Valves: Experimental, Theoretical, and Computational Methods," *Ann. Rev. Fluid Mech.*, Vol. 14, pp. 235–259.

Peskin, C. S., and Wolfe, A. W., 1978, "The Aortic Sinus Vortex," *Fed. Proc.*, Vol. 37, pp. 2784–2792.

Peters, N., 1975, "Calculation of the Instationary Turbulent Flow Past a Flat Plate Using a Net-Free Numerical Method," *Proc. GAMM-Conference on Numerical Methods in Fluid Mechanics* (Ed. E. H. Hirschel), pp. 134–141.

Peters, N., and Thies, H.-J., 1982, "Random Walk and Diffusion in Two-Dimensional Lagrangian Systems," *Recent Contributions to Fluid Mechanics* (Ed. W. Haase), Springer-Verlag, pp. 205–212.

Pettersen, B., and Faltinsen, O., 1983, "Separated Flow Around Circular Cylinders," *Proc. Int. Workshop on Ship and Platform Motions*, Berkeley.

Phillips, W. R. C., 1981, "The Turbulent Trailing Vortex During Roll-Up," *J. Fluid Mech.*, Vol. 105, pp. 451–467.

Pien, P. C., 1964, "The Application of Wavemaking Resistance Theory to the Design of Ship Hulls with Lower Total Resistance," *Proc. Fifth Symp. on Naval Hydrodynamics*, Bergen, Norway.

Pierce, D., 1961, "Photographic Evidence of the Formation and Growth of Vorticity Behind Plates Accelerated from Rest in Still Air," *J. Fluid Mech.*, Vol. 11, pp. 460–464.

Piziali, R. A., 1966, "A Method of Predicting the Aerodynamic Loads and Dynamic Responds of Rotor Blades," CAL Rep. BB-1932-5-1, USAAVLABS TR 65-74.

Poincare, H., 1893, *Theorie des Tourbillons*, Ed. G. Carre, Chapt. 4. Paris: Deslis Freres, 211 pp.

Polhamus, E. C., 1966, "A Concept of the Vortex Lift of Sharp-Edged Delta Wings Based on a Leading-Edge Suction Analogy," NASA TN D-3767.

Polhamus, E. C., 1979, "Technical Evaluation Report on the FDPS on High Angle of Attack Aerodynamics," AGARD AR-145.

Poling, D. R., Dadone, L., and Telionis, D. P., 1987, "Blade-Vortex Interaction," AIAA-87-0497.

Poling, D. R., and Telionis, D. P., 1986, "The Response of Airfoils to Periodic Disturbances—The Unsteady Kutta Condition," *AIAA J.*, Vol. 24, No. 2, pp. 193-199.

Porthouse, D. T. C., and Lewis, R. I., 1981, "Simulation of Viscous Diffusion for Extension of the Surface Vorticity Method to Boundary Layer and Separated Flows," *J. Mech. Engng. Sci.*, Vol. 23, No. 3, pp. 157–167.

Portnoy, H., 1976, "The Initial Roll-up of a Thick Two-Dimensional Wake Behind a Finite Span," *Aeronaut J.*, Vol. 80, pp. 442–447.

Portnoy, H., 1977, "Thick Two-Dimensional Wake Roll-up Behind a Wing of Finite Span—Extended Calculations," *Aeron. J.*, Vol. 81, pp. 460-463.

Pozrikidis, C., and Higdon, J. J. L., 1985, "Nonlinear Kelvin-Helmholtz Instability of a Finite Vortex Layer," *J. Fluid Mech.*, Vol. 157, pp. 225–263.

Prandtl. L., 1919, "Tragflugeltheorie," *Gottingen Nachrichten, II Mitteilung*, pp. 107–137.

Puckett, E. G., 1987, "A Study of the Vortex Sheet Method and its Rate of Convergence," Lawrence Berkeley Lab., Preprint 23341.

Pullin, D. I., 1975, "Calculations of the Steady Conical Flow Past a Yawed Slender Delta Wing with Leading Edge Separation," Aero. R.&M. No. 3767.

Pullin, D. I., 1978, "The Large-Scale Structure of Unsteady Self-Similar Vortex Sheets," *J. Fluid Mech.*, Vol. 88, Part 3, pp. 401–430.

Pullin, D. I., 1979, "Vortex Formation at Tube and Orifice Openings," *Phys. Fluids*, Vol. 22, pp. 401–403.

Pullin, D. I., and Perry, A. E., 1980, "Some Flow Visualization Experiments on the Starting Vortex," *J. Fluid Mech.*, Vol. 97, Part 2, pp. 239–256.

Pumir, A., and Siggia, E. D., 1987, "Vortex Dynamics and the Existence of Solutions to the Navier-Stokes Equations," *Phys. Fluids*, Vol. 30, No. 6, pp. 1606–1626.

Quartapelle, L., and Napolitano, M., 1983, "Force and Moment in Incompressible Flows," *AIAA J.*, Vol. 21, No. 6, pp. 911–913.

Raj, P., and Brennan, J., 1987, "Improvements to an Euler Aerodynamic Method for Transonic Flow Analysis," AIAA-87-0040.

Rayleigh, Lord, 1916, "On the Dynamics of Revolving Fluids," *Scientific Papers*, Vol. 6, pp. 447–453, Cambridge Univ. Press, Cambridge.

Rehbach, C., 1973, "Calculation of Flow Around Zero-Thickness Wings with Evolute Vortex Sheets," NASA TT F-15.

Rehbach, C., 1977, "Numerical Investigation of Vortex Sheets Issuing from a Separation Line Near the Leading Edge," NASA TM-F 15.

Rehbach, C., 1978, "Numerical Calculation of Unsteady Three-Dimensional Flows with Vortex Sheets," AIAA Paper No. 78–111.

Ribaut, M., 1983, "A Vortex Sheet Method for Calculating Separated Two-Dimensional Flows," *AIAA J.*, Vol. 12, No. 8, pp. 1079–1084.

Richardson, L. F., 1922, *Weather Prediction by Numerical Process*, Cambridge Univ. Press, London.

Rizzi, A., 1988, "Multi-Cell Vortices Computed in Large-Scale Difference Solution to the Incompressible Euler Equations," *J. Comput. Phys.*, Vol. 77, pp.207–220.

Rizzi, A., and Engquist, B., 1987, "Selected Topics in the Theory and Practice of Computational Fluid Dynamics," *J. Comput. Phys.*, Vol. 72, pp. 1–69.

Rizzi, A., and Eriksson, L-E., 1985, "Computation of Inviscid Incompressible Flow with Rotation," *J. Fluid Mech.*, Vol. 153, pp. 275–312.

Rizzi, A., and Muller, B., 1988, "Comparison of Euler and Navier-Stokes Solutions for Vortex Flow over a Delta Wing," *Aeronautical J.*, pp. 145–153.

Rizzi, A., and Purcell, C. J., "On the Computation of Transonic Leading-Edge Vortices Using the Euler Equations," *J. Fluid Mech.*, Vol. 181, pp. 163–195.

Rizzetta, D. P., and Shang, J. S., 1986, "Numerical Simulation of Leading-Edge Vortex Flows," *AIAA J.*, Vol. 24, No. 2, pp. 237–245.

Roberts, A. J., 1983, "A Stable and Accurate Numerical Method to Calculate the Motion of a Sharp Interface Between Fluids," *IMA J. Appl. Maths.*, Vol. 31, pp. 13–35.

Roberts, S., 1985, "Accuracy of the Random Vortex Method for a Problem with Non-Smooth Initial Conditions," *J. Comput. Phys.*, Vol. 58, pp. 29–43.

Rogler, H., 1978, "The Interaction Between Vortex-Array Representations of Free Stream Turbulence and Semi-Infinite Flat Plates," *J. Fluid Mech.*, Vol. 87, pp. 583–606.

Rom, J., and Almosnino, D., 1978, "Studies of Nonlinear Aerodynamic Characteristics of Finned Slender Bodies at High Angle of Attack," Israel Inst. of Tech., TAE No. 349.

Rom, J., Almosnino, D., and Gordon, R., 1981, "Method for the Calculation of the Non-Linear Aerodynamic Characteristics of Thick Wings and Bodies Including Symmetric Vortex Separation in Subsonic Flows," Dept. of Aero. Engng., Technion, Haifa, TAE Rep. 437.

Rosenhead, L., 1930, "The Spread of Vorticity in the Wake Behind a Cylinder," *Proc. Roy. Soc.*, Series A, Vol. 127, pp. 590–612.

Rosenhead, L., 1931, "The Formation of Vortices from a Surface of Discontinuity," *Proc. Roy. Soc.* Series A, Vol. 134, pp. 170–192.

Roshko, A., 1976, "Structure of Turbulent Shear Flows: A New Look," *AIAA J.*, Vol. 14, pp. 1349–1357.

Rossow, V. J., 1977, "Convective Merging of Vortex Cores in Lift-Generated Wakes," *J. Aircraft*, Vol. 14, pp. 283–290.

Rott, N., 1956, "Diffraction of a Weak Shock with Vortex Generation," *J. Fluid Mech.*, pp. 111–128.

Rottman, J. W., Simpson, J. E., and Stansby, P. K., 1987, "The Motion of a Cylinder of Fluid Released from Rest in a Cross Flow," *J. Fluid Mech.*, Vol. 177, pp. 307–337.

Roy, M., 1957, "Sur La Theorie de l'aile en Delta: Tourbillons d'Apex et Nappes en Cornet," *Recherche Aeronautique*, No. 56, pp. 3–12.

Rusak, Z., Wasserstrom, E., and Seginer, A., 1983, "Numerical Calculation of Nonlinear Aerodynamics of Wing-Body Configurations," *AIAA J.*, Vol. 21, No. 7, pp. 929–936.

Sacks, A. H., Lundberg, R. E., and Hanson, C. W., 1967, "A Theoretical Investigation of the Aerodynamics of Slender Wing-Body Combinations Exhibiting Leading-Edge Separation," NASA CR-719.

Saffman, P. G., 1970, "The Velocity of Viscous Vortex Rings," *Stud. Appl. Math.*, Vol. 49, 1970, pp. 371–380.

Saffman, P. G., 1974, "The Structure and Decay of Trailing Vortices," *Arch. Mech.*, Vol. 26, pp. 423–439.

Saffman, P. G., 1978, "The Number of Waves on Unstable Vortex Rings," *J. Fluid Mech.*, Vol. 84, pp. 625–639.

Saffman, P. G., 1979, "The Approach of a Vortex Pair to a Plane Surface in Inviscid Fluid," *J. Fluid Mech.*, Vol. 92, pp. 497–503.

Saffman, P. G., 1981, "Dynamics of Vorticity," *J. Fluid Mech.*, Vol. 106, pp. 49–58.

Saffman, P. G., and Baker, G. R., 1979, "Vortex Interactions," *Ann. Rev. Fluid Mech.*, Vol. 11, pp. 95–122.

Saffman, P. G., and Meiron, D. I., 1986, "Difficulties with Three-Dimensional Weak Solutions for Inviscid Incompressible Flow," *Phys. Fluids*, Vol. 29, pp. 2373–2375.

Saffman, P. G., and Schatzman, J. C., 1981, Properties of a Vortex Street of Finite Vortices," *SIAM J. Sci. Stat. Comput.*, Vol. 2, pp. 285–295.

Saffman, P. G., and Schatzman, J. C., 1982a, "Stability of a Vortex Street of Finite Vortices," *J. Fluid Mech.*, Vol. 117, pp. 171–185.

Saffman, P. G., and Schatzman, J. C., 1982b, "An Inviscid Model for the Vortex-Street Wake," *J. Fluid Mech.*, Vol. 122, pp. 467–486.

Sarpkaya, T., 1963, "Lift, Drag, and Added-Mass Coefficients for a Circular

Cylinder Immersed in a Time-Dependent Flow," ASME *Journal of Applied Mechanics*, Vol. 85, pp. 13–15.

Sarpkaya, T., 1966, "Separated Flow About Lifting Bodies and Impulsive Flow about Cylinders," *AIAA J.*, Vol. 4, pp. 414–420.

Sarpkaya, T., 1968a, "Separated Flow About a Rotating Plate," *Developments in Mechanics*, Vol. 4, pp. 1485–1499.

Sarpkaya, T., 1968b, "An Analytical Study of Separated Flow About Circular Cylinders," ASME *Journal of Basic Engineering*, Vol. 90, pp. 511–520.

Sarpkaya, T., 1969, "Analytical Study of Separated Flow About Circular Cylinders," *Phys. of Fluids*, Vol. 12, Supplement II, p. 145.

Sarpkaya, T., 1971, "On Stationary and Traveling Vortex Breakdowns," *J. Fluid Mech.*, Vol. 45, pp. 545–559.

Sarpkaya, T., 1975a, Comment on "Theoretical Study of Lift-Generated Vortex Wakes Designed to Avoid Roll-up," *AIAA J.*, Vol. 13, pp. 1680–1681.

Sarpkaya, T., 1975b, "An Inviscid Model of Two-Dimensional Vortex Shedding for Transient and Asymptotically Steady Separated Flow over an Inclined Flat Plate," *J. Fluid Mech.*, Vol. 68, pp. 109–128.

Sarpkaya, T., 1976, "Vortex Shedding and Resistance in Harmonic Flow about Smooth and Rough Circular Cylinders at High Reynolds Numbers," Report No: NPS-59SL76021, Naval Postgraduate School, Monterey, CA.

Sarpkaya, T., 1978a, "Fluid Forces on Oscillating Cylinders," *J. WPCO Div.*, ASCE, Vol. 104, No. WW4, pp. 275–290.

Sarpkaya, T., 1978b, "Impulsive Flow About a Circular Cylinder," Naval Postgraduate School Report No. NPS-69SL-78-008.

Sarpkaya, T., 1979, "Vortex-Induced Oscillations—A Selective Review," ASME *Journal of Applied Mechanics*, Vol. 46, pp. 241–258.

Sarpkaya, T., 1983, "Trailing Vortices in Homogeneous and Density Stratified Media," *J. Fluid Mech.*, Vol. 136, pp. 85–109.

Sarpkaya, T., 1985, "Past Progress and Outstanding Problems in Time-Dependent Flows about Ocean Structures," *Separated Flow Around Marine Structures*, pp. 1–36. Trondheim: The Norwegian Institute of Technology.

Sarpkaya, T., 1986a, Oscillating Flow over Bluff Bodies in a U-Shaped Water Tunnel," *Proc. AGARD Symposium on Aerodynamic and Related Hydrodynamic Studies Using Water Facilities*, AGARD CP-413, Paper No. 6.

Sarpkaya, T., 1986b, "Forces on a Circular Cylinder in Viscous Oscillating Flow at Low Keulegan-Carpenter Numbers," *J. Fluid Mech.*, Vol. 165, pp. 61–71.

Sarpkaya, T., 1986c, "Trailing-Vortex Wakes on the Free Surface," *Proc. 16th Symposium on Naval Hydrodynamics*, National Academy Press, pp. 38-50.

Sarpkaya, T., 1987, "Oscillating Flow About Smooth and Rough Cylinders," ASME *Journal Offshore Mechanics and Arctic Engineering*, Vol. 109, pp. 307–313.

Sarpkaya, T., and Daly, J. J., 1987, "Effect of Ambient Turbulence on Trailing Vortices," *J. Aircraft*, Vol. 24, No. 6, pp. 399–404.

Sarpkaya, T., and Elnitsky, J., and Leeker, R. E., 1988, "Wake of a Vortex Pair on the Free Surface," *Proc. 17th Symposium on Naval Hydrodynamics*, The Hague, The Netherlands, pp. 47–54.

Sarpkaya, T., and Ihrig, C. J., 1986, "Impulsively Started Flow About Rectangular Prisms: Experiments and Discrete Vortex Analysis," ASME JOURNAL OF FLUIDS ENGINEERING, Vol. 108, pp. 47–54.

Sarpkaya, T., and Isaacson, M., 1981, *Mechanics of Wave Forces on Offshore Structures*, Van Nostrand Reinhold, New York.

Sarpkaya, T., and Kline, H. K., 1982, "Impulsively-Started Flow About Four Types of Bluff Body," ASME JOURNAL OF FLUIDS ENGINEERING, Vol. 104, No. 2, pp. 207–213.

Sarpkaya, T., Mostafa, S. I. M., and Munz, P. D., 1987, "Unsteady Flow About Cambered Plates," Technical Report No. NPS-69-87-012, Naval Postgraduate School, Monterey, CA.

Sarpkaya, T., and Shoaff, R. L., 1979a, "An Inviscid Model of Two-Dimensional Vortex Shedding for Transient and Asymptotically Steady Separated Flow Over a Cylinder," *AIAA J.*, Vol. 17, No. 11, pp. 1193–1200.

Sarpkaya, T., and Shoaff, R. L., 1979b, "A Discrete-Vortex Analysis of Flow About Stationary and Transversely Oscillating Circular Cylinders," Naval Postgraduate School Technical Report No: NPS-69SL79011, Monterey, CA.

Savage, S. B., 1979, "The Role of Vortex and Unsteady Effects During the Hovering of Dragonflies," *J. Experimental Biology*, Vol. 83, pp. 59–77.

Sawaragi, T., and Nakamura, T., 1979, "Analytical Study of Wave Force on a Cylinder in Oscillatory Flow," *Coastal Structures*, Vol. 1, pp. 154–173, ASCE, New York.

Schewe, G., 1986, "Sensitivity of Transition Phenomena to Small Perturbations in Flow Round a Circular Cylinder," *J. Fluid Mech.*, Vol. 172, pp. 33–46.

Schindel, L., 1969, "Effects of Vortex Separation on Lift Distribution of Elliptic Cross-Section," *J. Aircraft*, Vol. 6, No. 6, pp. 537–543.

Schindel, L. H., and Chamberlain, T. E., 1967, "Vortex Separation on Slender Bodies of Elliptic Cross Section," TR 138, MIT Aerophysics Lab., Cambridge, MA.

Schlichting, H., 1932, "Berechnung ebener Periodischer Grenzschichtstromungen," *Phs. Zeit.*, Vol. 33, pp. 327–335.

Schmidt, D. W. von., and Tilmann, P. M., 1972, "Uber die Zikulationsentwicklung in Nachlaufen von Rundstaben," *Acustica*, Vol. 27, pp. 14–22.

Schroder, W., 1980, "Theoretical Estimation of Non-Linear Longitudinal Characteristics of Wings with Small and Moderate Aspect Ratio by the Vortex Method in Incompressible Flow," European Space Agency Technical Translation, ESA-TT-585.

Schumann, U., and Sweet, R. A., 1988, "Fast Fourier Transforms for Direct Solution of Poisson's Equation with Staggered Boundary Conditions," *J. Comput. Phys.*, Vol. 75, pp. 123–137.

Schwartz, K. W., 1982, "Generation of Superfluid Turbulence Deduced from Simple Dynamical Rules," *Phys. Rev. Lett.*, Vol. 49, pp. 283–285.

Schwartz, L. W., 1981, "A Semi-Analytic Approach to the Self-Induced Motion of Vortex Sheets," *J. Fluid Mech.*, Vol. 111, pp. 475–490.

Sears, W. R., 1956, "Some Recent Developments in Airfoil Theory," *J. Aero. Sci.*, Vol. 23, pp. 490–499.

Sears, W. R., 1976, "Unsteady Motion of Airfoils with Boundary-Layer Separation," *AIAA J.*, Vol. 14, pp. 216–220.

Sears, W. R., and Telionis, D. P., 1975, "Boundary Layer Separation in Unsteady Flow," *SIAM J. on Appl. Math.*, Vol. 28, No. 1, pp. 215–235.

Seshadri, S. N., and Narayan, K. Y., 1988, "Possible Types of Flow on Lee-Surface of Delta Wings at Supersonic Speeds," *Aeronaut. J.*, Vol. 92, No. 915, pp. 185–199.

Sethian, J. A., 1984, "Turbulent Combustion in Open and Closed Vessels," *J. Comput. Phys.*, Vol. 54, pp. 425–456.

Sethian, J. A., and Ghoniem, A. F., 1988, "Validation Study of Vortex Methods," *J. Comput. Phys.*, Vol. 74, pp. 283–317.

Shamroth, S. J., 1979, "A Viscous Flow Analysis for the Tip Vortex Generation Process," NASA CR-318.

Sheen, Q. Y., 1986, "Potential Flow Analysis of Unsteady Joukowski Airfoil in the Presence of Discrete Vortices," Ph.D. thesis, Univ. of Colorado, Boulder.

Shestakov, A. I., 1979, "A Hybrid Vortex-ADI Solution for Flow of Low Viscosity," *J. Comput. Phys.*, Vol. 31, pp. 313–334.

Shigemi, M., 1987, "Application of Discrete Vortex Method to Analysis of Separated Flow Around Aerofoils," *Trans. Japan Soc. for Aeronautical and Space Sci.*, Vol. 29, pp. 207–219.

Shirayama, S., and Kuwahara, K., 1987, "Patterns of Three-Dimensional Boundary Layer Separation," AIAA-87-0461.

Shirayama, S., Ohta, T., and Kuwahara, K., 1987, "Three-Dimensional Flow Past a Two-Dimensional Body," AIAA-87-0605.

Shivananda, T. P., and Oberkampf, W. L., 1981, "Prediction of the Compressible Vortex Wake for Bodies at High Incidence," AIAA-81-0360.

Shoaff, R. L., and Franks, C. B., 1981, "A Discrete Vortex Analysis of Flow About Non-Circular Cylinders," *Proc. 3rd Int. Conf. on Numerical Ship Hydrodynamics*, Paris, pp. 319–333.

Siddiqi, S., 1987, "Trailing Vortex Roll-up Computations using the Point Vortex Method," AIAA-87-2479.

Siggia, E. D., 1985, "Collapse and Amplification of a Vortex Filament," *Phys. Fluids*, Vol. 28, No. 3, pp. 794–805.

Simpson, R. L., 1981, "A Review of Some Phenomena in Turbulent Flow Separation," ASME JOURNAL OF FLUIDS ENGINEERING, Vol. 103, pp. 520–533.

Simpson, R. L., 1987, "Two-Dimensional Turbulent Separated Flow," *AIAA J.*, Vol. 25, No. 6, pp. 775–776.

Skomedal, N. G., and Vada, T., 1985, "The Vortex-in-Cell Method. Capability of Numerical Simulation of the Flow Past one Circular Cylinder in Laminar and Turbulent Flow," Report 85-2043, A. A. Veritas Research, Hovik, Norway.

Skomedal, N. G., and Vada, T., 1987, "Numerical Stimulation of Vortex Shedding Induced Oscillations of a Circular Cylinder," *Proc. 2nd int. Conf. on Advances in Numerical Methods in Engng. Theory and Applications*, Swansea, Wales, pp. 1–7.

Smith, J. H. B., 1966, "Improved Calculations of Leading-Edge Separation From Slender Delta Wings," RAE TR No. 66070.

Smith, J. H. B., 1968, "Improved Calculations of Leading-Edge Separation from Slender, Thin, Delta Wings," *Proc. Roy. Soc. London*, Ser. A., Vol. 306, pp. 67–90.

Smith, J. H. B., 1980, "Vortical Flows and Their Computation," RAE TM Aero-1866, Roy. Aircraft Establishment, Farnborough, Hants, UK.

Smith, J. H. B., 1986, "Vortex Flows in Aerodynamics," *Ann. Rev. Fluid Mech.*, Vol. 18, pp. 221–242.

Smith, P. A., 1986, "Computation of Viscous Flows by the Vortex Method," Ph. D. thesis, Univ. of Manchester.

Smith P. A., and Stansby, P. K., 1985, "Wave-Induced Bed Flows by a Lagrangian Vortex Scheme," *J. Comput. Phys.*, Vol. 60, No. 3, pp. 489–516.

Smith P. A., and Stansby, P. K., 1987, "Generalized Discrete Vortex Method for Cylinders Without Sharp Edges," *AIAA J.*, Vol. 25, No. 2, pp. 199–200.

Soh, W. K., and Fink, P. T., 1971, "On Potential Flow Modelling of the Action of Ship's Bilge Keels," *Proc. 4th Aust. Conf. Hyd. Fluid Mech.*, Monash Univ.

Spalart, P. R., 1982, "Numerical Simulation of Separated Flows," Ph.D. dissertation, Univ. of CA, Berkeley.

Spalart, P. R., and Leonard, A., 1981, "Computation of Separated Flows by a Vortex-Tracing Algorithm," AIAA-81-1246.

Spalart, P. R., Leonard, A., and Baganoff, D., 1983, "Numerical Simulation of Separated Flows," NASA TM-84328.

Spalding, D. B., 1986, "The Two-Fluid Model of Turbulence Applied to Combustion Phenomena," *AIAA J.*, Vol. 24, No. 6, pp. 876–884.

Spreiter, J. R., and Sacks, A. H., 1951, "The Rolling up of the Trailing Vortex and its Effect of the Downwash behind Wings," *J. Aeronaut. Sci.*, Vol. 18, pp. 21–32.

Squire, H. B., 1954, "The Growth of a Vortex in Turbulent Flow," ARC-16666, F.M. 2053. (Also in *Aeronaut. Quart.*, Vol. 16, 1965, pp. 302–306).

Sreenivasan, K. R., Strykowski, P. J., and Olinger, D. J., 1987, "Hope Bifurcation, Landau Equation, and Vortex Shedding Behind Circular Cylinders," *Forum on Unsteady Flow Separation* (Ed. K. N. Ghia), ASME, FED-Vol. 52, pp. 1-13.

Srinivasan, G. R., McCroskey, W. J., Baeder, J. D., and Edwards, T. A., 1986, "Numerical Simulation of Tip Vortices of Wings in Subsonic and Transonic Flows," AIAA-86-1095.

Stansby, P. K., 1977, "An Inviscid Model of Vortex Shedding From a Circular Cylinder in Steady and Oscillatory Far Flows," *Proc. Inst. Civ. Eng.*, Vol. 63, Part 2, pp. 865-880.

Stansby, P. K., 1979, "Mathematical Modeling of Vortex Shedding from Circular Cylinders in Planar Oscillatory Flows, Including Effects of Harmonics," *Mechanics of Wave-Induced Forces on Cylinders* (Ed. T. L. Shaw), Pitman, London, pp. 450-460.

Stansby, P. K., 1981, "A Numerical Study of Vortex Shedding from One and Two Circular Cylinders," *Aeronaut. Quart.*, Vol. 32, Pt. 1, pp. 48-68.

Stansby, P. K., 1985, "A Generalized Discrete-Vortex Method for Sharp-Edged Cylinders," *AIAA J.*, Vol. 23, No. 6, pp. 856-861.

Stansby, P. K., and Dixon, A. G., 1982, "The Importance of Secondary Shedding in Two-Dimensional Wake Formation at Very High Reynolds Numbers," *Aeronaut. Quart.*, Vol. 33, pp. 105-123.

Stansby, P. K., and Dixon, A. G., 1983, "Simulation of Flows Around Cylinders by a Lagrangian Vortex Scheme," *Appl. Ocean Res.*, Vol. 5, pp. 167-178.

Stansby, P. K., Smith, P. A., and Penoyre, R., 1987, "Flow Around Multiple Cylinders by the Vortex method," *Proc. International Conf. on Flow Induced Vibrations*, British Hydromechanics Res. Assoc., pp. 41-50.

Staufenbiel. R. W., 1984, "Structure of Lift-Generated Rolled-up Vortices," *J. Aircraft*, Vol. 21, No. 10, pp. 737-744.

Stratford, B. S., 1957, "Flow in Laminar Boundary Layers Near Separation," Rep. & Mem. Aero. Res. Counc. London, No. 3002.

Stratford, B. S., 1959, "The Prediction of Separation of the Turbulent Boundary Layer," *J. Fluid Mech.*, Vol. 5, pp. 1-16.

Strickland, J. H., Webster, B. T., and Nguyen, T., 1979, "A Vortex Model of the Darrieus Turbine: An Analytical and Experimental Study, ASME JOURNAL OF FLUIDS ENGINEERING, Vol. 101, pp. 500-505.

Summers, D. M., Hanson, T., and Wilson, C. B., 1985, "A Random Vortex Simulation of Wind-Flow Over a Building," *Int. J. for Num. Meth. in Fluids*, Vol. 5, pp. 849-871.

Sychev, V. V., 1972, "On Laminar Separation," *Izv. Akad. Nauk. Mech. Zhid. Gaza*, No. 3, pp. 47-59. Translated in *Fluid Dynamics*, Plenum, March/April 1974, pp. 407-419.

Takada, H., 1975, "An Extension to the Critical Flow of Stratford's Theory for Predicting the Turbulent Separation Position," *J. Physical Soc. Japan*, Vol. 39, No. 4, pp. 1106-1112.

Takami, H., 1964, "A Numerical Experiment with Discrete Vortex Approximation, with Reference to the Rolling up of a Vortex Sheet," Dept. Aero. and Astronaut. Stanford Univ. Rep. SUDAER 202, 1964.

Tamura, T., Tsuboi, K., and Kuwahara, K., 1988, "Numerical Simulation of Unsteady Flow Patterns Around a Vibrating Cylinder," AIAA-88-0128.

Taneda, S., 1977, "Visual Study of Unsteady Separated Flows around Bodies," *Prog. Aerospace Sci.*, Vol. 17, pp. 287-348.

Taneda, S., 1980, "Definition of Separation," *Reports of Research Institute for Applied Mechanics*, Kyushu Univ., Vol. 28, No. 89, pp. 73-81.

Telionis, D. P., 1979, "Review—Unsteady Boundary Layers, Separated and Attached," ASME JOURNAL OF FLUIDS ENGINEERING, Vol. 101, pp. 29-43.

Telionis, D. P., and Mathioulakis, D. S., 1984, "On the Shedding of Vorticity at Separation," *Unsteady Separated Flows* (Ed. M. W. Luttges), pp. 106-116. AFOSR, SRL, Univ. of Colorado.

Teng, Z. H., 1982, "Elliptic-Vortex Method for Incompressible Flow at High Reynolds Number," *J. Comput. Phys.*, Vol. 46, pp. 54-68.

Thom, A., 1933, "The Flow Past Circular Cylinders at Slow Speeds," *Proc. Roy. Soc.* London, Series A, Vol. 141, pp. 651-669.

Thoman, D. C., and Szewczyk, A. A., 1969, "Time-Dependent Viscous Flow Over a Cylinder," *Phys. of Fluids*, Vol. 12, Supplement II, pp. 76-86.

Thomas, J. L., Taylor, S. L., and Anderson, K., 1987, "Navier-Stokes Computations of Vortical Flows Over Low Aspect Wings," AIAA-87-0207.

Thompson, K. S., and Morrison, D. F., 1971, "The Spacing Position, and Strength of Vortices in the Wake of Slender Cylindrical Bodies at Large Incidence," *J. Fluid Mech.*, Vol. 50, Part 4, pp. 751-783.

Thrasher, D. F., 1982, "Application of the Vortex-Lattice Concept to Flows with Smooth-Surface Separation," Proc. ONR Symposium on Naval Hydrodynamics, Ann Arbor, MI. (see also DTNSRDC-85/041, 1985).

Tiemroth, E. C., 1986a, "Simulation of the Viscous Flow Around a Cylinder by the Random Vortex Method," Ph.D. thesis, Univ. of Calif., Berkeley.

Tiemroth, E. C., 1986b, "The Simulation of the Viscous Flow over a Cylinder in a Wave Field," *Proc. 16th Symp. Naval Hydrodynamics,* U. of CA, Berkeley (Ed. W. C. Webster), National Academy Press, pp. 490-513.

Tomassian, J. D., 1979, "The Motion of a Vortex Pair in a Stratified Medium," Ph.D. thesis, Univ. of CA, Los Angeles.

Townsend, A. A., 1956, *The Structure of Turbulent Shear Flow*, Cambridge Univ. Press.

Tryggvason, G., 1988a, "Numerical Simulations of the Rayleigh-Taylor Instability," *J. Comp. Phys.*, Vol. 75, pp. 253-282.

Tryggvason, G., 1988b, "Deformation of a Free Surface as a Result of Vortical Flows," *Phys. Fluids*, Vol. 31, No. 5, pp. 955-957.

Vada, T., and Skomedal, N. G., 1986, "Simulation of Supercritical Viscous Flow around Two Cylinders in Various Configurations," Report No. 86-2020, A. S. Veritas Research, Hovik, Norway.

van der Vegt, J. J. W., 1988, "A Variationally Optimized Vortex Tracing Algorithm for 3-Dimensional Flows around Solid Bodies," Ph.D. thesis, Maritime Research Inst., The Netherlands.

van der Vegt, J. J. W., and de Boom, W. C., 1985, "Numerical Simulation of Flow Around Circular Cylinders at High Reynolds Numbers," *Proc. BOSS'85*, pp. 227-238, Amsterdam: Elsevier Science Publishers.

van der Vegt, J. J. W., and Huijsmans, R. H. M., 1984, "Numerical Simulation of Flow Around Bluff Bodies at High Reynolds Numbers," *15th Symp. Naval Hydro.*, Hamburg, pp. 569-585.

Van der Vooren A. I., 1980, "A Numerical Investigation of the Rolling-up of Vortex Sheets," *Proc. Roy. Soc. London*, Series A, Vol. 373, pp. 67-91. (Also Math. Inst. Groniengen Rep. TW-21, 1965; and also IUTAM Conf., Ann Arbor, Mich., July 1964).

Van Dommelen, L. L., 1981, "Unsteady Boundary-Layer Separation," Ph.D. thesis, Cornell Univ., New York.

Van Dommelen, L. L., 1987, "Unsteady Separation from a Lagrangian Point of View," *Proc. Forum on Unsteady Flow Separation* (Ed. K. N. Ghia), ASME FED-Vol. 52, pp.81-84.

Van Dommelen, L. L., and Shen S. F., 1983, "An Unsteady Interactive Separation Process," *AIAA J.*, Vol. 21, No. 3, pp.358-362.

Van Tuyl, A. H., 1988, "Vortex Filament Model of the Wake Behind a Missile at High Angle of Attack," *AIAA J.*, Vol. 26, No. 3, pp. 264-270.

von Kerczek, C., and Tuck, E. O., 1969, "The Representation of Ship Hulls by Conformal Mapping Functions," *J. Ship Research*, Vol. 13, No. 4, pp. 284-298.

Wai, J. C., Baillie, J. C., and Yoshihara, H., 1985, "Computation of Turbulent Separated Flows over Wings," *Proc. 3rd Symp. on Num. and Physical Aspects of Aerod. Flows*, Paper No. II, Long Beach, CA.

Wang, S. S., 1977, "Grid-Insensitive Computer Simulation of the Kelvin-Helmholtz Instability and Shear Flow Turbulence," Ph.D. thesis, Stanford Univ., Inst. for Plasma Res. Rep. No. 710.

Ward, E. G., and Dalton, C., 1969, "Strictly Sinusoidal Flow Around a Stationary Cylinder," ASME *Journal of Basic Engineering.*, Vol. 91, pp. 141-174.

Wardlaw, A. B., 1974, "Prediction of Yawing Force at High Angle of Attack," *AIAA J.*, Vol. 12, pp. 1142-1144.

Wardlaw, A. B. Jr., 1975, "Multivortex Model of Asymmetric Shedding on Slender Bodies at High Angle of Attack," AIAA Paper No. 75-123.

Webster, W. C., 1975, "The Flow About Arbitrary, Three-Dimensional Smooth Bodies," *J. Ship Res.*, Vol. 19, pp. 206-218.

Weihs, D., and Boasson, M., 1979, "Multiple Equilibrium Vortex Positions in Symmetric Shedding from Slender Bodies," *AIAA J.*, Vol. 17, No. 2, pp. 213-214.

Westwater, F. L., 1935, "The Rolling up of a Surface of Discontinuity Behind an Airfoil of Finite Span," ARC R&M 1692.

Widnall, S. E., 1975, "The Structure and Dynamics of Vortex Filaments," *Ann. Rev. Fluid Mech.*, Vol. 7, pp. 141-165.

Widnall, S. E., 1985a, "Review of Three-Dimensional Vortex Dynamics: Implications for the Computation of Separated and Turbulent Flows," *Studies of Vortex Dominated Flows*, (Eds. M. Y. Hussaini and M. D. Salas), pp. 16-32, Springer-Verlag.

Widnall, S. E., 1985b, "Three-Dimensional Instability of Vortices in Separated Flows," *Proc. Symposium on Separated Flow Around Marine Structures*, Norwegian Inst. of Tech., Trondheim, Norway, June 26-28.

Widnall, S. E., and Bliss, D. B., 1971, "Slender-Body Analysis of the Motion and Stability of a Vortex Filament Containing an Axial Flow," *J. Fluid Mech.*, Vol. 50, pp. 335-353.

Widnall, S. E., Bliss, D. B., and Salay, A., 1971, "Theoretical and Experimental Study of the Stability of a Vortex Pair," *Aircraft Wake Turbulence and Its Detection* (Eds. J. Olsen et al.), pp. 305-338. Plenum.

Widnall, S. E., and Sullivan, J. P., 1972, "On the Stability of Vortex Rings," *Proc. Roy. Soc. London*, Series A, Vol. 332, pp. 335-353.

Winant, C. D., and Browand, F. K., 1974, "Vortex Pairing: The Mechanism of Turbulent Mixing Layer Growth at Moderate Reynolds Number," *J. Fluid Mech.*, Vol. 63, pp. 237-255.

Xieyuan, Y., 1985, "Roll-up of Strake Leading/Trailing-Edge Vortex Sheets for Double-Delta Wings," *J. Aircraft*, Vol. 22, No. 1, pp. 87-89.

Yang, H. T., and Bar-Lev, M., 1976, "Potential Flow Model for an Impulsively Started Circular Cylinder," ASME *Journal of Applied Mechanics*, Vol. 43, pp. 213-216.

Yeh, D. T., and Plotkin, A., 1986, "Vortex Panel Calculation of Wake Roll-up Behind a Large Aspect Ratio Wing," *AIAA J.*, Vol. 24, No. 9, pp. 1417-1423.

Zabusky, N. J., 1980, "Contour-Dynamics: A Boundary-Integral Evolutionary Method for Incompressible Dissipationless Flows," *Numerical Methods for Engineering*, GAMNI 2nd Int. Congr., (Ed. E. Absi et al.), pp. 503-513, Paris: Dunod.

Zabusky, N. J., 1981, "Recent Developments in Contour Dynamics for the Euler Equations," *Ann. NY Acad. Sci.*, Vol. 373, pp. 160-170.

Zabusky, N. J., Hughes, M. H., and Roberts, K. V., 1979, "Contour Dynamics for the Euler Equations in Two Dimensions," *J. Comput. Phys.*, Vol. 30, pp. 96-106.

Zalosh, R. G., 1976, "Discretized Simulation of Vortex Sheet Evolution with Buoyancy and Surface Tension Effects," *AIAA J.*, Vol. 14, pp. 1517-1523.

Zaroodny, S. J., and Greenberg, M. D., 1973, "On a Vortex Sheet Approach to the Numerical Calculation of Water Waves," *J. Comp. Phys.*, Vol. 11, pp. 440-446.

**T. Ogawa**
Professor.

**H. Yoshida**
Professor.

Department of Practical Life Studies,
Hyogo University of Teacher Education,
Yashiro, Hyogo, 673-14 Japan

**Y. Yokota**
Instructor,
Division of Technical Arts,
Mikaho Junior High School,
Sapporo, Hokkaido, 064 Japan

# Development of Rotational Speed Control Systems for a Savonius-Type Wind Turbine

*An attempt is made here to increase the output of a Savonius rotor by using a flow deflecting plate. When the deflecting plate is located at the optimum position, the rotor power increases nearly 30 percent over that when no deflecting plate is present. The rotor torque was found to become almost zero, when the plate is placed just in front of the rotor. In addition, two systems to control the rotational speed of a Savonius rotor are developed. These permit the rotor to be stopped in strong wind. Operating characteristics of the two control systems are investigated.*

## Introduction

Savonius-type wind turbines cannot compete with high-speed propeller and Darrieus type wind turbines from the standpoint of aerodynamic efficiency. Nevertheless, they are simple to construct, insensitive to wind direction and self-starting. In considering these advantages, it is clear that Savonius wind turbines would be used more often if their rotor performance could be improved.

Since Savonius published the results of an experimental study of this type of wind turbine in 1931 [1], numerous experimental attempts have been made to improve rotor performance. For example, refer to Bach [2], Khan [3], Sheldahl et al. [4] and Ushiyama et al. [5]. These experimental studies examined factors such as the section shape of a rotor bucket, the number of the buckets and the overlap ratio of the buckets.

On the other hand, an analytical model was developed for performance analysis by Wilson et al. [6]. Similarly, Van Dusen and Kirchhoff [7] presented a vortex sheet model. Although these models have contributed to the improvement of Savonius rotors, a number of important issues have yet to be considered. For example, flow separation from bucket tips of the rotor has been ignored. To remedy this, Ogawa [8] attempted to analyze the flow around the Savonius rotor using a discrete vortex method. As the next step of the research, several experimental studies on the Savonius rotor with various auxiliary devices have been conducted to further enhance the performance. Sabzevari [9] and Sivasegaram [10] used an asymmetrical box with a funnel-shaped wind inlet in which the Savonius rotor was placed. Ogawa et al. [11] investigated rotor performance by the use of the guide vanes placed around the Savonius rotor. Recently, experimental studies to enhance rotor performance by the applicaton of the effects due to mutual interaction between two closely spaced Savonius rotors were performed by Charwat [12] and Ogawa et al. [13].

In the present work, a flow deflecting plate, which consists of a simple flat plate, is used to increase the rotor output. The upstream flow is deflected by the plate, and the velocity of the flow which streams into the concave face of the bucket is increased. The effects of the deflecting plate parameters, i.e., the plate width, A, the distance between the rotor and plate, B, and the azimuthal angle of the plate, $\theta$, are individually examined.

For practical application of a wind turbine, a rotational speed control device or a protection device for strong winds is essential. It is neither reliable nor safe to use only a mechanical braking device, e.g., a disk brake, for speed control. To accomplish rotational speed control of a wind turbine it is necessary to control the aerodynamic force which operates on the rotor. In this study, two systems of rotational speed control are developed by moving the deflecting plate around the

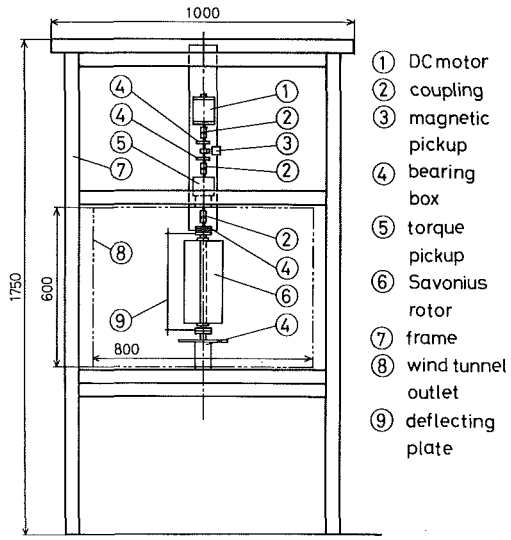


**Fig. 1 Test apparatus**

Contributed by the Fluids Engineering Division for publication in the JOURNAL OF FLUIDS ENGINEERING. Manuscript received by the Fluids Engineering Division June 23, 1987.

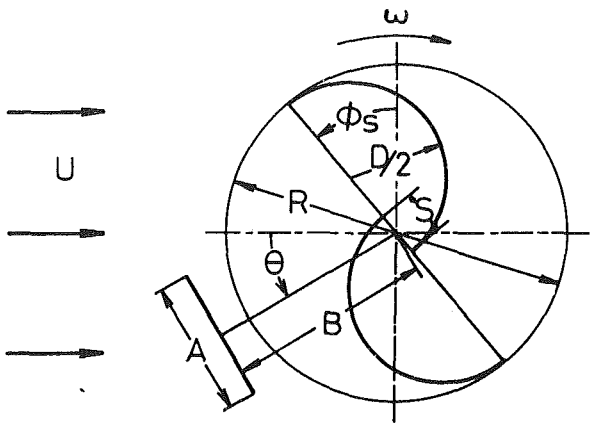


Fig. 2 Configuration of a Savonius rotor and a deflecting plate

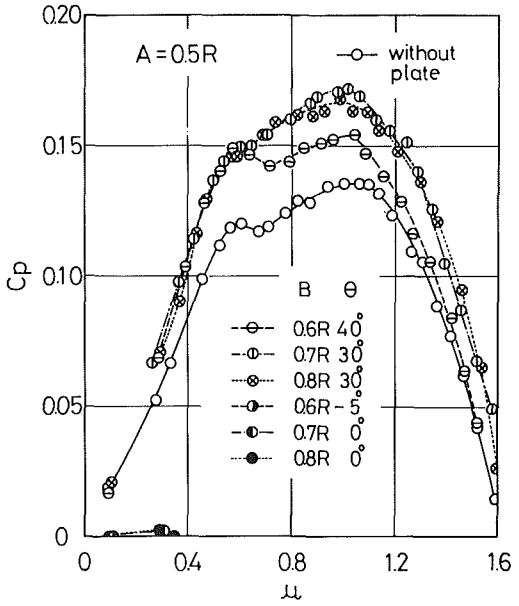


Fig. 3 Effects of B on Cp

rotor, and the characteristics of the control systems are investigated with a wind tunnel.

## The Effects of a Deflecting Plate

The test apparatus and instrumentation are shown in Fig. 1. The rotational speed of the rotor is controlled by a DC motor ①, and the motor shaft is connected to the rotor shaft via a torque pickup ⑤. The number of revolutions is measured by using a magnetic pickup ③ and a counter. The Savonius rotor consists of two buckets with a circular camber (180 deg) and two end plates. The rotor diameter $R$, rotor height, $H$, overlap ratio, $S/D$, and wind velocity, $U$, are 0.140m, 0.295m, 0.2 and approximately 7m/s, respectively.

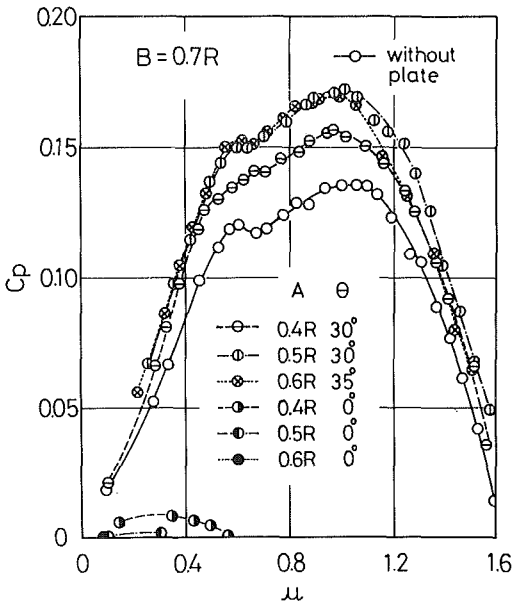


Fig. 4 Effects of A on Cp

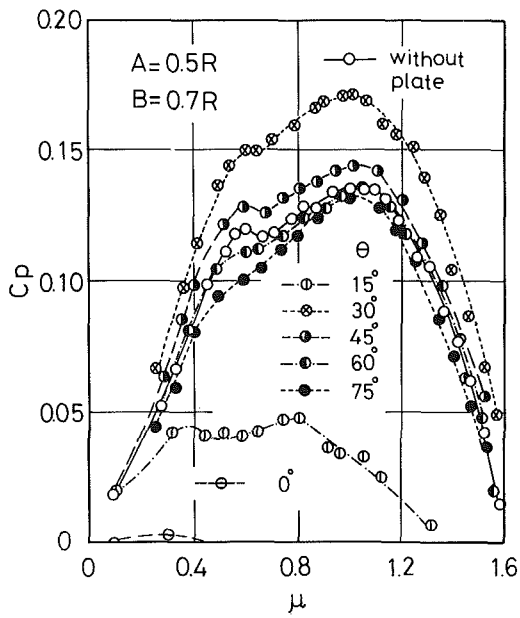


Fig. 5 Effects of θ on Cp

Fig. 3, 4, and 5 Uncertainty in $Cp = \pm 0.04$, in $\mu = \pm 0.01$ at 20:1 odds

An attempt to enhance the performance of a Savonius rotor by the application of a deflecting plate was previously reported by the authors [14]. In that study, the effects of the section shape of the deflecting plate on the rotor performance were investigated. It was concluded that a simple flat plate

## Nomenclature

$A$ = width of a deflecting plate, m (Fig. 2)
$B$ = distance between a deflecting plate and rotor center, m (Fig. 2)
$Cp$ = power coefficient ($=2T\omega/\rho U^3 RH$)
$D$ = diameter of a rotor bucket, m
$H$ = rotor height, m
$n$ = rotational speed of a rotor, rpm
$R$ = rotor diameter, m
$r_A$, $r_B$ = arm lengths of tail wing (Fig. 7)
$S$ = overlap distance of two buckets, m
$T$ = rotor torque, N•m
$U$ = wind velocity, m/s
$\Theta$ = angle of wind direction
$\theta$ = azimuthal angle of a deflecting plate (Fig. 2)
$\mu$ = tip-speed ratio ($=R\omega/2U$)
$\rho$ = air density, kg/m$^3$
$\omega$ = angular velocity of rotation, rad/s

produced the best results. The current investigation is a followup to the previous study, and the effects of the flat deflecting plate parameters (Fig. 2), i.e., A, B, and $\theta$ on the rotor performance are investigated in detail.

Results of the experiments for the determination of best combination of the parameters A, B, and $\theta$ are shown in Figs. 3 to 5. Figure 3 presents the effects of varying the distance, B, on the power coefficient, *Cp*, for a given value of $A$ ($=0.5R$). The optimum value for B was found to be $0.7R$, i.e., *Cp* becomes smaller for any other B value. The values of *Cp* for the cases in which $A=0.5R$ and $0.6R$ are nearly the same as is shown in Fig. 4. Based on these results and because a smaller plate is better as an attached apparatus, a deflecting plate with $A=0.5R$ was adopted.

Changes in the angle $\theta$ influences the output power considerably as shown in Fig. 5. At $\theta=30$ deg ($A=0.5R$, $B=0.7R$), the maximum value of *Cp* becomes approximately 27 percent larger than that of the rotor without the deflecting plate, while the output becomes almost zero, when the plate is placed just in front of the rotor ($\theta=0$ deg). Apparently, the aerodynamic force which operates on the rotor can be controlled by moving the deflecting plate around the rotor. The plate should be maintained at $\theta=30$ deg, if the wind velocity or the rotation speed of the rotor is lower than the designed value. In such a case more wind energy can be extracted than when the deflecting plate is not used. In a strong wind, or if the rotor rotates beyond the design speed, the rotor rotation can be decreased by moving the deflection plate towards the $\theta=0$ deg position. In this study, two systems to control the rotational speed of the Savonius rotor are developed by varying the location of the deflection plate.

## Control With Tail Wings

Several kinds of tail wings which have been tested in this study are presented in Fig. 6. Figure 6(*a*) shows a single tail wing, that is 0.75R wide and is connected to the deflecting plate. An attempt was made to keep the deflecting plate at $\theta=30$ deg by balancing the aerodynamic forces on the deflecting plate and tail wing. But it was not possible to stop the deflecting plate at $\theta=30$ deg. The plate invariably swung laterally $\pm 10$ deg around $\theta=30$ deg. Subsequently, an attempt was made to stop the deflecting plate at $\theta=0$ deg by changing the setting angle of the tail wing from 135 to 160 deg (Fig. 6(*b*)), but the swinging motion of the deflecting plate and tail wing remained. The reason for this swinging motion is thought to be due to the fact that the tail wing is located in the wake region which is disturbed by the rotating rotor. To circumvent this, as a next attempt, a mechanism which has two tail wings of width $0.5R$ were tested. The length of two arms shown in Fig. 6(*c*) is $0.8R$. In this case, the swinging motion was found to be smaller than that of the case with one tail wing, but it is still present. Figures 6(*d*) and 6(*e*) show the two tail wings system with longer arms ($1.1R$). In each case, the wings are located outside of the wake region and the deflecting plate remains still at $\theta=30$ deg, when the setting angles of wings are 130 and 110 deg. As shown in Fig. 6(*e*), the deflecting plate is moved to the position of $\theta=0$ deg and remains motionless, when the setting angle of the left-hand side tail wing is changed from 130 to 90 deg. Accordingly, it is possible to move the deflecting plate by changing one of the setting angles of two tail wings. In this study, a coil spring is attached to the left-hand side tail wing to change the setting angle automatically at a strong wind as shown in Figs. 6(*d*) and 6(*e*).

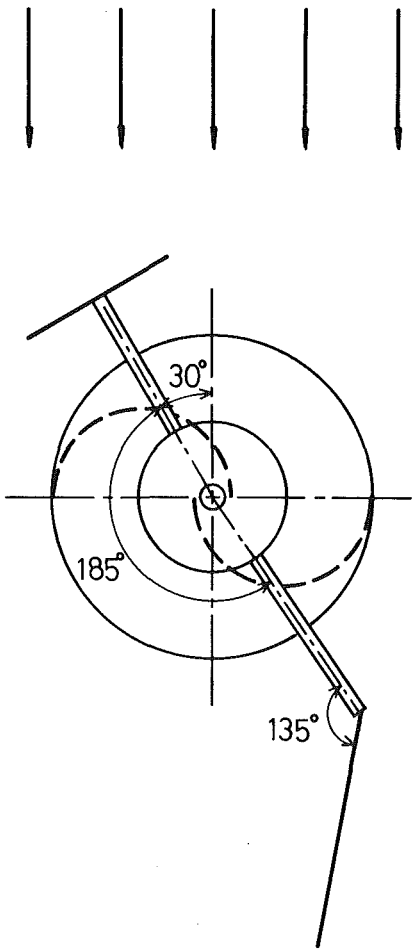


Fig. 6(*a*)

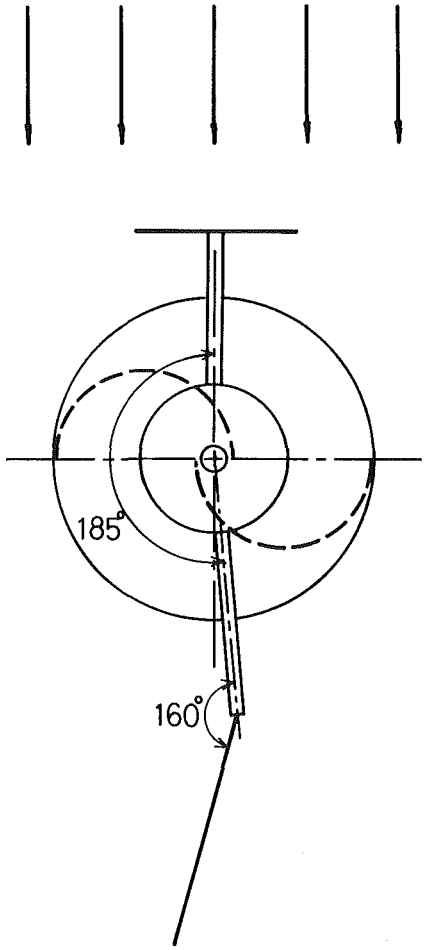


Fig. 6(*b*)

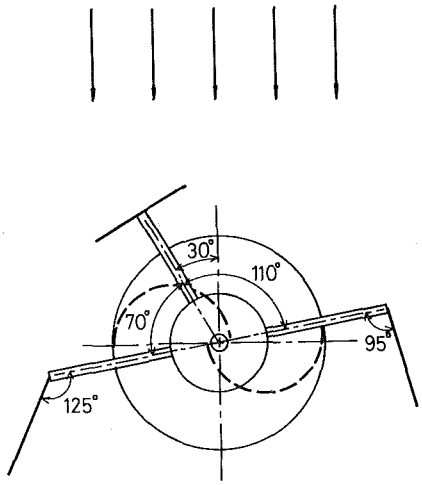


Fig. 6(c)

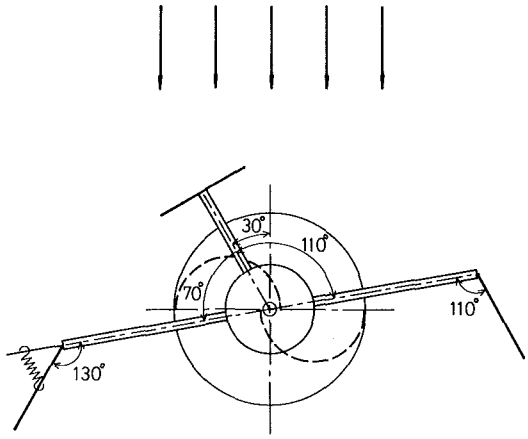


Fig. 6(d)

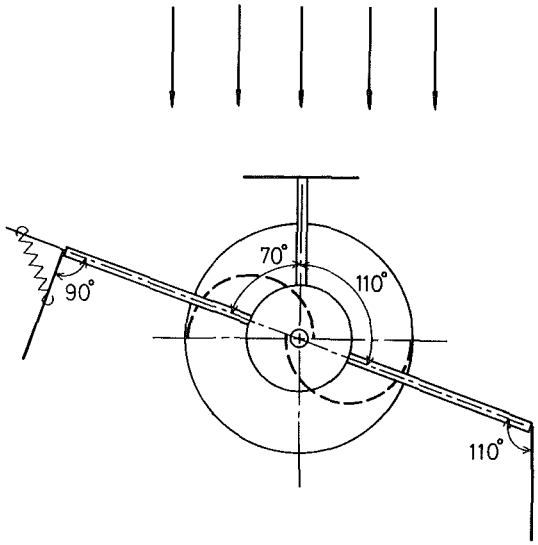


Fig. 6(e)

**Fig. 6 Tail wings**

In Fig. 7, an anemoscope, a Savonius rotor with two tail wings, and the guide vanes to change direction of the wind are presented. The wind direction, Θ, is changed by altering the setting of the guidevanes using a DC motor. The range of the variation in the wind direction is ±25 deg. The wind direction is recorded as the voltage change of the potentiometer which is attached to the axis of the anemoscope. The wind velocity, $U$, is varied by the damper of a sirocco fan of the wind tunnel and is measured with a hot-wire anemometer.

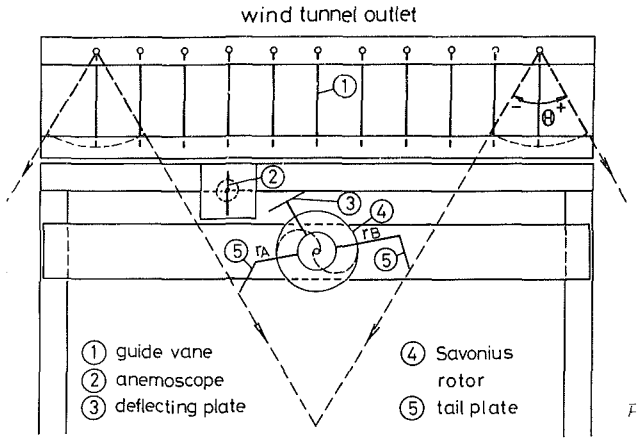


**Fig. 7 Experimental devices of rotational speed control**

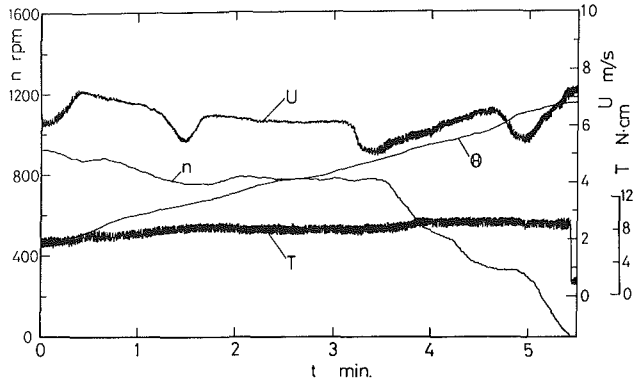


***Fig. 8 The change in $n$ without control (in case the wind direction, Θ, varies)***

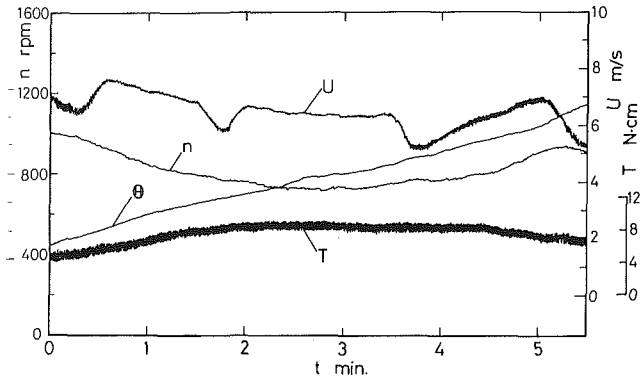


**Fig. 9 The control of $n$ with tail wings presented in Fig. 6($d$) (in case the wind direction, Θ, varies)**

The change in the rotational speed, $n$, when the deflecting plate is fixed, the rotor torque, $T$, the wind speed and the wind direction variations are presented in Fig. 8. The rotational speed begins to decrease as Θ becomes greater than about 5 deg, and $n$ becomes nearly zero when the wind blows directly against the deflecting plate. As shown in Fig. 8, the rotational speed changes markedly, if the deflecting plate does not track the change in the wind direction. The defects in the record of the velocity, $U$, indicate the wakes after the guidevanes. When the deflecting plate is moved by the tail wings (Fig. 6($d$)) which follow to the change in the wind direction, the rotational speed does not decrease (Fig. 9). In the case when the wind velocity increases and the deflecting plate is fixed at $\theta = 30$ deg, $n$ increases as shown in Fig. 10.

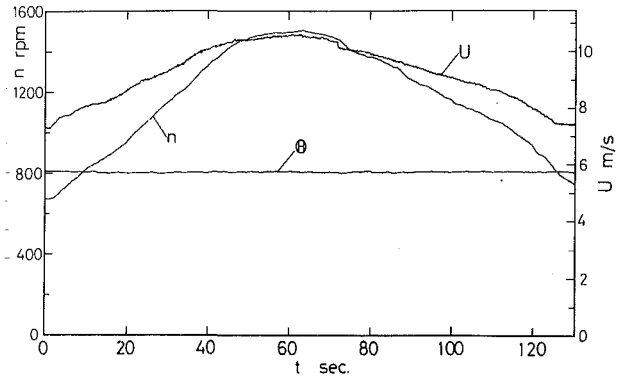


**Fig. 10 The change in *n* without control (in case the wind velocity, *U*, increases)**

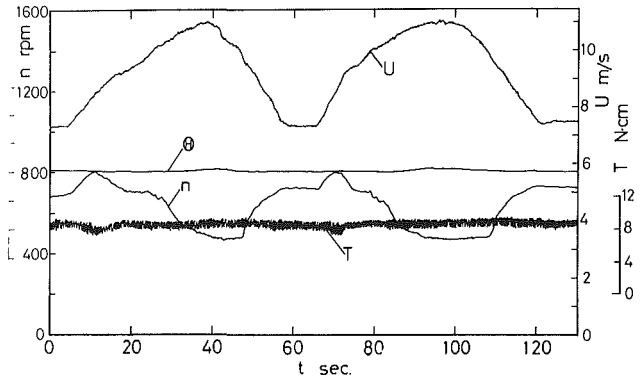


**Fig. 11 The control of *n* with tail wings presented in Fig. 6(*d*) (in case the wind velocity, *U*, increases)**

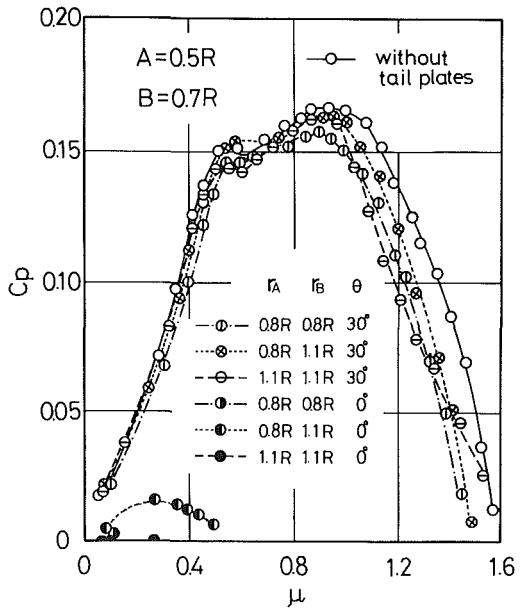


**Fig. 12 The effects of tail wings on *Cp* (Uncertainty in *Cp* = ± 0.04, in *μ* = ±0.01 at 20:1 odds)**

Figure 11 presents the characteristics of the control system which is shown in Fig. 6(*d*). When the wind velocity increases, the coil spring lengthens and the deflecting plate moves toward $\theta = 0$ deg position (Fig. 6(*e*)). Then, the rotational speed *n* decreases. It is possible to keep *n* constant or to let the rotor stop by selecting the spring factor properly. The effects of the existence of tail wings on the power coefficient *Cp* were investigated, and as may be seen in Fig. 12, there is almost no effect on performance.

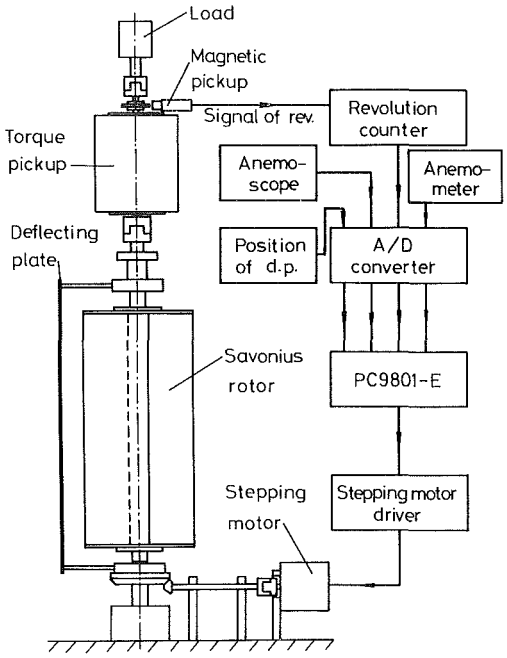


**Fig. 13 Schematic of the control system with a stepping motor**

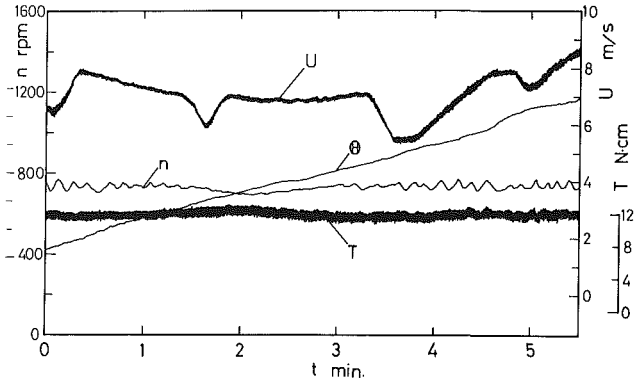


**Fig. 14 The control of *n* with a stepping motor (in case the wind direction, θ, varies)**

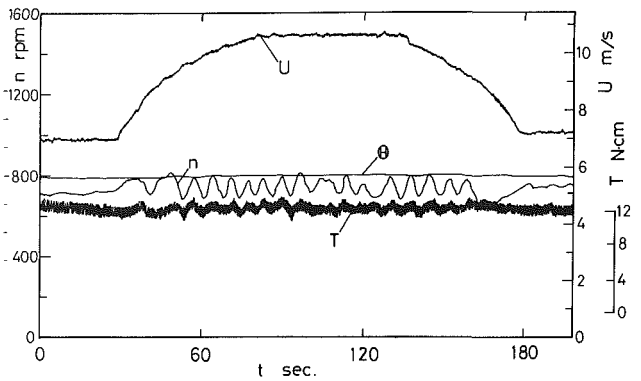


**Fig. 15 The control of *n* with a stepping motor (in case the wind velocity, *U*, increases)**

## Control With a Stepping Motor

In an effort to design a self-regulating control system, a computer controlled system was developed. The rotational speed, wind velocity and the wind direction are fed into a per-

sonal computer via an A/D converter and processed. A stepping motor is connected with the deflecting plate and moves it on the basis of the processed results (Fig. 13). The characteristics of this system are presented in Figs. 14 and 15. Figure 14 shows the results of the case in which it is programmed for the deflecting plate to move based on the information of the wind direction. The results when the wind direction, $\Theta$, is constant and the wind velocity varies are presented in Fig. 15. As shown in Figs. 14 and 15, the rotational speed, $n$, is kept almost constant, and it is proved that more precise control than that with tail wings is possible.

## Conclusions

In this study, experiments to improve the performance of a Savonius wind turbine rotor by using a flat deflecting plate are conducted. The effects of the deflecting plate on the power coefficient are investigated in detail. It was found that the rotor power was approximately 27 percent greater than that of a rotor without the deflecting plate, when the plate with $A = 0.5R$ and $B = 0.7R$ is placed at $\theta = 30$ deg. The rotor torque was shown to vary considerably with the azimuthal angle, $\theta$, of the deflecting plate. Two systems to control the rotational speed by using the deflecting plate were developed. Experimental attempts of mechanical control with tail wings revealed that this is an effective means to control rotational speed, especially as one of the protection devices for strong winds. It was also shown that the other system, a computer controlled closed loop system, is also applicable and more appropriate for precise control than that with the tail wings.

## References


1 Savonius, S. J., "The S-Rotor and Its Applications," *Mechanical Engineering*, Vol. 53, No. 5, 1931, pp. 333–338.

2 Bach, G., "Untersuchungen über Savonius-Rotoren und verwendte Strömungsmaschinen," Forschung, 2.Bd./Heft 6, 1931, pp. 218–231.

3 Khan, M. H., "Model and Prototype Performance Characteristics of Savonius Rotor Windmill," *Wind Engineering*, Vol. 2, No. 2, 1978, pp. 75–85.

4 Sheldahl, R. E., Blackwell, B. F., and Feltz, L. V., "Wind Tunnel Performance Data for Two- and Three-Bucket Savonius Rotors," *AIAA Journal of Energy*, Vol. 2, No. 3, 1978, pp. 160–164.

5 Ushiyama, I., Nagai, H., and Shinoda, J., "Experimentally Determining the Optimum Design Configuration for Savonius Rotors," *Trans. JSME*, Vol. 52, No. 480, 1986, pp. 2973–2982 (in Japanese).

6 Wilson, R. E., Lissaman, P. B. S., and Walker, S. N., "Aerodynamic Performance of Wind Turbines," ERDA/NSF/04014-76/1, 1976, pp. 111–164.

7 Van Dusen, E. S., and Kirchhoff, R. H., "A Two Dimensional Vortex Sheet Model of a Savonius Rotor," *Fluids Engineering in Advanced Energy Systems*, ASME, 1978, pp. 15–31.

8 Ogawa, T., "Theoretical Study on the Flow About Savonius Rotor," ASME JOURNAL OF FLUIDS ENGINEERING, Vol. 106, 1984, pp. 85–91.

9 Sabzevari, A., "Performance Characteristics of a Concentrator Augmented Savonius Wind Rotor," *Wind Engineering*, Vol. 1, No. 3, 1977, pp. 198–206.

10 Sivasegaram, S., "Concentration Augumentation of Power in a Savonius-Type Wind Rotor," *Wind Engineering*, Vol. 3, No. 1, 1979, pp. 52–61.

11 Ogawa, T., Tahara, K., and Suzuki, N., "Wind Tunnel Performance Data of the Savonius Rotor with Circular Guide Vanes," *Bulletin of JSME*, Vol. 29, No. 253, 1986, pp. 2109–2114.

12 Charwat, A. F., "Performance of Counter- and Corotating Arrays of Savonius Turbines," *AIAA Journal of Energy*, TN, Vol. 2, No. 1, 1978, pp. 61–63.

13 Ogawa, T., Sugiura, S., and Yoshida, H., "A Study on a Savonius Rotor (4th Report, Effects of Mutual Interaction Between Two Rotors)," *Trans.* JSME, Series B, Vol. 52, No. 481, 1986, pp. 3259–3265 (in Japanese).

14 Ogawa, T., and Yoshida, H., "The Effects of a Deflecting Plate and Rotor End Plates on Performances of Savonius-Type Wind Turbine," *Bulletin of JSME*, Vol. 29, No. 253, 1986, pp. 2115–2121.

## A Note of Caution and Apology

Accidents are shocking, not only because they are serious, but also because they are unexpected and rare. The odds are with us, so we routinely forget to buckle up, delay vehicle maintenance, and drive carelessly and too fast. Our behavior would be quite different if we cracked up our cars twice a week!

The mails are similarly seductive. We routinely send the most precious things through the various delivery services, counting on their safe arrival. This seems especially true of authors, editors, and printers. This note is to remind you that lightning does strike, accidents do happen, and authors should take care to back up their precious material such as original drawings and photos.

In late December, for the 41st consecutive quarter, our JFE Office packed up the 'next' issue (March 1989 in this case) and sent it to New York to the ASME Production Editor, via United Parcel Service. This box, containing sixteen original manuscripts, never arrived and is now declared officially lost. It helps little to know that UPS says "it might be in their Atlanta warehouse." Our JFE secretary, Terry Brown, frantically scrambled to contact authors and get back-up figures and photos; we could of course make good copies of typed material from our files. Regrettably, some authors did not have such back-up material and will have to reprocess them. The present issue prints only what we were able to recover, and we hope to make good with everyone in the June issue.

As editor, I sincerely apologize to all our authors and readers for this unfortunate occurrence. In the future, we will 1) get another delivery service; 2) break up our mailings into smaller packets; and 3) reinforce our warnings to authors that accidents do happen. Editors are deplorably human – please keep good back-up copies of your manuscript material against the next Black Monday.

**Frank M. White**
**Technical Editor**

# Numerical Computation of Turbulent Flow in a Square-Sectioned 180 Deg Bend

**Y. D. Choi**[1]
**H. Iacovides**
**B. E. Launder**
Fellow ASME.

Department of Mechanical Engineering,
UMIST, Manchester, England

*Fine-grid computations are reported of turbulent flow through a square sectioned U-bend corresponding to that for which Chang et al. (1983a) have provided detailed experimental data. A sequence of modeling refinements is introduced: the replacement of wall functions by a fine mesh across the sublayer; the abandonment of the PSL approximation (in which pressure variations across the near-wall sublayer are neglected); and the introduction of an algebraic second-moment (ASM) closure in place of the usual $k-\epsilon$ eddy-viscosity model. Each refinement is shown to lead to an appreciable improvement in the agreement between measurement and computation. Direct comparisons with the measured rms turbulent velocity give further support to the view that the ASM scheme achieves a generally satisfactory description of the Reynolds stress field. Even with the most refined model some discrepancies between the experiment and computed development are apparent. It is suggested that their removal may require the use of a turbulent transport model in the semi-viscous sublayer in place of the van Driest (1956) mixing-length treatment used at present.*

## Introduction

Chang et al. (1983a) have provided detailed experimental data of the development of a turbulent flow around a 180 deg square-sectioned bend with a bend radius equal to 3.375 times the hydraulic diameter of the duct. The flow geometry is shown in Fig. 1(*a*) and the flow Reynolds number based on the hydraulic diameter was 58,000. An upstream inlet tangent of some 30 hydraulic diameters meant that the boundary layers filled the duct at entry. The secondary flows induced by flow around the bend were thus stronger than in a flow with thin inlet boundary layers. The experiment was designed to provide a searching test for turbulent-flow computational schemes and in that respect it succeeded admirably. At 90 deg into the bend a large "hole" developed in the streamwise velocity towards the inside of the bend, Fig. 1(*b*), a feature that both Chang's (1983) own computations and subsequently those of Johnson (1984) (see also Chang et al. (1983b)) and Birch (1984) entirely failed to mimic.

These computations were based on a semi-elliptic discretization of the Reynolds equations in which streamwise diffusion was dropped but where fully three-dimensional effects were included in the pressure field. Thus, the pressure was stored over the full flow domain while all other dependent variables (which included, besides the velocity components, the turbulence energy and its dissipation rate) were held on two adjacent planes only, the values being successively overwritten as the solution sequence made repeated streamwise sweeps around the bend until convergence.

The choice of a semi-elliptic solver allowed a considerably finer mesh than had been possible in earlier fully elliptic studies (e.g., Humphrey, 1981). This refinement, together with the use of quadratic upstream differencing for convection (in place of some more stable but highly dispersive first-order, upwind scheme) led to the conclusion that numerical errors were of only minor significance. For example, Johnson (1984) reduced the mean forward step size to 1 deg over the first 90 deg of the bend (compared with 2 deg in Chang et al.); this produced a small improvement in predictions over the first 45 deg of the bend where the secondary motion was becoming established but virtually no change to the computed flow pattern at 90 deg.

Most of the computations reported in the above studies employed the standard $k-\epsilon$ eddy-viscosity model (EVM) of turbulence whose adequacy in a strongly curved, highly three-dimensional flow is at least suspect. Chang (1983) and Johnson (1984) both attempted computations with an algebraic second-moment (ASM) closure which has a track record of capturing much better than EVMs the effects of streamline curvature on the Reynolds stresses. However, this type of turbulence model gives rise to numerical instabilities and, as a result, in those studies residuals could not be reduced to convincingly negligible levels even when standard upwind differencing was used.

The present paper reports the outcome of our subsequent computational work at UMIST aimed at resolving the causes of the very severe disagreement between the computed and measured behavior of the 180 deg square bend flow. The springboard for this study was provided by parallel work on flow through bends of *circular* cross section. Those computations (Iacovides and Launder (1984a), Azzola et al. (1986)) re-

[1] Present address: Department of Mechanical Engineering, Korea University, Seoul, Korea.

*Contributed by the Fluids Engineering Division for publication in the* JOURNAL OF FLUIDS ENGINEERING. Manuscript received by the Fluids Engineering Division July 17, 1987.

tained the $k-\epsilon$ EVM but discarded the "wall functions" employed in the square-sectioned bend to bridge the viscous sublayer and buffer region adjacent to the walls. In their place a fine near-wall mesh was used in which the turbulent viscosity was obtained from Van Driest's (1956) version of the mixing-length hypothesis generalized to the case of nonplanar flows. The extra fine mesh was achieved with no extra core penalty by neglecting the very small pressure variations across this near-wall sublayer—the so-called PSL approximation (Iacovides and Launder (1984b)). In contrast to the case of the square-sectioned bend, the computations achieved quite satisfactory agreement with the experimental data. Further improvements for the circular-sectioned bend (albeit fairly minor) arose from including an ASM in place of the eddy-viscosity model (Iacovides and Launder, 1985). Our efforts, as described in the remainder of the paper, have therefore been directed at importing these various physical and numerical refinements into a solving procedure for rectangular sectioned bends, a flow which from both numerical and physical standpoints has emerged as a considerably more complex flow than the circular-sectioned bend.

## The Mathematical and Numerical Model

The equations of mean motion for the turbulent flow around a square-sectioned bend are conveniently expressed in cylindrical coordinates. $X$ and $Y$ map the cross-sectional plane, while progress around the bend is expressed through angle $\phi$. Thus:

*Continuity*

$$\frac{1}{r_c}\left[\frac{\partial}{\partial X}(\rho r_c U)+\frac{\partial}{\partial Y}(\rho r_c V)+\frac{\partial}{\partial \phi}(\rho W)\right]=0 \qquad (1)$$

*Mean Momentum*

$$\rho C(\Psi)+S_c(\Psi)=D(\Psi)+S_D(\Psi)-\rho R(\Psi)+S_R(\Psi)+S_p(\Psi)$$

where $\Psi$ refers to the velocity component in question and the operators $C(\Psi)$, $D(\Psi)$, and $R(\Psi)$ have the following significance:

$$C(\Psi)=\frac{1}{r_c}\left\{\frac{\partial}{\partial X}(r_c U\Psi)+\frac{\partial}{\partial Y}(r_c V\Psi)+\frac{\partial}{\partial \phi}(W\Psi)\right\}$$

$$D(\Psi)=\frac{1}{r_c}\left\{\frac{\partial}{\partial X}\left(r_c\mu\frac{\partial \Psi}{\partial X}\right)+\frac{\partial}{\partial Y}\left(r_c\mu\frac{\partial \Psi}{\partial Y}\right)+\frac{1}{r_c}\frac{\partial}{\partial \phi}\left(\frac{\mu\partial\Psi}{\partial\phi}\right)\right\}$$

$$R(\Psi)=\frac{1}{r_c}\left\{\frac{\partial}{\partial X}(r_c\overline{u\psi})+\frac{\partial}{\partial Y}(r_c\overline{v\psi})+\frac{\partial}{\partial \phi}(\overline{w\psi})\right\}$$

The term $R(\Psi)$ expresses the action of the turbulent stresses, $\psi$ denoting the fluctuation component of velocity in question and the overbar the usual Reynolds averaging. The quantities $S_p(\Psi)$, $S_c(\Psi)$, $S_D(\Psi)$ and $S_R(\Psi)$ differ according to the velocity component as indicated in Table 1.

| $\Psi$ | $S_p(\Psi)$ | $S_c(\Psi)$ | $S_R(\Psi)$ |
|---|---|---|---|
| $U$ | $-\frac{\partial p}{\partial X}$ | $\frac{W^2}{r_c}$ | $\frac{\overline{w^2}}{r_c}$ |
| $V$ | $-\frac{\partial p}{\partial Y}$ | 0 | 0 |
| $W$ | $-\frac{1}{r_c}\frac{\partial p}{\partial \phi}$ | $-\frac{UW}{r_c}$ | $-\frac{\overline{uw}}{r_c}$ |

For both turbulence models considered, the following closed-form transport equations are solved for the turbulent kinetic energy and its dissipation rate:

*Turbulence Energy*

$$C(k)=D(k)+S_D(k)+P-\rho\epsilon \qquad (3)$$

## Nomenclature

ASM = Algebraic Stress Model
$C_i$ = turbulence model constants
$C(\Psi)$ = convection of $\Psi$
$D$ = duct diameter
$D(\Psi)$ = diffusion of $\Psi$
EVM = Effective Viscosity Model
$k$ = turbulent kinetic energy
$l_m$ = turbulent mixing length
$P$ = turbulent kinetic energy generation rate or pressure
$P_{ij}$ = turbulent stress $\overline{u_i u_j}$ generation rate
PSL = Parabolic Sub-Layer
$R_c$ = bend radius of curvature
$r_c$ = local radius of curvature $R_c+D/2-X$
$R(\Psi)$ = turbulent mixing of $\Psi$
$S_C(\Psi)$ = convective curvature source term
$S_D(\Psi)$ = diffusive curvature source term
$S_P(\Psi)$ = pressure gradient source term
$S_R(\Psi)$ = turbulent stress curvature source term
$U$ = radial mean velocity component
$u$ = radial velocity fluctuation
$\overline{u_i u_j}$ = Reynolds stress tensor
$U_\tau$ = resultant shear velocity $\sqrt{\tau_{r/\rho}}$
$V$ = normal mean velocity component
$v$ = normal velocity fluctuation
$W$ = streamwise mean velocity component
$W_b$ = bulk velocity
$w$ = streamwise velocity fluctuation
$X$ = radial coordinate
$Y$ = normal coordinate
$y$ = physical distance from the wall
$y^+$ = dimensionless distance from the wall = $y \cdot U_\tau/\nu$
$\delta_{ij}$ = Kronecker delta
$\epsilon$ = turbulent kinetic energy dissipation rate
$\mu$ = molecular dynamic viscosity
$\mu_T$ = turbulent dynamic viscosity
$\nu$ = molecular kinematic viscosity
$\nu_T$ = turbulent kinematic viscosity
$\rho$ = density
$\tau_r$ = resultant wall shear stress
$\phi$ = bend angle
$\Phi_{ij}$ = turbulent kinetic energy redistribution terms
$\Psi$ = general velocity component

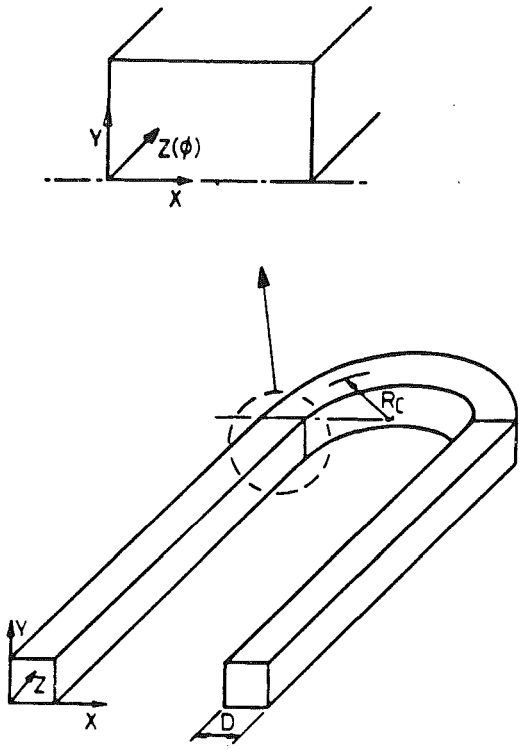


Fig. 1(*a*) Flow geometry and coordinate system used

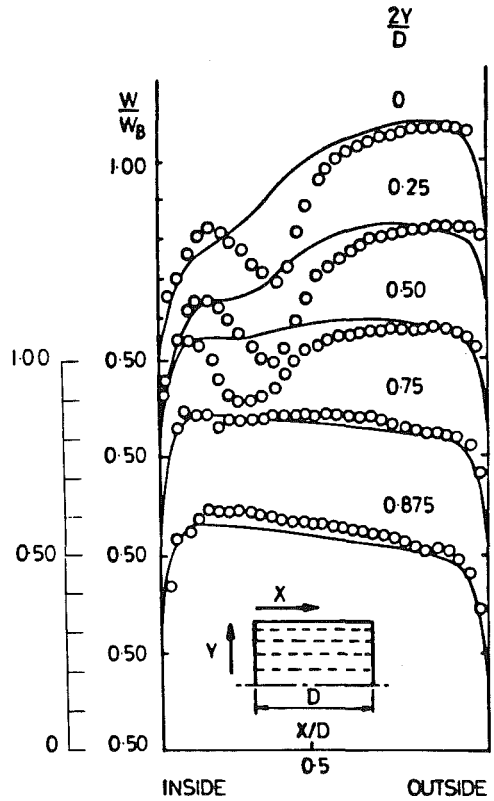


Fig. 1(*b*) Streamwise mean velocity profiles at 90 deg station. o o Measurements, Chang et al. (1983a); —— computations, Johnson (1984) using $k-\epsilon$ model with wall functions

where

$$C(k)=\frac{1}{r_c}\left\{\frac{\partial}{\partial X}\,(\rho r_c U k)+\frac{\partial}{\partial Y}\,(\rho r_c V k)+\frac{\partial}{\partial \phi}\,(\rho W k)\right\}$$

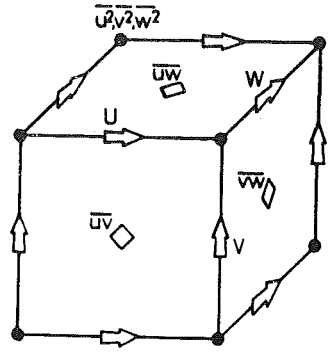


Fig. 1(*c*) Staggered three-dimensional stress field

**Table 1 Details of diffusion terms**

| $\Psi$ | $S_D(\Psi)$ |
|---|---|
| $U$ | $\frac{1}{r_c}\frac{\partial}{\partial X}\left\{r_c\mu\frac{\partial U}{\partial X}\right\}+\frac{\partial}{\partial Y}\left\{\mu\frac{\partial V}{\partial X}\right\}+\frac{\partial}{\partial \phi}\left\{\mu\frac{\partial}{\partial X}\left(\frac{W}{r_c}\right)\right\}-2\mu\left\{\frac{U-\partial W/\partial\phi}{r_c^2}\right\}$ |
| $V$ | $\frac{1}{r_c}\frac{\partial}{\partial x}\left\{r_c\mu\frac{\partial U}{\partial Y}\right\}+\frac{\partial}{\partial X}\left\{\mu\frac{\partial V}{\partial Y}\right\}+\frac{1}{r_c}\frac{\partial}{\partial \phi}\left\{\mu\frac{\partial W}{\partial Y}\right\}$ |
| $W$ | $\frac{1}{r_c}\frac{\partial}{\partial X}\left\{\mu\left(\frac{\partial U}{\partial \phi}+W\right)\right\}+\frac{1}{r_c}\frac{\partial}{\partial Y}\left\{2\mu\frac{\partial V}{\partial \phi}\right\}+\frac{1}{r_c^2}\frac{\partial}{\partial \phi}\left\{\mu\left(\frac{\partial W}{\partial \phi}-2U\right)\right\}-\mu\frac{\partial}{\partial X}\left(\frac{W}{r_c}\right)-\frac{\mu}{r_c^2}\frac{\partial U}{\partial \phi}$ |

$$D(k)=\frac{1}{r_c}\left\{\frac{\partial}{\partial X}\left[r_c\left(\mu+\rho C_k\frac{k}{\epsilon}\overline{u^2}\right)\frac{\partial k}{\partial X}\right]+\frac{\partial}{\partial Y}\left[r_c\left(\mu+\rho C_k\frac{k}{\epsilon}\overline{v^2}\right)\frac{\partial k}{\partial Y}\right]+\frac{1}{r_c}\frac{\partial}{\partial \phi}\left[\left(\mu+\rho C_k\frac{k}{\epsilon}\overline{w^2}\right)\frac{\partial k}{\partial \phi}\right]\right\}$$

$$S_D(k)=\frac{\rho C_k}{r_c}\left\{\frac{\partial}{\partial X}\left[r_c\frac{k}{\epsilon}\left(\overline{uv}\frac{\partial k}{\partial Y}+\frac{\overline{uw}}{r_c}\frac{\partial k}{\partial \phi}\right)\right]+\frac{\partial}{\partial Y}\left[r_c\frac{k}{\epsilon}\left(\overline{uv}\frac{\partial k}{\partial X}+\frac{\overline{vw}}{r_c}\frac{\partial k}{\partial \phi}\right)\right]+\frac{1}{r_c}\frac{\partial}{\partial \phi}\left[\frac{k}{\epsilon}\left(\overline{uw}\frac{\partial k}{\partial X}+\overline{vw}\frac{\partial k}{\partial Y}\right)\right]\right\}$$

$$P=-\rho\left\{\overline{u^2}\frac{\partial U}{\partial X}+\overline{v^2}\frac{\partial V}{\partial Y}+\overline{w^2}\left(\frac{1}{r_c}\frac{\partial W}{\partial \phi}-\frac{U}{r_c}\right)+\overline{vw}\left(\frac{\partial W}{\partial Y}+\frac{1}{r_c}\frac{\partial V}{\partial \phi}\right)+\overline{uw}\left(\frac{1}{r_c}\frac{\partial U}{\partial \phi}+\frac{\partial W}{\partial X}+\frac{W}{r_c}\right)+\overline{uv}\left(\frac{\partial V}{\partial X}+\frac{\partial U}{\partial Y}\right)\right\}$$

**Turbulence Energy Dissipation Rate**

$$C(\epsilon)=D(\epsilon)+S_D(\epsilon)+c_{\epsilon 1}\frac{\epsilon}{k}P-c_{\epsilon 2}\frac{\rho\epsilon^2}{k} \tag{4}$$

where operators $C(\epsilon)$, $D(\epsilon)$, $S_D(\epsilon)$, and $P_k$ are as defined for the turbulence energy equation but with $c_k$ replaced by $c_\epsilon$.

The turbulent stresses themselves are obtained from one of two routes. With the eddy-viscosity model:

$$\left(\overline{u^2}-\frac{2}{3}k\right)=-2\nu_t\frac{\partial U}{\partial X};\ \left(\overline{v^2}-\frac{2}{3}k\right)=-2\nu_t\frac{\partial V}{\partial Y}$$

$$\overline{uv}=-\nu_t\left(\frac{\partial U}{\partial Y}+\frac{\partial V}{\partial X}\right);\ \overline{vw}=-\nu_t\left(r_c\frac{\partial}{\partial Y}\left(\frac{W}{r_c}\right)+\frac{1}{r_c}\frac{\partial V}{\partial\phi}\right);\ \overline{uw}=-\nu_t\left(\frac{\partial W}{\partial X}+\frac{1}{r_c}\frac{\partial V}{\partial\phi}+\frac{W}{r_c}\right) \tag{5}$$

where $\nu_t=c_\mu k^2/\epsilon$ and $r_c$ denotes the local radius of curvature from the bend center.

When the ASM scheme is used, the stresses are obtained from the following tensor statement of the model:

$$\frac{\left(\overline{u_iu_j}-\frac{2}{3}\delta_{ij}k\right)}{k}=\frac{(1-c_2)}{(c_1-1+P/\epsilon)}\frac{\left(P_{ij}-\frac{2}{3}\delta_{ij}P\right)}{\epsilon}+\frac{(\phi'_{ij1}+\phi'_{ij2})}{\epsilon}\frac{1}{(c_1-1+P/\epsilon)} \tag{6}$$

where

$$\phi'_{ij(1)}=-c'_1\frac{\epsilon}{k}\left\{\overline{u_qu_m}n_qn_m\delta_{ij}-\frac{3}{2}\overline{u_iu_q}n_qn_j-\frac{3}{2}\overline{u_ju_q}n_in_q\right\}f\left(\frac{l}{n_pr_p}\right)$$

$$\phi'_{ij(2)}=-c'_2\left\{\Phi_{qm(2)}n_qn_m\delta_{ij}-\frac{3}{2}\Phi_{qi(2)}n_qn_j-\frac{3}{2}\Phi_{jq(2)}n_qn_i\right\}f\left(\frac{l}{n_pr_p}\right)$$

$$l\equiv\frac{k^{3/2}}{c_l\epsilon},$$

$n_q$ denotes the unit vector normal to the wall and

$$\phi_{ij(2)}\equiv-c_2\left[P_{ij}-\frac{2}{3}\delta_{ij}P\right]$$

When expressed in cylindrical coordinates, this form gives rise to a lengthy set of equations which, nevertheless, for completeness are given in the Appendix. The constants appearing in the turbulence equations are assigned the values indicated in Table 2; these values are the same as in our circular-bend computations, and, indeed, are those that have been used in several other studies with the same turbulence model.

From the duct wall to a distance 0.04 times the duct hydraulic diameter,[2] the above models were replaced by adding to the molecular viscosity a turbulent viscosity given by the mixing-length hypothesis:

$$\nu_t=l_m^2\frac{\partial U_i}{\partial x_j}\sqrt{\left(\frac{\partial U_i}{\partial x_j}+\frac{\partial U_j}{\partial x_i}\right)} \tag{7}$$

[2]This corresponds to a distance where the $y^+$ value is greater than 50 at all positions; at the first node the $y^+$ value was around 3. (At different bulk Reynolds numbers one would probably want to choose a different thickness for the mixing-length region to keep the $y^+$ values in the same range).

**Table 2 Values of model coefficients**

| $c_{\epsilon 1}$ | $c_{\epsilon 2}$ | $c_k$ | $c_\epsilon$ | $c_1$ | $c_2$ | $c'_1$ | $c'_2$ | $c_\mu$ | $c_l$ |
|---|---|---|---|---|---|---|---|---|---|
| 1.44 | 1.92 | 0.22 | 0.15 | 1.8 | 0.6 | 0.5 | 0.3 | 0.09 | 2.55 |

where a generalized Van Driest form is used for the mixing length:

$$l_m=0.419x_n(1-\exp-(x_nU_{\tau r}/26\nu)) \tag{8}$$

Here $x_n$ is the distance from the (nearest) wall and $U_{\tau r}$ is the resultant wall shear velocity at the point on the surface reached by dropping a perpendicular from the point in question. Within the partially turbulent region where this model is applied, the velocity profile is highly skewed; for example, on the flat surfaces of the bend the maximum secondary flow occurs for $x_nU_{\tau r}/\nu\simeq 5$. The mixing-length hypothesis was chosen on the basis of the satisfactory agreement achieved with it in computing flows on spinning discs, cones and cylinders (e.g., Koosinlin et al. 1974) where, as here, the skewing of the velocity in the semi-turbulent sublayer is also large.

The standard grid employed to cover the half cross-section of the duct between the symmetry plane and on each wall was $25\times 47$ in the normal and radial directions respectively with eight nodes covering the near-wall sublayer where the mixing length model was employed. Initially the PSL approximation was applied over this same region. The standard forward step in the bend section was 2 deg arc. Thus, 90 planes were required for the full bend; a further 10 planes were employed for the inlet and exit tangents extending respectively two diameters upstream and downstream. The absence of streamwise recirculation allows the computation to be terminated shortly after the bend exit. Variations from this standard are noted in the text.

The finite-volume solving procedure employed in the calculations has been described in earlier contributions (Iacovides and Launder, 1985; Iacovides, 1986, Azzola et al. 1986), so here only a brief summary is provided.

- The usual staggered arrangement of $U$, $V$, $W$, $P$ nodes is adopted, iterated either by way of the SIMPLER (Patankar, 1980) or SIMPLE (Patankar and Spalding, 1972) algorithm. Generally the former was found to be faster when residuals were large, the latter when convergence was approached.
- The nondiffusive QUICK approximation of Leonard (1979) is used for discretizing convective transport in the cross-sectional plane of the duct.
- Although in the initial stages of iteration streamwise sweeps were made with all coefficients evaluated upstream, as the residuals fell to moderate levels first one, then two, in-plane iterations were introduced.
- Successive streamwise passes continued until the normalized mass and momentum residuals on any plane had fallen below 0.04 percent.
- When the ASM scheme was employed, the turbulent stresses were staggered relative to the velocity nodes in order that they were situated on the boundaries of the momentum control volumes on which they acted, as shown in Fig. 1(*c*). This practice reduced interpolation and assisted stability.
- Nevertheless, various stability-enhancing measures proved necessary to secure convergence with the ASM. (Numerically the flow proved to be very much more difficult than the flows reported earlier in the toroidal bend, Iacovides and Launder (1985)). The stresses themselves were solved in a pointwise manner as recommended by Huang and Leschziner (1985).
- When, during iteration with the ASM scheme, the turbulent kinetic energy production fell below that given by the $k-\epsilon$ EVM, the latter was adopted as the production rate of $k$ and the (negative) balance was credited to the energy dissipation

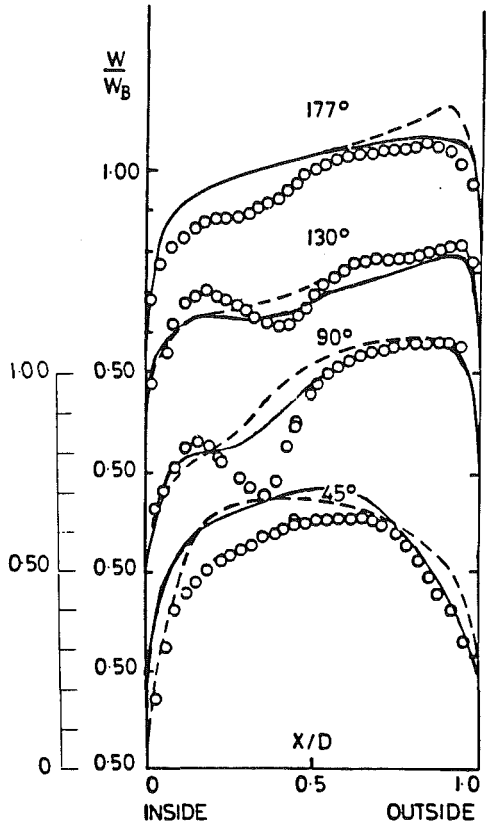


**Fig. 2 Computed and measured development of streamwise velocity profile on symmetry plane.**
**o o Measurements, Chang et al. (1983a);**
**---- Computations, Johnson (1984);**
**—— Computations, present study using $k-\epsilon$ model-mixing length with PSL approximation**

rate. This reassignment from "production" to "dissipation" brought major stability improvements due in part to the different ways that sources and sinks are handled in the solver.

The introduction of the ASM increased the overall CPU time required for a fully converged solution by roughly a factor of 2.

Finer meshes have been employed for checking purposes to establish the sufficiency of the numerical resolution in the case of *fully developed* flow in a circular-sectioned bend. (In this limiting case only three streamwise planes are needed allowing major refinement on the cross-sectional plane.) Two studies carried out by Iacovides and Launder (1985, 1987) concerning circular-bend flows and rotating square-duct flows (where the flow field is similar to that of a U-bend) indicate that, provided a sensible grid distribution is chosen across the wall layer, a minimum of about 25 nodes from the wall to the duct center is sufficient to obtain a grid-independent velocity field at this level of turbulence modelling for bend flows without recirculation. These earlier computations and Johnson's (1984) explorations, coupled with the fact that the non-diffusive QUICK scheme was here employed for approximating cross-stream convection, indicate that the flow field as a whole was free from significant numerical error. Especially sensitive quantities such as the local wall shear stress may, at locations where the friction factor falls to low values, be in error by a few percent.

## Presentation and Discussion of Computations

The first set of computations began three diameters upstream of the bend employing as starting conditions a careful fit to the measured mean velocity at this station (Chang et al. 1983a). The turbulence energy at node points was likewise obtained from an interpolation of measured profiles. The inlet energy dissipation rate is obtained from $\epsilon = k^{3/2}/l$ where close to the wall $l$ increases linearly with distance from the wall with slope 2.44 and levels off to a nearly uniform level in the core of approximately 0.5D. This distribution is broadly similar to that previously assumed in computing flow in straight square ducts (e.g., Launder and Ying, 1973). The development of the center plane profile of mean streamwise velocity around the bend obtained in the present computations is compared both with the experiments of Chang et al. (1983a) and Johnson's (1984) computations in Fig. 2. The latter, it is recalled, used precisely the same model of turbulence but, as is usual in elliptic and three-dimensional flows, adopted wall functions to bridge the near-wall viscous region. From this comparison it may be said that the present fine-grid near-wall treatment brings the flow development over the first 45 deg of the bend into close agreement with the measurements. Further around the bend the present computations can still be said to do better than the earlier ones though, compared with the difference from the measured behavior, the improvement is slight. The relative improvement along the other data-traverse lines (displaced from the center plane) is in fact even less than shown in Fig. 2.

The above computations applied the PSL approximation (Iacovides and Launder, 1984b) in the immediate wall vicinity to avoid having to store the three-dimensional pressure field there. This scheme had worked admirably in the case of circular sectioned bends (Iacovides and Launder, 1984a, Azzola et al., 1986) but, in searching for a cause of the large differences that remained between the computed and measured behavior, it came increasingly into question. While pressure differences across the sublayer around most of the duct perimeter would assuredly be negligible, in the corners it was the pressure variation normal to the wall that mainly caused the secondary flow to change abruptly its direction from (say) running along the flat end wall to flowing down the convex inside wall. So, full inclusion of pressure variations was arguably important to capture the secondary flow properly. A further run was therefore made in which the pressure-correction equation was solved even within the thin near-wall sublayer. Since by this stage our interest had strongly focused on the behavior at 90 and 130 deg, the computations were terminated at the end of the bend (180 deg) in order to make better use of computing resource. At the bend exit a uniform streamwise pressure gradient was imposed. Our experiences are (Iacovides and Launder, 1984a) that this inaccurate exit prescription of pressure does not contaminate the flow field more than about 25 deg upstream of the exit plane with the present bend curvature ratio. A different initialization procedure was also employed in this case in that the starting profiles upstream of the bend were obtained from a separate computation of flow developing in a straight duct. These exhibited some systematic (albeit small)) differences from the measured entry profiles principally because with an eddy-viscosity stress-strain law no "turbulence-driven" secondary flow are created. The differences between measured and computed velocity at three diameters upstream of the bend nowhere differed by more than 3 percent of the bulk mean velocity from the data. In view of the experience of Johnson (1984), Birch (1984) and ourselves that the flow at 90 deg and beyond is insensitive to inlet conditions,[3] we do not believe that the small difference in the prescribed inlet profiles can have made a significant con-

[3] *Experimental* evidence of this insensitivity has been provided by measurements by Johnson and Launder (1985) in an identically proportioned U-bend. These showed a dynamic behavior at 90 deg essentially unaltered when the inlet tangent was increased from 30 to 90 hydraulic diameters.

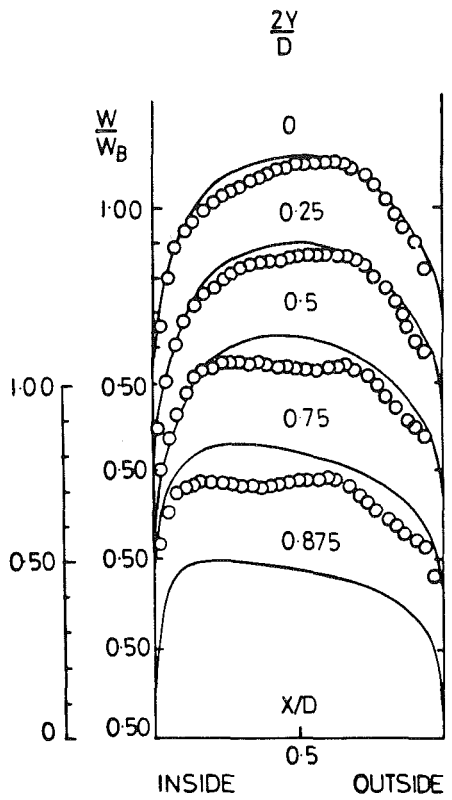


Fig. 3 Streamwise mean velocity profiles at 45 deg station.
o o Measurements, Chang et al. (1983a);
—— Computations, present study using $k-\epsilon$/mixing length without PSL approximation

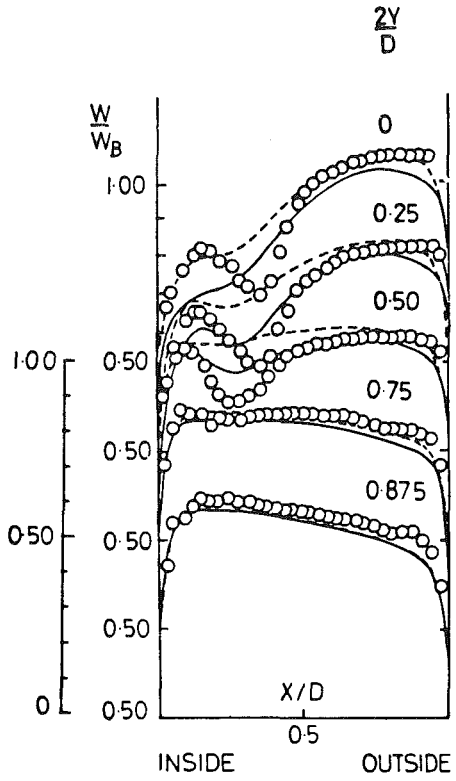


Fig. 4 Streamwise mean velocity profiles at 90 deg station.
o o Measurements, Chang et al. (1983a);
—— Computations, present study using $k-\epsilon$/mixing length without PSL;
---- Computations, present study using $k-\epsilon$/mixing length with PSL

tribution to the differences in the computed behavior noted below.

The streamwise velocity profiles along the center plane and four other lines parallel to it obtained from dropping the PSL approximation are shown in Figs. 3–5 at 45, 90 and 130 deg. Clearly the inclusion of pressure variations across the sublayer has brought about a marked improvement in the level of agreement with the measured velocity profiles. There is now an appreciable trough in streamwise velocity near the inside of the bend at 90 and 130 deg—broadly similar to but less pronounced than the experimental data. The very great differences between these computations and those previously obtained using wall functions (e.g., Chang et al., 1983b) do strongly suggest that the latter approach ought not to be used in computing three-dimensional flows with strong secondary motions.

Despite the improvement, substantial differences still remained between the computed and measured flow development. The computations were therefore repeated employing the algebraic second-moment (ASM) closure described in the previous section; again, the PSL approximation was not adopted. The inlet conditions were generated by an ASM computation in a straight duct. The resultant streamwise mean velocity profiles at 90 and 130 deg are compared with experiments in Figs. 6 and 7. What is plainly evident from these figures is that the ASM computations are in considerably closer agreement with the measured data than those obtained from the eddy-viscosity model. The agreement is particularly close at 130 deg.

A key factor in obtaining the correct primary flow is the prediction of the strong secondary motion. Certainly, as shown in Fig. 8, the three different computational models of the flow discussed above produce markedly different secondary flow patterns. The pattern obtained when using the PSL approximation is nearly the same as that of Johnson (1984) us-

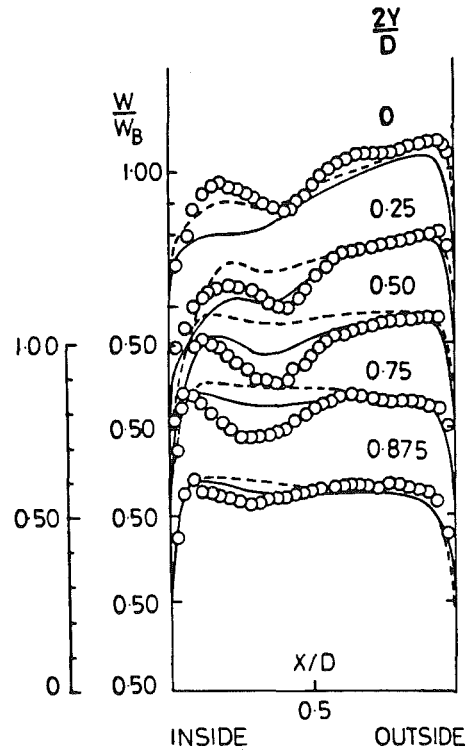


Fig. 5 Streamwise mean velocity profiles at 130 deg station. Key as Fig. 4.

ing wall functions. This is consistent with the axial velocity profile at 130 deg being nearly the same for these two cases. The adoption of a fine grid without the PSL approximation, Figs. 8(*c*) and 8(*d*), produces a multi-cellular secondary flow

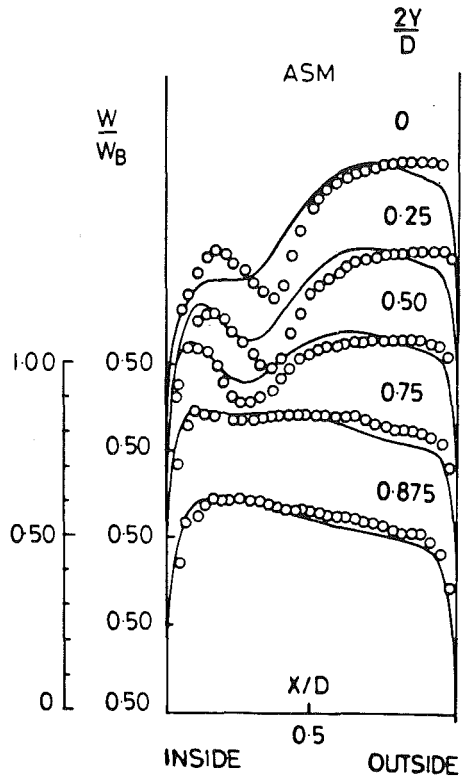


**Fig. 6 Streamwise mean velocity profiles at 90 deg station.**
**o o Measurements, Chang et al. (1983a);**
**—— Computations, present study using ASM/mixing length without PSL approximation**

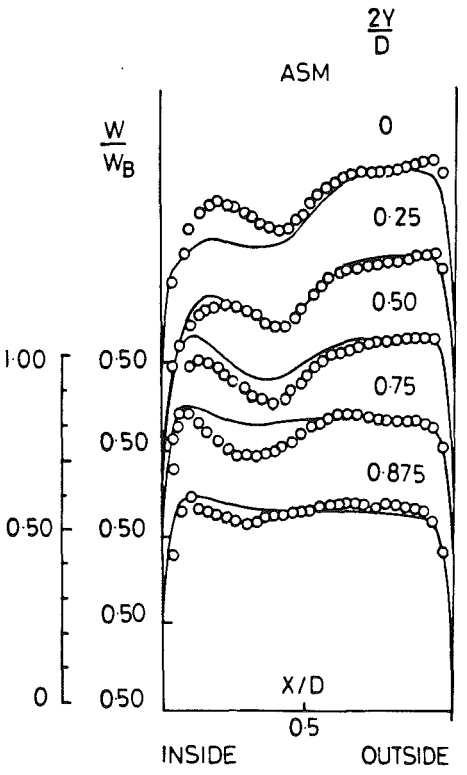


**Fig. 7 Streamwise mean velocity profiles at 130 deg station. Key as Fig. 6.**

pattern with the ASM model (Fig. 8(*d*)) producing one extra vortex than the EVM computations. While it is not possible to construct a corresponding diagram from the limited experimental secondary flow data, there seems little doubt that

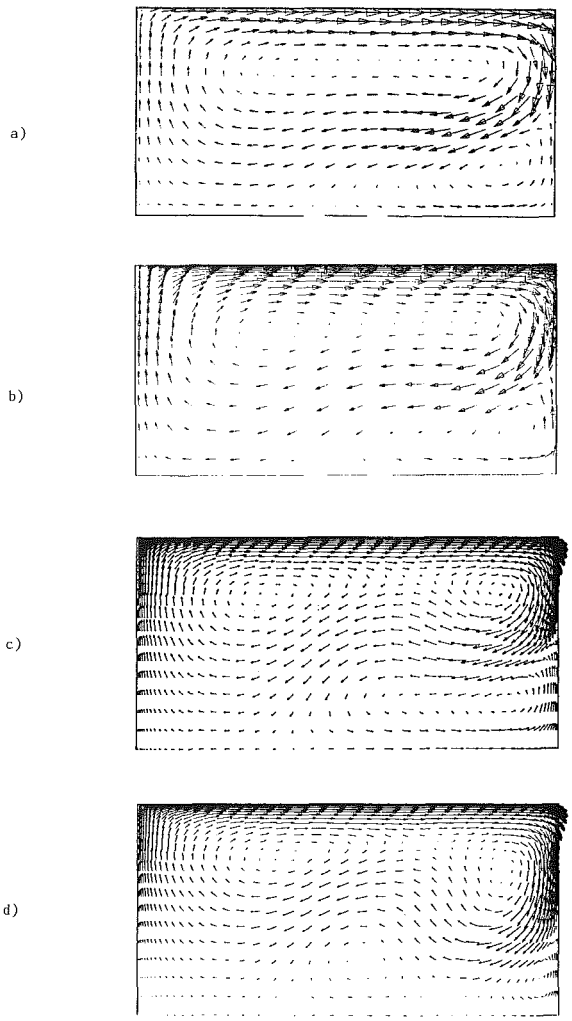


**Fig. 8 Secondary flow vectors at 130 deg station.**
**(*a*) Johnson (1984);**
**(*b*) present study, $k-\epsilon$/mixing length with PSL;**
**(*c*) present study, ($k-\epsilon$/mixing length without PSL;**
**(*c*) present study, ASM/mixing length without PSL**

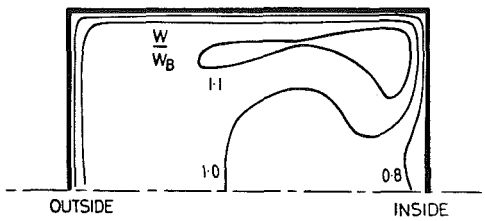


**Fig. 9 Axial velocity contours at 130 deg station**

the multi-cellular behavior generated by the ASM computations corresponds most closely to the real flow. The figure also helps us infer the sequence of developments that gives rise to the trough in streamwise velocity near the inside of the bend. Over the initial part of the bend the conventional single secondary vortex carries near-wall fluid to the inside of the bend. Due to this accumulation, slow-moving fluid near the symmetry plane is pushed away from the inside wall towards the outside of the bend. However, because its streamwise velocity is low it cannot proceed far against the radial pressure gradient: the fluid is deflected at roughly right angles to the symmetry plane and then turns back on itself towards the inside of the bend. Thus, the interaction of primary and secondary flow leads to a progressive vortex breakdown. The streamwise velocity contours shown in Fig. 9 are distorted in an obvious

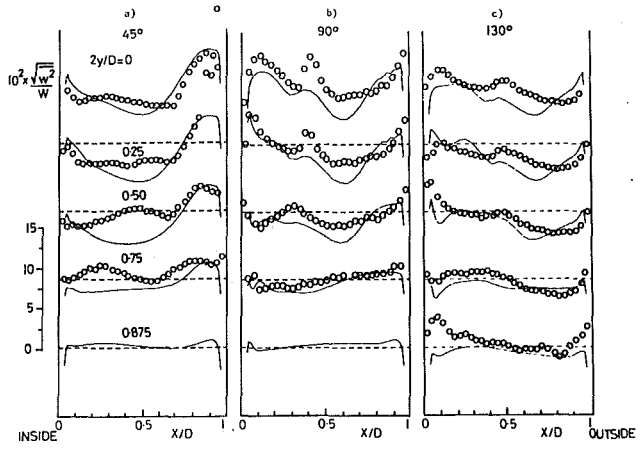


**Fig. 10 RMS streamwise turbulent velocity fluctuations.**
**o o Measurements, Chang et al. (1983a);**
**—— Present ASM computations**
**(a) 45 deg; (b) 90 deg; (c) 130 deg**

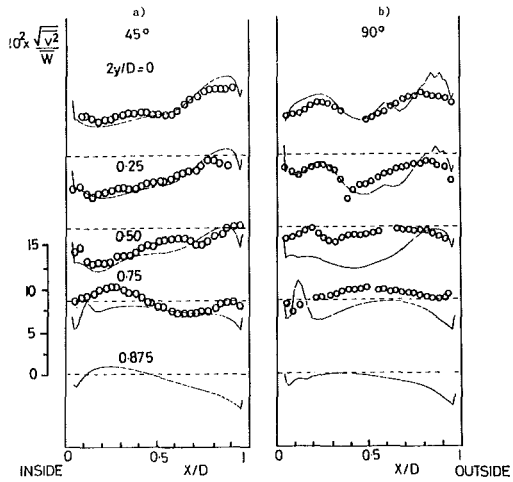


**Fig. 11 RMS radial turbulent velocity fluctuations. Key as Fig. 10.**
**(a) 45 deg; (b) 90 deg**

way by this secondary flow pattern and it is clearly this that leads to the appearance of the trough in the profiles in Fig. 7.

The ASM scheme yields predictions of the turbulent as well as the mean velocity components. In Figs. 10 and 11 the rms streamwise and radial fluctuating velocity profiles are shown along lines parallel with the symmetry plane (the corresponding mean velocity profiles being those of Figs. 6 and 7). On the whole the computed profiles exhibit distributions very similar to the measurements of Chang et al. (1983a), though there are a few points of discrepancy. For example, the measured sharp spike in $\sqrt{w^2}$ near the symmetry plane at 90 deg is only hinted at in the computations, presumably because the radial gradient in streamwise mean velocity there (the main agency for generating the normal-stress component) is under-predicted, c.f. Fig. 6. A considerably too low level of $\sqrt{v^2}$ is also observed at this station along the line midway beween the symmetry plane and the end wall.

## Conclusions

The present paper has reported four refinements on earlier computer simulations of the 180 deg U-bend experiment of Chang et al. (1983a). The following conclusions may be drawn:

1. The successive refinement of the mesh has, on its own, had only a very minor effect on the computed flow pattern. Purely numerical errors were thus not a major factor in the failure of earlier computations to produce a flow field close to the measured one—at least not where the QUICK scheme had been used for discretizing convective terms.
2. The replacement of wall functions by a fine grid to resolve the buffer and viscous sublayers (even though only the very simple mixing-length hypothesis was used in this region) has led to a marked increase in the realism of the computed flow.
3. Due to the very rapid variation of pressure normal to the passage walls in the corners of the duct, the use of the parabolic sublayer approximation (PSL) introduced serious errors. Attempts to drop the approximation in the corner region did not prove successful.
4. The replacement of the standard $k-\epsilon$ eddy-viscosity model by a standard algebraic second-moment closure led to a further significant improvement in the level of agreement of the computed flow with experiment.
5. Obtaining a reasonable representation of the primary flow is intimately bound up with predicting the secondary flow with reasonable fidelity. The present computations suggest that the troughs in the primary flow arise from a "blockage" of the return secondary current near the symmetry plane by about 90 deg of arc accompanied by a breakdown of the secondary motion into a very complex multi-cellular pattern.

Finally, it should be said that, despite the marked improvements in the accuracy of the computations, not insignificant differences still remain between the computed and measured distributions. It must remain at present a matter of speculation whether these differences are mainly due to failures of the turbulence model in the conventional sense or possibly to the secondary motion developing a certain periodicity giving rise to a "sloshing" about the plane of geometric symmetry (Humphrey, 1984). Our computations of the thermal field, which will be reported in a future communication, suggest that the neglect of turbulent transport by the strong secondary motion in the near-wall sublayer (as is implicit in the use of the mixing-length hypothesis there) is probably the most significant contributor to the remaining discrepancies—at least so far as the surface heat transfer coefficients are concerned.

## Acknowledgments

Different phases of this research have been sponsored by the U.S. Office of Naval Research and Rolls-Royce plc. The work has proceeded in close collaboration with that of Professor J. A. C. Humphrey and his group at the University of California, Berkeley. Young Don Choi gratefully acknowledges the award of sabbatical leave and overseas travel scholarship by the Korea University. Mrs. L. J. Ball has painstakingly prepared the manuscript for publication.

## References

Azzola, J., Humphrey, J. A. C., Iacovides, H., and Launder, B. E., 1986, ASME Journal of Fluids Engineering, Vol. 108, pp. 214–221.

Birch, N., 1984, "The Calculation of 3D Flow in Curved Ducts Using Q385," Report TSG0161, Rolls-Royce Theoretical Sciences Group, Derby.

Chang, S. M., 1983, PhD Thesis, Dept. of Mechanical Engineering, University of California/Berkeley.

Chang, S. M., Humphrey, J. A. C., and Modavi, A., 1983a, *Physico-Chemical Hydrodynamics*, Vol. 4, pp. 243–269.

Chang, S. M., Humphrey, J. A. C., Johnson, R. W., and Launder, B. E., 1983b, *Proc. 4th Symp. on Turbulent Shear Flows*, pp. 6.20–6.25, Karlsruhe.

Huang, P. G., and Leschziner, M. A., 1985, *Proc. 5th Symp. on Turbulent Shear Flows*, Cornell, p. 20.7

Humphrey, J. A. C., 1984, Personal communication.

Iacovides, H., 1986, "Momentum and Heat Transport in Flow through 180° Bends of Circular Cross Section," PhD thesis, Faculty of Technology, University of Manchester.

Iacovides, H., and Launder, B. E., 1984a, *Proc. Ist U.K. National Heat Transfer Conf.*, Symp. Series No. 86, pp. 1097–1114, Leeds.

Iacovides, H., and Launder, B. E., 1984b, ASME Journal of Fluids Engineering, Vol. 106, p. 241.

Iacovides, H., and Launder, B. E., 1985, *Proc. 4th Int. Conf. Num. Meth. in Laminar and Turbulent Flow*, Pineridge Press, Swansea, pp. 1023–1045.
Iacovides, H., and Launder, B. E., 1987, *Numerical Heat Transfer*, Vol. 12, p. 475.
Johnson, R. W., "Turbulent Convecting Flow in a Square Duct with a 180° Bend," PhD thesis, Faculty of Technology, University of Manchester.
Johnson, R. W., and Launder, B. E., 1985, *Int. J. Heat and Fluid Flow*, Vol. 6, pp. 171–180.
Koosinlin, M. L., Launder, B. E., and Sharma, B. I., 1974, ASME *Journal of Heat Transfer*, Vol. 98, p. 204.
Launder, B. E., and Ying, W. M., 1973, Proc I.Mech.E., Vol. 187, 37/73, pp. 455–461.
Leonard, B. P., 1979, *Comp. Meth. Appl. Mech. Eng.*, Vol. 19, p. 59.
Patankar, S. V., 1980, *Numerical Heat Transfer and Fluid Flow*, Hemisphere Publishing Corp., McGraw-Hill.
Patankar, S. V., and Spalding, D. B., 1972, *Int. J. Heat Mass Transfer*, Vol. 15, p. 1787.
Van Driest, E. R., 1956, *J. Aero, Sci.*, Vol. 23, p. 1007.

## APPENDIX

### Cylindrical Version of Algebraic Stress Equations

**Component Stress Equations.** Transformation of the tensorial ASM equations to cylindrical polar form produces the following very cumbersome set of equations for the component stresses. These equations can be rearranged as

$$A_{ij}\overline{u^2}+B_{ij}\overline{u^2}+C_{ij}\overline{w^2}+D_{ij}\overline{uv}+E_{ij}\overline{uw}+F_{ij}\overline{vw}=G_{ij} \tag{A-1}$$

Let us first introduce the following abbreviations

$$\begin{aligned}
\alpha &= I-C_2\\
\beta &= C_1-1+P/\epsilon\\
d &= \beta\epsilon/\alpha k\\
\wedge X_2 &= \left(\frac{C_2'C_2}{1-C_2}\right)f(l/X)\\
\wedge Y_2 &= \left(\frac{C_2'C_2}{1-C_2}\right)f(l/Y)\\
\wedge X_1 &= \left(\frac{C_1'}{1-C_2}\right)f(l/X)\\
\wedge Y_1 &= \left(\frac{C_1'}{1-C_2}\right)f(l/Y)
\end{aligned} \tag{A-2}$$

The functions $f(l/X)$ and $f(l/Y)$ denote the wall-pressure-reflection effects associated with two opposite walls and are given by

$$\begin{aligned}
f\left(\frac{l}{X}\right) &= \frac{l}{X}+\frac{l}{D-X}\\
f\left(\frac{l}{Y}\right) &= \frac{l}{Y_p}+\frac{l}{D-Y_p}
\end{aligned} \tag{A-3}$$

The expressions for $A_{ij}$ . . . . . $G_{ij}$ may then be written:

*$\overline{u^2}$ Equation*

$$\begin{aligned}
A_{11} &= (2+4\wedge X_2+\wedge Y_2)\frac{\partial U}{\partial X}+3\wedge X_1\frac{\epsilon}{k}+\frac{3d}{2}\\
B_{11} &= -(1+2\wedge X_2+2\wedge Y_2)\frac{\partial V}{\partial Y}-\frac{3}{2}\wedge Y_1\frac{\epsilon}{k}\\
C_{11} &= -(1+2\wedge X_2-\wedge Y_2)\left(\frac{1}{r_c}\frac{\partial W}{\partial\phi}-\frac{U}{r_c}\right)\\
D_{11} &= -\frac{\partial V}{\partial X}(1+2\wedge X_2+2\wedge Y_2)\\
&\quad -\frac{\partial U}{\partial Y}(-2-4\wedge X_2-\wedge Y_2)\\
E_{11} &= -\frac{\partial W}{\partial X}(1+2\wedge X_2-\wedge Y_2)\\
&\quad +\left(\frac{1}{r_c}\frac{\partial U}{\partial\phi}+\frac{W}{r_c}\right)(2+4\wedge X_2-\wedge Y_2)\\
F_{11} &= -\frac{\partial W}{\partial Y}(1+2\wedge X_2-\wedge Y_2)\\
&\quad +\frac{1}{r_c}-\frac{\partial V}{\partial\phi}(1+2\wedge X_2-2\wedge Y_2)\\
G_{11} &= \beta\epsilon/\alpha
\end{aligned} \tag{A-4}$$

*$\overline{v^2}$ Equation*

$$\begin{aligned}
A_{22} &= -\frac{\partial U}{\partial X}(1+2\wedge X_2+\wedge Y_2)-\frac{3}{2}\wedge X_1\frac{\epsilon}{k}\\
B_{22} &= \frac{\partial V}{\partial Y}(2+\wedge X_2+4\wedge Y_2)+3\wedge Y_1\frac{\epsilon}{k}+\frac{3d}{2}\\
C_{22} &= -\left(\frac{1}{r_c}\frac{\partial W}{\partial\phi}-\frac{U}{r_c}\right)(1-\wedge X_2+2\wedge Y_2)\\
D_{22} &= -\frac{\partial U}{\partial Y}(1+2\wedge X_2+2\wedge Y_2)\\
&\quad -\frac{\partial V}{\partial X}(-2-\wedge X_2-4\wedge Y_2)\\
E_{22} &= -\frac{\partial W}{\partial X}(1-\wedge X_2-2\wedge Y_2)\\
&\quad -\left(\frac{1}{r_c}\frac{\partial U}{\partial\phi}+\frac{V}{r_c}\right)(1+2\wedge X_2+2\wedge Y_2)\\
F_{22} &= -\frac{\partial W}{\partial Y}(1-\wedge X_2+2\wedge Y_2)\\
&\quad -\frac{1}{r_c}\frac{\partial V}{\partial\phi}(-2+\wedge X_2-4\wedge Y_2)\\
G_{22} &= \beta\epsilon/\alpha
\end{aligned} \tag{A-5}$$

*$\overline{w^2}$ Equation*

$$\begin{aligned}
A_{33} &= -\frac{\partial U}{\partial X}(1+2\wedge X_2-\wedge X_2)+\frac{3}{2}\wedge X_1\frac{\epsilon}{k}\\
B_{33} &= -\frac{\partial V}{\partial Y}(1-\wedge X_2+2\wedge Y_2)+\frac{3}{2}\wedge Y_1\frac{\epsilon}{k}\\
C_{33} &= \left(\frac{1}{r_c}\frac{\partial W}{\partial\phi}-\frac{U}{r_c}\right)(2+\wedge X_2+\wedge Y_2)\\
D_{33} &= -\frac{\partial U}{\partial Y}(1+2\wedge X_2-\wedge Y_2)\\
&\quad -\frac{\partial V}{\partial X}(1-\wedge X_2+2\wedge Y_2)\\
E_{33} &= -\left(\frac{1}{r_c}\frac{\partial U}{\partial\phi}+\frac{W}{r_c}\right)(1+2\wedge X_2-\wedge Y_2)\\
&\quad -\frac{\partial W}{\partial X}(-2-\wedge X_2-\wedge Y_2)\\
F_{33} &= \frac{1}{r_c}\frac{\partial V}{\partial\phi}(1-\wedge X_2+2\wedge Y_2)
\end{aligned} \tag{A-6}$$

$$-\frac{\partial W}{\partial Y}(-2-\wedge X_2-\wedge Y_2)$$

$$G_{33}=\beta\epsilon/\alpha$$

*$\overline{uv}$ Equation*

$$A_{12}=\frac{\partial V}{\partial X}\left(1+\frac{3}{2}\wedge X_2+\frac{3}{2}\wedge Y_2\right)$$

$$B_{12}=\frac{\partial U}{\partial Y}\left(1+\frac{3}{2}\wedge X_2+\frac{3}{2}\wedge Y_2\right)$$

$$C_{12}=0$$

$$D_{12}=\left(\frac{\partial U}{\partial X}+\frac{\partial V}{\partial Y}\right)\left(1+\frac{3}{2}\wedge X_2+\frac{3}{2}\wedge Y_2\right)+\frac{3}{2}(\wedge X_1+\wedge Y_1)\frac{\epsilon}{k}+d$$

$$E_{12}=\frac{1}{r_c}\frac{\partial V}{\partial\phi}\left(1+\frac{3}{2}\wedge X_2+\frac{3}{2}\wedge Y_2\right) \quad \text{(A-7)}$$

$$F_{12}=\left(\frac{1}{r_c}\frac{\partial U}{\partial\phi}+\frac{W}{r_c}\right)\left(1+\frac{3}{2}\wedge X_2+\frac{3}{2}\wedge Y_2\right)$$

$$G_{12}=0$$

*$\overline{uw}$ Equation*

$$A_{13}=\frac{\partial W}{\partial X}\left(1+\frac{3}{2}\wedge X_2\right)$$

$$B_{13}=0$$

$$C_{13}=\left(\frac{1}{r_c}\frac{\partial U}{\partial\phi}+\frac{W}{r_c}\right)\left(1+\frac{3}{2}\wedge X_2\right)$$

$$D_{13}=\frac{\partial W}{\partial Y}\left(1+\frac{3}{2}\wedge Y\right) \quad \text{(A-8)}$$

$$E_{13}=\left(\frac{1}{r_c}\frac{\partial W}{\partial\phi}-\frac{U}{r_c}+\frac{\partial U}{\partial X}\right)\left(1+\frac{3}{2}\wedge X_2\right)+\frac{3}{2}\wedge X_1\frac{\epsilon}{k}+d$$

$$F_{13}=\frac{\partial U}{\partial Y}\left(1+\frac{3}{2}\wedge X_2\right)$$

$$G_{13}=0$$

*$\overline{vw}$ Equation*

$$A_{23}=0$$

$$B_{23}=\frac{\partial W}{\partial Y}\left(1+\frac{3}{2}\wedge Y_2\right)$$

$$C_{23}=\frac{1}{r_c}\frac{\partial V}{\partial\phi}\left(1+\frac{3}{2}\wedge Y_2\right) \quad \text{(A-9)}$$

$$D_{23}=\frac{\partial W}{\partial X}\left(1+\frac{3}{2}\wedge Y_2\right)$$

$$E_{23}=\frac{\partial V}{\partial X}\left(1+\frac{3}{2}\wedge Y_2\right)$$

$$F_{23}=\left(\frac{1}{r_c}\frac{\partial W}{\partial\phi}-\frac{U}{r_c}+\frac{\partial V}{\partial Y}\right)\left(1+\frac{3}{2}\wedge Y_2\right)+\frac{3}{2}\wedge Y_1\frac{\epsilon}{k}+d$$

$$G_{23}=0$$

# Measurements in Vertical Plane Turbulent Plumes

**B. R. Ramaprian**
Professor of Mechanical and Materials Engineering, Washington State University, Pullman WA.
Mem. ASME

**M. S. Chandrasekhara**
Adjunct Research Professor, Department of Aeronautics and Astronautics, Naval Postgraduate School, Monterey, CA
Assoc. Mem. ASME

*Mean-flow and turbulence measurements have been obtained in two-dimensional vertical turbulent plumes in a nominally still ambient. The plumes were generated by injecting hot water vertically upwards from the bottom of a reservior containing cold water. A two-component Laser Doppler Anemometer (LDA) and a "cold-film" resistance thermometer were used to obtain instantaneous velocity and temperature measurements in the plume. The present mean-flow measurements have confirmed many of the earlier measurements on plane plumes, but have also indicated some important differences. The use of the two-component LDA made it possible to obtain data on turbulent intensities, turbulent fluxes and other details of the structure of turbulence in plane plumes. The turbulence measurements have shown that the eddy viscosity and turbulence are significantly higher in the plume compared to an isothermal jet. Detailed measurements of energy balance suggest that buoyant production contributes substantially to this increase.*

## Introduction

There are several practical applications for the study of turbulent plumes, for example, cooling-tower and chimney exhausts, and hot-water discharges from power plants to lakes and rivers. The plume is also an interesting complex flow in which turbulent motions are strongly influenced by buoyancy. Study of the plume may lead to a better understanding of the role of buoyancy in turbulent shear flows. Early methods of prediction of buoyant jets were based on the well-known integral techniques [1–4] using empirical physical assumptions about the flow (e.g., the value of an entrainment coefficient). More recent methods [5–8] involve solution of the complete set of governing partial differential equations using turbulence models of varying degrees of complexity.

The empirical input required in either of the above approaches is to be obtained from detailed experiments. There have been only a few such experiments reported in the literature. These include the early experiments such as those of Rouse, Yih, and Humphreys [9] on round and plane plumes, and Lee and Emmons [10] on a plane plume; the more recent round-plume experiments [11–13] and the plane buoyant-jet and plume experiments of Kotsovinos [14] reported in [15]. Of the above, the experiments of Kotsovinos represent the only extensive study on plane buoyant jets and plumes, reported in the literature. These experiments were performed in water using a one-component Laser Doppler Anemometer (LDA) for instantaneous velocity measurements and a microthermistor for temperature measurements. Extensive as the work was, the single-component LDA used in [14] did not allow the direct measurement of the turbulent transport of momentum and heat in the cross-stream direction. While detailed data of these turbulent fluxes are available for the round plume from [13], similar information is not available for the plane plume. The present experiments were designed primarily to obtain this information for the plane plume. In the present experiments, as in those of Kotsovinos and List [15] (referred to henceforth as KL) heat was used to produce buoyancy. A two-component LDA system, coupled with a microresistance thermometer (cold film) was used to measure two instantaneous velocity components $U$ and $V$ and the instantaneous temperature excess $\Delta T$ above the ambient. The study was focused on the asymptotic plume rather than on the entire range of buoyant-jet flows. This was done because the asymptotic plume is independent of the initial conditions and hence, represents a well-defined flow configuration. It is, therefore, ideal both for the study of buoyancy effects on turbulence and for use as a basic test case in the development of predictive models for buoyancy-driven flows.

## Experimental Conditions and Procedure

The experiments were conducted in a hydraulic flume 7 m long × 0.45 m wide × 0.75 m deep, which served in the present experiments, simply as a large reservior. A nozzle 5 mm in width (D) and 250 mm in span, located at the bottom of the flume served as the source of the two-dimensional vertical submerged buoyant jet. The flow was confined between two plexiglas false side walls spaced 250 mm apart, to improve the two-dimensionality of the flow. The two-component LDA used had a spatial resolution of about 1.1 mm in the spanwise direction and 0.1 mm in the other two directions. The temperature sensor was located within about 1 mm downstream of the center of the focal volume of the LDA. The experimental apparatus, instrumentation and procedure were identical to those used for the study of nonbuoyant jets reported in [16]. Special problems associated with LDA measurements in a nonisothermal flow and with the contamination of the ambient by the heated fluid, as well as the

Contributed by the Fluids Engineering Division for publication in the JOURNAL OF FLUIDS ENGINEERING. Manuscript received by the Fluids Engineering Division June 17, 1987.

means to assess and minimize these problems are also described in that paper. These will not, therefore, be discussed here. Note that the measurements extended up to a height of 60 D above the nozzle exit and that the last measurement station was about 60 D below the free surface. The results for the plane jet presented in [16] also showed that there are no significant free-surface effects on the flow in the region of measurements.

Flow rate through the nozzle was measured using an orifice meter. The temperature of the jet fluid $T_j$ and the ambient $T_a$ were measured using thermistors. The flow rate was maintained constant to within 1 percent and the temperature excess $\Delta T_j (= T_j - T_a)$ to within 5 percent over the duration of the experiment. Their average values were used to define the (span averaged) *nominal* exit conditions for velocity, temperature excess and fluxes of mass, momentum, buoyancy and heat. It may be noted that the accurate knowledge of the exit conditions is not essential for the study of the asymptotic plume and that the exit conditions have been used only for either nondimensionalizing the data or deriving a length scale *representative* of the axial distance at which the flow can be expected to transform to the asymptotic plume state. The nominal values of these exit conditions are adequate for this purpose. The experiments pertained to four cases of plume flows. These are designated as MSC3, MSC3X, MSC3Y and MSC4. The nominal exit conditions corresponding to the flows are as shown in Table 1. The coefficient of thermal expansion of water, $\alpha$ in the above table, was obtained from the following expression suggested in [14]:

$$\alpha = (-0.073 + 0.19T - 0.0027T^2 + 0.00002T^3) \times 10.^{-4} \quad (1)$$

where $T$ is the temperature of the water in degrees centigrade. $R_j$ is the exit Richardson number defined by

$$R_j = \frac{\alpha g \Delta T_j D}{U_j^2} \quad (2)$$

**Table 1 Experimental conditions**

| Flow Designation | $U_j$ cm/s | $\Delta T_j$ °C | $T_a$ °C | $\alpha_j \times 10^4$ $(^\circ C)^{-1}$ | $R_j$ |
|---|---|---|---|---|---|
| MSC3 | 10 | 23.2 | 24.4 | 4.42 | 0.050 |
| MSC3X | 10 | 19.0 | 21.0 | 3.85 | 0.036 |
| MSC3Y | 10 | 22.0 | 22.4 | 4.18 | 0.045 |
| MSC4 | 5 | 22.3 | 21.1 | 4.10 | 0.179 |

Even though the flows MSC3X and MSC3Y do not differ significantly in their exit conditions from MSC3, these experiments were performed on different days and can therefore be used to ascertain the repeatability of the experimental results. The exit conditions in all the cases were such as to cause the laminar flow to become unstable almost immediately after exit (say within $x/D = 1$), as observed from dye visualization tests. Transition to turbulence can be expected to have been complete typically in the range $20 < x/D < 30$, as inferred from the transition criterion of Bill and Gebhart (see List [17]), namley the Grashoff number Gr at the transition point $x_{tr}$ is given by

$$\mathrm{Gr} = g x_{tr}^3 \alpha (\Delta T_m)/\nu^2 = 3 \times 10^8 \quad (3)$$

Thus the plumes studied can be expected to be turbulent over most of the measurement range. It will also be shown that all the flows reached practically the asymptotic *turbulent* plume state by $x/D = 30$ with regard to the mean, and by $x/D = 40$ with regard to *most* turbulent properties. They, however, exhibited mild evolving trends in respect of some *details* of the turbulent structure in the measurement range $30 < x/D < 60$. The conservation of the (kinematic) heat flux integral $H$, defined by the two-dimensional, integral energy equation

$$H = \int_{-\infty}^{+\infty} (U\Delta T)\,dy = \int_{-\infty}^{+\infty} (\bar{U}\Delta\bar{T} + ut)\,dy \quad (4)$$

is a good test of not only the two-dimensionality of the flow in the neighborhood of the measurement plane, but also the

## Nomenclature

$B$ = kinematic buoyant force, $\int_{-\infty}^{+\infty} -\frac{\Delta\gamma}{\rho}\,dy$

$b$ = half width, defined as the value of $y$ at $\bar{U} = \frac{U_m}{2}$ $\left(\text{or at } \Delta\bar{T} = \frac{\Delta T_m}{2}\right)$

$C_E$ = entrainment coefficient (equation (23))

$C_p$ = growth parameter (equation (20))

$D$ = jet width at exit

Gr = Grashoff number (equation (3))

$g$ = acceleration due to gravity

$H$ = kinematic heat flux (mean + turbulent)

$K_1$ = spreading rate $\frac{db}{dx}$ (equation (11))

$M$ = kinematic momentum flux (equation (7))

$M^*$ = nondimensional momentum flux (equation (8))

Pr = Prandtl number

$Q$ = kinematic mass flux (equation (6))

$Q^*$ = nondimensional mass flux (equation (19))

$q$ = square root of turbulent kinetic energy per unit mass

R = Richardson number (equation (5))

$T$ = temperature

$\Delta T$ = excess temperature above the ambient

$\Delta T_m^*$ = nondimensional maximum excess temperature (equation (24))

$t$ = temperature fluctuation

$U$ = axial velocity component

$u$ = turbulent fluctuation in $U$

$V$ = cross-stream velocity component

$v$ = turbulent fluctuation in $V$

$w$ = turbulent fluctuation in the spanwise direction

$x$ = axial coordinate

$x^*$ = nondimensional axial coordinate, $x\beta_j^{2/3}/M_j$

$y$ = cross-stream coordinate

$\alpha$ = coefficient of thermal expansion

$\beta$ = kinematic buoyancy flux (equation (8))

$\epsilon$ = rate of dissipation of turbulent kinetic energy (equation (28))

$\gamma$ = specific weight

$\Delta\gamma$ = excess specific weight above the ambient

$\eta$ = $y/b$

$\rho$ = density

$\sigma$ = coefficient

$\nu$ = kinematic viscosity

**Subscripts**

$a$ = ambient

max, m = maximum value

cl = centerline of the jet

$j$ = jet exit

$M$ = pertaining to momentum

$o$ = virtual origin

$t$ = pertaining to temperature

$u$ = pertaining to velocity

30 = pertaining to station $x/D = 30$

**Other Notations**

overbar = time-mean value

prime = rms value

Table 2 Experimental data of mean-flow properties

| Flow designation and virtual origins ($x_{oM}/D$; $x_{ot}/D$) | $\frac{x}{D}$ | $\Delta T_j$ | $M$ | $Q$ | $\beta$ | B | $H$ | $b_u$ | $b_t$ | $U_m$ | $\Delta T_m$ | R |
|---|---|---|---|---|---|---|---|---|---|---|---|---|
| | | °C | $cm^3/s^2$ | $cm^2/s$ | $cm^3/s^3$ | $cm^2/s^2$ | $\frac{cm^2-°C}{s}$ | cm | cm | cm/s | °C | |
| Uncertainties: | ±0.005 | ±0.20 | ±4.0 | ±0.50 | ±1.00 | ±0.70 | ±2.0 | ±0.05 | ±0.05 | ±0.25 | ±0.20 | ±0.040 |
| MSC3X | 30 | 21.80 | 122.8 | 24.50 | 31.90 | 7.03 | 114.5 | 2.04 | 2.84 | 7.01 | 5.47 | 0.253 |
| (−1.0; −6.0) | 40 | 21.60 | 159.7 | 31.45 | 31.71 | 7.25 | 117.1 | 2.24 | 3.00 | 6.68 | 4.18 | 0.242 |
| | 50 | 22.20 | 168.1 | 37.30 | 28.35 | 6.70 | 107.0 | 2.54 | 3.52 | 6.41 | 3.37 | 0.310 |
| | 60 | 21.80 | 225.7 | 49.80 | 31.71 | 6.57 | 125.3 | 3.44 | 4.69 | 6.58 | 3.00 | 0.340 |
| MSC3Y | 30 | 19.55 | 115.9 | 24.96 | 29.70 | 7.04 | 111.3 | 1.80 | 2.24 | 6.60 | 5.41 | 0.297 |
| (0.0; −5.0) | 40 | 18.63 | 131.1 | 30.47 | 25.85 | 6.36 | 102.1 | 2.32 | 3.16 | 6.09 | 4.06 | 0.325 |
| | 50 | 19.96 | 185.3 | 38.93 | 33.43 | 7.27 | 132.1 | 2.77 | 3.26 | 6.53 | 4.01 | 0.310 |
| | 56 | 19.09 | 179.3 | 40.60 | 30.59 | 7.59 | 122.8 | 3.14 | 4.52 | 6.19 | 3.49 | 0.355 |
| MSC3 | 20 | 23.40 | 119.7 | 19.90 | 47.20 | 8.69 | 145.8 | 1.24 | 1.51 | 8.13 | 8.67 | 0.216 |
| (−4.0; −5.0) | 30 | 22.80 | 160.6 | 28.00 | 43.78 | 8.32 | 139.5 | 1.72 | 1.96 | 7.97 | 6.15 | 0.232 |
| | 40 | 23.20 | 185.5 | 33.20 | 39.34 | 7.09 | 133.7 | 2.16 | 2.46 | 7.58 | 4.79 | 0.225 |
| | 50 | 23.30 | 240.0 | 44.90 | 41.79 | 8.27 | 144.4 | 3.25 | 3.77 | 7.26 | 3.76 | 0.273 |
| | 60 | 23.40 | 296.0 | 53.50 | 39.80 | 6.96 | 137.5 | 3.52 | 3.80 | 7.78 | 3.23 | 0.235 |
| MSC4 | 30 | 22.39 | 76.8 | 17.20 | 25.60 | 6.66 | 89.99 | 1.50 | 1.87 | 5.69 | 6.19 | 0.287 |
| (6.0; 6.0) | 40 | 22.29 | 90.0 | 22.20 | 20.30 | 5.60 | 76.60 | 1.93 | 2.28 | 5.51 | 4.52 | 0.305 |
| | 50 | 22.46 | 113.0 | 28.40 | 17.65 | 5.73 | 70.50 | 2.23 | 2.60 | 5.60 | 3.54 | 0.280 |
| | 56 | 21.85 | 87.0 | 27.70 | 9.22 | 2.67 | 40.90 | 2.35 | 2.33 | 4.96 | 2.39 | 0.298 |

absence of any stratification of the ambient. Figure 1 shows results for the different flows in the measurement range $20 < x/D < 60$. The data are normalized using the value of $H$ at $x/D = 30$. It is seen that flows MSC3 and MSC3X are reasonably two-dimensional and are free from any significant stratification effects. The result for flow MSC3Y is marginally acceptable. The flow MSC4 was particularly difficult to set up and measure, because of very low velocities and very large temperature fluctuations associated with this flow. It is possible that three-dimensional and stratification effects were present in this flow. Even so, some results from this experiment are presented to demonstrate that flows originating from substantially different initial conditions evolve towards the same asymptotic plume state. The experimental uncertainties in the case of the other three flows are: $\bar{U} = \pm 2.5$ mm/s; $\Delta\bar{T} = 0.2°C$; $u'$, $v'$, $t' = 5$ percent; $\overline{uv}$, $\overline{ut}$, $\overline{vt} = 10$ percent; $\overline{u^2 v}$, $\overline{v^3} = 15$ percent. Uncertainty estimates for the other derived quantities were obtained from an error-propopagation analysis in some cases and from the standard deviation of the data, in the other cases. These are indicated on the respective figures.

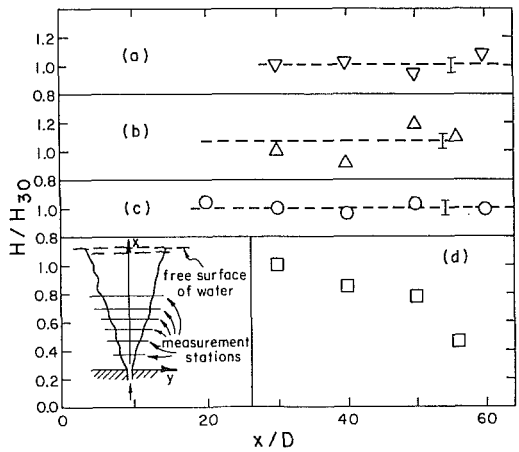


Fig. 1 Conservation of kinematic heat flux. (a) MSC3X, (b) MSC3Y, (c) MSC3, (d) MSC4. Dashed lines represent mean through data. Vertical bars represent uncertainty in the measurements.

## Theoretical Framework

The theoretical framework for the analysis of the asymptotic plume has been well developed in the earlier literature [9, 15] and also briefly reviewed by List [17]. A dimensionless number often used to characterize plane vertical buoyant jets is the Richardson number R, which following KL, is defined as

$$\mathrm{R}(x) = (Q/M)^3 \beta \tag{5}$$

with

$$Q = \int_{-\infty}^{+\infty} \bar{U} dy \tag{6}$$

$$M = \int_{-\infty}^{+\infty} \overline{U^2} = \int_{-\infty}^{+\infty} (\bar{U}^2 + \overline{u^2}) dy \tag{7}$$

$$\beta = -\int_{-\infty}^{+\infty} \frac{1}{\rho} \overline{U \Delta\gamma} dy = -\int_{-\infty}^{+\infty} \frac{1}{\rho} (\bar{U}\Delta\bar{\gamma} + \overline{u\Delta\gamma'}) dy \tag{8}$$

being the kinematic fluxes of mass, momentum and buoyancy, respectively. All heated jets can be expected to reach eventually an asymptotic state in which all the flow properties assume selfsimilar distributions. Under such conditions, it can be shown [9] that the behavior of a fully turbulent plume is completely described by specifying only the initial kinematic buoyancy flux $\beta_j$ defined by

$$\beta_j = \alpha_j g H_j \tag{9}$$

and that the following functional relationships can be written for such a plume:

$$\mathrm{R} = \text{constant} \tag{10}$$

$$b = K_1 x \tag{11}$$

$$Q = \sigma_Q \beta_j^{1/3} x \tag{12}$$

$$M = \sigma_M \beta_j^{2/3} x \tag{13}$$

$$U_m = \sigma_u \beta_j^{1/3} \tag{14}$$

and

$$\alpha g \Delta T_m = -\frac{\Delta\gamma_m}{\rho} = \beta_j^{2/3} / (x \sigma_t) \tag{15}$$

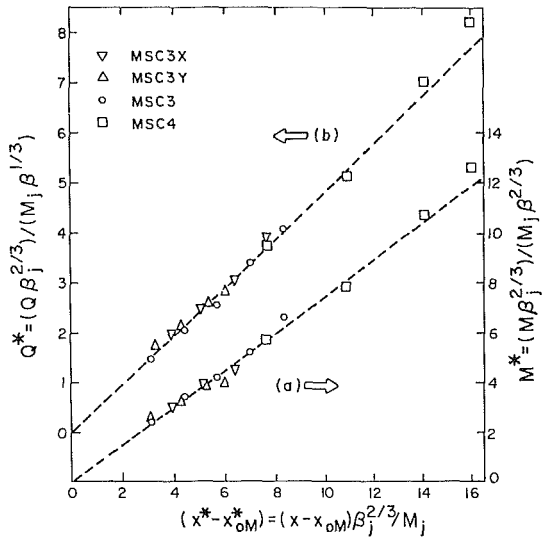


**Fig. 2 Variations of kinematic fluxes of mass and momentum. Symbols as in Figs. 1. Uncertainties: $x^*$: ±0.3; $Q^*$: ±2.2 percent; $M^*$: ±3.3 percent.**

where $b$ is a characteristic width of the plume (usually the half-width), and $K_1$, $\sigma_Q$, $\sigma_M$, $\sigma_u$ and $\sigma_t$ are universal constants.

The above relations are based on the assumption of conservation of buoyancy flux in the plume, which is equivalent to the assumption of constant $\alpha$, since heat flux is unconditionally conserved. In practice, there may be a significant decrease in the buoyancy flux with downstream distance in the near-field of the source, because of the rapid decrease in temperature (and hence $\alpha$) along the plume axis. But changes in buoyancy flux will be very small in the far field (see for example Table 2). In such cases, it is still reasonable to assume that the above relationships will be valid, provided one uses, instead of the initial buoyancy flux $\beta_j$, the local buoyancy flux $\beta(x)$ defined in equation (8), which can also be written as

$$\beta=\int_{-\infty}^{+\infty}\alpha(x)g(\Delta\bar{T}\bar{U}+\overline{ut})dy \tag{16}$$

It was found adequate in the present studies to assume a constant average value $\alpha(x)$ (equal to the value at the plume centerline) across the asymptotic plume ($x/D\geq 30$) without introducing substantial error into the evaluation of $\beta$.

## Results and Discussion

**Mean Flow Properties.** Table 2 gives a summary of the important measured mean-flow properties. Note that the quantities $M$ and $\beta$ will be referred to as "mean-flow" quantities, even though they contain turbulent contribution. It is seen from Table 2 that except in the downstream part of MSC4 the buoyancy flux $\beta$ remains reasonably constant (to within 10 percent) in the range $30<x/D<60$.

*Kinematic Fluxes of Momentum and Mass.* The experimental data on the kinematic momentum flux $M(x)$ obtained for each of the different flows were found to exhibit, within experimental scatter, a linear variation with axial distance of the form

$$M=A(x-x_{oM}) \tag{17}$$

where $A$ is a constant and $x_{oM}$ is the location of the virtual origin for each flow. Figure 2($a$) shows a plot of the momentum-flux data for all the flows in normalized coordinates. The axial coordinate $x^*$ chosen is suggested by KL. Hence, $(x^*-x^*_{oM})$ is the ratio of the distance $(x-x_{oM})$ from the virtual origin to the typical distance $(M/\beta_j^{2/3})$ required for the flow to transform to the (asymptotic) plume state. The value of $(x^*-x^*_{oM})$ should therefore be equal to (or preferably, sufficiently greater than) 1 to insure that the flow has reached the asymptotic-plume state. The scaling used for the vertical coordinate $M^*$ is suggested by equation (13). It is seen from Fig. 2($a$) that the flows studied are all in the asymptotic plume state and that most of the data collapse reasonably well on to the straight line

$$M^*=(M/\beta^{2/3})\left(\frac{\beta_j^{2/3}}{M_j}\right)=\sigma_M\frac{(x-x_{oM})}{M_j}\beta_j^{2/3}=\sigma_M(x^*-x^*_{oM}) \tag{18}$$

in conformity with equation (13). A least-square fit indicates a value of 0.74 for the universal constant $\sigma_M$.

The results for the kinematic mass flux are shown in Fig. 2($b$), plotted in normalized coordinates suggested by equation (12). These data also indicate the linear relation as implied by this equation, namely

$$Q^*=\left(\frac{Q}{\beta^{1/3}}\right)\left(\frac{\beta_j^{2/3}}{M_j}\right)=\sigma_Q(x^*-x^*_{oM}) \tag{19}$$

with a value of 0.48 for the universal constant $\sigma_Q$. The values of $\sigma_M$ and $\sigma_Q$ from [9] are 0.72 and 0.57, respectively. A growth parameter $C_p$ defined as

$$C_p\equiv\frac{Q}{M^{1/2}(x-x_{oM})^{1/2}} \tag{20}$$

along with the Richardson number R, was introduced in [15] to characterize the plane buoyant jet. Both $C_p$ and R attain universal values in the asymptotic plume. The value of $C_p$ for the plume was found from their experiments to be 0.54. Now, $C_p$ can be written as

$$C_p\equiv\left[\frac{Q}{\beta^{1/3}(x-x_{oM})}\right]\left[\frac{\beta^{1/3}(x-x_{oM})^{1/2}}{M^{1/2}}\right]=\frac{\sigma_Q}{\sigma_M^{1/2}} \tag{21}$$

Using the present values of $\sigma_Q$ and $\sigma_M$, one gets $C_p\approx 0.56$ which is in reasonable agreement with the KL data.

*Centerline Velocity.* The asymptotic theory suggests that the centerline velocity in the plume is constant (equation 14). The results for the various plumes are shown in Fig. 3($a$). It is seen from the figure that the normalized variable $U_m/\beta^{1/3}$ remains nearly constant for all the flows as implied by equation (14). There is some scatter in the data but a least-square fit indicates an average value of 2.13, with a standard deviation (indicated by the vertical bar in the figure) of 0.1. Hence,

$$\sigma_u=\frac{U_m}{\beta^{1/3}}=2.13 \tag{22}$$

This value is significantly higher than the value of 1.66 reported by KL and the value of 1.8 reported by Rouse, Yih, and Humphreys [9]. The probable reasons for this difference, especially with the former experiments and its implications will be discussed later.

*Entrainment Rate.* The entrainment coefficient $C_E$ for the asymptotic plume, can now be computed from the usual definition

$$C_E=\frac{1}{U_m}\frac{dQ}{dx} \tag{23}$$

With $\sigma_Q=0.48$ and $\sigma_u=2.13$, equation (23) yields: $C_E=0.225$. Ths value is in agreement with the value of about 0.22 observed by KL and confirms the earlier conclusions of [14, 17] that the entrainment rate in a plume is nearly twice that in an isothermal jet ($C_E$ for jet = 0.110).

*Decay of Centerline Excess Temperature.* It is known that the excess temperature in the asymptotic nonbuoyant jet

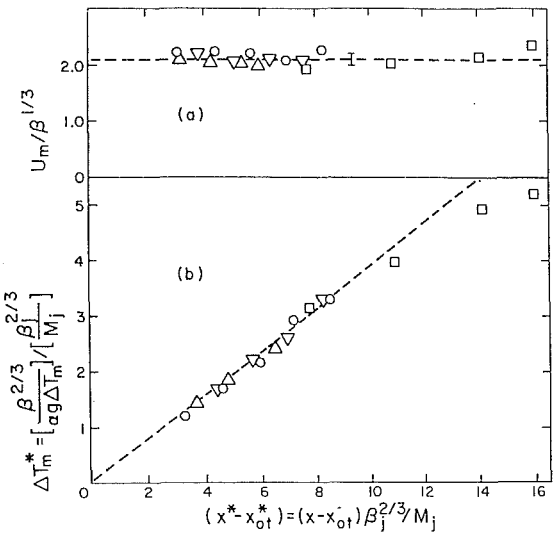


**Fig. 3 Variations of centerline velocity and centerline excess temperature along the plume. Symbols as in Figs. 1. Uncertainties: $x^*$: ±0.3; $U_m$: ±0.1; $\Delta T_m$: ±2.8 percent.**

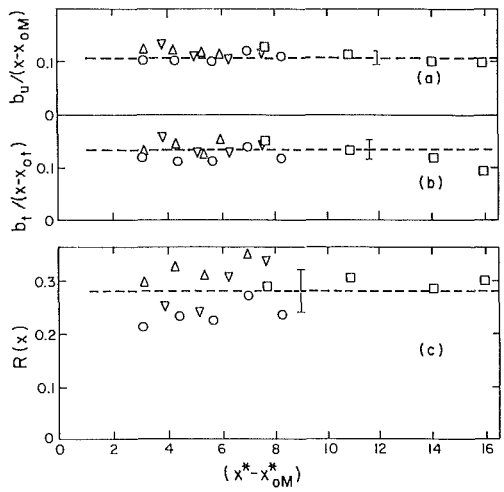


**Fig. 4 Variations of the spreading rates and Richardson number Symbols as in Fig. 1. Uncertainties: $x^*$: ±0.3; rest shown by vertical bars.**

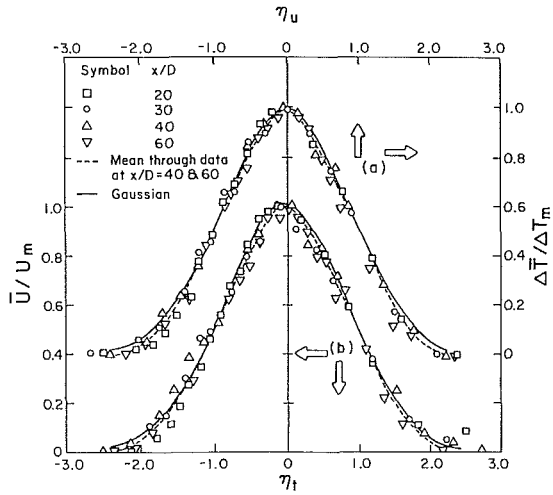


**Fig. 5 Velocity and temperature distributions across the plume. Uncertainties: $\eta$: ±0.06, $U$: ±0.015; $\Delta T$: ±0.015.**

decays as the inverse square root of the distance from the origin [16]. The temperature-decay results for the different plumes are shown in Fig. 3(*b*), after shifting the origin (by an amount $x_{ot}$) as necessary in each case. This figure demonstrates that the axial temperature decays nearly as $(x^*-x_{ot}^*)^{-1}$ as indicated by equation (15). The large departure from this trend in the case of the MSC4-data is caused by contamination and possibly three dimensional effects already referred to. The temperature decay in all the flows can be approximated by the law

$$\Delta T_m^* = \left(\frac{\beta^{2/3}}{\alpha g \Delta T_m}\right)\left(\frac{\beta_j^{2/3}}{M_j}\right) = \sigma_t (x^* - x_{ot}^*) \tag{24}$$

with $\sigma_t = 0.39$. The values for $\sigma_t$ reported by KL, and Rouse, Yih, and Humphreys are 0.42 and 0.385, respectively, and considering experimental uncertanties, these are not too different from the present value. It may be noted that for small temperature differences, $\sigma_t$ can also be taken to be the slope corresponding to the decay of the centerline specific-weight defect, $-\Delta\gamma_m$.

*Velocity and Temperature Half Widths.* If the asymptotic plume is selfpreserving, it is reasonable to define, in the usual way, half widths $b_u$ and $b_t$ of the velocity and temperature distributions across the plume, as two characteristic length scales. They can be obtained directly from the measured velocity and temperature distributions. These data were found to exhibit very nealy linear growth rates for both $b_u$ and $b_t$ as indicated by equation (11). The results for the ratios, $b_u/(x-x_{oM})$ and $b_t/(x-x_{ot})$ are shown for all the plumes in Figs. 4(*a*) and 4(*b*). It may be noted that $x_{oM}$ and $x_{ot}$ are the same virtual origins as have already been introduced. The data show considerable scatter especially in the case of $b_t$, but the following average values are obtained for the growth rates

$$K_{1u} = \frac{db_u}{dx} \approx \frac{b_u}{(x-x_{oM})}$$
$$= 0.11 \text{ (with a standard deviation of 0.01)} \tag{25}$$

$$K_{1t} = \frac{db_t}{dx} \approx \frac{b_t}{(x-x_{ot})}$$
$$= 0.133 \text{ (with a standard deviation of 0.014)} \tag{26}$$

The unduly large departure, from the general trend, of the MSC4 data for $K_{1t}$ is due to reasons already mentioned. The present values of $K_{1u}$ and $K_{1t}$ in reasonable agreement with the values ($K_{1u} = 0.097$ and $K_{1t} = 0.130$) reported by KL. The corresponding values of Rouse, Yih, and Humphreys [9] are $K_{1u} = 0.147$, $K_{1t} = 0.130$, but the uncertainty in their velocity measurement can be expected to be large.

*Richardson Number.* A significant parameter in the study of buoyant jets and plumes is the Richardson number. Figure 4(*c*) show the variation of the Richardson number $R(x)$ obtained from equation (5) using the actual values of $Q$, $M$, and $b$ computed from the measured distribution of $U$, $u'$, $\Delta T$, and $\overline{ut}$ in the various flows. There is considerable scatter in the data, because of the uncertainties in the estimation of $Q^3$, $M^3$, and $\beta$. Nevertheless, the data for $(x^*-x_{oM}^*)$ are seen to tend toward an average value of 0.28 with a standard deviation of 0.04, as indicated by the vertical bar in the figure. Based on this and the other results presented so far, it is reasonable to state that all the flows studied have attained near-asymptotic state of turbulent plume, within the limits of experimental uncertainties.

*Mean Velocity and Temperature Distributions.* Profiles of the longitudinal mean velocity $\bar{U}$ and the temperature excess $\Delta\bar{T}$ are shown in Fig. 5 typically for the flow MSC3. In Fig. 5(*a*) the distributions are plotted after centering them with respect to the axis of the flow in order to correct for any small asymmetry in the flow. Also, corrections for the zero shift (in

Table 3 Turbulent properties of the asymptotic plume

| Description | $\frac{u'_{cl}}{U_m}$ | $\frac{v'_{cl}}{U_m}$ | $\frac{t'_{cl}}{\Delta T_m}$ | $\frac{\lvert\overline{uv}\rvert_{max}}{U_m^2}$ | $\frac{\lvert\overline{vt}\rvert_{max}}{U_m \Delta T_m}$ | $\frac{\overline{ut}_{max}}{U_m \Delta T_m}$ | Pr |
|---|---|---|---|---|---|---|---|
| Plane plume present experiments) | 0.275 (0.015) | 0.23 (0.02) | 0.42 (0.02) | 0.031 (0.003) | 0.045 (0.005) | 0.064 (0.006) | 0.46–0.70 |
| Plane plume (Kotsovinos, [21]) | 0.38 | | 0.4 | | | 0.26 | |
| Plane nonbuoyant jet at $x/D=40$ (Ramaprian and Chandrasekhara, [16]) | 0.20 | 0.18 | 0.18 | 0.20 | 0.018 | 0.025 | 0.75 |
| Predictions of plane plumes (Malin and Spalding, [6]) | | | 0.44<br>0.46 | 0.035<br>0.031 | 0.048<br>0.055 | 0.078<br>0.078 | Variable<br>0.5 |
| Axisymmetric plume (Beuther, Capp, and George, [13]) | 0.27 | 0.22 | 0.4 | 0.024 | 0.032 | 0.039–0.07 | 0.95 |

Note: cl denotes centerline values. The numbers in parentheses represent standard deviations.

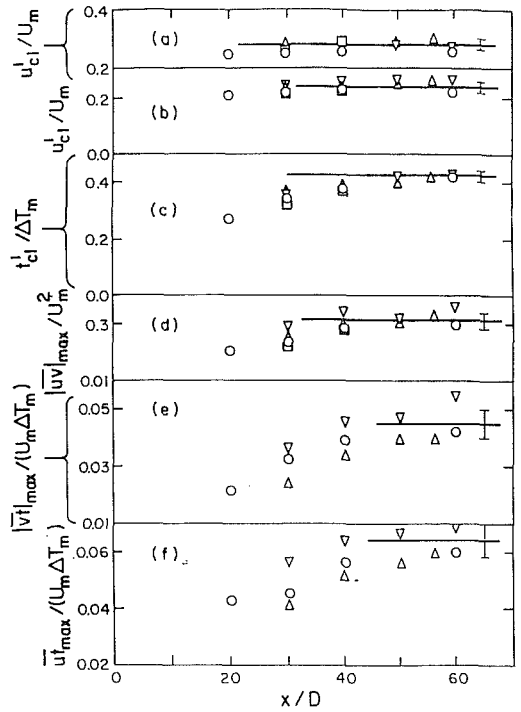


Fig. 6 Evolution of the turbulence properties along the centerline. Symbols as in Fig. 1. The horizontal line in each case is the expected asymptotic behavior. Uncertainties: shown by vertical bars.

the instrumentation) and ambient contamination have been applied (for details see [19]). The profiles show some scatter but this is acceptable considering the difficulty in making these measurements. All the profiles exhibit near-selfsimilarity for $x/D>20$. Also shown in these figures are the universal Gaussian curves

$$\frac{\bar{U}}{U_m}=\exp(-0.69\eta_u^2);\quad \frac{\Delta\bar{T}}{\Delta T_m}=\exp(-0.69\eta_t^2) \tag{27}$$

While the velocity and temperature distributions are not drastically different from Gaussian, it is possible to detect a small but consistent difference, especially in the case of the temperature distribution. Of course, there is no reason to expect that the velocity or the temperature distribution should be exactly Gaussian.

The lateral mean velocities ($\bar{V}$) were also obtained from the LDA output. These velocities were, however, very small, being of the order of 0.5-1 cm/s. The uncertainty in their determination was therefore rather large and hence are not presented here.

## Turbulence Properties

*Centerline and Maximum Values.* The data presented so far have shown that all the flows studied have reached an asymptotic plume state in respect of the mean flow properties at $x/D\geq 30$. The axial evolution of the turbulence properties of the flow can be seen from Fig. 6. The evolution of these properties is shown in terms of the physical distance $x/D$ instead of the normalized coordinate $x^*$ used earlier. This is because the interest here is primarily in the (constant) asymptotic values of these properties. Furthermore, the evolution depends on the details of the turbulence structure in the boundary layers at the nozzle exit and not just on the momentum or buoyancy flux at the exit. It is seen that the centerline turbulence intensities ($u'_{cl}/U_m$) and ($v'_{cl}/U_{max}$) and the maximum Reynolds shear stress $\lvert\overline{uv}\rvert_{max}/U_m^2$ reach their respective asymptotic values (within experimental scatter) by $x/D=40$ in all the flows studied. The thermal properties such as $t'_{cl}/\Delta T_m$, $\lvert\overline{vt}\rvert_{max}/(U_m\Delta T_m)$ and $\overline{ut}_{max}/(U_m\Delta T_m)$ take longer to develop. In fact, the last two properties seem to have barely reached their terminal values at $x/D=60$. The experimental scatter is also larger in this case. It is possible that these properties are still evolving at this station. However, judging from the data trend, it seems reasonble to assume that most of the evolution has already taken place and that they tend towards the asymptotic values indicated by the horizontal lines in each figure within the uncertainty indicated by the vertical bars. Table 3 summarizes these average symptotic values along with the standard deviations. In the case of $u'$, $v'$, $\overline{uv}$ and $t'$, these averages are based on the results for $40\leq x/D\leq 60$. In the case of $vt$ and $ut$, these are based on the results for $50\leq x/D\leq 60$. The data from the last two stations of MSC4 have been excluded for reasons already mentioned. Table 3 also includes the available data from KL for plane plumes, data for round plumes from Beuther, Capp, and George [13] and, for comparison, the values for a nonbuoyant jet (at $x/D=40$) from Ramaprian and Chandrasekhara [16]. Lastly, the results of recent numerical calculations by Malin and Spalding [8] using a complex turbulence model (the so-called $k-\omega$ model) are also presented in the table. It can be seen that buoyancy substantially increases the turbulent intensities and turbulent transport. For example, there is a 50 percent increase in the Reynolds shear stress and about 150 percent increase in the turbulent heat fluxes in the plume relative to

the nonbuoyant jet. The table also shows that the centerline turbulent intensities $u'_{cl}$, $v'_{cl}$ and $t'_{cl}$ are approximately the same in plane and axisymmetric plumes. The maximum fluxes $|\overline{uv}|_{max}$, $|\overline{vt}|_{max}$ and $|\overline{ut}|_{max}$ are, however, about 30–35 percent higher in the plane plume. One of the two sets of results from Malin and Spalding shown in the table corresponds to a constant Prandtl number of 0.5. The other set corresponds to a variable Prandtl number. In this case, the Prandtl number was assumed to depend on a local buoyancy parameter via an empirical algebraic function. It is seen that both the numerical solutions predict the correct trends though they appear to over-predict the fluxes by 15–25 percent. The data of [14] agree with the present measurements in respect of $t'_{cl}$ but differ significantly with regard to $u'_{cl}$ and $ut_{max}$. In particular, their value of 0.26 for $ut_{max}$ is several times larger than the typical values measured in other plume experiments (plane or axisymmetric) or predicted by numerical calculations.

*Distributions of the Turbulent Properties Across the Plume.* For the sake of brevity, only the distributions of the transport terms $\overline{uv}$, $\overline{ut}$ and $\overline{vt}$ across the plume are shown. Also, results are shown only for the plume MSC3, as a typical example. Similar results were obtained in other cases. The full lines are the mean (drawn by eye judgement) through the last two measurement stations. Also presented for comparison are similar results for an isothermal and a heated but nonbuoyant jet from [16]. More detailed results can be found in [18].

**Reynolds shear stress:** The Reynolds shear stress distributions are shown in Fig. 7(*a*). The data show acceptable symmetry and no significant scatter. Also the results for the isothermal jet agree well with those for the heated jet, thereby confirming that there are no significant effects of the refractive index fluctuations on the measurements. The measurement technique used can therefore be considered satisfactory. The peak value $|\overline{uv}|_{max}/U_m^2$ of the shear stress for the isothermal jet, as measured by the LDA is seen to be about 0.020. This is lower (by about 15–20 percent) than the value generally obtained by other investigators using hot-wire anemometry. It is, however, reasonable to compare the results obtained for the isothermal and buoyant flows from the same procedure. It is seen from Fig. 7(*a*) that the data show selfsimilarity especially beyond $x/D=40$. The shear stress values are generally much higher than those measured in the isothermal/nonbuoyant jet. As already mentioned, the measured dimensionless asymptotic peak shear stress of about 0.03 in the buoyant jet is about 50 percent higher than the corresponding value measured in the isothermal/nonbuoyant jet. The accuracy of the shear stress measurements can be assessed by examining consistency with the momentum equation. Assuming selfsimilar distributions and asymptotic growth and decay laws for $b_u$, $U_m$, and $\Delta T_m$, the momentum equation can be integrated to obtain the distribution of $\overline{uv}$ across the plume (for details see [19]). This calculated distribution is shown by the dashed line in Fig. 7(*a*). It is seen that the shear stress distribution obtained from direct measurements is in agreement with the distribution obtained indirectly from the momentum equation within the limits of experimental uncertainty of about 10 percent. This agreement can be taken as a measure of consistency between the turbulence measurements and the mean flow measurements.

**Transverse turbulent heat flux:** Figure 7(*b*) shows the distributions of $\overline{vt}$, which is proportional to the transverse turbulent heat flux $\rho c_p \overline{vt}$, for the plume MSC3. While these distributions evolve more slowly than the shear stress distributions, the data for the last 2 stations exhibit a strong trend toward self-similarity. The data for the other plumes gave similar results. The figure also shows the distribution of $\overline{vt}$ in the nonbuoyant jet at $x/D=40$. It is very clear that the turbulent heat flux $\overline{vt}$ is spectacularly affected by buoyancy. Again, as in the case of the shear stress, it is possible to assess the accuracy of the turbulence heat flux measurements in the plume by comparing the measured $\overline{vt}$ distribution obtained from direct measurements with that obtained indirectly from the thermal energy equation for the plume. Integration of this equation under similar assumptions as before and using measured velocity and temperature values yields the dashed line in Fig. 7(*b*). On comparison, it is seen that the level of agreement between the direct measurement and that calculated from the thermal energy equation is poorer than in the case of shear stress. For example, the measured peak value $|\overline{vt}|_{max}/(U_m\Delta T_m)$ is on the average about 20 percent lower than the calculated value of 0.051. Part of this discrepancy is perhaps due to the fact that the flow MSC3 is possibly still evolving as is suggested by Fig. 6. It can also be seen from Fig. 6 that the flow MSC3X does indeed exhibit peak values of $|\overline{vt}|$, more nearly in agreement with the calculated value. The recommended asymptotic value of 0.045 is, however, still lower than the calculated value by about 10 percent. Some of the discrepancy may also arise from the physical separation between the points of velocity and temperature measurements.

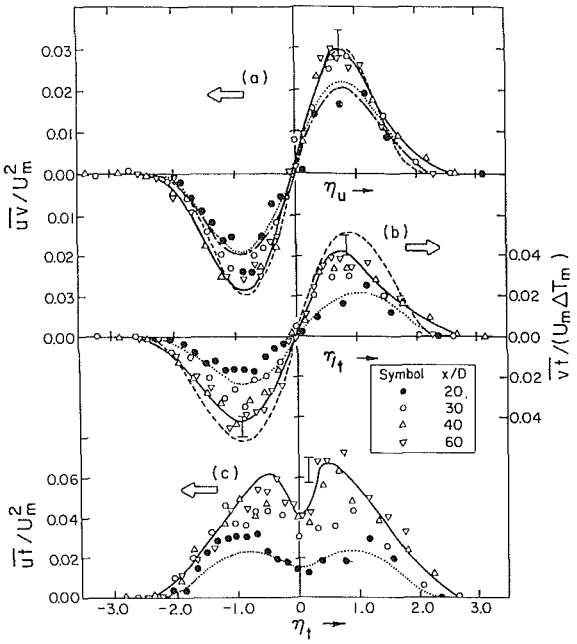


**Fig. 7 Distributions of the turbuelnt transport terms across the plume MSC3. The full lines are the mean through the downstream data. The chain link and dotted lines are respectively for an isothermal and a heated but nonbuoyant jet, from [16]. The dashed lines are obtained from the momentum equation in (*a*) and the energy equation in (*b*). Uncertainties: shown by vertical bars.**

**Longitudinal heat flux:** The distributions of $\overline{ut}$ (proportional to the longitudinal heat flux and for constant $\alpha$, also proportional to the longitudinal turbulent buoyant flux) for the plume MSC3 are shown in Fig. 7(*c*). The profiles are again seen to evolve toward a self-similar state. The results for the heated nonbuoyant jet at $x/D=40$ are also shown in this figure for comparison. Again, $\overline{ut}/(U_m\Delta T_m)$ shows a drastic increase in the plume in comparison with the results for the nonbuoyant jet. The area under the $\overline{ut}$- curve for MSC3 in Fig. 7(*c*) is defined as the kinematic turbulent heat flux integral (proportional to the turbulent buoyancy flux intregral). Its magnitude is about 0.18, indicating that the total turbulent heat flux across the horizontal plane is a significant fraction of the total mean heat flux. Similar results were obtained with the other plumes also. The corresponding value for the nonbuoyant jet at $x/D=40$ is about 0.03 to 0.04. Measurements in a round plume [11, 13] also gave results similar to the present

measurements. While the effect of buoyancy on $\int \bar{u}\bar{t}dy$ is thus very significant, it is not, however, as large as was measured by KL (abut 0.5 as against the present value of 0.18 for the integral).

Autocorrelation measurements of $u$ (or $v$) and $t$ signals showed that the integral length scale was several times larger than the separation between the points of velocity and temperature measurement. It was estimated from these measurements that the maximum reduction in the measured values of $\bar{v}\bar{t}$ (and $\bar{u}\bar{t}$), due to this separation is about 10 percent. Hence, the difference between the present heat-flux results and those of KL is likely to be due primarily to the disagreement between the velocity measurements in the two cases. The temperature measurements as well as the two-dimensionality of the flows appear to be satisfactory in both the investigations.

### *Detailed Structure of Turbulence*

**Turbulent kinetic energy balance:** The turbulent kinetic energy equation for the plane buoyant jet at any axial location $x$ can be written in the following nondimensional form using the half-width of the velocity profile and the centerline velocity as the normalizing length and velocity scales respectively [19].

$$\left[\frac{b_u}{U_m^3}\bar{U}\frac{\partial \overline{q^2}/2}{\partial x}+\frac{b_u}{U_m^3}\bar{V}\frac{\partial \overline{q^2}/2}{\partial y}\right]+\left[\frac{\overline{uv}}{U_m^2}\frac{\partial(U/U_m)}{\partial(y/b_u)}\right]-\left[\frac{\alpha g \bar{t} b_u}{U_m^3}\right]+\left[\frac{1}{U_m^3}\frac{\partial(\overline{vq^2})}{\partial(y/b_u)}-\overline{vq^2}/2\right]+\left[\frac{1}{U_m^3}\frac{\partial(\overline{pv/\rho})}{\partial(y/b_u)}\right]+\left[\frac{\epsilon b_u}{U_m^3}\right]=0 \tag{28}$$

This equation is the same as the usual kinetic energy equation for an isothermal jet except for the additional production term due to buoyancy (fourth term). Since $\overline{w^2}$ was not measured in the experiments, $\overline{q^2}$ was obtained from the usual assumption (see [20]),

$$\overline{q^2}=(\overline{u^2}+\overline{v^2}+\overline{w^2})=\frac{3}{2}(\overline{u^2}+\overline{v^2}) \tag{29}$$

Similarly, $\overline{q^2 v}$ was assumed to be given by

$$\overline{q^2 v}=(\overline{u^2 v}+\overline{v^3}+\overline{w^2 v})=\frac{3}{2}(\overline{u^2 v}+\overline{v^3}) \tag{30}$$

These approximations are acceptable for the purpose of comparing the essential features of jets and plumes. Some of the energy balance terms, in equation (28), were measured in the plume MSC3. These are presented and compared in Figs. 8(*a*) and 8(*b*), with the corresponding results for an isothermal jet from [16]. As is the usual convention, positive quantities in the figure denote a "loss" (or flux out of the control volume) and negative quantities denote a "gain" or flux into the control volume. It is seen that there is no significant effect of buoyancy on the diffusion term (fifth term). On the other hand, it is clear that the rate of turbulent energy production by shear (third term) is increased significantly by buoyancy. This is a direct consequence of the increase in the Reynolds shear stress in the plume, since the nondimensional velocity gradient $[\partial(\bar{U}/U_m)/\partial(y/b_u)]$ is very nearly the same in the isothermal jet and plume. In addition to this, there is also a direct production of turbulent energy by buoyancy. The total buoyant production across the plume can be estimated from Fig. 8(*b*) to be about 30 percent of the energy produced by shear. Previous studies by Kotsovinos [14] as well as the spectral and intermittency results obtained in the present study (but not presented in this paper) seem to show that the buoyant contribution occurs through the generation of large-scale eddies by gravitational disturbances. These are created by the destabilizing effect of the fluctuating buoyancy. The model suggested for this process in [21] appears to be reasonable. Buoyancy thus increases turbulent energy in two ways, directly by generating large-scale disturbances and indirectly by raising the turbulence level (and thereby the Reynolds shear stress) which in turn extracts more turbulent energy from the mean flow. The most striking difference between the jet and plume is with regard to the contribution to the turbulent energy balance by advection (first two terms in equation (28)). The advection is zero at the plume centerline and is very small in the vicinity of the centerline as opposed to large and negative values at and around the centerline of the isothermal jet. The zero advection at the plume centerline is a result of the constancy of $U_m$ and hence of the turbulent energy $(\overline{q^2}/2)$ which scales with $U_m^2$ in the $x$-direction. In a jet on the other hand, the turbulent energy at the centerline decays as $x^{-1}$. In fact, a study of the continuity requirement would show that the streamlines in the plume are convergent everywhere except at the centerline where they are parallel. In the jet, the streamlines are convergent in the outer regions and divergent in the central part. The difference between the advection curves in the jet and plume is predominantly due to this difference in their streamline patterns.

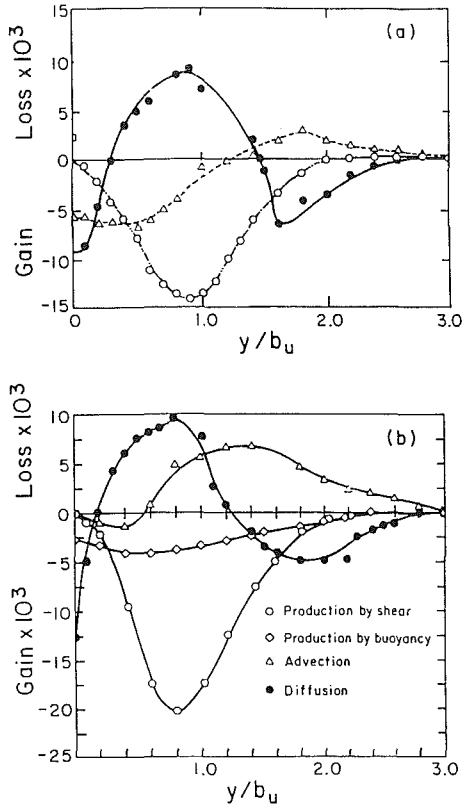


**Fig. 8 Comparison of the energy balance terms form equation (26) for the plume MSC3 with the isothermal jet of [16]. (*a*) isothermal jet; (*b*) plume. Uncertainties: $y/b_u$: ± 0.06; Production: ± 15 percent; Advection: ± 15 percent; diffusion: ± 20 percent; [best estimates].**

## Conclusions

1. The study confirms many of the results from earlier studies on the asymptotic two-dimensional plume. For example, the study has confirmed that all plane buoyant jets reach a universal asymptotic state in respect of both the mean and tur-

bulent flow properties. However, the present mean-flow measurements, while indicating the constancy of $U_m$ and Richardson number R in the asymptotic plume, yield larger values for $U_m$ (and hence, for R) than measured by Kotsovinos and List [15]. Future experiments will hopefully resolve this difference.

2. Buoyancy causes a significant increase in the turbulent intensities and turbulent fluxes and transport coefficients. The order of increase observed in the present experiments is similar to that observed by Beuther, Capp, and George in round plumes [13], but significantly smaller than that observed in [15].

3. The turbulent kinetic energy balance shows increased production by Reynolds shear stress and also significant buoyant production near the central region of the plume. Production from these two sources is responsible for the sustenance and enhancement of turbulence in the plume.

## Acknowledgment

The study reported in this paper was supported by the U.S. National Science Foundation under Grant Nos. ENG77-22756 and CME 80-06797. This support is gratefully acknowledged.

## References

1 Priestly, C. H. B., and Ball, F. K., "Continuous Convection from Isolated Source of Heat," *Quart. J. Roy. Met. Soc.*, Vol. 81, 1955, pp. 144–157.

2 Morton, B., Taylor, G. I., and Turner, J. S., "Turbulent Gravitational Convection From Maintained and Instantaneous Sources," *Proc. Roy. Soc.*, Vol. A234, 1956, pp. 1–23.

3 Fan, L. N., and Brooks, N. H., "Numerical Solutions of Turbulent Buoyant Jet Problems," W. M. Keck Laboratory of Hydraulics and Water Resources Report No. KH-R-18, California Institute of Technology, Pasadena, 1969.

4 Brooks, N. H., and Koh, R. C. Y., "Discharge of Sewage Effluent From a Line Source Into a Stratified Ocean," Eleventh Congress of Int. Assoc. for Hydraulic Research, Paper No. 2.19, 1965.

5 Madni, I. K., and Pletcher, R. H., "Prediction of Turbulent Forced Plumes Issuing Vertically Into Stratified or Uniform Ambients," ASME *Journal of Heat Transfer*, Vol. 99, No. 1, 1976, pp. 99–104.

6 Chen, C. J., and Rodi, W., "A Mathematical Model For Stratified Turbulent Flows and Its Application to Buoyant Jets," Paper C4, 16th Congress of the Int. Assoc. of Hyd. Research, Sao Paulo, Brazil, 1975.

7 Hossain, M. S., and Rodi, W., "A Mathematical Model for Buoyant Flows and Its Application to Vertical Buoyant Jets," *Turbulent Jets and Plumes*. ed. W. Rodi, Pergamon Press, Oxford, 1982.

8 Malin, M. R., and Spalding, D. B., "The Prediction of Turbulent Jets and Plumes by Use of the k-$\omega$ Model of Turbulence," *Physiochemical Hydrodynamics*, Vol. 5, No. 2, 1984, pp. 153–198.

9 Rouse, H., and Yih, C. S., and Humphreys, H. W., "Gravitational Convection From a Boundary Source," *Tellus*, Vol. 3, 1952, pp. 201–210.

10 Lee, S. L., and Emmons, H. W., "A Study of Natural Convection Above a Line Fire," *J. Fluid Mech.*, Vol. 11, 1961, pp. 353–368.

11 Nakagome, H., and Hirata, M., "The Structure of Ambient Diffusion in an Axisymmetric Thermal Plume," *Proc. Int. Conf. on Heat and Mass Transfer*, Seminar on Turbulent Buoyant Convection, Dubrovnik, Yugoslavia, 1976, pp. 361–372.

12 George, W. K., Alpert, R. L., and Tamanini, F., "Turbulence Measurements in an Axisymmetric Buoyant Plume," *Int. J. Heat and Mass Transfer*, Vol. 20, 1977, pp. 1145–1154.

13 Beuther, P. D., Capp, S. P., and George, W. K., Jr., "Momentum and Temperature Balance Measurements in an Axisymmetric Turbulent Plume," ASME Paper No. 79-HT-42, Joint ASME/AIChE 18th National Heat Transfer Conference, San Diego, California, Aug. 6–8, 1979.

14 Kotsovinos, N. E., "A Study of the Entrainment and Turbulence in a Plane Buoyant Jet," W. M. Keck Laboratory of Hydraulics and Water Resources Report No. KH-R-32, California Institute of Technology, Pasadena, 1975.

15 Kotsovinos, N. E., and List, E. J., "Plane Turbulent Buoyant Jets. Part I. Integral Properties," *J. Fluid Mech.*, Vol. 81, Part 1, 1977, pp. 25–44.

16 Ramaprian, B. R., and Chandrasekhara, M. S., "LDA Measurements in Plane Turbulent Jets," ASME JOURNAL OF FLUIDS ENGINEERING, Vol. 107, 1985, pp. 264–271.

17 List, E. J., "Turbulent Jets and Plumes," *Ann. Rev. Fluid Mech.*, Vol. 14, 1982, pp. 189–212.

18 Ramaprian, B. R., and Chandrasekhara, M. S., "Study of Plane Turbulent Jets and Plumes," IIHR Report No. 257, The Institute of Hydraulic Research, University of Iowa, Iowa City, Iowa, 1983.

19 Chandrasekhara, M. S., "Study of Vertical Plane Turbulent Jets and Plumes," PhD thesis, Mechanical Engineering Department, University of Iowa, Iowa City, Iowa, 1983.

20 Bradshaw, P., "The Turbulence Structure of Equilibrium Boundary Layers," *J. Fluiid Mech.*, Vol. 29, 1967, pp. 625–645.

21 Kotsovinos, N. E., "Plane Turbulent Buoyant Jets. Part 2. Turbulence Structure," *J. Fluid Mech.*, Vol. 81, Part 1, 1977, pp. 45–62.

# Studies on Two-Dimensional Curved Nonbuoyant Jets in Cross Flow

**H. Haniu**
Associate Professor,
Department of Mechanical Engineering,
Kitami Institute of Technology,
Hokkaido, Japan

**B. R. Ramaprian**
Professor,
Department of Mechanical and Materials Engineering,
Washington State University,
Pullman, Wash.
Mem. ASME

*An experimental study of two-dimensional, curved, heated (but essentially nonbuoyant) jets is reported. The experiments were conducted in a hydraulic flume in which a curved jet was produced by injecting a plane jet of slightly heated water vertically upwards in to a small cross flow. The data presented include mean and turbulent flow properties obtained from the measurement of instantaneous velocity and temperature, using two-component Laser Doppler Anemometry (LDA) and microresistance thermometry. The measurements extended over the near-to-intermediate field, namely,* $y/D < 60$, *where* y *is the distance along the flume and* D *is the width of the jet at the exit. The study has demonstrated the stabilizing effects of streamline curvature in the inner (lower) portion and the destabilizing effects of curvature and the coflowing ambient in the outer (upper) portion of the curved jet in cross flow. The quantitative effects on the mean and turbulent properties are presented and discussed in this paper.*

## Introduction

Curved jets in cross flow are encountered in many environmental flow problems. Some examples are cooling tower plumes, smoke stack exhaust, thermal discharges to rivers, vents of liquified natural gas carriers, etc. These flows are generally three-dimensional and buoyancy driven. However, in certain regions of the flow or under certain conditions, three-dimensional and buoyancy effects may not be significant. Traditionally, buoyant jets in cross flow have been predicted (with moderate success), using empirical relations for plume rise, dilution, etc., or by using integral methods in combination with similarity and entrainment assumptions [1, 2]. While these methods are still being studied [3], the present trend is increasingly toward the use of differential methods based on complex models of turbulence [4, 5]. Streamline curvature and buoyancy are two important aspects that require careful consideration in the development of such turbulence models. This is especially so for the correct prediction of the near-to-intermediate field of these flows (say, within 100 characteristic diameters from the source), which is often of practical interest. A third aspect which may also have some significance in turbulence modeling is the presence of a moving stream external to the jet. The study of the first and third aspects is described in this paper. Studies on the effects of buoyancy are reported separately [6].

The effect of streamline curvature on turbulent boundary layers has been studied extensively over the last 20 years. In fact, Bradshaw [7] invoked the concept of an analogy between streamline curvature and buoyancy to derive the so-called "curvature Richardson numbers" that characterize curvature effects in a turbulent shear flow. It is now known from his work and the others following it [8–10] that the effect of streamline curvature is such as to increase the turbulent shear stress in a curved shear layer, when the local curvature Richardson number $R_c$ defined as

$$R_c = \frac{2\bar{U}/r}{(\partial \bar{U}/\partial n + \bar{U}/r)} \tag{1}$$

is negative. The shear stress is decreased if this quantity is positive. In the first case, the curvature is said to be destabilizing and in the second case, it is said to be stabilizing. It is easily seen from Fig. 1(*a*) that in the case of a jet in cross flow, the outer part of the jet is destabilized while the inner part is stabilized. Irwin and Smith [11] demonstrated the importance of extra production terms appearing in the Reynolds stress equation for curved flows. Sawyer [12] in his study of reattaching jets, showed, from a first order analysis, that the difference between the entrainment rates in the outer and inner portions of the jet is proportional to the ratio of shear layer thickness to the radius of curvature. Castro and Bradshaw [13] studied curvature effects on a curved mixing layer and the details downstream, as the flow relaxed back from curvature effects. The Reynolds stresses were found in this case, to decrease in the region of large curvature, then overshoot the self-preserving values before finally relaxing to the original values. The stable shear layer studied by them corresponds roughly to the outer part of a convexly curved boundary layer or the inner portion of a curved jet in cross flow. The differences from the curved jet, however, are in the curvature history imposed and the absence of recirculation (flow reversal) in the inner portion of the shear layer. More important is the fact that the curved mixing layer has no counterpart of the unstable outer part of the curved jet. Pelfrey and Liburdy [14] studied a two-dimensional curved jet, in which streamline curvature was introduced by discharging the jet a small distance

Contributed by the Fluids Engineering Division for publication in the JOURNAL OF FLUIDS ENGINEERING. Manuscript received by the Fluids Engineering Division, June 17, 1987.

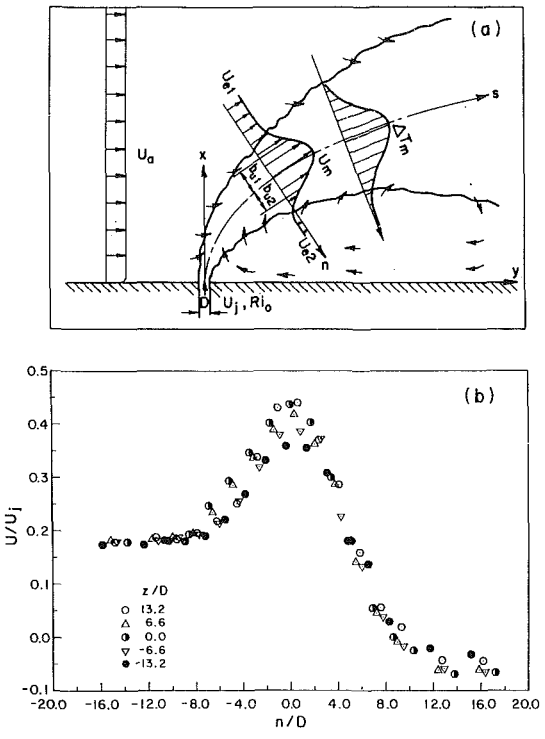


**Fig. 1** *(a)* **Flow configuration studied;** *(b)* **Two dimensionality check. (z is the spanwise coordinate),** $x/D = 40.94$.
**Uncertainties:** $n/D$: $\pm 0.005$; $U/U_j$: $\pm 0.001$.

away from a parallel wall. There was no external flow in their experiment except for the recirculation induced by the jet itself. They have reported some mean and turbulent flow properties in this offset jet, which were measured using a single-component LDA. These limited data indicate the stabilizing effects of curvature on the inner side of the curved jet and the destabilizing effects on the outer side.

In the case of a jet in cross flow, the external flow on the outer side of the curved jet has a finite velocity component along the axis of the jet ($s$-direction). This $s$-component "edge velocity" or "freestream velocity" may be particularly large along the outer edge of the jet. The $s$-component velocity at the inner edge may be negative (in the presence of recirculation) though its magnitude is generally smaller than that at the outer edge. Everitt and Robins [15] studied the effect of external flow parallel to a plane jet. When the centerline velocity is large with respect to the freestream velocity, the flow (often known as a "strong jet") is similar to that of a jet in still air and is approximately self preserving. However, at larger freestream velocities, the jet is not self-preserving except in the other extreme case of the freestream velocity being very nearly equal to the centerline velocity. Such a jet is known as a "weak jet" and behaves very much similar to an asymptotic small-defect wake. In the intermediate state, the flow develops slowly due to the presence of the moving stream, and the spreading rate is not constant and is less than that of a jet in still air. The rms turbulent velocity at the centerline of the jet, normalized with respect to the difference between the local maximum velocity and the external flow velocity, increases as the external flow velocity increases. In a jet in cross flow, additional complexities are introduced by the facts that the edge velocity changes in the $s$-direction thereby introducing nonequilibrium effects and that the edge velocity is negative in the lower part of the jet.

One of the main objectives of the present experimental study was to obtain detailed data necessary for the testing and development of turbulence models and calculation procedures for jets in cross flow. In order to achieve this objective with a minimum of experimental complexity, it was decided to keep the flow configuration as simple as possible. Hence two-dimensional flows with only mild recirculation behind the jet were selected for the study. The jets were nonbuoyant but were characterized by significant streamline curvature and variation of external flow velocity parallel to the jet centerline. By varying the ratio of jet velocity to crossflow velocity, it was possible to vary the relative magnitudes of the curvature and external-flow effects. Resuls from such tests have been used, with some success, to separate the effects of curvature from those of the external flow.

## Experimental Details

**The Apparatus and Instrumentation.** The experiments were conducted in a hydraulic flume, 7.0 m long × 45 cm wide × 75 cm deep, with transparent side walls. The freestream tur-

## Nomenclature

$b$ = half width
$C_E$ = entrainment coefficient (defined by equation (15))
$D$ = jet width at exit
$E$ = entrainment rate $dQ/ds$
$g$ = acceleration due to gravity
$H$ = total kinematic heat flux in the $s$-direction
$h$ = turbulent heat flux in the $s$-direction
$H_u$ = height of the trajectory above the origin
$K$ = $U_j/U_a$
$k$ = curvature of the trajectory
$l_m$ = momentum length scale (defined by equation (4))
$M$ = kinematic momentum flux
$n$ = coordinate normal to the trajectory
$Q$ = kinematic mass flux
$R$ = radius of curvature of the trajectory
$R_b$ = buoyancy Richardson number
$R_c$ = local curvature Richardson number
$\hat{R}_c$ = global curvature Richardson number
$r$ = local radius of curvature of the streamline
$s$ = coordinate along the trajectory of the jet
$T$ = temperature
$\Delta T$ = temperature excess above the ambient
$t$ = turbulent fluctuation in temperature
$U$ = $s$-component velocity
$u$ = $s$-component turbulent velocity
$V$ = $n$-component velocity
$v$ = $n$-component turbulent velocity
$x$ = vertical coordinate
$y$ = horizontal (downwind) coordinate
$z$ = spanwise coordinate
$\rho$ = density
$\Delta\rho$ = $\rho - \rho_a$

**Subscripts**

$a$ = ambient
$e$ = edge of jet
$j$ = jet exit
$m$ = maximum value
$t$ = refers to temperature
$u$ = refers to velocity
1 = upper part of jet
2 = lower part of jet

**Other Symbols**

overbar = time average
prime = rms value

bulence intensity in the flume is typically 1 percent at a velocity of 20 cm/s. The hot-water jet was introduced vertically from a rectangular nozzle 250 mm (span) × 5 mm (width) located near the floor of the flume. A small flow was maintained along the flume to simulate the "cross flow." The flow was confined between two false side walls made of plexiglas and spaced 250 mm apart. These walls, which extended from 800 mm upstream to 600 mm downstream of the jet injection slot served to limit the upstream boundary layer thickness to less than 5 cm and improve the two-dimensionality of the flow. Likewise, the nozzle assembly was located flush with a false bottom extending 300 mm upstream of the injection slot. This arrangement served to limit the bottom wall boundary layer to less than 2 cm. The nozzle assembly and the hot water system are the same as those used for the vertical-jet studies described in [16]. More details of the apparatus can also be found in [17]. Figure 1(*a*) shows the flow configuration studied and the nomenclature used in the paper to describe the flow.

A two-component, frequency-shifted LDA, powered by a 15 mW helium-neon laser was used for the measurement of instantaneous velocity in the flow. The LDA had an effective spatial resolution of about 1.1 mm in the spanwise direction and 0.1 mm in the other two directions. Two Disa Type 55R11 hot-film sensors were used (one in the flow and the other in the ambient) differentially in a "cold-film" anemometer circuit to measure instantaneous temperature differences. The LDA and the temperature probe were both mounted on a three-dimensional traverse that could be located to an accuracy of 0.025 mm. The cold-film sensor in the flow was located within 1 mm downstream of the point of velocity measurement. The error introduced by this spatial separation in to the determination of the correlations $\overline{ut}$ and $\overline{vt}$ is estimated to be less than 10 percent (see [16]). Velocity traverses were made across the curved jet at several spanwise stations. These measurements indicated that the flow was acceptably two-dimensional (to within 5 percent in mean velocities) over the central half of the span. This is seen typically from Fig. 1(*b*) which shows the distribution of the streamwise velocity $\bar{U}$ across the jet at $x/D \approx 40$. All the measurements reported in this paper were made in this central region of two-dimensional flow.

**Experimental Conditions and Procedures.** Three main (M series) flow configurations were studied. The average initial conditions for these flows are given in Table 1.

It is seen that flow 301000M is an isothermal flow. In the other two flows, the magnitude of the exit buoyancy Richardson number $R_{bj}$ (defined by $R_{bj} = [(\Delta\rho_j g D)/(\rho_a U_j^2)]$ is very small. These jets are therefore essentially nonbuoyant, with heat simply playing the role of a passive scalar. In addition, some results are presented from a series of repeated experiments (D series) in which the flow conditions were nominally the same as in the main experiments. The nominal jet exit velocity (based on the measured flow rate and the area of the slot) was 30 cm/s in all the experiments. This corresponds to an exit Reynolds number of about 1500 at which the flow remains fully turbulent over the region of measurement as seen from previous studies [16]. The exact velocity distribution at the exit could not be measured because of the limitations imposed by the instrumentation. However, because of the large (8:1) flow contraction through the nozzle immediately before the exit, the velocity can be expected to have a nearly top-hat distribution at the exit.

**Table 1 Experimental conditions**

| Jet no. | $U_j$ (cm/s) | $U_a$ (cm/s) | $K$ | $\Delta T_j$(°C) | $\lvert R_{bj} \rvert$ | $T_a$ |
|---|---|---|---|---|---|---|
| 301000M | 30.0 | 3.0 | 10.0 | 0.0 | 0.0000 | 24.9 |
| 300905M | 30.0 | 3.3 | 09.0 | 6.7 | 0.0009 | 21.3 |
| 300605M | 30.0 | 5.0 | 06.0 | 5.7 | 0.0009 | 26.4 |

Cross flow velocities were uniform to within ±2 percent in the absence of the jet. At velocity ratios $K$ greater than 10, the jet was found to bend too quickly. Preliminary tests showed that at large inclinations of the jet to the vertical, unstable stratification in the flume caused secondary flows to be generated, destroying the two-dimensionality of the flow. It was found that the inclination of the jet had to be kept within 30 degrees to the vertical in order that the flow could be maintained acceptably two-dimensional (to within 5 percent in mean velocity). This condition was satisfied up to the last measurement station (at $s/D \approx 55$) in all the tests. Also, the last station was about 60 D below the free surface. Previous tests [16] suggest that there are no significant free-surface effects on the flow at this depth.

The cross-sectional planes and locations of measurements at each cross section were selected after ascertaining the approximate boundaries of the curved jet from preliminary dye visualization experiments. In this manner, the measurement locations could be distributed efficiently over the flow. The measurements covered the range $0 < s/D < 60$. An HP 1000 minicomputer and a Preston analog-to-digital converter were used for the acquisition and processing of the experimental data. The flow properties (which included the mean and turbulent quantities) were first obtained in the flume coordinates $(x,y)$. Then, the position of maximum velocity and the direction of the tangent to the jet centerline (which is the locus of the maximum velocity points) were obtained graphically from the mean-flow data. All the results calculated in the $x-y$ coordinates were then transformed into the jet coordinates $(s, n)$. Only selected data from this extensive set of experiments are presented and discussed in this paper. Full details of the experiments and a complete set of tabulated experimental data are reported in [17]. The data are also available on magnetic tape. Based on previous experience with this facility and instrumentation [16, 18], the following are the experimental uncertainty estimates of the flow properties actually measured. $\bar{U}$: ±2.5 mm/s, $\bar{V}$: ±1.5 mm/s, $\Delta\bar{T}$: ±0.2°C, $u'$, $v'$, $t'$: ±5 percent, $uv$, $ut$, $\overline{vt}$: ±10 percent. Uncertainty estimates of the results presented in the various figures were obtained from an error-propagation analysis and are indicated on each figure.

## Results

**Trajectories.** Trajectories of maximum velocity points for several flow conditions are shown in Fig. 2(*a*). Fourth order polynomials were fitted to the trajectory data in $x-y$ coordinates to calculate the distance along the jet $s$, and the curvature $k$ of the trajectory. These results are presented in Fig. 2(*b*). Note that while the curvatures of the three jet trajectories are not very different from one another beyond $s/D = 40$, the trajectory of the jet 300605M has the largest curvature and that of the jet 301000M the least in the region $0 < s/D < 40$.

Except very near the source, and in the absence of significant buoyancy effects, the jet behavior can be expected to depend only on its initial (kinematic) momentum flux $M_j$ (defined by $M_j = U_j^2 D$), and the cross flow velocity $U_a$ [19]. One can then write, for the asymptotic rise of the jet,

$$f(H_u, y, U_a, M_j) = 0 \tag{2}$$

Dimensional analysis yields

$$H_u \propto \frac{M_j^{1/2} y^{1/2}}{U_a} \tag{3}$$

Introducing a momentum length scale $l_m$ defined as

$$l_m = \frac{M_j}{U_a^2} \tag{4}$$

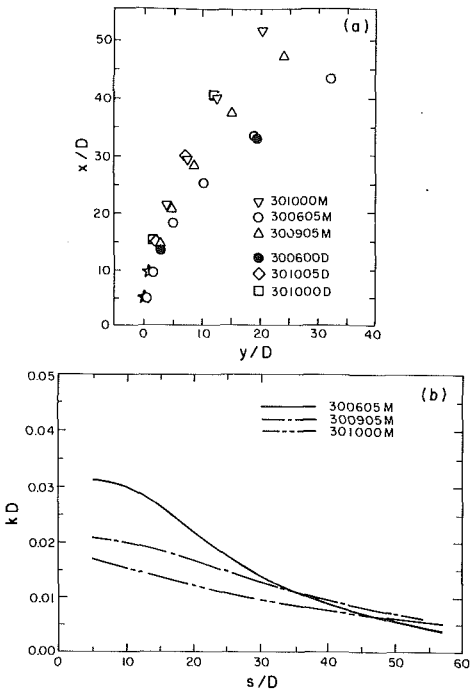


*Fig. 2 Trajectory of the maximum velocity point and its curvature in the different flows studied.*
**Uncertainties: *y/D*: ±0.005; *x/D*: ±0.005; *s/D*: ±0.070; *kD*: ±0.001.**

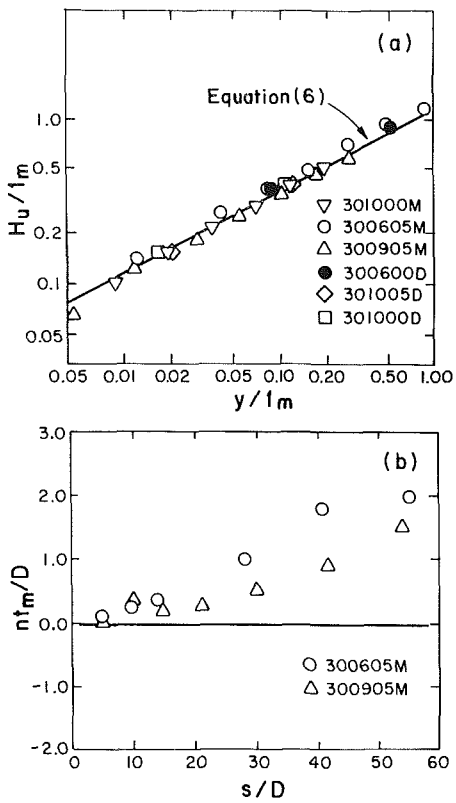


**Fig. 3 (a) Correlation of the jet-rise with momentum length scale; (b) Trajectory of the maximum-temperature point relative to that of the maximum-velocity point.**
**Uncertainties: $y/L_m$: ±5 percent; $H_u/l_m$: ±5 percent; *s/D*: ±0.070; $n_{tm}/D$: ±0.1.**

one gets

$$\frac{H_u}{l_m} \propto \left(\frac{y}{l_m}\right)^{1/2} \tag{5}$$

The experimental results for the trajectory are presented in Fig. 3(*a*) for different nonbuoyant jets. It is seen that all the data with the exception of those very near the exit approximately fall on the curve

$$\frac{H_u}{l_m} = 1.2\left(\frac{y}{l_m}\right)^{0.54} \tag{6}$$

indicating agreement with equation (5).

The location of the temperature maximum in the case of the heated nonbuoyant jet can be obtained from the measured mean temperature distributions. The trajectories of the maximum temperature points for the two heated jets studied are shown in Fig. 3(*b*). It is seen that all the values of $\eta_{tm}$ are positive which means that in all cross-sectional planes, the point of maximum temperature in the jet lies below the point of maximum velocity.

**Spreading Rate.** The half width $b_u$ of a symmetrical jet is defined as the distance from the center of the jet to the location where $\bar{U} = (U_m + U_e)/2$. In the case of the jet issuing into still surroundings ($U_e = 0$), it is known that $b_u \propto s$. In the presence of cross flow, the jet is generally asymmetrical about the *s*-axis. One can define, in this case, half-widths $b_{u1}$ and $b_{u2}$ for the upper and lower parts of the flow, based on $(U_m + U_{e1})/2$ and $(U_m + U_{e2})/2$ points, respectively. Note that not only $U_{e1} \neq U_{e2} \neq 0$, but also $U_{e1}$ and $U_{e2}$, in general, vary along the *s*-direction. As will be shown later, the curvature of the jet trajectory produces stronger mixing in the upper part of the jet and reduced mixing in the lower part. This should result in a larger growth rate of the upper part and a smaller growth rate of the lower part. However, the presence of finite edge velocity (coflowing on the upper part and contraflowing on the lower) counteracts these trends. The spreading-rate data shown in Fig. 4(*a*) for the three nonbuoyant jets reflect the results of these interactions. The figure also shows the straight line of slope 0.11 corresponding to the asymptotic spreading rate of a two-dimensional vertical isothermal jet [16]. It is seen that the jet 300605M with the strongest initial curvature shows the largest spreading rate for the lower part beyond the 5th station. This is due to the presence of the strongest recirculation below this jet. The mildly curved isothermal jet 301000M jet behaves almost like a vertical jet, while the jet 300905M of "intermediate" initial curvature exhibits an intermediate trend. It is also seen from the figure that the overall average spreading rate of the curved jet, based on $b_u = (b_{u1} + b_{u2})/2$, is slightly (but not significantly) larger than that of an isothermal vertical jet and increases with curvature. Pelfrey and Liburdy [14] found the average spreading rate of curved offset jets (in the absence of an imposed external flow) to be nearly the same as that of a straight jet.

The temperature half widths $b_{t1}$ and $b_{t2}$ (defined as the distance from the location of maximum temperature excess to the locations of half the maximum temperature excess in the upper and lower parts of the jet) are presented in Fig. 4(*b*) for the two heated nonbuoyant jets. The broken lines in Fig. 4(*b*) have a slope of 0.154, which is the "average" value for vertical nonbuoyant jets from a number of experiments [16]. From the figure, it is seen that the temperature half widths in the curved nonbuoyant jet are affected approximately in the same way as velocity half widths. The average half width increases faster in the more strongly curved jet. The lower part of the temperature profile spreads faster as recirculation becomes stronger.

**Mass Flux and Entrainment.** The mass flux across any plane normal to the axis of the nonbuoyant jet can be obtained by integrating the velocity profiles across the jet, as

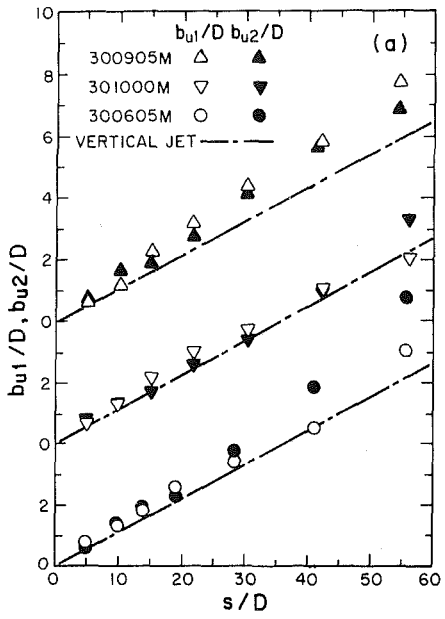


Fig. 4(a)

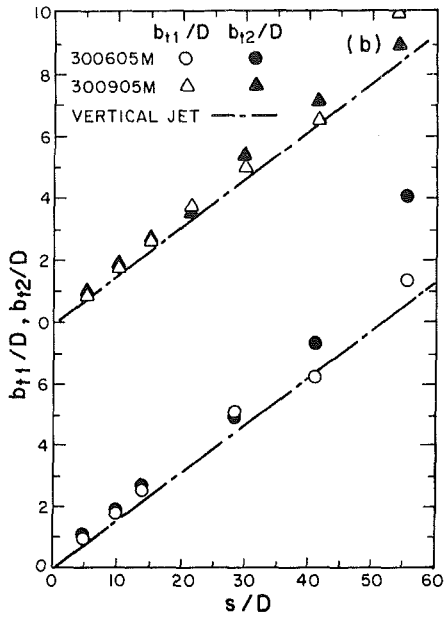


Fig. 4(b)

**Fig. 4 Spreading rates of velocity and temperatures half-widths. Uncertainties: $s/D$: ±0.070; $b_u/D$: ±0.1.**

$$Q = \int_{n_{e1(s)}}^{n_{e2(s)}} \bar{U} dn \tag{7}$$

However, since the $s$-component velocity does not go to zero at the "edges" of the jet, the limits of integration, $n_{e1}$ and $n_{e2}$ have to be carefully defined. In the present case, it was found that beyond $|n| = 3b_u$, the $n$-component velocity (entrainment velocity) was practically constant on both sides of the jet. Hence for the calculation of entrainment, we define $|n_{e1}| = |n_{e2}| = 3b_u$. It was also found from measurements in the range $5 < s/D < 60$ that

$$\left|\frac{n_{e1}}{D}\right| = \left|\frac{n_{e2}}{D}\right| \approx 0.42(s/D) \tag{8}$$

The integral continuity equation for the curved jet can be shown to be

$$\frac{dQ}{ds} = \frac{d}{ds}\int_{n_{e1}}^{n_{e2}} \bar{U} dn = U_{e2}\left(\frac{dn_{e2}}{ds}\right) - U_{e1}\left(\frac{dn_{e1}}{ds}\right) + \left(1 + \frac{n_{e1}}{R}\right) V_{e1} - \left(1 + \frac{n_{e2}}{R}\right) V_{e2} \tag{9}$$

or, using equation (8), one gets

$$\frac{dQ}{ds} = 0.42U_{e1} + 0.42U_{e2} + \left(1 + \frac{n_{e1}}{R}\right) V_{e1} - \left(1 + \frac{n_{e2}}{R}\right) V_{e2} \tag{10}$$

At very large distances from the jet exit, $|n_{e1}/R|$ and $|n_{e2}/R|$ will be small compared with unity and $U_{e1}$ and $U_{e2}$ will become nearly constant. Also, if the cross flow velocity $U_a$ is sufficiently large, $0.42(U_{e1} + U_{e2})$ will be much larger than the last two terms in equation (10). Thus at asymptotically large $s/D$, the mass flux will follow the relation

$$Q \propto s \tag{11}$$

Equation (11) indeed represents the mass flux increase in a "weak jet" i.e., a jet in cross flowing ambient with

$$\frac{(U_m - U_{e1})}{U_m} << 1 \tag{12}$$

At the other extreme, if the cross flow is very small compared with the jet velocity (as for $s/D \to 0$), the jet rises nearly vertically. In this case, the mass flux follows the well known isothermal vertical-jet ("strong" jet) relation [16], namely

$$Q \propto s^{1/2} \tag{13}$$

The curved nonbuoyant jet can be expected to behave somewhat in between these two asymptotic trends. Data on the two curved jets 300905M and 300605M are presented in Fig. 5(*a*). It can be seen from the figure that both the jets tend toward the half-power, strong-jet relation (equation (13)) at small values of $s/D$ and the linear, weak-jet relation (equation (11)) for larger $s/D$. The data for the vertical jet (from [16]) are also shown in Fig. 5(*a*) by the dashed line. The comparison shows a larger entrainment rate in the curved jets. As one can see from equation (9), the increase of entrainment is not only due to the increase in the contribution from the terms containing $V_{e1}$ and $V_{e2}$ but also due to the presence of the first two terms representing the expansion of the jet boundary. The mass fluxes $Q_1$ and $Q_2$ through the outer and inner portions of the jet are presented in Figs. 5(*b*) and 5(*c*). It is seen that the inner portion of the jet behaves somewhat like a strong jet while the outer portion behaves like a weak jet. Similar conclusions were reached from a study of the momentum flux also. Details of this analysis are described in [17].

In vertical jets (in still surroundings), the entrainment rate is simply the algebraic sum of the entrainment velocities at the two edges of the jet, i.e.,

$$E = \frac{dQ}{ds} = V_{e1} - V_{e2} = 2V_{e1} \tag{14}$$

since $V_{e2} = -V_{e1}$. In the case of jets in cross flow, it is given by equation (10). The edge velocities $U_{e1}$, $U_{e2}$, $V_{e1}$, $V_{e2}$ can be different from each other in sign and/or magnitude. This was indeed found to be the case in the two flows studied. It was also found that the jets were significantly asymmetric, with $U_{e1} > U_{e2}$. The entrainment rate is therefore different on the two sides of the jet. The overall entrainment rate $dQ/ds$ can, however, be obtained from the measured rate of change of the kinematic mass flux along the jet shown in Fig. 5(*a*). The

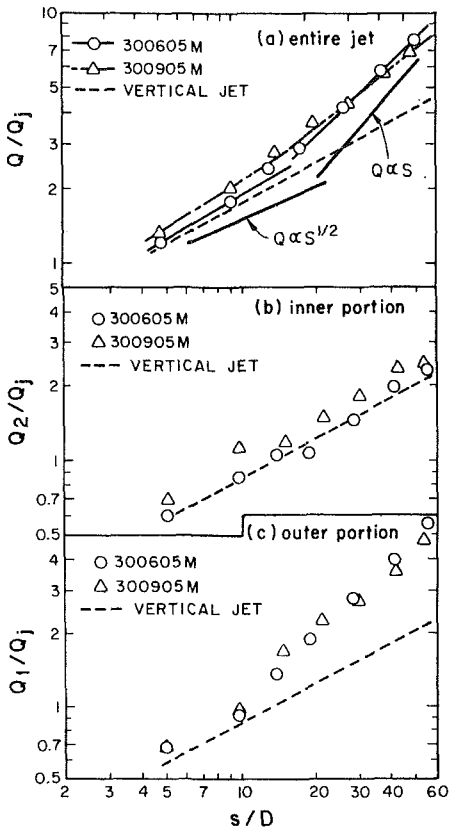


**Fig. 5 Variation of kinematic mass flux along the curved jet. Uncertainties: s/D: ±0.070; $Q/Q_j$: ±3 percent.**

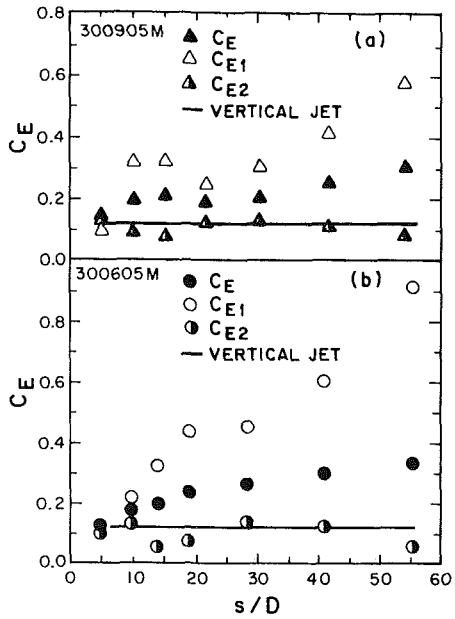


**Fig. 6 Entrainment coefficient in the curved jet. Uncertainties: s/D: ±0.070; $C_E$: ±0.017.**

results are shown in Fig. 6 where the nondimensional entrainment coefficient $C_E$ defined by

$$C_E = \frac{dQ/ds}{U_m} \tag{15}$$

is plotted. It can be seen that there is a significant increase in the entrainment rate compared with that of a vertical jet in still surroundings, for which $C_E \approx 0.12$ (see [16]). The entrainment

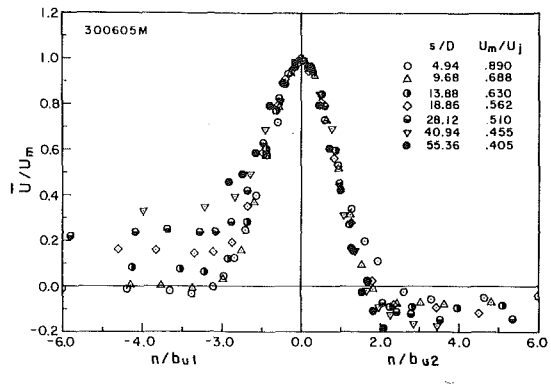


**Fig. 7 s-component mean velocity distributions across the curved jet. Uncertainties: $n/b_u$: ±0.06; $\bar{U}/U_m$: ±0.015.**

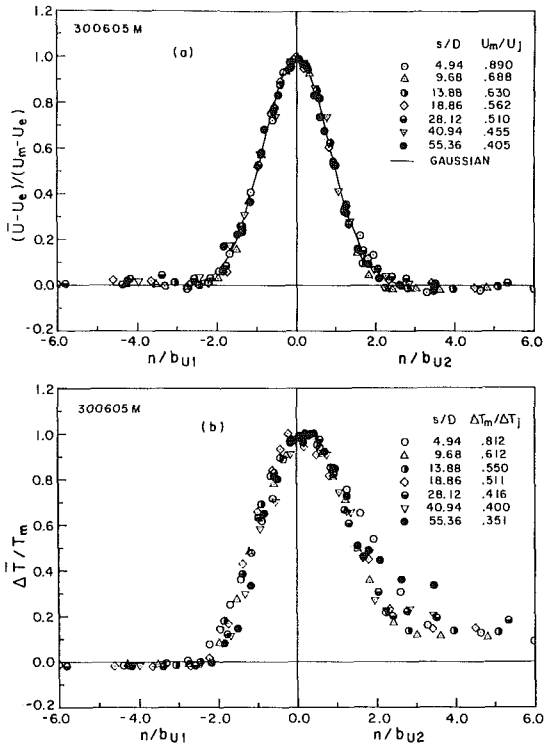


**Fig. 8 s-component excess velocity and temperature distributions. Uncertainties: $n/b_u$: ±0.06; velocity: ±0.015; temperature: ±0.056.**

rates (based on $n_e = \pm 3b_u$) obtained separately for the upper and lower portion of the jet from the respective mass fluxes $Q_1$ and $Q_2$ are also shown in Fig. 6. The respective entrainment coefficients are defined as

$$C_{E1} = 2\frac{dQ_1/ds}{(U_m - U_{e1})} \tag{16}$$

$$C_{E2} = 2\frac{dQ_2/ds}{(U_m - U_{e2})} \tag{17}$$

The effect of cross flow $U_a$ on the entrainment rate is very clearly seen. The entrainment rate in the upper part of the jet is increased due to the presence of positive edge velocity while, in the lower part, the jet behaves more nearly like a vertical jet.

**Mean Velocity and Temperature Distributions.** Typical *s*-component mean velocity profiles are presented in Fig. 7 for the jet with the strongest cross flow, namely 300605M. In this figure, $U_m$ has been used as the velocity scale for normalization. The cross-stream coordinate $n$ is normalized using $b_{u1}$ in

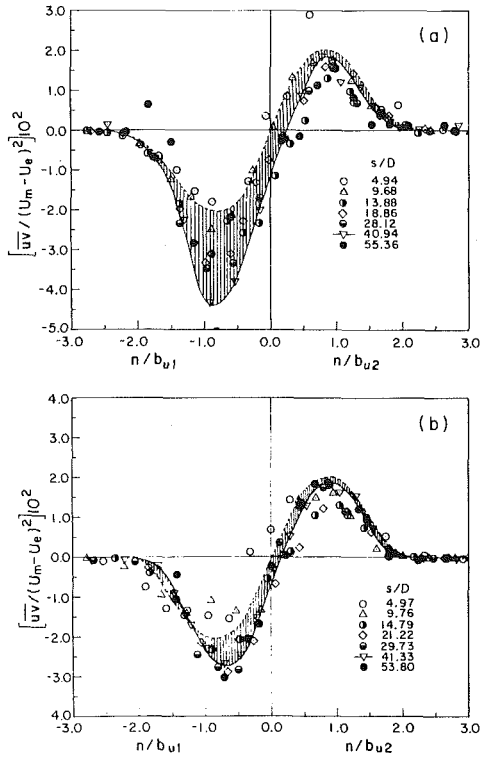


**Fig. 9 Turbulent shear stress distributions in the two curved nonbuoyant jets (a) 300605M (b) 300905M.**
**Uncertainties: $n/b_u$: ±0.06; $\overline{uv}$: $\pm 0.3 \times 10^{-2}$.**

the outer part and $b_{u2}$ in the inner part. It is clearly seen that there is a positive $s$-component edge velocity along the outer edge of the jet and a smaller negative edge velocity due to recirculation at the inner edge. The distributions at different axial locations do not exhibit self-similarity in the coordinates chosen. In fact, a strong evolutionary trend is observed especially near the outer edge. Everitt and Robins [15] observed that jets in a coflowing ambient exhibit self-similarity in the profiles of the excess mean velocity $[\bar{U}-U_e/U_m-U_e]$. The present data were also found to exhibit a similar trend as seen from the typical results for the jet in Fig. 8($a$). In this figure, the data are presented as excess mean velocity $[\bar{U}-U_{e1}/U_m-U_{e1}]$ for the outer part and $[\bar{U}-U_{e2}/U_m-U_{e2}]$ for the inner part. The $n$-coordinate is normalized as before using the appropriate half width on each side. It is seen that the distributions are fairly symmetric, self-similar and very nearly Gaussian (shown by the solid line).

Figure 8($b$) shows typical excess temperature distributions in the same nonbuoyant jet. One can see from this figure that all the temperature profiles are shifted toward the right side of the $n=0$ axis (i.e., toward the lower side of the jet). Also, substantial excess temperature can be observed beyond the inner edge of the jet, which is a result of the recirculation below the jet. The recirculation and reentrainment of the jet fluid, in fact, caused the excess temperature $\Delta T_{e2}$ at the inner edge to remain nearly constant at all $s/D$, rather than scale with the local maximum excess temperature $\Delta T_m$. The velocity and temperature distributions in the other jets with smaller cross flow were qualitatively similar. The evolution of the flow as well as the recirculation and reentrainment phenomena were, however, less pronounced in those cases.

**Turbulence Properties.** Turbulence measurements were made in each of the three jets 301000M, 300905M and 300605M. Of these flows, the first two with nearly the same cross-flow velocity ratios (namely 10 and 9), were found to exhibit almost similar turbulence properties. Hence, only the data on the second and third flows will be presented and discussed here. These two jets had nearly the same streamline curvature in the region $10<x/D<60$. The cross flow velocities in the jet 300905M were, however, much smaller than those in the jet 300605M. The influence of the ratio $U_e/U_m$ and its variation along the jet (nonequilibrium effect) was thus different in these two flows. The severity of streamline curvature can conveniently be characterized by a global *curvature* Richardson number which can be defined, for each side of the jet as follows:

$$\hat{R}_{c1}=2kb_{u1};\quad \hat{R}_{c2}=-2kb_{u2} \tag{18}$$

These definitions follow from equation (1) if one assumes that $|\partial\bar{U}/\partial n|\sim\bar{U}/b_u$ and $b_u<<R$. Both the heated jets exhibited $\hat{R}_c$ values of the order of $\pm 0.1$ over the most part (note that $k$ is negative). This value is very similar to that observed in the curved-jet experiments of [14].

The distributions of turbulent shear stress in the two jets are presented in Fig. 9($a$) and 9($b$). The full line drawn through the data at $x/D=40.34$ shows the trend. The dotted line corresponds to the distribution in a vertical jet and is taken from [16]. Since the dimensionless maximum shear stress for a vertical jet is approximately 0.022, an appreciable enhancement of the shear stress in the outer portion and a slight reduction in this stress in the inner portion can be observed. Since both the curved jets (with $0<U_e<0.4U_m$) can be considered to be "strong jets," the finite velocity of the free stream alone should not cause any significant change in the turbulence structure of these jets. Thus, considering a typical location such as $s/D\approx 40$, one can regard the shaded regions in these figures to represent, in principle, the combined effect of nonequilibrium (*variation* of $U_e/U_m$) and streamline curvature. While it is difficult to isolate precisely their individual effects from these results, it is reasonable to conclude that, since the edge velocities are very small in magnitude on the inner side of these jets, any change from the vertical-jet behavior in this side is due largely to the curvature effects. The same statement can be made (though with a little less certainty) also with respect to the outer portion of the jet 300905M (which has a smaller cross flow), in view of the relatively small edge velocities ($U_{e1}/U_j<0.1$) observed in that case. One can thus speculate that the shaded region in the inner portion represents approximately the *stabilizing* effect of curvature in *both* the jets, whereas the shaded region in the outer portion represents the *destabilizing* curvature effect in the case of the jet 300905M. Similar observations were made from the $u'$ and $v'$ distributions also. Hence, if the present estimates are correct, it seems that while the effect of streamline curvature on turbulence in curved nonbuoyant jets is significant, it is not as large as has been observed in earlier boundary-layer and free-shear-flow studies [8, 9, 10, 13]. This is presumably due to the existence of streamline curvature effects of opposite sign in the two parts of the curved jet—a feature not present in any of the other curvature studies, cited above.

The thermal properties of the curved jet in cross flow are shown typically for the jet 300605M, in Fig. 10. Note that, as already mentioned, heat essentially plays the role of a passive scalar in this flow. Again, the data for $s/D=40.34$ are joined by a full line to show the trend. A larger rms intensity of temperature fluctuations is seen in the outer portion compared to the inner portion (Fig. 10($a$)). Also one can see from the figure that the temperature fluctuations evolve continuously along the jet in both the outer and inner portions of the jets. The distributions are similar to those observed in plane vertical heated jets except for the asymmetry about the jet axis. A comparison of the maximum values of $t'/\Delta T_m$ in the outer and inner parts of this jet with the value of 0.28 obtained in a vertical jet [16] leads to similar conclusions regarding curvature effects, as were reached from the study of the velocity fluctuations.

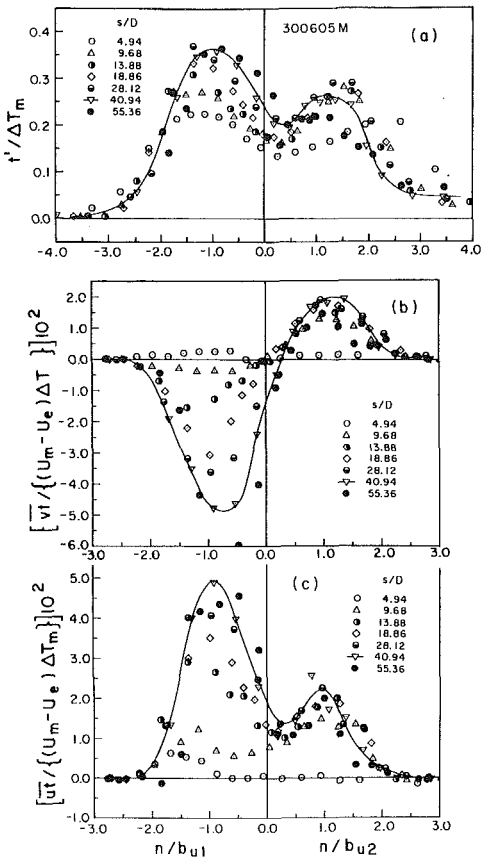


**Fig. 10 Thermal properties in the curved nonbuoyant jet 300605M. Uncertainties: $n/b_u$: ±0.06; $t'$: ±0.02; $\overline{vt}$: $\pm 0.4 \times 10^{-2}$; $\overline{ut}$: $\pm 0.4 \times 10^{-2}$.**

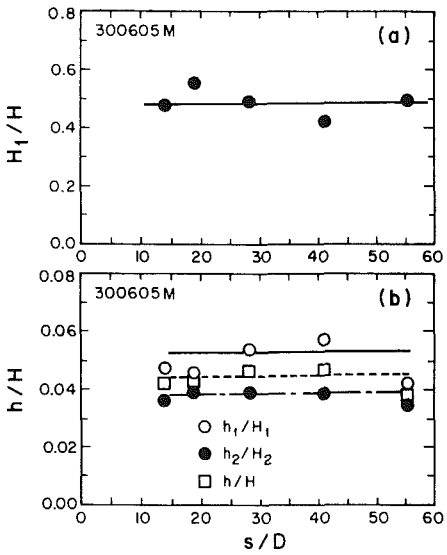


**Fig. 11 *s*-component heat flux in the curved nonbuoyant jet. (*a*) total heat flux (*b*) turbulent heat flux. Uncertainties: $s/D$: ±0.070; $H_1/H$: ±0.028; $h/H$: ±0.005.**

The distributions of $\overline{vt}$ and $\overline{ut}$, respectively proportional to the $n$- and $s$-component of the turbulent heat flux are shown in Figs. 10(*b*), (*c*). It is seen that beyond $s/D = 10$, these quantities are significantly larger in the outer portion than in the inner portion. Also, comparing with the maximum values of $\overline{vt}/U_m\Delta T_m$ and $\overline{ut}/U_m\Delta T_m$ in the inner part of the jet with those reported in [16] for a vertical jet, namely 0.018 and 0.024, respectively, it can once again be concluded that the effect of curvature alone on the curved jet is not spectacularly large. The large effect observed in the outer portion should again be interpreted as being due primarily to the nonequilibrium of the flow. Results consistent with the above conclusions were obtained from the jet 300905M also.

The total (kinematic) $s$-component heat flux $H$ across the jet is composed of the mean heat flux $H$ and the turbulent heat flux $h$, and can be obtained from integrating the measured distributions of $\bar{U}$, $\Delta\bar{T}$ and $\overline{ut}$, respectively, across the jet. The fraction of the total heat flux carried by the outer portion, $H_1/H$ is shown in Fig. 11(*a*). This value is around 0.5 everywhere and indicates no significant difference between the outer and inner portions of the jet. The different heat flux ratios namely, $h_1/H_1$, $h_2/H_2$ and $h/H$ are presented in Fig. 11(*b*). It is seen that a larger fraction of the total heat flux is carried as turbulent heat flux (approximately 5.5 percent of $H_1$) in the outer portion compared with the inner portion (4 percent of $H_1$). The overall value of $h/H$ for the jet lies in between the values for the outer and inner portions. This value is about 4.5 percent which is slightly higher than the value (3–4 percent) reported in [16] for vertical nonbuoyant jets. From the experimental data obtained, it is possible to estimate the eddy transport coefficients for momentum and heat, and hence the turbulent Prandtl number. The turbulent Prandtl number estimated in this manner was found to have a typical value of 0.9 in the outer portion and 0.5 in the inner portion of the curved jet, as compared to a value of about 0.75 in a vertical jet.

## Conclusions

The experimental study reported in this paper has lead to the following conclusions.

1. The rise of the two-dimensional nonbuoyant jet in cross flow is proportional to $y^{0.54}$ in the region $0.1 < y/l_m < 30$ and the trajectory (of the point of velocity maximum) is described by equation (6). The maximum temperature in the jet occurs slightly below the point of maximum velocity. This is due to the recirculation present in the lower part of the jet.
2. The overall width of the curved jet increases at a slightly faster rate than that of a vertical jet.
3. There is a substantial increase in the entrainment rate, turbulent intensities and turbulent transport in the outer part of the nonbuoyant curved jet. This is predominantly due to the presence of a continuously evolving, coflowing edge velocity, and to a lesser extent, due to the destablizing effect of streamline curvature.
4. There is a small reduction in the entrainment rate and turbulent properties in the inner portion of the jet. Since the edge velocities in this part are very small, this reduction is due primarily to the stabilizing effect of streamline curvature.
5. The curvature effects in this flow are substantially smaller than those observed in earlier studies on curved boundary layers and free shear flows characterized by a single sign of curvature Richardson number. This is presumably due to the opposing effect of curvature on the two sides of the curved jet in cross flow.

## Acknowledgment

The study reported in this paper was supported by the U.S. National Science Foundation, Grant No. CME-8006707. This support is gratefully acknowledged.

## References

1 Slawson, P. R., and Csanady, G. T., "On the Mean Path of Buoyant, Bent-Over Chimney Plumes," *J. Fluid Mech.*, Vol. 28, 1967, pp. 311-322.

2 List, E. J., and Imberger, J., "Turbulent Entrainment in Buoyant Jets and Plumes," *J. Hydraulic Division, Proc. ASCE*, Vol. 99, 1973, pp. 1461-1474.

3 Chiang, H. C., and Sill, B. L., "Entrainment Models and Their Application to Jets in A Turbulent Cross Flow," *Atmos. Environment*, Vol. 19, No. 9, 1985, pp. 1425–1438.

4 Launder, B. E., "On the Effects of a Gravitational Field on the Turbulent Transport of Heat and Momentum," *J. Fluid Mech.*, Vol. 67, Part 3, 1975, pp. 569–581.

5 Gibson, M. M., and Rodi, W., "A Reynolds-Stress Closure Model of Turbulence Applied to the Calculation of a Highly Curved Mixing Layer," *J. Fluid Mech.*, Vol. 103, 1981, pp. 161–182.

6 Ramaprian, B. R., and Haniu, H., "Measurements in Two-Dimensional Buoyant Jets in Cross Flow," To appear in ASME JOURNAL OF FLUIDS ENGINEERING, June 1989.

7 Bradshaw, P., "The Analogy Between Streamline Curvature and Buoyancy in Turbulent Shear Flow," *J. Fluid Mech.*, Vol. 36, 1969, pp. 177–191.

8 So, R. M. C., and Mellor, G. L., "Experiment on Convex Curvature Effects in Turbulent Boundary Layers," *J. Fluid Mech.*, Vol. 60, 1973, pp. 43–62.

9 Ramaprian, B. R., and Shivaprasad, B. G., "The Structure of Turbulent Boundary Layers Along Mildly Curved Surfaces," *J. Fluid Mech.*, Vol. 85, 1978, pp. 273–303.

10 Gillis, J. C., and Johnston, J. P., "Turbulent Boundary-Layer Flow and Structure on a Convex Wall and Its Redevelopment on a Flat Wall," *J. Fluid Mech.*, Vol. 135, 1983, pp. 123–153.

11 Irwin, H. P. A. H., and Smith, P. A., "Prediction of the Effect of Streamline Curvature on Turbulence," *Phys. Fluids*, Vol. 18, 1975, pp. 624–630.

12 Sawyer, P. A., "Two-Dimensional Reattaching Jet Flows Including the Effects of Curvature on Entrainment," *J. Fluid Mech.*, Vol. 17, 1963, pp. 481–498.

13 Castro, I. P., and Bradshaw, P., "The Turbulence Structure of a Highly Curved Mixing Layer," *J. Fluid Mech.*, Vol. 73, 1976, pp. 265–304.

14 Pelfrey, J. R. R., and Liburdy, J. A., "Effect of Curvature on the Turbulence of a Two-Dimensional Jet," *Experiments In Fluids*, Vol. 4, 1986, pp. 143–149.

15 Everitt, W. K., and Robins, G. A., "The Development and Structure of Turbulent Plane Jets," *J. Fluid Mech.*, Vol. 88, 1978, pp. 563–583.

16 Ramaprian, B. R., and Chandrasekhara, M. S., "LDA Measurements in Plane Turbulent Jets," JOURNAL OF FLUIDS ENGINEERING, Vol. 107, 1985, pp. 264–271.

17 Ramaprian, B. R., and Haniu, H., "Turbulence Measurements in Plane Jets and Plumes in Cross Flow," IIHR Report No. 266, University of Iowa, Iowa City, 1983.

18 Ramaprian, B. R., and Chandrasekhara, M. S., "Measurements in Vertical Plane Turbulent Plumes," ASME JOURNAL OF FLUIDS ENGINEERING, Vol. 111, published in this issue, pp. 69–77.

19 Wright, S. J., "Buoyant Jets in Density-Stratified Cross Flow," *J. Hydraulic Engrg.*, ASCE, Vol. 110, 1984, pp. 643–656.

**K. Isomoto**
Design Engineer,
Advanced Engineering Department,
Civil Aero-Engine Development Div.,
IHI Co., Ltd.,
Tanashi, Tokyo, 188 Japan

**S. Honami**
Professor,
Mechanical Engineering Dept.,
Science University of Tokyo,
Kagurazaka, Shinjuku,
Tokyo, 162 Japan
Mem. ASME

# The Effect of Inlet Turbulence Intensity on the Reattachment Process Over a Backward-Facing Step

*Behavior of a separated shear layer over a backward-facing step and its reattachment is presented when a two-dimensional cavity or rod is installed upstream of the step in order to change local turbulence intensity in addition to grid turbulence in the free-stream. The reattachment length has a strong negative correlation with maximum turbulence intensity near the wall at the separation point. Turbulence in the entrainment region immediately downstream of the step plays an important role in determining the reattachment length.*

## Introduction

A backward-facing step flow has been an important subject of concern as a model of separated flows. Numerous studies on a backward-facing step flow have been made, e.g., by Bradshaw and Wong [1], Eaton and Johnston [2] and Etheridge and Kemp [3]. The data accumulation has also been required in order to evaluate turbulence modeling in prediction codes. Some recent studies have been focussed on understanding parameters which affect the reattachment process over a backward-facing step from the viewpoint of suppression and control of the separation process, while major emphasis has been placed on observation of such a flow field. The effect of Reynolds number as one of the important parameters was studied by Eaton and Johnston [4], Adams et al. [5], and Durst and Tropea [6]. Inlet condition as a ratio of boundary layer thickness to step height was clarified by Adams et al. [5]. The effect of streamline curvature on the reattachment length was examined in the experiments in curved channels by Honami and Nakajo [7]. An extensive study on the expansion ratio was made by Durst and Tropea [6]. No systematic and comprehensive study of the effect of turbulence has been made, though freestream turbulence was expected to be an effective parameter as pointed out by Eaton and Johnston [2].

The present authors observed in a preliminary experiment that as the turbulence level in the freestream region upstream of the step became higher, the reattachment length became shorter. It was impossible to find out which local turbulence in the transvere direction, i.e., in the freestream or near wall region, at the separation point influences the reattachment length which is a representative parameter of the reattachment process. The objective of the present paper is to provide answers to the aforementioned problem, and to understand extensively the effect of inlet turbulence intensity by systematically varying the local turbulence in the transverse direction by use of a rod or cavity in addition to freestream turbulence.

## Experimental Apparatus and Procedures

Figure 1 shows schematics of the experimental apparatus and test geometry. The precise geometry of the step and a

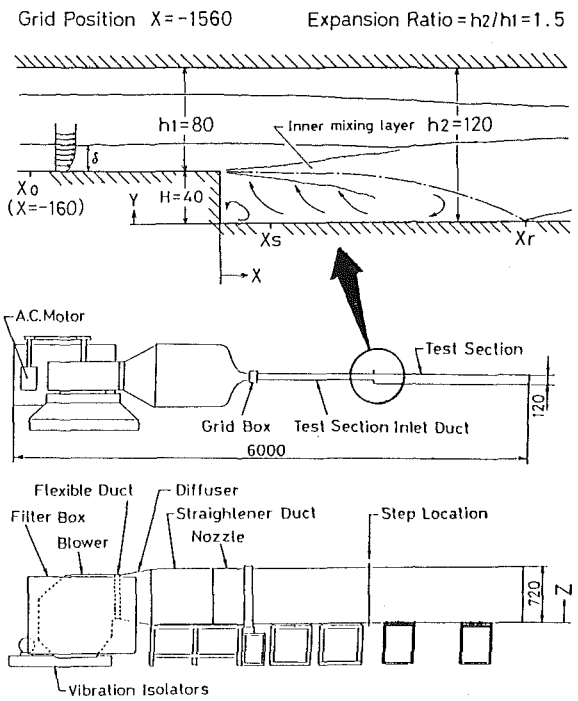


**Fig. 1 Experimental apparatus (dimensions in mm)**

Contributed by the Fluids Engineering Division for publication in the JOURNAL OF FLUIDS ENGINEERING. Manuscript received by the Fluids Engineering Division September 22, 1987.

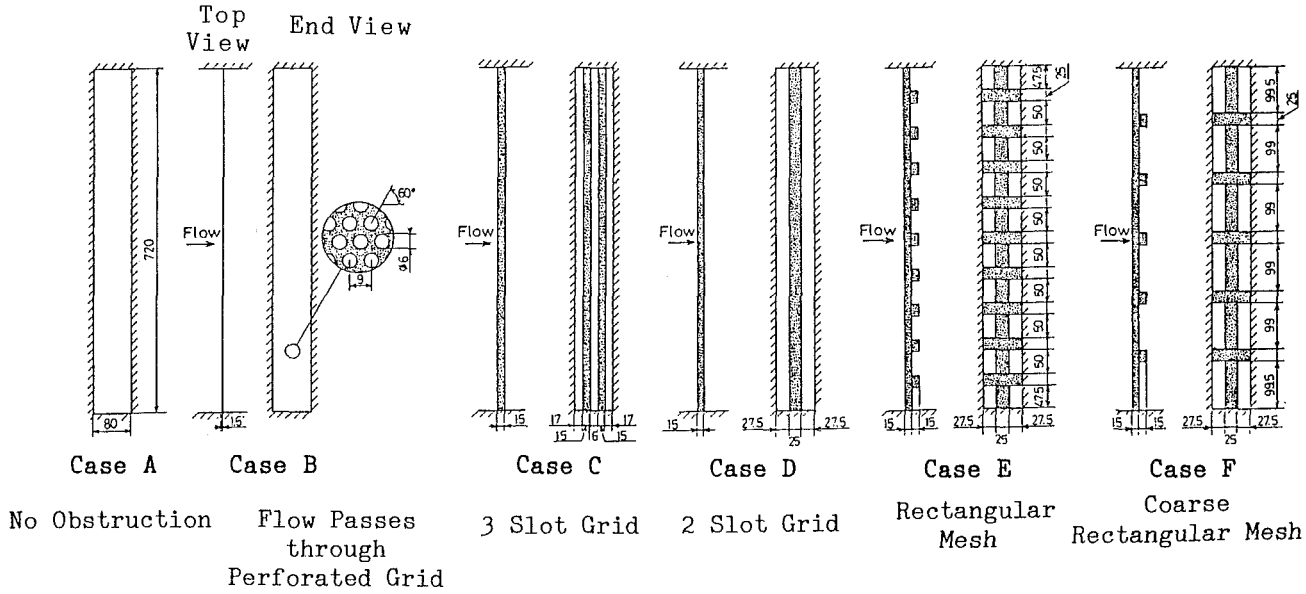


**Fig. 2 Grid configuration (dimensions in mm)**

coordinate system where Z coordinate is taken in the spanwise direction of the step are also illustrated in Fig 1. The air flow tunnel consists of an inlet duct of 1560 mm in length (in some cases 1500 mm) and a test section of 2000 mm in length. The inlet duct of 1500 mm in length is used for the experiments on the effect of free-stream turbulence with and without the grid. In these cases, the terminology such as case A and F, which corresponds to the lowest and highest freestream turbulence, is used. The other of 1560 mm in length is utilized to install the cavity or rod near the step. The reference station is located 160 mm (150 mm in case A to F) upstream of the separation point. Furthermore, the terminology in those cases is changed to add "0" like case A0 or F0 to the aformentioned case such as case A or F. After the inlet section is extended by 60 mm, the change in the reattachment length is within $\pm 0.1\ H$. The same velocity and turbulence intensity profiles were also obtained at the same distance from the step before and after extension of the inlet section. Therefore, experiments in case A and A0 were conducted under the same inlet condition at the step in spite of the extension, i.e., case A was the same as case A0. The aspect ratio of the test section width to the step height is 18. An expansion ratio of the test section height $h2$ to the inlet section height $h1$ is 1.5. A fully developed turbulent boundary layer ($\delta_{99}/H = 0.5$) is obtained at the step. The free-stream velocity at the reference point is 12 m/s. The step height Reynolds number ReH is $3.2 \times 10^4$. Turbulence intensity, $Tu$, is defined as the root mean square of the fluctuating velocity, $u'$, obtained by a single hot-wire probe normalized by the free-stream velocity, $Uo$, at the reference point, i.e., $\sqrt{u'^2}/Uo$.

Figure 2 shows a grid configuration which is located as a grid box at the nozzle exit upstream of the inlet duct. No grid was used in case A and A0.

Figure 3 shows an arrangement of a rod or two-dimensional cavity near the step in order to change local turbulence intensity in the transverse location in addition to grid turbulence. The cavity was installed to increase near-wall turbulence without a substantial change in the velocity profile, adding "−C" in the terminology like case A0-C. The rod was placed 100 mm upstream of the step. Each distance of the rod from the wall, which corresponds to the region at a half distance of the boundary layer thickness, at the boundary layer edge, and in the free-stream, is 11.5 mm, 20 mm, and 40 mm, respectively. The terminology in those cases is distinguished by adding "−R1", "−R2" or "−R3" like case A0-R1. The installation of the rod makes the local turbulence level high, though the velocity profile has defect by a wake due to the rod.

The reattachment length, $Xr$, was determined by forward flow fraction measurements using a wall flow direction probe flush-mounted on the test surface. Mean velocity and turbulence intensity at the separation point and in the separated shear layer were measured by a hot-wire anemometer which was a linearized constant temperature type. The data in the highly turbulent region where local turbulence intensity was

## Nomenclature

$Cf/2$ = skin friction coefficient
$d$ = rod diameter (ex., d5 means 5 mm in diameter)
$Er$ = expansion ratio, $h2/h1 (= 1.5)$
$H$ = step height (= 40 mm)
$H12$ = shape factor
$h1$ = channel height of inlet test section (= 80 mm)
$h2$ = channel height of downstream of step (= 120 mm)
ReH = Reynolds number based on step height
$\mathrm{Re}_\theta$ = Reynolds number based on momentum thickness
$Tu$ = turbulence intensity, $Tu = \sqrt{u'^2}/Uo$
$u'$ = longitudial velocity fluctuation
$u_\tau$ = friction velocity
$U$ = streamwise mean velocity
$X$ = streamwise distance from step base
$Xr$ = reattachment length
$Xs$ = reseparation point
$W$ = channel width (= 720 mm)
$Y$ = transverse distance from wall on step side
$Y+$ = transverse distance in wall law scale, $Yu_\tau/\nu$
$Z$ = spanwise distance from side wall
$\delta$ = boundary layer thickness
$\nu$ = kinematic viscosity
$\theta$ = momentum thickness

### Subscripts

0 = reference point, $X = -160$ mm
$p$ = freestream

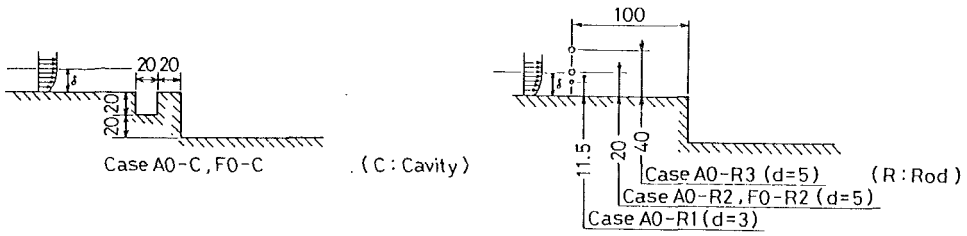


Fig. 3 Cavity or rod arrangement

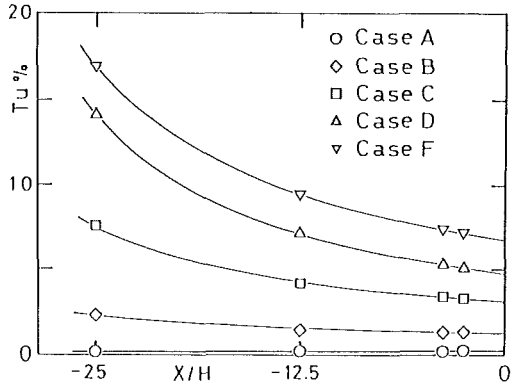


Fig. 4 Decay process of freestream turbulence

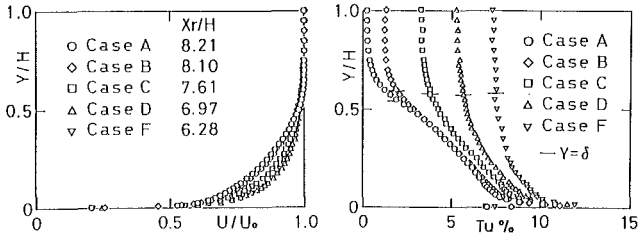


Fig. 5 Velocity and turbulence intensity profiles at reference point (Uncertainty in $U/Up = \pm 0.005$, in $Tu = \pm 0.001$ at 20:1 odds)

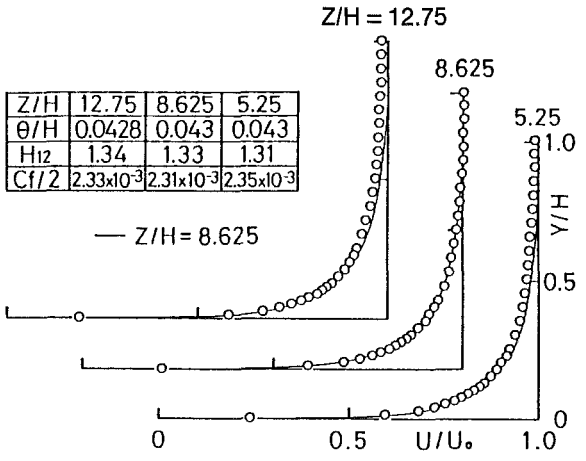


Fig. 6 Velocity profiles at three spanwise stations in case F

more than 30 percent were excluded because of the constraints on accuracy.

## Results and Discussions

**Inlet Condition.** Figure 4 shows the decay process of freestream turbulence in the inlet section. Turbulence intensity in all cases except case A is still in the process of decaying. As turbulence intensity in the freestream decreases at most by 0.7 percent from the separation point to the reattachment point in case F, the effect of the decay rate on the reattachment process seems insubstantial.

Table 1 Boundary layer parameters at reference point

| | Case A | Case B | Case C | Case D | Case E | Case F |
|---|---|---|---|---|---|---|
| $Tu_\infty$ % | 0.25 | 1.3 | 3.3 | 5.3 | 5.7 | 7.4 |
| $Re_\theta$ | $2.07\times10^3$ | $2.00\times10^3$ | $1.65\times10^3$ | $1.41\times10^3$ | $1.36\times10^3$ | $1.39\times10^3$ |
| $\delta/H$ | 0.548 | 0.598 | 0.586 | 0.589 | 0.577 | 0.588 |
| $\theta/H$ | 0.0638 | 0.0618 | 0.0508 | 0.0435 | 0.0420 | 0.0430 |
| $H_{12}$ | 1.37 | 1.36 | 1.35 | 1.33 | 1.34 | 1.33 |
| $Cf/2$ | $1.88\times10^{-3}$ | $1.92\times10^{-3}$ | $2.11\times10^{-3}$ | $2.36\times10^{-3}$ | $2.33\times10^{-3}$ | $2.31\times10^{-3}$ |
| $Xr/H$ | 8.21 | 8.10 | 7.61 | 6.97 | 6.91 | 6.28 |

Uncertainty in $\delta/H = \pm0.01$, in $\theta = \pm0.03$ mm in $H12 = \pm0.01$, $Cf/2 = \pm0.00002$ at 20:1 odds

Table 2 Reattachment length

| Case | Xr/H |
|---|---|
| A0 | 8.14 |
| C0 | 7.54 |
| D0 | 7.00 |
| F0 | 6.28 |
| A0-C | 8.27 |
| A0-R1 | 8.43 |
| A0-R2 | 7.23 |
| A0-R3 | 7.94 |
| F0-C | 6.29 |
| F0-R2 | 6.09 |

(Uncertainty in Xr/H = ±0.1 at 20:1 odds)

Figure 5 shows the velocity and turbulence intensity profiles at the reference point among the cases. Table 1 shows the boundary layer parameters at the reference point and the reattachment length $Xr/H$.

**Two-Dimensionality.** It is important to obtain a uniform freestream and the two-dimensional boundary layer flow upstream of the step, even if the grid which might cause the non-uniformity is used. The two-dimensionality in the boundary layer and the uniformity in the free-stream within the range of 300 mm in the spanwise direction were checked at the reference point by the hot-wire measurement.

Figure 6 shows the velocity profiles at the three spanwise stations of the reference point in case F which is the case of highest turbulence intensity and is the worst case of two-dimensionality. In spite of the worst case, the similar boundary layer parameters are obtained.

According to the spanwise measurements of forward flow fraction in the reattachment region, variations across the span $6.9 \leq Z/H \leq 11.8$ were within 2 percent for all the cases. The reattaching shear layer is almost two-dimensional in the sense of a long time average.

**Flow Characteristics at Separation Point.** Figure 7 depicts the turbulence intensity distributions in a wall law scale at the separation point with and without a grid. As no detailed measurement at the separation point for cases B and E was made, the results on the cases A, C, D, and F will be discussed in detail. Table 2 shows the reattachment length for all the cases. The wall friction velocity is determined carefully by the

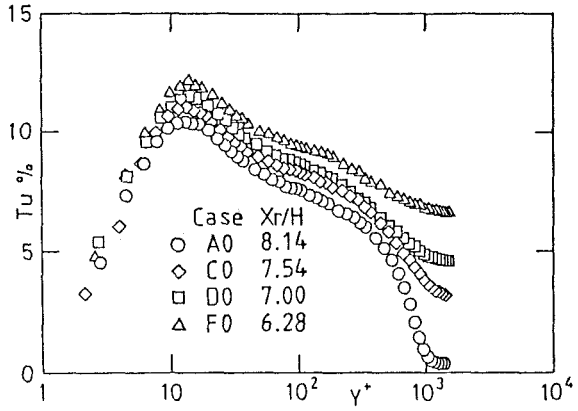


Fig. 7 Turbulence intensity profiles at separation point

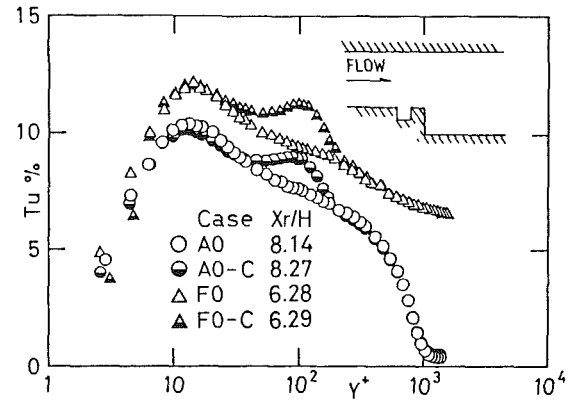


Fig. 8 Turbulence intensity profiles with and without cavity

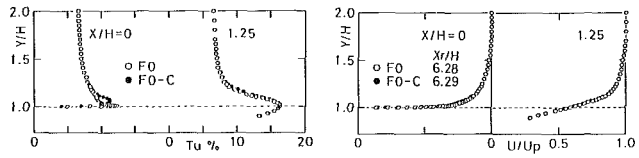


(a) turbulence intensity (b) velocity

Fig. 9 Turbulence intensity and velocity profiles near the step

Clauser's plot. All the cases show the logarithmic law in the near wall region under the different inlet condition. As the turbulence level becomes higher, the reattachment length becomes shorter. It is impossible to find out which turbulence in the transverse direction affects the reattachment length, since the turbulence level shifts in the same manner even in the boundary layer as well as the freestream among 4 cases.

**Effect of Local Turbulence.** Figure 8 shows the turbulence intensity distributions at separation with the cavity of case A0-C and F0-C, and without the cavity of case A0 and F0. A local increase of turbulence can be observed at $Y+ \simeq 100$ because of the cavity. It is possible to evaluate precisely the effect of local turbulence due to the cavity, since the profile of case F0-C shows the same as that of case F0 except near $Y+ = 100$.

Figure 9(*a*) depicts the turbulence intensity distributions at $X/H = 0$ and 1.25 in cases F0-C and F0. No change in turbulence intensity in the region from the peak to the step side can be observed in $X/H = 1.25$. Figure 9(*b*) also shows the velocity distribution at the same stations. Small defect of the velocity at the near-wall region which corresponds to the region of the local increase of turbulence is observed at separation. But, the same profiles are obtained 1.25 H downstream

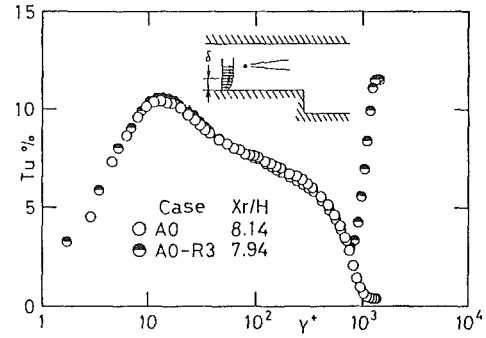


Fig. 10 Turbulence intensity profiles when a rod is placed in the freestream

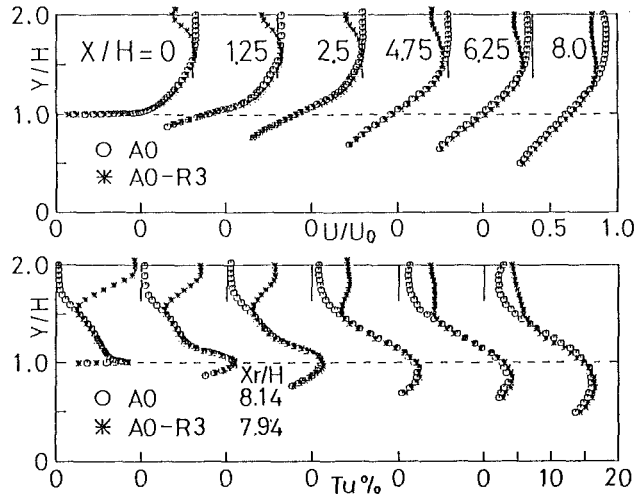


Fig. 11 Velocity and turbulence intensity profiles for the two cases with and without a rod in the freestream

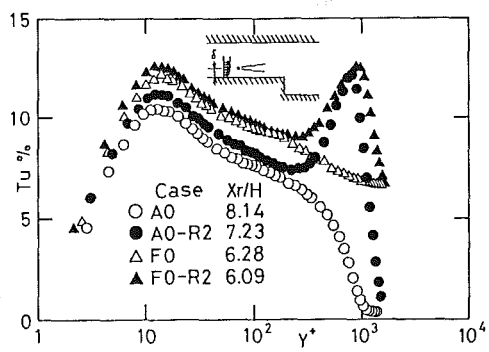


Fig. 12 Turbulence intensity profiles when a rod is placed at the boundary layer edge

of the step. Although the turbulence intensity distributions are locally different, the reattachment length is the same. This means that local turbulence near $Y+ \simeq 100$ generated by the cavity has no effect on the reattachment process.

Figure 10 depicts the turbulence intensity distributions at separation, when the rod of 5 mm in diameter is in the freestream. The turbulence level is almost the same except in the freestream region. It allows us to estimate the effect of free-stream turbulence.

Figure 11 shows the distributions of mean velocity and turbulence intensity in the downstream direction in the cases with and without a rod, case A0-R3 and A0. Profiles of velocity and turbulence intensity are almost identical in both cases within the shear layer. These results indicate that freestream turbulence seems not to directly affect the development of the

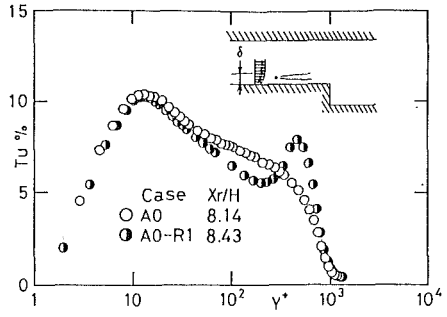


Fig. 13 Turbulence intensity profiles when a rod is placed in the outer boundary layer

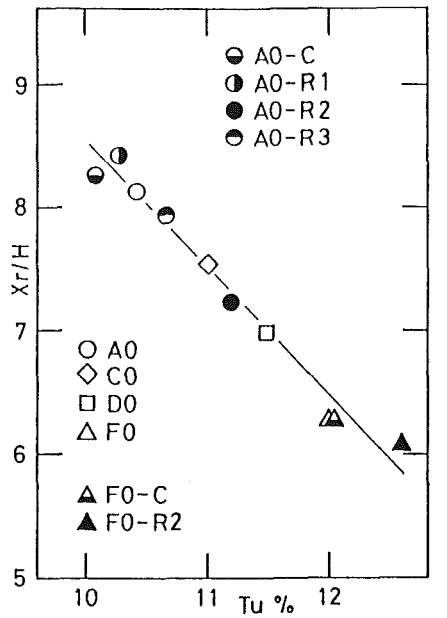


Fig. 14 Reattachment length versus maximum turbulence intensity near the wall at the separation point

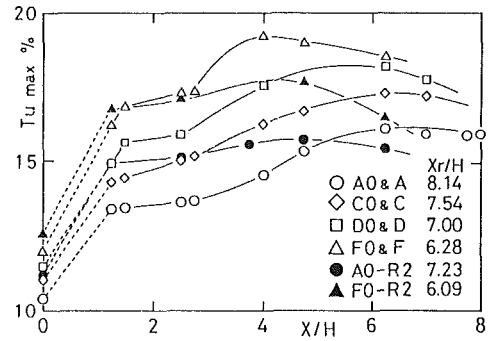


Fig. 15 Maximum values of streamwise turbulence intensity

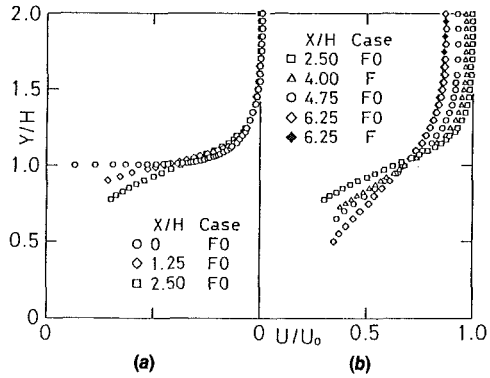


Fig. 16 Velocity profiles in the downstream station

inner mixing layer and the reattachment processes in the separated shear layer.

Figure 12 shows the turbulence intensity profiles at separation when the rod of 5 mm in diameter is placed at the edge of the boundary layer. A local increase of turbulence intensity near the boundary layer edge ($Y+ \simeq 1000$) and an overall increase from the near wall to the inner boundary layer are observed. The reattachment length shows a remarkable difference among the two cases (A0-R2 and F0-R2), while the turbulence level near the edge of the boundary layer for these two cases is almost the same. Furthermore, the reattachment length of case F0 is shorter than that of case A0-R2, though turbulence intensity near the boundary layer edge of the latter case is about twice as the case F0. Correlation between the reattachment length and the turbulence intensity level at the boundary layer edge is quite low.

Figure 13 shows the turbulence intensity profiles when the rod of 3 mm in diameter is placed in the outer boundary layer. Although a local increase of turbulence is obviously found at $Y+ \simeq 500$, the reattachment length in the case with the rod becomes longer than that in the case without the rod. Furthermore, local turbulence at $Y+$ of 100–200 was found not to affect the reattachment length as mentioned in the case with the cavity in Fig. 8, though a local decrease is observed there. Therefore, turbulence intensity in the region where $Y+$ is more than 50 is considered to have no direct effect on the reattachment process from the experimental results with the cavity or rod.

Figure 14 shows the reattachmert length versus maximum turbulence intensity near the wall at the separation point. The maximum turbulence intensity is closely related to the reattachment length. A correlation factor among them is 0.987 and extremely high, even if the mean velocity defect due to the rod installation is encountered. It is quite interesting to note that only a change in 2 percent of turbulence intensity near the wall introduces a change of 2 step heights in the reattachment length. These experimental results show that the near wall turbulence at the separation point is one of the representative and dominant parameters which affect the development of the separated shear layer and the reattachment process.

Figure 15 shows the maximum turbulence intensity distributions in the streamwise direction. All the cases A to F and the corresponding cases A0 to F0 with a rod show a plateau of constant intensity from $X/H = 1.5$ to 2.5 after a rapid increase downstream of the step. Turbulence intensity in four cases with a grid increases to a peak value just upstream of reattachment, then decays. However, the other cases with a rod (case A0-R2 and F0-R2) show a somewhat different trend downstream of $X/H = 2.5$. In comparison of case F0 with case F0-R2, maximum turbulence intensity in case F0 at the separation point is lower than that in case F0-R2. Reverse of intensity occurs near the plateau of constant intensity ($X/H = 2.5$). Further downstream, the difference between the two cases becomes remarkable. Although the development of turbulence in the separated shear layer shows a different manner, the reattachment length in case F0 is longer than that in case F0 with the rod. An examination of the previous results suggests that turbulence from the step to 2.5 H plays an important role in the reattachment process, and turbulence in the separated shear layer downstream of 2.5 H does not strongly influence the reattachment process.

**Characteristics of Inner Mixing Layer.** The velocity and turbulence intensity are examined in detail in the region from the step to 2.5 $H$ in order to make the entrainment process clear. Figure 16 is a velocity distribution in the downstream

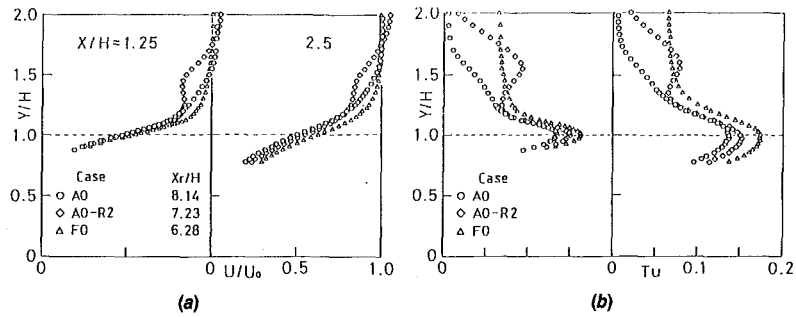


**Fig. 17 Velocity and turbulence intensity profiles in the entrainment region for the three cases**

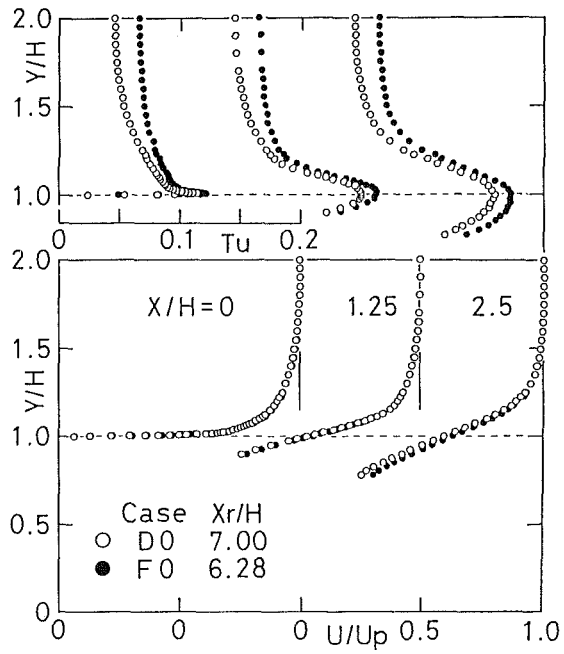


**Fig. 18 Turbulence intensity and velocity profile in the entrainment region for the two cases with the same inlet velocity profile**

direction in case F and F0 which is the case of the highest turbulence intensity. There is no change in the free-stream and outer shear layer ($Y/H > 1.2$) velocity up to $X/H = 2.5$, but the inner region ($Y/H < 1.2$) shows significant variations. This suggests that the flow rate from the free-stream to the inner mixing layer is quite small, while the entrainment flow rate from the step corner region is large. Therefore, the development process in the inner mixing layer up to 2.5 $H$ is dominated by the entrainment process. Hereafter the region up to 2.5 H from the step is called an "entrainment region." Further downstream a change both in the free-stream and mixing layer regions can be observed as shown in Fig. 16(*b*). The similar process is also observed in the other cases. Much attention will be paid to the development of the inner mixing layer in the entrainment region where turbulence plays an important role as shown in Fig. 15.

Figure 17(*a*) shows the velocity profiles in the entrainment region for the three cases. The change in the reattachment length is about one step height with one another. At $X/H = 1.25$ the velocities in the outer layer differed from case to case, while in the inner layer the velocities were nearly identical. The difference of the entrainment flow rate in the region from the step to $X/H = 1.25$ is small among the three cases. However, more remarkable difference of the entrainment flow rate might be observed in the region from $X/H = 1.25$ to 2.5, since the inner velocity profiles are different for the 3 cases. Figure 17(*b*) shows the turbulence intensity profiles at the same stations. It can be clearly demonstrated that the entrainment flow rate becomes larger and the inner mixing layer development becomes faster, as turbulence intensity in the inner region of the mixing layer is higher.

Figure 18 also shows the turbulence intensity and velocity change from separation to $X/H = 2.5$ in case D0 and F0. It might be easy to compare the following two cases D0 and F0 on the development of the inner mixing layer, since the velocity profiles at separation is about the same but the turbulence level is different. Case F0 which corresponds to the case of the shorter reattachment length shows the higher turbulence level in the inner mixing layer and faster development of the inner mixing layer. According to the comparison of the three cases and the two cases mentioned above, turbulence intensity near the wall at the separation point plays a significant role in the development of the inner mixing layer, and correspondingly leads to faster reattachment.

## Conclusions

The present study is focussed on understanding behavior of separated shear layer over a backward-facing step and its reattachment, when a two-dimensional cavity or rod is installed upstream of the step in order to change local turbulence intensity in addition to grid turbulence in the freestream.

The following conclusions are obtained.

(1) The reattachment length has a strong negative correlation with maximum turbulence intensity near the wall at separation, while the effect of the velocity distribution through the inlet boundary layer on the reattachment process is weak.

(2) Turbulence in the entrainment region immediately downstream of the step plays an important role in determining the reattachment length.

## Acknowledgments

The authors wish to thank Messrs. T. Ikeda, H. Imaizumi, and K. Watanabe, who assisted in the data acquisition.

## References

1 Bradshaw, P., and Wong, F. Y. F., "The Reattachment and Relaxation of a Turbulent Shear Layer," *Journal Fluid Mechanics*, Vol. 52, 1972, pp. 113-135.

2 Eaton, J. K., and Johnston, J. P., "A Review for Research on Subsonic Turbulent Reattachment," *AIAA Journal*, Vol. 19, 1981, pp. 1092-1100.

3 Etheridge, D. W., and Kemp, P. H., "Measurements of Turbulent Flow Downstream of a Rearward-Facing Step," *Journal Fluid Mechanics*, Vol. 86, 1978, pp. 545-566.

4 Eaton, J. K., and Johnston, J. P., "Turbulent Flow Reattachment: An Experimental Study of the Flow and Structure Behind a Backward-Facing Step," Stanford University Report MD-39, 1980.

5 Adams, E. C. et al., "Experiments on the Structure of Turbulent Reattaching Flow," Stanford University Report MD-43, 1984.

6 Durst, F., and Tropea, C., "Turbulent, Backward-Facing Step Flows in Two-Dimensional Ducts and Channels," *Proc. 3rd Symp. Turbulent Shear Flows*, Davis, 1981, pp. 18.1-6.

7 Honami, S., and Nakajo, I., "A Reattaching Shear Layer to the Curved Surfaces Over a Backward Facing Step," ASME paper 86-WA/FE-9, 1986.

Journal of Fluids Engineering

Technical Briefs

# Effect of 90 Degree Flap on the Aerodynamics of a Two-Element Airfoil

**J. Katz and R. Largman**

*The aerodynamic performance of a two-element airfoil with a 90 deg. trailing edge flap was experimentally investigated. The 5 percent-chord long flap, significantly increased the lift of the baseline airfoil, throughout a wide range of angles of attack. The maximum lift coefficient of the flapped wing increased too, whereas the lift/drag ratio decreased.*

## Introduction

High speed ground vehicles, such as race cars, can improve their performance and particularly their cornering speeds by generating aerodynamic downforce. This additional downforce increases the tires' adhesion and is generated by wings added onto the vehicle's body (reference [1]). Because of considerations, such as sufficient rear view, the geometry and position of these wings are restricted by regulations. Frequently, these requirements result in a limit on the wing angle-of-attack range or on its chamber shape. In situations when maximum negative lift is desired, race-car designers have used short (up to 5 percent chord long), 90 deg. trailing edge flaps to increase the aerodynamic down-force (these flaps are frequently called "Gurney-flaps"). This very high deflection and short flap (compared to aircraft type flaps) will cause the flow to separate locally and its effectiveness for this application is not well documented.

In this study, the performance of a typical two-element race-car rear wing was examined experimentally to determine the effectiveness of the 90 deg. flap.

## Experimental Procedure

The geometry of the two element airfoil section that was used is shown in Fig. 1. This airfoil shape differs slightly from multielement airfoils used on aircraft [2–5] at the gap region between the two elements, since the second element does not retract into the main wing. The wing had a rectangular planform with an aspect-ratio of 4.6 and had two small end-plates with the contours shown in Fig. 1. The main function of these end-plates was to structurally hold the wing elements in place but they also increased the lift slope by about 10 percent. To investigate the effect of the flap, a 5 percent-chord long, thin metal sheet was attached to the wing trailing edge, as shown in Fig. 1. Since within the operational angle-of-attack range of the baseline wing ($2 < \alpha < 12$ deg.), the flow over the two airfoil elements was attached, the effect of the open gap between the two airfoil elements was briefly investigated by taping it along the dashed lines shown in Fig. 1.

The wing was tested in a closed circuit wind tunnel with a cross section of 0.8 m × 1.15 m, and at a Reynolds No. of $0.3 \times 10^6$ (based on wing chord). Because of the attached flow conditions (within the operating range of $\alpha$) for both the 1/4-scale model and for the full-scale wing, it is assumed that this Reynolds no. is sufficient for lift measurements. Model to test-section cross-section area-ratio varied between 1–2 percent, so the effect of wind tunnel walls and the required blockage corrections were minimum. Also, the balance system accuracy for the lift and drag components was less than ±0.1 pounds.

## Results

The lift coefficient versus angle-of-attack for the baseline wing alone, with the 90 deg flap, and with the sealed gap is presented in Fig. 2. The lift of the basic wing (with an aspect ratio of 4.6) is competitive with two-element aircraft wing sections (reference [5]). The wing with the flap clearly has a much higher lift than the baseline shape over the whole range of angle-of-attack. Flow visualizations (see inset to Fig. 2) indicated that the flow is always separated on the suction side, behind the flap. Furthermore, on the pressure side ahead of the flap and above the wing, a small flow-recirculation area was observed. Therefore the lift increase can be attributed to the additional twisting of the streamlines at the vicinity of the airfoils trailing edge. When the gap between the two wing elements was closed, the lift dropped further down, showing the positive interaction between the elements and the advantage of the multielement design [4]. The most important effect of the "Gurney flap", as shown in Fig. 2, is the increase in the maximum lift coefficient, even though wing stall is initiated at smaller angles-of-attack (with the flap).

Another important aspect of wing design is its efficiency in generating the aerodynamic force, which can be weighted by

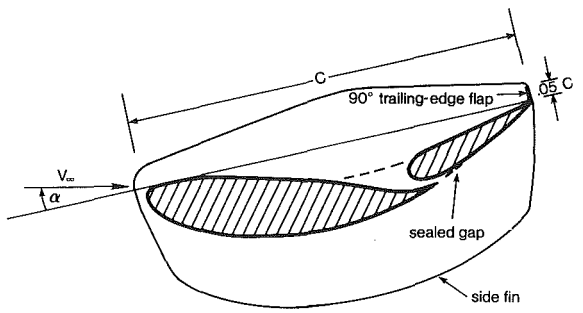


**Fig. 1 Geometry of the two element airfoil and the 90 deg. flap ($c = 0.102$ meter, also note the definition of positive $\alpha$)**

Professor and Graduate Student, respectively, Department of Aerospace Engineering, SDSU, San Diego, CA 92182.

Contributed by the Fluids Engineering Division of THE AMERICAN SOCIETY OF MECHANICAL ENGINEERS. Manuscript received by the Fluids Engineering Division July 21, 1987.

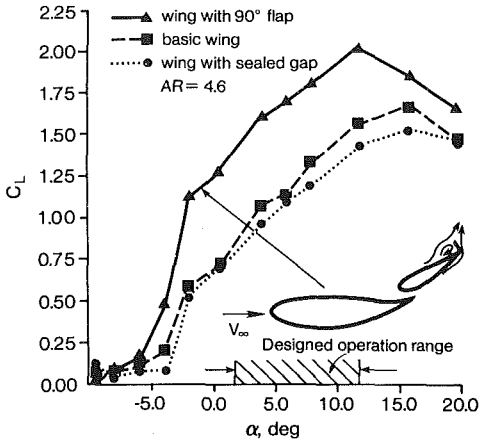


**Fig. 2 Lift coefficients for the baseline and the modified wings ($AR$ = wing span/wing chord, uncertainty in $C_L = \pm 0.02$, in $\alpha = \pm 0.2$ deg.)**

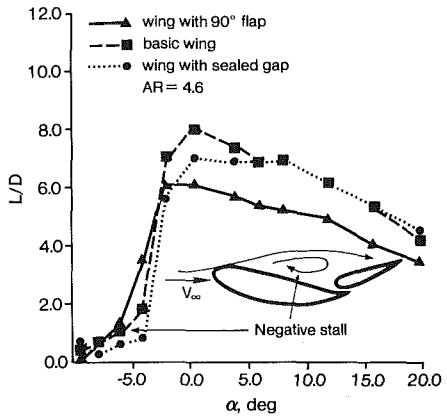


**Fig. 3 Lift/drag ratios for the three airfoil configurations. (Uncertainty in $L/D = \pm 0.25$, and in $\alpha = \pm 0.2$ deg.)**

analyzing the lift/drag ratio diagram (Fig. 3). Here the wing with the flap is the least efficient over the whole practical range ($2 < \alpha < 12$ deg.). The baseline wing is more efficient at the beginning of this "design angle-of-attack range" (shown in Fig. 2), but has similar $L/D$ as the sealed-gap wing for the higher angles of attack.

At the lower angles-of-attack ($\alpha < 2$ deg.) the performance of the wing has dropped considerably because of a large flow separation pattern on its pressure side, as shown in the inset in Fig. 3. Therefore if a wing has to operate at this region a different shape, perhaps with less camber, should be designed.

## Concluding Remarks

The above data show that for high aerodynamic efficiency the 90 deg. flap is not the most effective choice. However, if wing chord and span are limited (as the case for most race cars) and if maximum downforce is sought, then higher down force coefficients can be obtained by this simple add-on, without a redesign of the airfoil shape.


## Acknowledgments

This work was partially supported by NASA Ames Research Center, under Grant No. NCC-2-458, with Dr. Larry Olson as project monitor. The author also acknowledges the wind-tunnel model support and the valuable information provided by Mr. Lee Dykstra of Special Chassis Inc., Indianapolis, Ind.


## References


1 Katz, J., "Aerodynamic Model for Wing-Generated Down Force on Open-Wheel-Racing-Car Configurations," SAE Paper No. 86-0218, Feb. 1986.

2 Tinoco, E. N., Ball, D. N., and Rice, F. A., "PAN AIR Analysis of a Transport High-Lift Configuration," AIAA Paper No. 86-1811, 1986.

3 Seetharam, H. C., and Wentz, W. H. Jr., "Studies of Flow Separation and Stalling on One and Two-Element Airfoils at Low Speeds," SAE Paper No. 77-0442, 1977.

4 Smith, A. M. O., "High Lift Aerodynamics," *J. Aircraft*, Vol. 12, 1975.

5 Nichols, J. H. Jr., and Taylor, D. W., "Development of High Lift Devices for Application to Advanced Navy Aircraft," *Proceeding of the V/STOL Aircraft Aerodynamics Conference*, Monterey CA, Vol. 2, May 1979, pp. 777–849.


# A Modified Van Driest Formula for the Mixing Length of Turbulent Boundary Layers in Pressure Gradients


**P. S. Granville**[1]



*A modified van Driest formula is proposed for the mixing length of turbulent boundary layers in pressure gradients. The slope and intercept of the logarithmic similarity law are satisfied asymptotically unlike existing modified van Driest formulas.*


## Introduction

Algebraic formulas for mixing lengths represent the simplest type of turbulence modelling and have often proved to be the most reliable [1, 2] for predicting the development of turbulent boundary layers. The van Driest formula [3] for mixing lengths has almost become the standard for the near-wall region of turbulent boundary layers. The physical basis of mixing lengths in general has been examined recently by Kutateladze [4] and by Landahl [5].

The original van Driest formula predicts very well the velocity profile of the viscous sublayer, the buffer layer and asymptotically the log layer of turbulent boundary layers in zero longitudinal pressure gradient on smooth surfaces. However it has proved unsatisfactory for non-zero pressure gradients. Consequently various modifications have been proposed to the van Driest formula which are listed in the Table 1.

The proposed modifications should satisfy asymptotically the experimental fact that the inner logarithm velocity law is invariant in usual pressure gradients [6, 7] with respect to both slope and intercept.

It is shown that all the formulas listed in the Table 1, references [8 to 12], with the exception of that of Nituch et al. [13] fail with respect to predicting asymptotically the slope of the log law. It is also shown that the formula of Nituch et al.[13] which predicts the slope, fails to predict the correct intercept.

It is proposed that the formula of Nituch et al. be further improved by relating the van Driest factor to a modified pressure-gradient parameter so as to predict the correct intercept as well as slope of the log law. A numerical relation is determined in this respect and incorporated into the proposed formula.

The proposed mixing-length formula may be used for the Baldwin-Lomax model [14, 15].

## Velocity Profile

In a recent experiment Salam [7] shows again that the inner log law for the velocity profile near a wall does not vary in pressure gradients even close to separation

$$u^* = (1/\kappa) \ln y^* + B_1 \tag{1}$$


[1]Research Physicist, David Taylor Research Center, Bethesda, MD 20084-5000.



Contributed by the Fluids Engineering Division of THE AMERICAN SOCIETY OF MECHANICAL ENGINEERS. Manuscript received by the Fluids Engineers Division April 9, 1988.

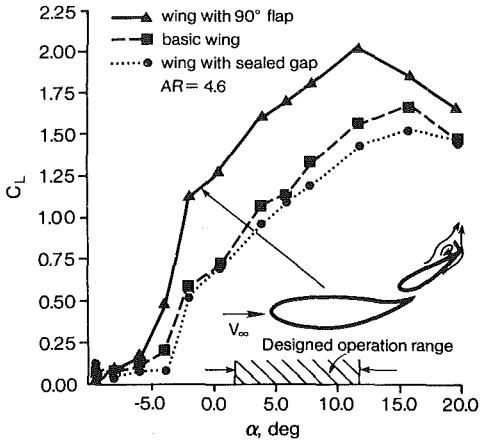


**Fig. 2 Lift coefficients for the baseline and the modified wings (*AR* = wing span/wing chord, uncertainty in $C_L = \pm 0.02$, in $\alpha = \pm 0.2$ deg.)**

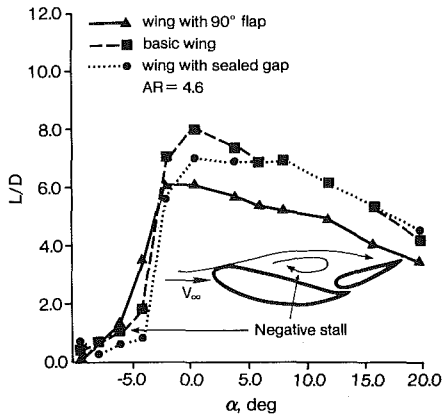


**Fig. 3 Lift/drag ratios for the three airfoil configurations. (Uncertainty in $L/D = \pm 0.25$, and in $\alpha = \pm 0.2$ deg.)**

analyzing the lift/drag ratio diagram (Fig. 3). Here the wing with the flap is the least efficient over the whole practical range ($2 < \alpha < 12$ deg.). The baseline wing is more efficient at the beginning of this "design angle-of-attack range" (shown in Fig. 2), but has similar $L/D$ as the sealed-gap wing for the higher angles of attack.

At the lower angles-of-attack ($\alpha < 2$ deg.) the performance of the wing has dropped considerably because of a large flow separation pattern on its pressure side, as shown in the inset in Fig. 3. Therefore if a wing has to operate at this region a different shape, perhaps with less camber, should be designed.

## Concluding Remarks

The above data show that for high aerodynamic efficiency the 90 deg. flap is not the most effective choice. However, if wing chord and span are limited (as the case for most race cars) and if maximum downforce is sought, then higher down force coefficients can be obtained by this simple add-on, without a redesign of the airfoil shape.


## Acknowledgments

This work was partially supported by NASA Ames Research Center, under Grant No. NCC-2-458, with Dr. Larry Olson as project monitor. The author also acknowledges the wind-tunnel model support and the valuable information provided by Mr. Lee Dykstra of Special Chassis Inc., Indianapolis, Ind.


## References


1 Katz, J., "Aerodynamic Model for Wing-Generated Down Force on Open-Wheel-Racing-Car Configurations," SAE Paper No. 86-0218, Feb. 1986.

2 Tinoco, E. N., Ball, D. N., and Rice, F. A., "PAN AIR Analysis of a Transport High-Lift Configuration," AIAA Paper No. 86-1811, 1986.

3 Seetharam, H. C., and Wentz, W. H. Jr., "Studies of Flow Separation and Stalling on One and Two-Element Airfoils at Low Speeds," SAE Paper No. 77-0442, 1977.

4 Smith, A. M. O., "High Lift Aerodynamics," *J. Aircraft*, Vol. 12, 1975.

5 Nichols, J. H. Jr., and Taylor, D. W., "Development of High Lift Devices for Application to Advanced Navy Aircraft," *Proceeding of the V/STOL Aircraft Aerodynamics Conference*, Monterey CA, Vol. 2, May 1979, pp. 777–849.


# A Modified Van Driest Formula for the Mixing Length of Turbulent Boundary Layers in Pressure Gradients


**P. S. Granville**[1]



*A modified van Driest formula is proposed for the mixing length of turbulent boundary layers in pressure gradients. The slope and intercept of the logarithmic similarity law are satisfied asymptotically unlike existing modified van Driest formulas.*


## Introduction

Algebraic formulas for mixing lengths represent the simplest type of turbulence modelling and have often proved to be the most reliable [1, 2] for predicting the development of turbulent boundary layers. The van Driest formula [3] for mixing lengths has almost become the standard for the near-wall region of turbulent boundary layers. The physical basis of mixing lengths in general has been examined recently by Kutateladze [4] and by Landahl [5].

The original van Driest formula predicts very well the velocity profile of the viscous sublayer, the buffer layer and asymptotically the log layer of turbulent boundary layers in zero longitudinal pressure gradient on smooth surfaces. However it has proved unsatisfactory for non-zero pressure gradients. Consequently various modifications have been proposed to the van Driest formula which are listed in the Table 1.

The proposed modifications should satisfy asymptotically the experimental fact that the inner logarithm velocity law is invariant in usual pressure gradients [6, 7] with respect to both slope and intercept.

It is shown that all the formulas listed in the Table 1, references [8 to 12], with the exception of that of Nituch et al. [13] fail with respect to predicting asymptotically the slope of the log law. It is also shown that the formula of Nituch et al.[13] which predicts the slope, fails to predict the correct intercept.

It is proposed that the formula of Nituch et al. be further improved by relating the van Driest factor to a modified pressure-gradient parameter so as to predict the correct intercept as well as slope of the log law. A numerical relation is determined in this respect and incorporated into the proposed formula.

The proposed mixing-length formula may be used for the Baldwin-Lomax model [14, 15].

## Velocity Profile

In a recent experiment Salam [7] shows again that the inner log law for the velocity profile near a wall does not vary in pressure gradients even close to separation

$$u^* = (1/\kappa) \ln y^* + B_1 \qquad (1)$$


[1]Research Physicist, David Taylor Research Center, Bethesda, MD 20084-5000.



Contributed by the Fluids Engineering Division of THE AMERICAN SOCIETY OF MECHANICAL ENGINEERS. Manuscript received by the Fluids Engineers Division April 9, 1988.

**Table 1 Prandtl–van Driest mixing-length formulas for turbulent boundary layers in pressure gradients**

| METHOD | Ref. | FORMULA | REMARKS |
|---|---|---|---|
| van Driest | [3] (1956) | $l^* = \kappa y^* \, [1 - \exp(-y^*/\lambda_0^*)]$ | zero pressure gradient |
| Patankar and Spalding | [8] (1968) | $l^* = \kappa y^* \, [1 - \exp(-y^*\sqrt{\tau^*}/\lambda_0^*)]$ | does not satisfy slope of log law |
| Cebeci | [9] (1970) | $l^* = \kappa y^* [1 - \exp(-y^* \sqrt{1 + 11.8p^+}/\lambda_0^*)]$, see note 3 | does not satisfy slope of log law |
| Launder and Pridden | [10] (1973) | 1) $l^* = \kappa y^* \, [1 - \exp(-y^*\tau^{*3/2}/\lambda_0^*)]$<br>2) $l^* = \kappa y^* \, [1 - \exp(-y^*\tau^{*2}/\lambda_0^*)]$ | does not satisfy slope of log law |
| Baker and Launder | [11] (1974) | $l^* = \kappa y^* \, [1 - \exp(-y^*\tau^*/\lambda_0^*)]$ | does not satisfy slope of log law |
| Kays and Moffat | [12] (1975) | $l^* = \kappa y^* \{1 - \exp[-y^*(1 + ap^+)/\lambda_0^*]\}$<br>$a = 14.2$ for $p^+ \geq 0$ $a = 30.2$ for $p+ < 0$ | does not satisfy slope of log law |
| Nituch, Sjolander and Head | [13] (1978) | $l^* = \kappa y^* \sqrt{\tau^*} \, [1 - \exp(-y^*/\lambda_0^*)]$ | satisfies slope but not intercept of log law |
| proposed | Equation 17 | $l^* = \kappa y^* \sqrt{\tau^*} \{1 - \exp[-y^* \sqrt{1 + b\,\hat{p}^+/26}]\}$<br>$b = 14.0$ for $\hat{p}^+ > 0$<br>$b = 16.4$ for $\hat{p}^+ < 0$ | satisfies both slope and intercept of log law |

Notes: 1. $\tau^* = 1 + \hat{p}^+ y^*$
2. $\hat{p}^+ = 0.9\, p^+$
3. The $p^+$ in the paper of Cebeci is defined as negative of $p^+$ used here
4. $\kappa = 0.4$, $\lambda_0^* = 26$

where $u^* = u/u_\tau$, $y^* = u_\tau\, y/\nu$, $\kappa$ = von Kármán constant, $1/\kappa$ = slope, $B_1$ = intercept, $u_\tau = \sqrt{\tau_w/\rho}$, $\tau_w$ = wall shear stress, $\rho$ = density of fluid, $\nu$ = kinematic viscosity, and $y$ = normal distance from wall.

The turbulent shear stress ($\tau_t$) may be given by the mixing length ($l$) as

$$\frac{\tau_t}{\rho} = l^2 \left(\frac{du}{dy}\right)^2 \tag{2}$$

or nondimensionally as

$$\frac{\tau_t}{\tau_w} = l^{*2} \left(\frac{du^*}{dy^*}\right)^2 \tag{3}$$

where $l^* = u_\tau l/\nu$.

The total shear stress ($\tau$) which has laminar and turbulent contributions may be expressed nondimensionally as

$$\tau^* = \frac{du^*}{dy^*} + l^{*2} \left(\frac{du^*}{dy^*}\right)^2 \tag{4}$$

where $\tau^* = \tau/\tau_w$. Consequently,

$$\frac{du^*}{dy^*} = \frac{2\tau^*}{1 + \sqrt{1 + (2l^*)^2\, \tau^*}} \tag{5}$$

From the equation of motion, the shear stress profile, $\tau^*$, close to the wall is given by

$$\tau^* = 1 + p^+ y^{*+} \ldots \tag{6}$$

where $p^+ = (\nu/\rho u \tau^3)\, dp/dx$, a pressure-gradient parameter. Here $p$ = pressure and $x$ is the streamwise coordinate.

The slope of the shear-stress profile, $\partial\tau^*/\partial y^*$, is $p^+$ at the wall and gradually decreases away from the wall due to the effect of the convective terms of the equation of motion. However since the layers near the wall which are being considered are relatively thin, the variation of the shear stress away from the wall is practically linear. This was noted by Townsend [16] from a study of measured data such that

$$\tau^* = 1 + cy^* \tag{7}$$

where $c$ is a constant in the $y$-direction and is close in value to that of $p^+$.

Patel [17] also recommends a linear relation

$$\tau^* = 1 + \left(\frac{\nu}{\rho u \tau^3} \frac{\partial \tau}{\partial y}\right) y^* = 1 + \frac{\partial \tau^*}{\partial y^*} \tag{8}$$

which, when integrated, becomes the same as that of Townsend.

Since $c$ is close in value to $p^+$, it will be designated as $\hat{p}^+$. Then in the wall region

$$\tau^* = 1 + \hat{p}^+ y^* \tag{9}$$

$\hat{p}^+$ may be related to $p^+$ by

$$\hat{p}^+ = \alpha\, p^+ \tag{10}$$

where $\alpha$ is an appropriate constant, $\alpha < 1$.

The original van Driest model incorporating the Prandtl mixing length is given nondimensionally as

$$l^* = \kappa y^* \, (1 - e^{-y/\lambda^*}) \tag{11}$$

where $\lambda^* = u_\tau\, \lambda/\nu$, $\lambda$ is the van Driest factor.

### Slope of Log Law

The van Driest mixing length model works well for zero pressure gradient in predicting the logarithmic velocity profile, equation (1), if $\lambda^* = \lambda_o^*$, the particular value for zero pressure gradient. For pressure gradients, however, agreement has been poor. This has prompted many investigators [8–13] to propose in effect modifications to $\lambda^*$ as shown in the Table 1. The presence of these many formulas would seem to indicate an underlying dissatisfaction.

Now, if the laminar contribution to the shear stress ($\tau$) is considered negligible at the higher values of $y^*$ in the log region, then from definitions

$$l^* = \kappa y^* \sqrt{\tau^*} \tag{12}$$

This conclusion was arrived at by various investigators such as Reeves [18], Glowacki and Chi [19] and Galbraith [20] as explained by Nituch et al. [13] who proposed for the viscous sublayer, buffer layer as well as the log layer

$$l^* = \kappa y^* \sqrt{\tau^*} \, (1 - e^{-y^*/\lambda_0^*}) \tag{13}$$

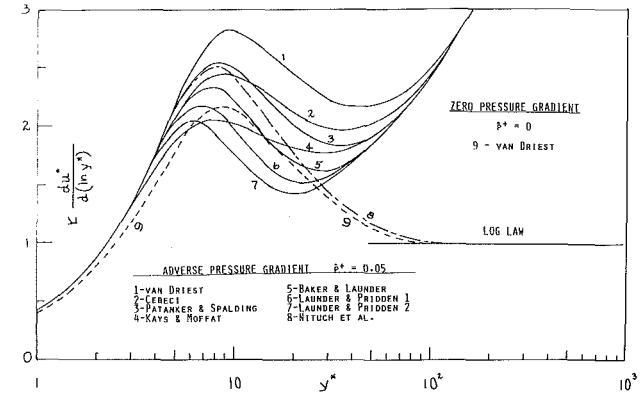


**Fig. 1 Variation of slope, $\kappa du^*/d(\ln y^*)$, with normal distance, $y^*$, using formulas in the table**

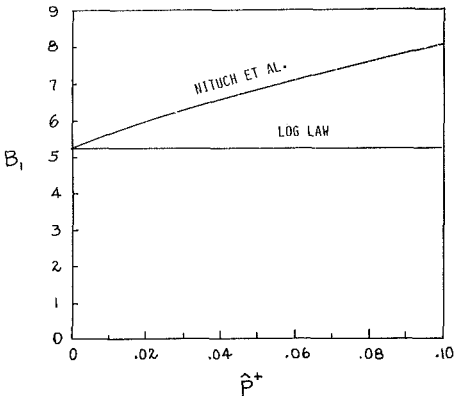


**Fig. 2 Prediction of intercept, $B_1$, as a function of pressure-gradient parameter, $\hat{p}^+$, according to method of Nituch et al. (reference [13])**

where $\lambda_0{}^*$ is again the value of $\lambda^*$ for zero pressure gradient.

Figure 1 illustrates the behavior of the various formulas given in the Table with respect to the slope of the velocity profile as given by equation (5) which is rewritten as

$$\kappa \frac{du^*}{d(\ln y^*)} = \frac{2\kappa\tau^* y^*}{1+\sqrt{1+(2l^*)^2\,\tau^*}} \tag{14}$$

For the log law, $\kappa\, du^*/d(\ln y^*) = 1$, and for laminar flow, $\kappa\, du^*/d(\ln y^*) = \kappa\tau^* y^*$. A representative display shown in Fig. 1 is for an adverse pressure gradient of $\hat{p}^+ = 0.05$. A standard value of $\kappa = 0.4$ is is used.

In Fig. 1 it is shown that both the van Driest formula for zero pressure gradient ($\hat{p}^+ = 0$) and the Nituch formula for an adverse pressure gradient ($\hat{p}^+ = 0.05$) asymptotically attain the slope of the log law. All the other modified van Driest formulas as listed in the Table fail markedly for pressure gradients in this respect and in fact tend towards $\kappa du^*/d(\ln y^*) = \sqrt{\tau^*}$. The van Driest plot for $\hat{p}^+ = 0.05$ represents the unmodified van Driest formula using a value of $\lambda_0{}^*$.

## Intercept

The mixing-length formula should also lead to a value of an intercept, $B_1$ which agrees with the log law. Equating the log law, equation (1), and the velocity profile obtained by integrating equation (5) results in

$$B_1 = \int_0^1 \frac{2\tau^*}{1+\sqrt{1+(2l^*)^2\tau^*}}\, dy^* + \int_0^{\ln \tilde{y}^*} \left[\frac{2\tau^* y^*}{1+\sqrt{1+(2l^*)^2\tau^*}} - \frac{1}{\kappa}\right] d(\ln y^*) \tag{15}$$

where $\tilde{y}^*$ is a sufficiently large value of $y^*$ in the log layer. The integrand of the second term becomes practically zero at the value of $\tilde{y}^*$.

For a value of $\lambda_0{}^* = 26$, $B_1 = 5.23$ for $\kappa = 0.4$ for zero pressure gradient, $\tau^* = 1$.

For the formula of Nituch et al. which uses $\lambda^* = \lambda_0{}^*$, $B_1$ increases with $\hat{p}^+$ as shown in Fig. 2 instead of remaining constant with pressure gradient.

### Proposed Mixing-Length Formula

To keep the intercept ($B_1$) constant for all pressure gradients as shown experimentally, it is necessary to have the van Driest factor ($\lambda^*$) as a function of pressure-gradient parameter $\hat{p}^+$. Then

$$l^* = \kappa y^* \sqrt{\tau^*}\,(1 - e^{-y^*/\lambda^*}) \tag{16}$$

where $\lambda^* = f[\hat{p}^+]$.

From numerical solutions of $B_1$ in equation (15), $\lambda^*$ is plotted against $\hat{p}^+$ in Fig. 3. Here $\kappa = 0.4$. A numerical fit to

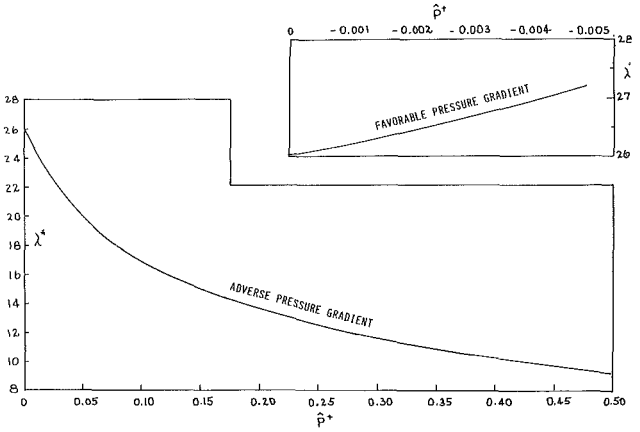


**Fig. 3 Variation of van Driest factor, $\lambda$ with pressure-gradient parameter, $\hat{p}^+$, according to proposed formula, equation (16)**

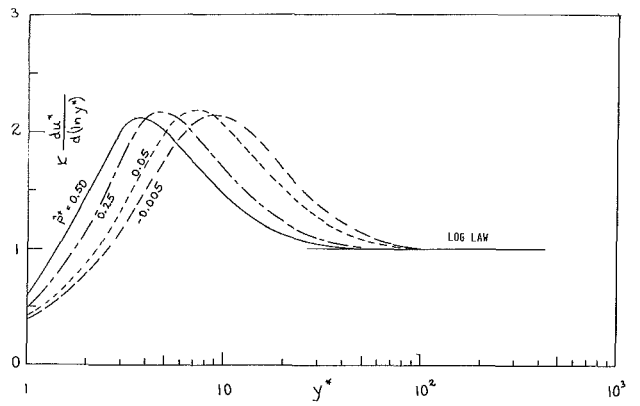


**Fig. 4 Variation of slope ($\kappa\, du^*/d(\ln y^*)$, with normal distance $y^*$, using proposed formula, equation (17), for various pressure gradients**

$(26/\lambda^*)^2 = 1 + b\,p^+$ gives $b = 14.0$ for $\hat{p}^+ > 0$ and $b = 16.4$ for $\hat{p}^+ < 0$. Then the proposed formula is

$$l^* = \kappa\, y^* \sqrt{\tau^*}\,(1 - e^{-y^*\sqrt{1+b\hat{p}^+}/26}) \tag{17}$$

where $b = 14.0$ for $p^+ > 0$ and $b = 16.4$ for $p^+ < 0$.

A plot of the slopes based on the proposed formula in Fig. 4 shows that the log law is satisfied asymptotically for representative pressure gradients, favorable and adverse.

The proposed formula, equation (17), is also recommended for the Baldwin-Lomax model [14, 15] near the wall instead of the unmodified van Driest model which has been used.

### Concluding Remarks

The proposed formula, equation (17), satisfies the slope of

the log law by using $\kappa y^* \sqrt{\tau^*}$ instead of just $\kappa y^*$ and the intercept by properly relating the van Driest factor $\lambda^*$ to pressure-gradient parameter $\hat{p}^+$. Although the existing formulas with the exception of that of Nituch et al. could immediately satisfy the slope of the log law by adding $\sqrt{\tau^*}$ to $\kappa y^*$, there still remains the problem of satisfying the intercept. Curiously, if the formula of Cebeci adds the $\sqrt{\tau^*}$ and uses a value of $\alpha = 0.84$ to convert the $p^+$ to $\hat{p}^+$, it exactly matches the proposed formula for adverse pressure gradients.

### References


1 Patel, V. C., Rodi, W., and Scheuerer, "Turbulence Models for Near-Wall and Low Reynolds Numbers Flows: A Review," *AIAA Journal*, Vol. 23, No. 9, 1985, pp. 1308–1319.

2 Cebeci, T., Chang, K. C., Li, C., and Whitelaw, J. H., "Turbulence Models for Wall Boundary Layers," *AIAA Journal*, Vol. 24, No. 3, 1986, pp. 359–360.

3 van Driest, E. R., "On Turbulent Flow Near a Wall," *Journal of Aeronautical Sciences*, Vol. 23, 1956, pp. 1007–1011, 1036.

4 Kutateladze, S. S., "The Mixing Length Hypothesis in the Turbulence Theory," *International Journal of Heat and Mass Transfer*, Vol. 27, No. 11, 1984, pp. 1947–1950.

5 Landahl, M. T., "Coherent Structures in Turbulence and Prandtl's Mixing Length Theory," *Zeitschrift für Flugwissenschaften und Weltraumforschung*, Vol. 8, No. 4, 1984, pp. 233–242.

6 McDonald, H., "The Effect of Pressure Gradient on the Law of the Wall in Turbulent Flow," *Journal of Fluid Mechanics*, Vol. 35, Part 2, 1969, pp. 311–336.

7 Salam, M. Y., "Measurement of the Viscous Sublayer in Near-Separated Flows," *Applied Scientific Research*, Vol. 39, No. 4, 1982, pp. 337–347.

8 Patankar, S. V., and D. B. Spalding, *"Heat and Mass Transfer in Boundary Layers,"* C.R.C. Press, Cleveland, 1968.

9 Cebeci, T., "Behavior of Turbulent Flow Near a Porous Wall with Pressure Gradient," *AIAA Journal*, Vol. 8, No. 12, 1970, pp. 2152–2156.

10 Launder, B. E., and Priddin, C. H., "A Comparison of Some Proposals for the Mixing Length Near a Wall," *International Journal of Heat and Mass Transfer*, Vol. 16, 1973, pp. 700–702.

11 Baker, R. J., and Launder, B. E., "The Turbulent Boundary Layer with Foreign Gas Injection II," *International Journal of Heat and Mass Transfer*, Vol. 17, No. 2, 1974, pp. 293–306.

12 Kays, W. M., and Moffat, R. J., "The Behavior of Transpired Turbulent Boundary Layers," *"Studies in Convection"* Vol. 1, B. E. Launder, ed., Academic Press, London, 1975, pp. 223–319.

13 Nituch, M. J., Sjolander, S., and Head, M. R., "An Improved Version of the Cebeci-Smith Eddy-Viscosity Model," *Aeronautical Quarterly*, Vol. 29, Part 3, 1978, pp. 207–225.

14 Baldwin, B. S., and Lomax, H., "Thin Layer Approximation and Algebraic Model for Separated Turbulent Flows," AIAA Paper 78–257, 1978.

15 Granville, P. S., "Baldwin-Lomax Factors for Turbulent Boundary Layers in Pressure Gradients," *AIAA Journal*, Vol. 25, No. 12, 1987, pp. 1624–1627.

16 Townsend, A. A., 1961, "Equilibrium Layers and Wall Turbulence," *Journal of Fluid Mechanics*, Vol. 11, Part 1, 1961, pp. 97–120.

17 Patel, V. C., "A Unified View of the Law of the Wall Using Mixing-Length Theory," *Aeronautical Quarterly*, Vol. 24, Part 1, 1973, pp. 55–70.

18 Reeves, B. L., "Two-Layer Model of Turbulent Boundary Layers," *AIAA Journal*, Vol. 12, No. 7, 1974, pp. 932–939.

19 Glowacki, W. J., and Chi, S. W., "Effect of Pressure Gradient on Mixing Length for Equilibrium Turbulent Boundary Layers," *AIAA Paper* 72–213, 1972.

20 Galbraith, R. A. McD., Sjolander and Head, M. R., "Mixing Length in the Wall Region of Turbulent Boundary Layers," *Aeronautical Quarterly*, Vol. 27, Part 2, 1977, pp. 97–110.


## Stability of the Flow Between Rotating Cylinders—Wide-Gap Problem


**H. S. Takhar,[1] M. A. Ali,[2] and V. M. Soundalgekar[3]**


### Introduction

Wide-gap stability of Couette flow was studied by many authors. Notable among these are Sparrow et al. [1], Astill and Chung [2], and Walowit et al. [3]. All other papers are referred in the reference list of reference [3]. However, cell-pattern and the radial eigenfunctions were not shown in detail earlier. So we now propose to show these in the present investigation.

Consider the flow of a viscous incompressible fluid between two concentric rotating cylinders with $R_1$ and $R_2$ as the radii and $\Omega_1$ and $\Omega_2$ as the angular velocities of the inner and outer cylinders, respectively.

Then the differential equation which governs the linear stability of the flow in a wide-gap region is given by [reference [3]]

$$(DD^* - a^2)^3 v = -a^2 T g(x) v \tag{1}$$

where $u$, $v$ are, respectively, the dimensionless amplitudes of the normal mode perturbations of the radial and azimuthal velocity components. These equations are to be solved with following boundary conditions:

$$v = (DD^* - a^2)v = D(DD^* - a^2)v = 0 \text{ at } x = 0,1 \tag{2}$$

Here $g(x) = \dfrac{\mu - \eta^2}{1-\eta^2} + \dfrac{\eta^2(1-\mu)}{1-\eta^2} \cdot \dfrac{1}{\epsilon^2}$, $\mu = \dfrac{\Omega_2}{\Omega_1}$, $\eta = \dfrac{R_1}{R_2}$

$$\epsilon = \frac{r}{R_2}, \quad d = R_2 - R_1, \quad a = \lambda d, \quad T = -\frac{4A^*\Omega_1 d^4}{\nu^2},$$

$$D = \frac{d}{dx}, \quad x = \frac{r - R_1}{d}, \quad D^* = \frac{d}{dx} + \frac{1-\eta}{\epsilon},$$

$$A^* = \frac{\Omega_1 {R_1}^2 - \Omega_2 {R_2}^2}{{R_1}^2 - {R_2}^2}. \tag{3}$$

The eigenvalue problem governed by equations (1) and (2) is solved numerically, following Harris and Reid [5]. The procedure starts by rewriting the governing equation (1) as a system of first order differential equations which are then integrated by using the Merson form of the Runge-Kutta method. The range of integration was divided into twenty equal increments. The integration was advanced from $x = 0$, over successive increments. The final value of one increment provides the initial value for the next. The integration increment is taken as 1/20. This procedure obtains an estimate of the local truncation error at each step and varies the step length automatically to keep this estimate below a specified error bound. If the step-length becomes less than $10^{-4}$ times the initial step length, the procedure stops the calculation and an error message is printed. For all calculations, the specified error bound was set equal to $10^{-4}$. The truncation error per step length is controlled by varying the step length. Over a number of steps the errors can accumulate in various ways and the total error may exceed the specified error bound. This can be controlled by reducing the error bound for a large number of steps. This was found to be unnecessary in the present problem.

These eigenfunctions and the corresponding cells at the onset of instability for different values of $\mu$, $\eta$ are shown in Figs. 1–4, and the numerical values of $a_c$, $T_c$ are listed in Table 1. Also variation of $a_c$, $T_c$ with $\mu$, $\eta$ is shown in Figs. 5–6. The Taylor number is defined in a different manner in references [1, 2]. The following relation exists between $T$ of our analysis and $T_{AC}$ of Astill and Chung [reference [2]].

$$T = 4(T_{AC})^2 \frac{\left(\dfrac{1}{\eta} - 1\right)^2}{\dfrac{1}{\eta^2} - 1}\left(1 - \frac{\mu}{\eta^2}\right). \tag{4}$$


[1]Department of Engineering, University of Manchester, Manchester M13 9PL, U.K.

[2]Department of Mathematics, University of Bahrain, Bahrain (Middle East).

[3]31A/12, Brindavan Society, Thane, 400601 India, Mem. ASME.



Contributed by the Fluids Engineering Division of THE AMERICAN SOCIETY OF MECHANICAL ENGINEERS. Manuscript received by the Fluids Engineering Division April 29, 1987.

the log law by using $\kappa y^* \sqrt{\tau^*}$ instead of just $\kappa y^*$ and the intercept by properly relating the van Driest factor $\lambda^*$ to pressure-gradient parameter $\hat{p}^+$. Although the existing formulas with the exception of that of Nituch et al. could immediately satisfy the slope of the log law by adding $\sqrt{\tau^*}$ to $\kappa y^*$, there still remains the problem of satisfying the intercept. Curiously, if the formula of Cebeci adds the $\sqrt{\tau^*}$ and uses a value of $\alpha = 0.84$ to convert the $p^+$ to $\hat{p}^+$, it exactly matches the proposed formula for adverse pressure gradients.

### References


1 Patel, V. C., Rodi, W., and Scheuerer, "Turbulence Models for Near-Wall and Low Reynolds Numbers Flows: A Review," *AIAA Journal*, Vol. 23, No. 9, 1985, pp. 1308–1319.

2 Cebeci, T., Chang, K. C., Li, C., and Whitelaw, J. H., "Turbulence Models for Wall Boundary Layers," *AIAA Journal*, Vol. 24, No. 3, 1986, pp. 359–360.

3 van Driest, E. R., "On Turbulent Flow Near a Wall," *Journal of Aeronautical Sciences*, Vol. 23, 1956, pp. 1007–1011, 1036.

4 Kutateladze, S. S., "The Mixing Length Hypothesis in the Turbulence Theory," *International Journal of Heat and Mass Transfer*, Vol. 27, No. 11, 1984, pp. 1947–1950.

5 Landahl, M. T., "Coherent Structures in Turbulence and Prandtl's Mixing Length Theory," *Zeitschrift für Flugwissenschaften und Weltraumforschung*, Vol. 8, No. 4, 1984, pp. 233–242.

6 McDonald, H., "The Effect of Pressure Gradient on the Law of the Wall in Turbulent Flow," *Journal of Fluid Mechanics*, Vol. 35, Part 2, 1969, pp. 311–336.

7 Salam, M. Y., "Measurement of the Viscous Sublayer in Near-Separated Flows," *Applied Scientific Research*, Vol. 39, No. 4, 1982, pp. 337–347.

8 Patankar, S. V., and D. B. Spalding, *"Heat and Mass Transfer in Boundary Layers,"* C.R.C. Press, Cleveland, 1968.

9 Cebeci, T., "Behavior of Turbulent Flow Near a Porous Wall with Pressure Gradient," *AIAA Journal*, Vol. 8, No. 12, 1970, pp. 2152–2156.

10 Launder, B. E., and Priddin, C. H., "A Comparison of Some Proposals for the Mixing Length Near a Wall," *International Journal of Heat and Mass Transfer*, Vol. 16, 1973, pp. 700–702.

11 Baker, R. J., and Launder, B. E., "The Turbulent Boundary Layer with Foreign Gas Injection II," *International Journal of Heat and Mass Transfer*, Vol. 17, No. 2, 1974, pp. 293–306.

12 Kays, W. M., and Moffat, R. J., "The Behavior of Transpired Turbulent Boundary Layers," *"Studies in Convection"* Vol. 1, B. E. Launder, ed., Academic Press, London, 1975, pp. 223–319.

13 Nituch, M. J., Sjolander, S., and Head, M. R., "An Improved Version of the Cebeci-Smith Eddy-Viscosity Model," *Aeronautical Quarterly*, Vol. 29, Part 3, 1978, pp. 207–225.

14 Baldwin, B. S., and Lomax, H., "Thin Layer Approximation and Algebraic Model for Separated Turbulent Flows," AIAA Paper 78–257, 1978.

15 Granville, P. S., "Baldwin-Lomax Factors for Turbulent Boundary Layers in Pressure Gradients," *AIAA Journal*, Vol. 25, No. 12, 1987, pp. 1624–1627.

16 Townsend, A. A., 1961, "Equilibrium Layers and Wall Turbulence," *Journal of Fluid Mechanics*, Vol. 11, Part 1, 1961, pp. 97–120.

17 Patel, V. C., "A Unified View of the Law of the Wall Using Mixing-Length Theory," *Aeronautical Quarterly*, Vol. 24, Part 1, 1973, pp. 55–70.

18 Reeves, B. L., "Two-Layer Model of Turbulent Boundary Layers," *AIAA Journal*, Vol. 12, No. 7, 1974, pp. 932–939.

19 Glowacki, W. J., and Chi, S. W., "Effect of Pressure Gradient on Mixing Length for Equilibrium Turbulent Boundary Layers," *AIAA Paper* 72–213, 1972.

20 Galbraith, R. A. McD., Sjolander and Head, M. R., "Mixing Length in the Wall Region of Turbulent Boundary Layers," *Aeronautical Quarterly*, Vol. 27, Part 2, 1977, pp. 97–110.


## Stability of the Flow Between Rotating Cylinders—Wide-Gap Problem


**H. S. Takhar,[1] M. A. Ali,[2] and V. M. Soundalgekar[3]**


### Introduction

Wide-gap stability of Couette flow was studied by many authors. Notable among these are Sparrow et al. [1], Astill and Chung [2], and Walowit et al. [3]. All other papers are referred in the reference list of reference [3]. However, cell-pattern and the radial eigenfunctions were not shown in detail earlier. So we now propose to show these in the present investigation.

Consider the flow of a viscous incompressible fluid between two concentric rotating cylinders with $R_1$ and $R_2$ as the radii and $\Omega_1$ and $\Omega_2$ as the angular velocities of the inner and outer cylinders, respectively.

Then the differential equation which governs the linear stability of the flow in a wide-gap region is given by [reference [3]]

$$(DD^* - a^2)^3 v = -a^2 T g(x) v \tag{1}$$

where $u$, $v$ are, respectively, the dimensionless amplitudes of the normal mode perturbations of the radial and azimuthal velocity components. These equations are to be solved with following boundary conditions:

$$v = (DD^* - a^2)v = D(DD^* - a^2)v = 0 \text{ at } x = 0,1 \tag{2}$$

Here $g(x) = \dfrac{\mu - \eta^2}{1-\eta^2} + \dfrac{\eta^2(1-\mu)}{1-\eta^2} \cdot \dfrac{1}{\epsilon^2}$, $\mu = \dfrac{\Omega_2}{\Omega_1}$, $\eta = \dfrac{R_1}{R_2}$

$$\epsilon = \frac{r}{R_2}, \quad d = R_2 - R_1, \quad a = \lambda d, \quad T = -\frac{4A^*\Omega_1 d^4}{\nu^2},$$

$$D = \frac{d}{dx}, \quad x = \frac{r - R_1}{d}, \quad D^* = \frac{d}{dx} + \frac{1-\eta}{\epsilon},$$

$$A^* = \frac{\Omega_1 {R_1}^2 - \Omega_2 {R_2}^2}{{R_1}^2 - {R_2}^2}. \tag{3}$$

The eigenvalue problem governed by equations (1) and (2) is solved numerically, following Harris and Reid [5]. The procedure starts by rewriting the governing equation (1) as a system of first order differential equations which are then integrated by using the Merson form of the Runge-Kutta method. The range of integration was divided into twenty equal increments. The integration was advanced from $x = 0$, over successive increments. The final value of one increment provides the initial value for the next. The integration increment is taken as 1/20. This procedure obtains an estimate of the local truncation error at each step and varies the step length automatically to keep this estimate below a specified error bound. If the step-length becomes less than $10^{-4}$ times the initial step length, the procedure stops the calculation and an error message is printed. For all calculations, the specified error bound was set equal to $10^{-4}$. The truncation error per step length is controlled by varying the step length. Over a number of steps the errors can accumulate in various ways and the total error may exceed the specified error bound. This can be controlled by reducing the error bound for a large number of steps. This was found to be unnecessary in the present problem.

These eigenfunctions and the corresponding cells at the onset of instability for different values of $\mu$, $\eta$ are shown in Figs. 1–4, and the numerical values of $a_c$, $T_c$ are listed in Table 1. Also variation of $a_c$, $T_c$ with $\mu$, $\eta$ is shown in Figs. 5–6. The Taylor number is defined in a different manner in references [1, 2]. The following relation exists between $T$ of our analysis and $T_{AC}$ of Astill and Chung [reference [2]].

$$T = 4(T_{AC})^2 \frac{\left(\dfrac{1}{\eta} - 1\right)^2}{\dfrac{1}{\eta^2} - 1}\left(1 - \frac{\mu}{\eta^2}\right). \tag{4}$$


[1]Department of Engineering, University of Manchester, Manchester M13 9PL, U.K.

[2]Department of Mathematics, University of Bahrain, Bahrain (Middle East).

[3]31A/12, Brindavan Society, Thane, 400601 India, Mem. ASME.



Contributed by the Fluids Engineering Division of THE AMERICAN SOCIETY OF MECHANICAL ENGINEERS. Manuscript received by the Fluids Engineering Division April 29, 1987.

With the help of this relation (4), we have converted some values of $a_c$, $T_c$ from reference [2] and these are plotted in Figs. 5–6. The agreement seems to be excellent. Also $a_c$, $T_c$-values are compared with those of Walowit et al. [3] and the agreement here is also excellent.

We observe from Fig. 1 that the maximum value of the radial eingenfunction $u(x)$ shifts toward the inner cylinder when the gap-width increases and the inner cylinder is only rotating. On Figs. 3 and 4 the cell-pattern is shown for $\eta = 0.9$ and $\mu = 0.0, -1.0$ respectively. On Fig. 5 the variation of $T_c$ with respect to $\eta$ is shown. We observe from this figure that when the gap-width is large, the flow is more stable when the two cylinders are counter-rotating. The flow is destabilized early when the two cylinders are corotating and the gap width is small or $\eta$ is large. However, we observe from this figure that for $\mu \geq 0.5$, $T_c$ is found to be unaffected by a change in

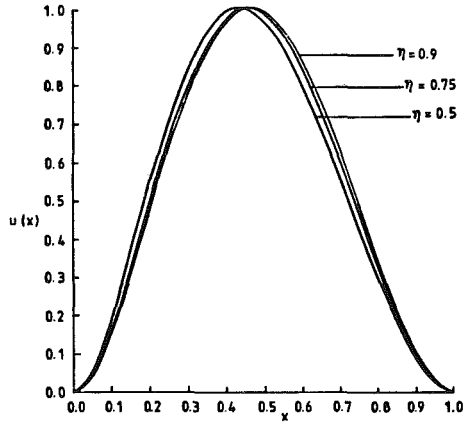


Fig. 1 The radial eigenfunction $u(x)$ for $\mu = 0.0$ and different values of $\eta$

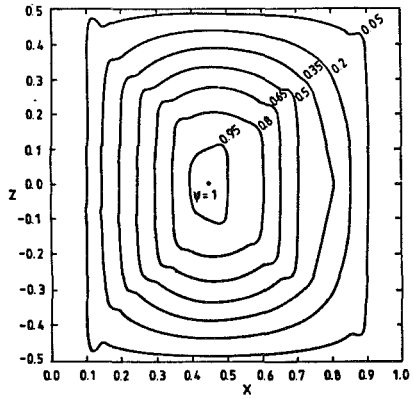


Fig. 3 The cell pattern at the onset of instability for $\eta = 0.9$ and $\mu = 0.0$

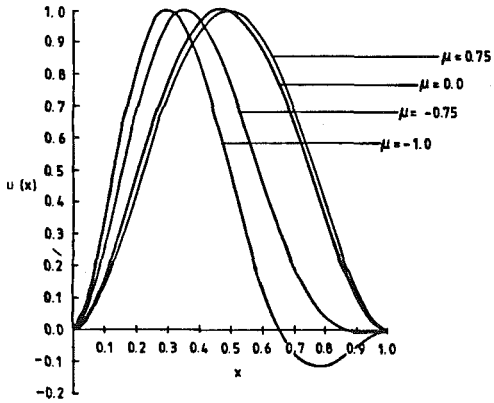


Fig. 2 The radial eigenfunction $u(x)$ for $\eta = 0.9$ and different values of $\mu$

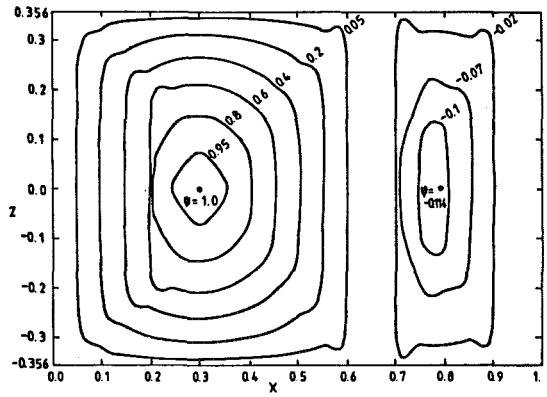


Fig. 4 The cell pattern at the onset of instability for $\eta = 0.9$ and $\mu = -1.0$

**Table 1 Critical values of $T$ and $a$ for various values of $\mu$, $\eta$**

| $\eta$ | $\mu$ | $a_c$ | $T_c$ | Walowit et al. | $\eta$ | $\mu$ | $a_c$ | $T_c$ | Walowit et al. |
|---|---|---|---|---|---|---|---|---|---|
| 0.9 | 0 | 3.129 | 3646.94 | 3648.15 | 0.3 | 0 | 3.215 | 11548.17 | 11555.55 |
| | 0.25 | 3.120 | 2847.8 | | | 0.01 | 3.210 | 10999.47 | |
| | 0.5 | 3.118 | 2332.13 | 2332.84 | | 0.08 | 3.19 | 7942.69 | 7942.33 |
| | 0.75 | 3.117 | 1973.13 | | | −0.01 | 3.219 | 12151.8 | |
| | −0.25 | 3.151 | 5033.71 | 5035.06 | | −0.09 | 3.329 | 20372.15 | |
| | −0.5 | 3.24 | 7877.26 | | | −0.1 | 3.361 | 22117.03 | |
| | −0.75 | 3.642 | 14651.31 | | 0.2 | 0 | 3.263 | 20715.78 | 20728.5 |
| | −1.0 | 4.41 | 27135.50 | | | 0.01 | 3.253 | 18991.39 | |
| | −1.5 | 5.58 | 69640.82 | | | 0.04 | 3.234 | 15158.94 | 15168.0 |
| 0.75 | 0 | 3.135 | 4204.45 | | | −0.01 | 3.276 | 22763.45 | |
| | 0.25 | 3.125 | 3096.38 | | | −0.04 | 3.358 | 31938.73 | |
| | 0.5 | 3.121 | 2445.5 | | | −0.1 | 4.250 | 82090.37 | |
| | −0.25 | 3.176 | 6457.4 | | | | | | |
| | −0.5 | 3.413 | 12485.02 | | 0.1 | 0 | 3.340 | 64597.31 | 65000 |
| | −0.75 | 4.312 | 27973.68 | | | 0.01 | 3.304 | 50628.78 | 50910 |
| 0.5 | 0 | 3.163 | 6199.2 | 6198.4 | | −0.01 | 3.424 | 87873.32 | |
| | 0.25 | 3.143 | 3828.49 | 3828.88 | | | | | |
| | −0.25 | 3.358 | 14778.13 | 14775.6 | | | | | |
| | −0.5 | 4.8 | 52217.36 | 53292.0 | | | | | |
| 0.4 | 0 | 3.184 | 7996.17 | 7994.38 | | | | | |
| | 0.1 | 3.166 | 5989.16 | | | | | | |
| | 0.16 | 3.162 | 5198.73 | 5198.81 | | | | | |
| | −0.1 | 3.236 | 11864.14 | | | | | | |
| | −0.16 | 3.33 | 16309.04 | | | | | | |
| | −0.25 | 3.811 | 30110.89 | 30191.25 | | | | | |

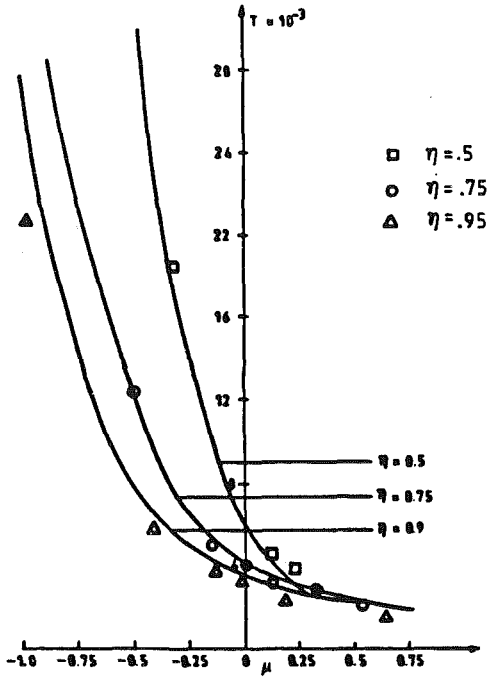


Fig. 5 Variation of critical Taylor number

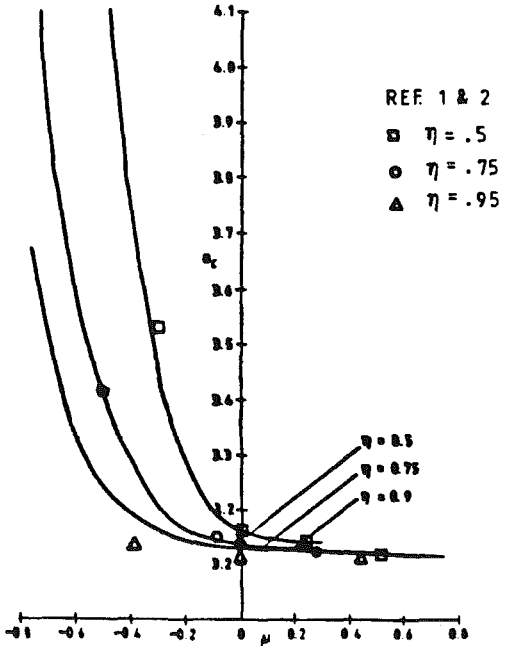


Fig. 6 Variation of the critical wave-number

the gap-width i.e., $T_c$ is not affected by the variation of $\mu$ for $\geq 0.5$.

On Fig. 6, the variation of $a_c$, the critical wave number, is shown against $\mu$ and for different values of $\eta$. An increase in $\eta$ i.e., by decreasing the gap-width, there is a decrease in the critical wave-number. When the two cylinders are counter-rotating the critical wave-number increases very fast, but when these cylinders are corotating, $a_c$ is not affected by the variation of $\eta$ when $\mu \geq 0.5$, i.e., by the variation of the gap-width.


### Acknowledgment

We are grateful to the referees for their valuable suggestions and help to improve the presentation of this matter in this paper.


### References


1 Sparrow, E. M., Munro, W. D., and Johnsson, V. K., "Instability of Flow Between Rotating Cylinders: The Wide Gap Problem," *Journal of Fluid Mechanics*, Vol. 20, 1964, pp. 35–46.

2 Astill, K. N., and Chung, K. C., "A Numerical Study of Instability of the Flow Between Rotating Cylinders," ASME Paper No. 76-FE-27, 1976.

3 Walowit, J., Tsao, S., and Di Prima, R. C., "Stability of Flow Between Arbitrarily Spaced Concentric Cylindrical Surfaces Including the Effect of a Radial Temperature Gradient," ASME *Journal of Applied Mechanics*, Vol. 31, 1964, pp. 583–593.

4 Harris, D. L., and Reid, W. M., "On the Stability of Viscous Flow Between Rotating Cylinders," *Journal of Fluid Mechanics*, Vol. 20, 1964, pp. 95–101.


## Passive Control of Three-Dimensional Separated Vortical Flow Associated With Swept Rearward-Facing Steps


G. V. Selby[1]



*Control of the three-dimensional separated-flow region downstream of a swept, rearward-facing step has been studied with the purpose of reducing the separated-flow region and attendant drag. Results have indicated that geometric modifications in the region downstream of the step where the spanwise vortex is formed has little effect on the extent of the separated flow, while "conical-lip" and "vortex-trough" base modifications lead to a significant reduction in reattachment distances. The "conical-lip" modification involves a step lip with variable radius and the "vortex troughs" are grooves in the surface upstream of the step which produce longitudinal vortices.*


### Introduction

Control of three-dimensional flow separation is of particular interest for drag reduction and high lift. The effectiveness of several boundary-layer control concepts in reducing flow separation on moderately and highly swept wings has been studied in references [1] and [2]. These concepts include slot blowing and suction, vortex generators and boundary layer fences. Previous investigators also examined techniques for controlling the separated, streamwise-directed vortical flow fields generated by the fuselages and wings of military fighter aircraft at high angle of attack (references [3]–[6]). In addition to blowing [3] and suction [4], these separated-flow control methods included the installation of add-on devices, such as vortex generators [5] and vertical flaps [6], at the leading edge of delta wings. The present paper considers separated-flow control for flow over a swept rearward-facing step, which is neither two-dimensional nor a complex three-dimensional flow.

### Discussion

The present research was conducted in a low-speed, low-turbulence wind tunnel operated by the Viscous Flow Branch of the High Speed Aerodynamics Division at NASA Langley Research Center. The model consisted of a splitter-plate with rearward-facing step heights ($h$) of 1.12, 1.27, and 2.38 cm and step sweep angles ($\Lambda$) of 30 and 60 deg. The incoming flow was tripped, using a 1-mm diameter wire located 5 cm downstream of the leading edge, resulting in a 2-cm thick turbulent boundary layer at the midspan of the step. The freestream


[1]Associate Professor, Department of Mechanical Engineering and Mechanics, College of Engineering and Technology, Old Dominion University, Norfolk, VA 23529-0247.



Contributed by the Fluids Engineering Division of THE AMERICAN SOCIETY OF MECHANICAL ENGINEERS. Manuscript received by the Fluids Engineering Division December 20, 1987.

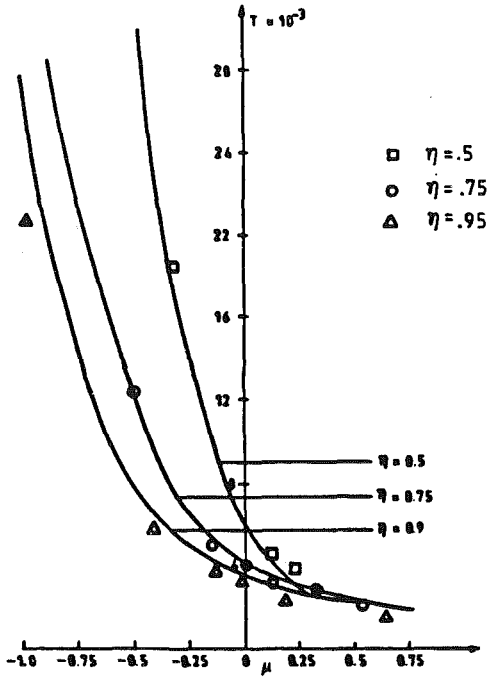


Fig. 5 Variation of critical Taylor number

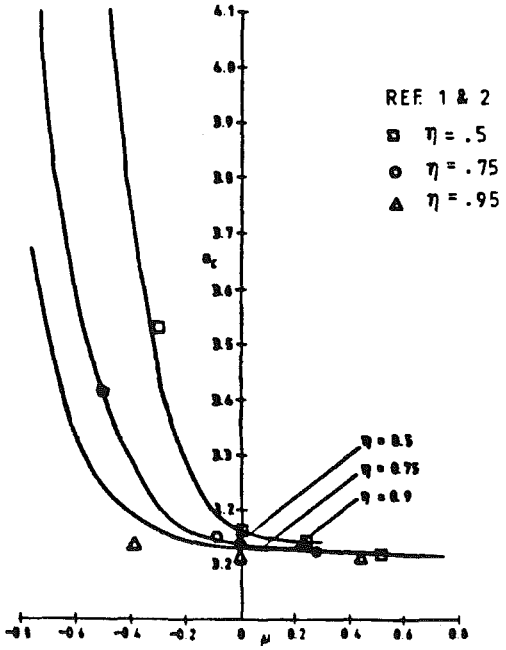


Fig. 6 Variation of the critical wave-number

the gap-width i.e., $T_c$ is not affected by the variation of $\mu$ for $\geq 0.5$.

On Fig. 6, the variation of $a_c$, the critical wave number, is shown against $\mu$ and for different values of $\eta$. An increase in $\eta$ i.e., by decreasing the gap-width, there is a decrease in the critical wave-number. When the two cylinders are counter-rotating the critical wave-number increases very fast, but when these cylinders are corotating, $a_c$ is not affected by the variation of $\eta$ when $\mu \geq 0.5$, i.e., by the variation of the gap-width.


### Acknowledgment

We are grateful to the referees for their valuable suggestions and help to improve the presentation of this matter in this paper.


### References


1 Sparrow, E. M., Munro, W. D., and Johnsson, V. K., "Instability of Flow Between Rotating Cylinders: The Wide Gap Problem," *Journal of Fluid Mechanics*, Vol. 20, 1964, pp. 35–46.

2 Astill, K. N., and Chung, K. C., "A Numerical Study of Instability of the Flow Between Rotating Cylinders," ASME Paper No. 76-FE-27, 1976.

3 Walowit, J., Tsao, S., and Di Prima, R. C., "Stability of Flow Between Arbitrarily Spaced Concentric Cylindrical Surfaces Including the Effect of a Radial Temperature Gradient," ASME *Journal of Applied Mechanics*, Vol. 31, 1964, pp. 583–593.

4 Harris, D. L., and Reid, W. M., "On the Stability of Viscous Flow Between Rotating Cylinders," *Journal of Fluid Mechanics*, Vol. 20, 1964, pp. 95–101.


## Passive Control of Three-Dimensional Separated Vortical Flow Associated With Swept Rearward-Facing Steps


G. V. Selby[1]



*Control of the three-dimensional separated-flow region downstream of a swept, rearward-facing step has been studied with the purpose of reducing the separated-flow region and attendant drag. Results have indicated that geometric modifications in the region downstream of the step where the spanwise vortex is formed has little effect on the extent of the separated flow, while "conical-lip" and "vortex-trough" base modifications lead to a significant reduction in reattachment distances. The "conical-lip" modification involves a step lip with variable radius and the "vortex troughs" are grooves in the surface upstream of the step which produce longitudinal vortices.*


### Introduction

Control of three-dimensional flow separation is of particular interest for drag reduction and high lift. The effectiveness of several boundary-layer control concepts in reducing flow separation on moderately and highly swept wings has been studied in references [1] and [2]. These concepts include slot blowing and suction, vortex generators and boundary layer fences. Previous investigators also examined techniques for controlling the separated, streamwise-directed vortical flow fields generated by the fuselages and wings of military fighter aircraft at high angle of attack (references [3]–[6]). In addition to blowing [3] and suction [4], these separated-flow control methods included the installation of add-on devices, such as vortex generators [5] and vertical flaps [6], at the leading edge of delta wings. The present paper considers separated-flow control for flow over a swept rearward-facing step, which is neither two-dimensional nor a complex three-dimensional flow.

### Discussion

The present research was conducted in a low-speed, low-turbulence wind tunnel operated by the Viscous Flow Branch of the High Speed Aerodynamics Division at NASA Langley Research Center. The model consisted of a splitter-plate with rearward-facing step heights ($h$) of 1.12, 1.27, and 2.38 cm and step sweep angles ($\Lambda$) of 30 and 60 deg. The incoming flow was tripped, using a 1-mm diameter wire located 5 cm downstream of the leading edge, resulting in a 2-cm thick turbulent boundary layer at the midspan of the step. The freestream


[1]Associate Professor, Department of Mechanical Engineering and Mechanics, College of Engineering and Technology, Old Dominion University, Norfolk, VA 23529-0247.



Contributed by the Fluids Engineering Division of THE AMERICAN SOCIETY OF MECHANICAL ENGINEERS. Manuscript received by the Fluids Engineering Division December 20, 1987.

Reynolds number (based on the distance from the leading edge of the splitter plate to the step at midspan) was $1.4 \times 10^6$ ($V_\infty$ = 21 m/s). The pertinent flow geometry is shown in Fig. 1, along with general flow features in the three-dimensional separated-flow region, as deduced from surface oil flow studies and flow angularity measurements. Reattachment length data presented herein were obtained exclusively using the oil drop flow visualization technique. Details of the separated-flow case without flow control are presented in reference [7].

As an initial sensitivity study, the step was swept either 30 or 60 deg relative to the freestream flow, as shown in Fig. 2, and several geometric modifications in the region where the vortex was formed were explored to examine their effect on flow parameters in the separated-flow region (60 deg swept-step model with $h$ = 1.27 cm). An examination of Fig. 3 indicates that the reattachment distance is effectively independent of the initial conditions beyond several step heights in the spanwise direction. The surface swirl angle and base pressure data of reference [7] further substantiate this conclusion. However, at $y/h > 20$, the data for the three configurations diverge due to wall effects. In Fig. 3, the estimated maximum uncertainty in the ordinate and the abscissa is ±0.12. (Stated uncertainty value also applies to Figs. 5 and 7.)

One set of models ($\Lambda$ = 30 deg, $h$ = 1.12 cm) were designed with conical-lip (CL) and vortex-trough (VT) base modifications (see Fig. 4). The CL model included a variable lip radius; i.e., the lip radius varied linearly with $y$ from 0 at $y$ = 0 to 0.6 $h$ at the downstream corner, while the VT model contained streamwise "V" grooves (30 deg half-angle, 0.635 cm depth,

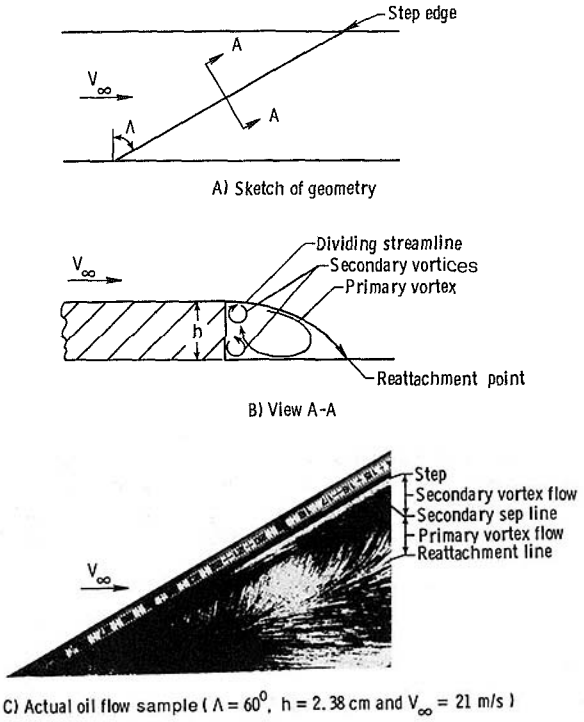


**Fig. 1 The swept rearward-facing step geometry and flow features**

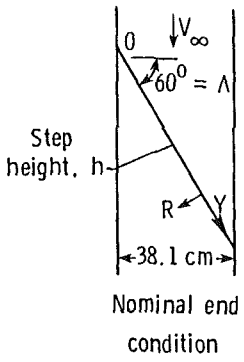


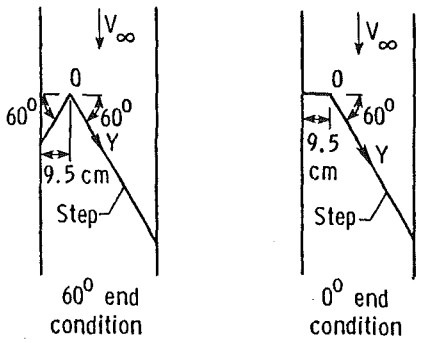


**Fig. 2 Geometric modifications to step initial conditions**

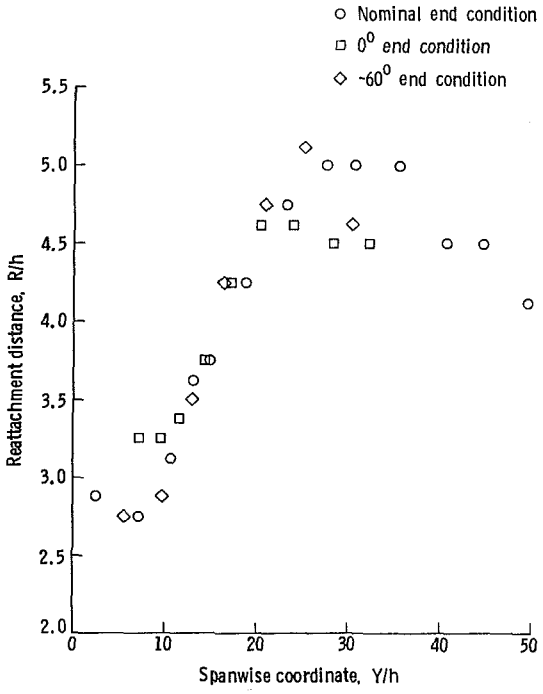


**Fig. 3 Reattachment distance perpendicular to step versus spanwise coordinate for the 60 deg basic swept-step model with various end conditions (Re = 1.4 × 10⁶ and $h$ = 1.27 cm)**

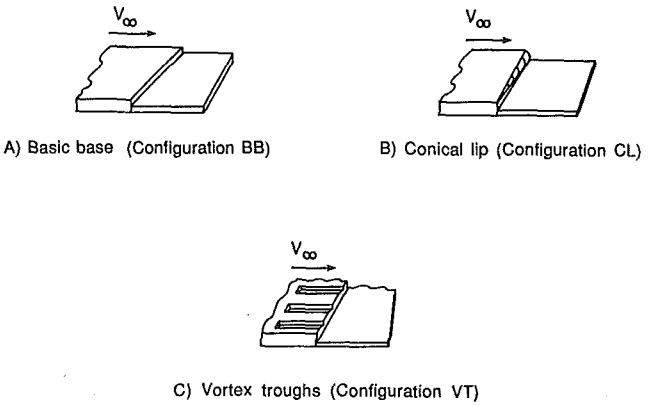


**Fig. 4 Basic, conical lip and vortex trough geometries**

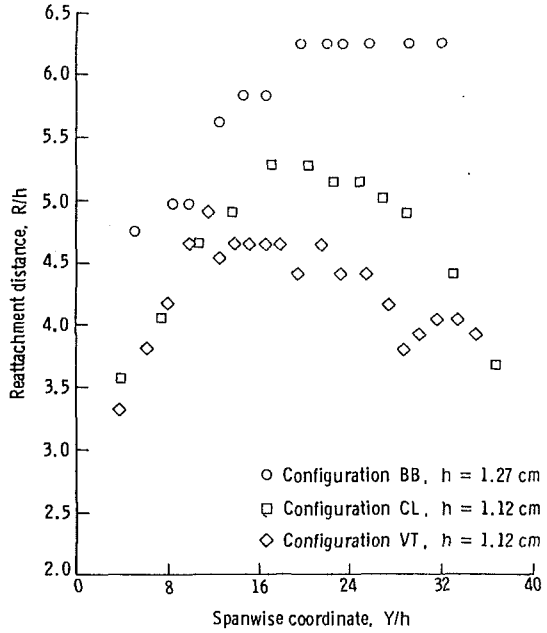


**Fig. 5 Reattachment distance perpendicular to step versus spanwise coordinate for configurations BB, CL, and VT ($\Lambda$ = 30 deg, $h$ = 1.12 cm, and Re = 1.4 × $10^6$)**

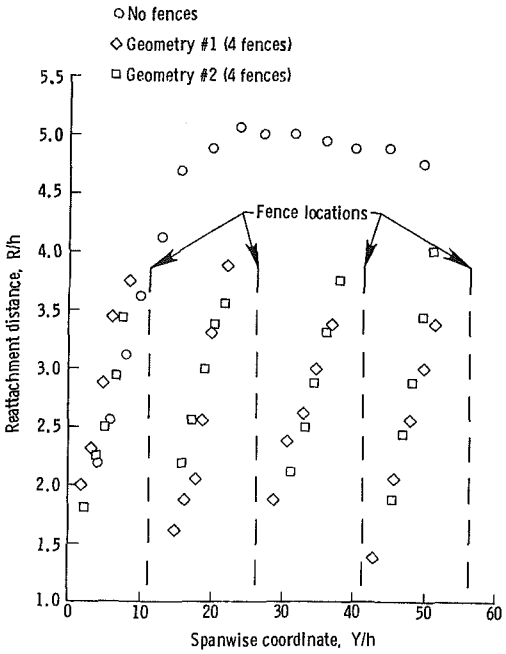


**Fig. 7 Reattachment distance perpendicular to step versus spanwise coordinate for the 60 deg basic swept-step model with and without fences (Re = 1.4 × $10^6$ and $h$ = 1.27 cm)**

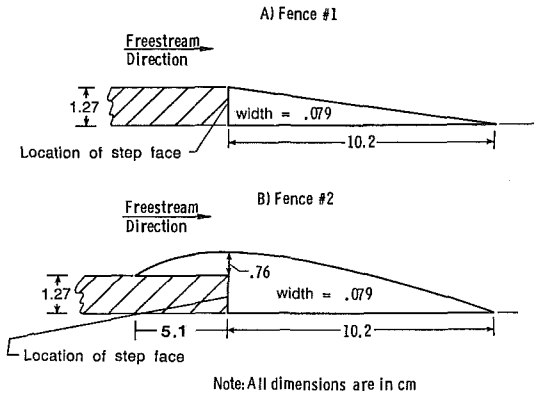


**Fig. 6 Sketch of boundary-layer fences**

25.4 to 43.2 cm length, 3.18 cm between groove centers) in the surface upstream of the step. Figure 5 indicates the reduction in the separated-flow region achieved with the aforementioned modifications. A pair of streamwise vortices is generated in each vortex trough [8]. These vortex pairs energize the separated-flow region, resulting in almost a 30 percent reduction to the maximum value of the non-dimensionalized reattachment distance, $R/h$. The effect of the finite lip radius is to delay separation and cause a reduction to the reattachment distance. Data presented in Fig. 5 suggest that the reattachment distance decreases with increasing lip radius. Therefore, a constant large lip radius is desirable for minimum reattachment distance.

Streamwise boundary-layer fences, as sketched in Fig. 6, were installed in the separated-flow region of the 60 deg basic swept-step model ($h$ = 1.27 cm) to determine their effect on reattachment distance. Similar surface oil flow patterns result from the two fence geometries. The reattachment distance data determined from surface oil flow patterns are displayed in Fig. 7 for one of several fence spacings examined. The reattachment distance increases from a minimum value at each fence-step junction to a maximum value at the adjacent fence, where a new vortex originates. Real-time surface oil flow patterns indicated that the fences turn the vortex flows toward the streamwise direction—probably causing either vortex liftup or breakdown in the process. Each fence geometry had essentially the same effect on the separated flow in terms of the reattachment distance. The general effect of the fences was to reduce the region of separated flow by over 50 percent for the fence spacing shown in Fig. 6. The effect of the fences and other modifications on base pressure was inconclusive due to an inadequate number of pressure orifices in the base region.

The present results have shown that the reattachment distances downstream of swept steps are independent of the upstream initial geometric condition. It has also been shown that simple base modifications can considerably reduce flow separation associated with the swept-step geometry. Further systematic study is being conducted (including detailed base pressure measurements) to determine if the present reduction in the extent of the separated-flow region can be optimized by varying control device geometry and translated into a reduction of the attendant drag.

## References

1 Kukainis, J., "Effects of Three Boundary-Layer Control Devices on a Quasi-Two-Dimensional Swept Wing at High Subsonic Speeds," Arnold Engineering Development Center, AEDC-TR-69-251, Dec. 1969.

2 Rao, D. M., and Johnson, T. D., Jr., "Investigation of Leading-Edge Devices for Drag Reduction of a 60-deg. Delta Wing at High Angles of Attack," AIAA-80-0310, AIAA 18th Aerospace Sciences Meeting, Pasadena, Calif., 14–16 Jan. 1980.

3 Peake, D. J., and Owen, F. K., "Control of Forebody Three-Dimensional Flow Separations," NASA TM-78593, May 1979.

4 Taylor, A. H., and Huffman, J. K., "Vortex Lift Augmentation by Suction on a 60° Swept Gothic Wing," AIAA-82-0231, AIAA 20th Aerospace Sciences Meeting, Orlando, Fla., 11–14, Jan. 1982.

5 Rao, D. M., and Johnson, T. D., Jr., "Alleviation of the Subsonic Pitch-Up of Delta Wings," AIAA-82-0129, AIAA 20th Aerospace Sciences Meeting, Orlando, Fla., 11–14, Jan. 1982.

6 Mattick, A. A., and Stollery, J. L., "Increasing the Lift-Drag Ratio of a Flat Delta Wing," *Aeronautical Journal*, Oct. 1981, pp. 379–386.

7 Selby, G. V., "Phenomenological Study of Subsonic Turbulent Flow Over a Swept Rearward-Facing Step," Ph.D. dissertation, University of Delaware, June 1982.

8 Zumwalt, G. W., "Experiments on Three-Dimensional Separating-and-Reattaching Flows," AIAA-81-0259, AIAA 19th Aerospace Sciences Meeting, St. Louis, Mo., 12–15, Jan. 1981.

# Effects of Excitation on Turbulence Levels in a Shear Layer

M. Nallasamy[1] and A. K. M. F. Hussain[2]

## Introduction

The phenomenon of turbulence suppression due to controlled excitation in circular jets was observed by Vlasov and Ginovskiy [1] and Petersen et al. [2] at certain frequencies of excitation. The first detailed study of turbulence suppression in free shear flows, however, was due to Zaman and Hussain [3]. They investigated the turbulence suppression due to controlled excitation (introduced acoustically or by ribbon oscillation) in a number of experimental facilities—circular jets, a plane jet, and a single-stream plane mixing layer. They found that the turbulence suppression (reduction in velocity fluctuations and Reynolds stress) in these shear flows was maximum when the shear layer was forced at around the maximally unstable frequency, i.e., $St_\theta \approx 0.017$ (Michalke [4]). Here, $St_\theta$ $(=f\theta_e/U_e)$ is the excitation Strouhal number, $f$ is the forcing frequency, $\theta_e$ and $U_e$ are the exit boundary layer momentum thickness and free stream velocity, respectively. The experiments were carried out with amplitudes of excitation in the range of 0.3 to 1 percent of $u_f'/U_e$; $u_f'$ is the rms velocity at the frequency of excitation. Hussain and Hasan [5] recently demonstrated that the turbulence suppression leads to jet noise reduction as well. A numerical simulation of the phenomenon of turbulence suppression in a plane shear layer by Nallasamy and Hussain [6] showed that at low amplitudes of excitation, the maximum suppression occurs at a Strouhal number of 0.017, consistent with experimental observation [3]. However, for high amplitudes of excitation, the above Strouhal number preference is lost. That is, the maximum turbulence suppression no longer occurs at the maximally unstable frequency, but occurs at a higher frequency. The present note presents experimental results of a study of turbulence suppression as a result of high amplitudes of external excitation in an axisymmetric mixing layer.

## Experiments

This study was carried out in a large axisymmetric mixing layer. An initially laminar axisymmetric mixing layer of a jet (of diameter D = 27 cm) was subjected to high amplitudes of controlled sinusoidal excitation at various frequencies (one frequency at a time). A periodic disturbance of a given frequency and amplitude was applied through an axisymmetric slit, at the jet lip [7], Fig. 1. The excitation was induced at the initiation of the shear layer without forcing the bulk flow. Data were taken using a miniature $X$-wire probe traversed by a computer. Velocity signals were digitized by an A/D converter at the rate of 51 Hz and then the mean and fluctuating components were computed. The rms value of the streamwise velocity fluctuations $u_f$ were measured using a spectrum analyzer (spectroscope SD335). For the measurements reported in this note, the initial boundary layer was laminar, the mean velocity profile agreeing with the Blasius profile (the agreement of the shape factors was excellent). The true initial condition must be measured upstream of the jet lip (i.e., the separation point). For an initially laminar boundary layer, it has been found that the mean velocity profile measured just downstream of the lip, in the region of the jet where transformation from the confined nozzle flow to a free shear layer takes place, agrees well with the Blasius profile (see also references [8 and 9]).

The initial condition (namely the profiles of mean and fluctuating velocities) and the amplitude of excitation were measured at $x/\theta_e = 20$. This is an optimum location; it is sufficiently downstream from the lip that the flow is independent of the excitation slit details; it is well within the range of linear growth in $x$ within the shear layer. The frequency and the amplitude of excitation were varied at a constant exit velocity ($U_e$ = 15 m/s) of the jet as in the experiments of Zaman and Hussain [3]. The exit boundary layer momentum thickness was 0.374 mm. Four amplitudes of excitation, namely $u_f'/U_e$ = 0.5, 2.5, 3.5 and 4.5 percent were considered. The frequency (i.e., $St_\theta$) of excitation was varied from 0.006 to 0.025.

## Discussion of Results

We define a suppression factor as the ratio of $u_{ex}'/u_{ux}'$ where $u_{ex}'$ is the maximum longitudinal (rms) velocity fluctuation at a section with excitation and $u_{ux}'$ is that without excitation at the same section. The variation of the suppression factor with the amplitude of excitation is shown in Fig. 2. The figure shows the suppression factor at a distance $x/\theta_e = 200$ where the suppression was found to be the maximum. We see that at an amplitude of 0.5, the maximum suppression occurs at the maximally unstable frequency predicted by the linear theory, $St_\theta = 0.017$, as in the experiments of Zaman and Hussain. However, the magnitude of the maximum suppression in the present study is only 12 percent in contrast to 80 percent in their study. This difference in magnitudes stems from the definition of the suppression factor. They define the suppression factor as the ratio of the longitudinal velocity fluctuations at a point with and without excitation. The suppression of 80 percent was found at a point $x$ = 10 cm in the jet, and $y$ = 0.5D-1.27 cm (D is the diameter of the jet). Such a definition of the suppression factor based on the intensities at a single point may not adequately characterize the turbulence in the flow field, for the following reasons: when a shear layer is acoustically excited, the vortical structures are displaced in radial/axial directions, pairing of vortical structures is induced, the location of vortex pairing is changed etc. It is thus possible that the intensities at a point with and without the structure are significantly different. The suppression defined on the basis of the peak intensities at any section with and without excitation as in the present study better represents the turbulence suppression. With the increase of amplitude to 2 percent, the maximum turbulence suppression occurs at a higher Strouhal number of about 0.0194. For an amplitude of 3.5 percent the maximum suppression still occurs at 0.0194. With a further increase in the amplitude of excitation to 4.5 percent, the maximum suppression shifts to $St_\theta = 0.022$. Thus, we see that the maximum turbulence suppression shifts to higher Strouhal numbers as the amplitude of excitation is increased in the range of amplitudes studied. This confirms the observation made in the numerical simulation of an excited shear layer [6].

The magnitude of suppression as a function of downstream distance is shown in Fig. 3, for four different Strouhal numbers, $St_\theta$ = 0.0067, 0.017, 0.0135, and 0.022, at the excitation amplitude of 4.5 percent. First we observe that the maximum suppression occurs at about the same downstream distance, $x/\theta_e = 200$, for all Strouhal numbers considered. Second, the maximum turbulence suppression now occurs at the higher Strouhal number of 0.022, rather than at 0.017. It is instructive to note that the axial location at which maximum suppression occurs is about 200 $\theta_e$ in contrast with about 400 $\theta_e$ observed in the previous study [3]. Thus it appears that the location of the maximum suppression is dependent on the initial condition of the shear layer.

[1]Sverdrup Technology, Inc., Cleveland, Ohio 44130.

[2]Department of Mechanical Engineering, University of Houston, Houston, TX 77004.

Contributed by the Fluids Engineering Division of The American Society of Mechanical Engineers. Manuscript received by the Fluids Engineering Division May 5, 1987.

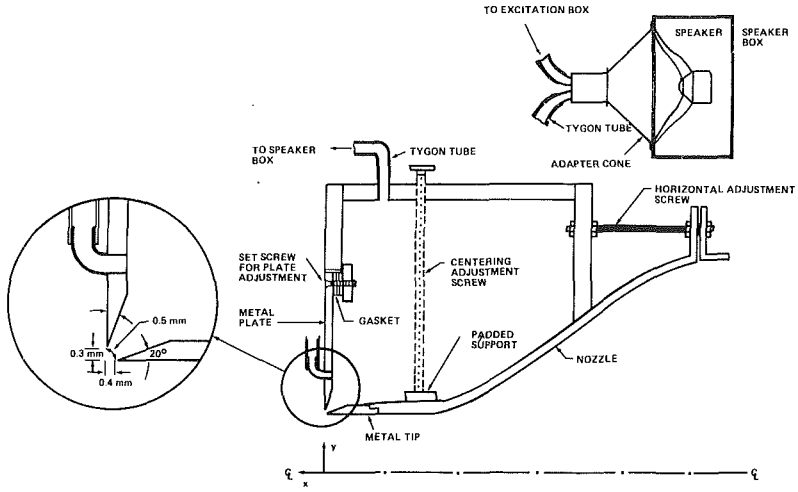


**Fig. 1 Sectional view of the shear layer excitation mechanism [7]**

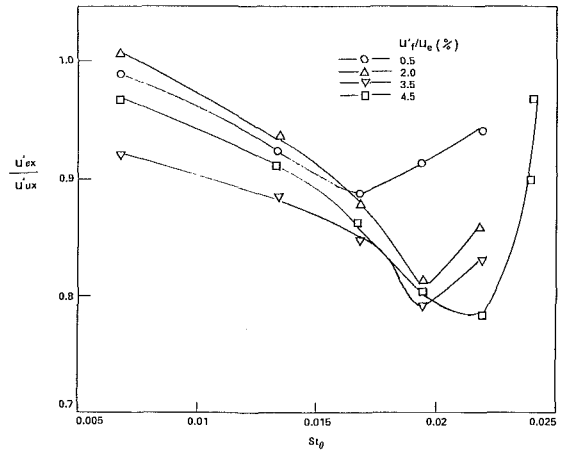


**Fig. 2 Variation of turbulence suppression with forcing frequency: Effect of forcing amplitude (uncertainty in turbulence intensity in the order of 3 percent)**

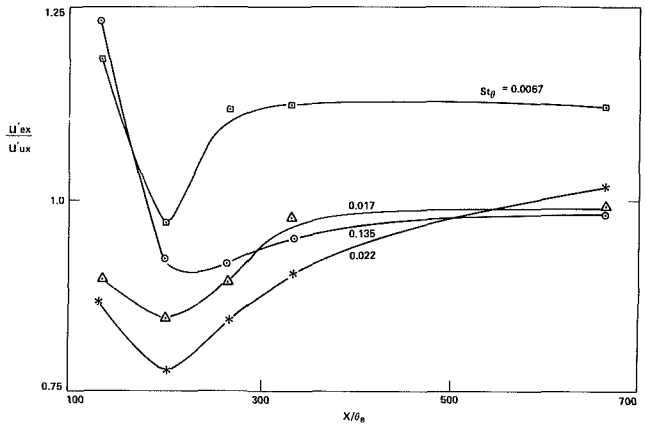


**Fig. 3 Axial variation of turbulence suppression for an excitation amplitude of 4.5 percent: Effect of forcing frequency (uncertainty in turbulence intensity in the order of 3 percent)**

An examination of the longitudinal velocity spectrum at different $x$ along the straight line corresponding to $U/U_e = 0.7$, shows that a higher amplitude forcing can hasten transition to turbulence only when the excitation frequency is greater than the maximally unstable frequency [10]. Table 1 shows the approximate axial location, $x/\theta_e$ at which the transition is complete for each frequency of excitation at an amplitude of 4.5 percent. The transition is taken to be complete when the peaks in the spectrum disappear and it resembles that of a fully turbulent flow. A similar definition for the completion of transition was employed by Sato and Saito [11] in their transition studies. At frequencies greater than the maximally unstable frequency, earlier saturation, lower level of saturation and faster transition occur. These nonlinear interactions lead to the observed turbulence suppression at high amplitudes of excitation. The faster transition appears to be the result of a nonlinear interaction mode which is the growth suppression [11] induced by a large amplitude. Recently Gaster et al. modeled the large scale vortex structures that occur in a high amplitude forced mixing layer by a linear stability theory [12]. They compared the magnitude and phase of the velocity fluctuations across various sections of the flow and found remarkable agreement with measurements. The overall integral behavior involving the amplification along the mixing layer was found to compare less favorably with calculations due to the neglect of nonlinear terms. It appears that the nonlinear interactions in the turbulence suppression at high amplitudes of forcing of a mixing layer can not be explained by employing a simple extension of the linear theory.

**Table 1**

| Frequency, $St_\theta$ | 0.0 | 0.0067 | 0.0135 | 0.017 | 0.0194 | 0.022 |
|---|---|---|---|---|---|---|
| Approximate $x/\theta_e$ for completion of transition | 200 | 500 | 335 | 270 | 170 | 135 |

## Conclusions

The present experimental investigation confirms the numerical simulations: at high amplitudes of excitation, the maximum turbulence suppression no longer occurs at the maximally unstable frequency, but occurs at a higher $St_\theta$ depending on the amplitude.

## References

1 Vlasov, Y. V., and Ginevski, A. S., "Generation and Suppression of Turbulence in Axisymmetric Turbulent Jet in the Presence of Acoustic Influence," NASA TT F 15721, 1974.

2 Petersen, R. A., Kaplan, R. E., and Laufer, J., "Ordered Structures and Jet Noise," NASA CR 134733, 1974.

3 Zaman, K. M. B. Q., and Hussain, A. K. M. F., "Turbulence Suppression in Free Shear Flows by Controlled Excitation," *J. Fluid Mech.*, Vol. 103, 1981, pp. 133–159.

4 Michalke, A., "On Spatially Growing Disturbances in an Inviscid Shear Layer," *J. Fluid Mech.*, Vol. 23, 1965, pp. 521-544.
5 Hussain, A. K. M. F., and Hasan, M. A. Z., "Turbulence Suppression in Free Turbulent Shear Flows Under Controlled Excitation, Part 2: Jet Noise Reduction," *J. Fluid Mech.*, Vol. 150, 1985, pp. 159-168.
6 Nallasamy, M., and Hussain, A. K. M. F., "Numerical Study of the Phenomenon of Turbulence Suppression in a Plane Shear Layer," *Turbulent Shear Flows*, Vol. 4, 1984, pp. 169-181.
7 Hussain, Z. D., Ph.D. thesis, University of Houston, 1982.
8 Browand, F. K., and Latigo, B. O., "Growth of the Two Dimensional Mixing Layer From Turbulent and Nonturbulent Boundary Layer," *Phys. Fluids*, Vol. 22, 1979, pp. 1011-1019.
9 Hussain, Z. D., and Husssain, A. K. M. F., "Axisymmetric Mixing Layer: Influence for the Initial and Boundary Conditions," *AIAA J.*, Vol. 17, 1979, pp. 48-55.
10 Nallasamy, M., "Turbulence Suppression at High Amplitudes of Excitation: Numerical and Experimental Study," *Bull. Am. Phys. Soc.*, Vol. 28, 1983, p. 1380.
11 Sato, H., and Saito, H., "Artificial Control of the Laminar-Turbulent Transition of a Two Dimensional Wake by External Sound," *J. Fluid Mech.*, Vol. 84, 1975, pp. 657-672.

## Comment on the Loss of Vorticity in the Near Wake of Bluff Bodies

**M. M. Zdravkovich**[1]

*Fage and his co-workers* [1, 2] *made a remarkable discovery in the 20's that only half of the vorticity generated by bluff bodies remained concentrated in shed vortices. This belated comment reconsiders Fage's method of "loss" calculation by examining nonlinear effects. The ignored effect of three dimensional distortion of vortex filaments before roll up might be another important cause for the "apparent" loss of vorticity.*

### 1 Introduction

Fage and Johansen [1, 2] have noted that less than half of the "*vorticity*" generated at the separation could be found in the fully formed vortices. This large "*loss of vorticity*" was confirmed by subsequent researchers as cited by Cantwell and Coles [3].

Fage and Johansen [1] calculated the *rate of vorticity* shed from each side of the bluff body in unit time by assuming that the width of the vortex sheet is infinitesimally *small* and that the *time-averaged* mean velocities on the outer and inner edges of the shear layer are $\bar{v}_1$ and $\bar{v}_2$, respectively. The elementary circulation $\delta\Gamma$ around a rectangle containing a length $\delta s$ of the vortex sheet is $\delta\Gamma = (\bar{v}_1 - \bar{v}_2)\,\delta s$ and $\delta s/\delta t = \frac{1}{2}(\bar{v}_1 + \bar{v}_2)$ hence

$$\delta\Gamma = (\bar{v}_1^2 - \bar{v}_2^2)\delta t/2 \tag{1}$$

Note that the mean velocity of the vortex sheet as written implies a linear variation of the velocity. This is true neither for the boundary layer nor for the shear layer. The total amount of circulation leaving each separation point during time $T$ is

$$\Gamma = \tfrac{1}{2}(\bar{v}_1^2 - \bar{v}_2^2)T \tag{2}$$

Fage and Johansen [1] measured $\bar{v}_1$ and $\bar{v}_2$ along the separated shear layer up to the rolling up. They found that loss of circulation amounted to 8 percent and was mostly due to the viscous increase in $\bar{v}_2$. At a distance of nine widths behind the plate about 60 percent of the vorticity leaving the edge is passing downstream in the form of large vortices having a definite individuality.

Fage and Johansen [1] inferred that an appreciable dissipation of vorticity occurs at the back of the plate. By counting fluid particles, Nielsen [4] found that only 4 percent of the generated vorticity was entrained into the region close to the rear of the body.

Fage and Johansen [1] further argued that a part of vorticity is dissipated immediately behind the plate, by a *mixture of positive and negative vorticity* from the two edges, and the rest possibly passes downstream as "unattached vortices," which are too small to appreciably affect the measured velocity fluctuations outside the wake.

Abernathy and Kronauer [5] simulated numerically a nonlinear interaction of two inviscid, infinite and uniform vortex sheets, initially a fixed distance apart, and subjected to a sinusoidal perturbation. Only one cluster of vorticity was formed for the spacing ratio 0.28 and contained net 62 percent of the vorticity i.e., +81 percent and −19 percent. It is still not clear how and whether the positive and negative vorticity will anihilate each other in a real viscous flow. The mechanism of mixing positive and negative vorticity has not yet been studied experimentally. In this note we reconsider the other possible mechanisms which could account for the loss of vorticity.

### 2 Reconsideration of the "Loss" Calculation

Fage and Johansen [1] based their calculation on the *time-averaged* vorticies $\bar{v}_1$ and $\bar{v}_2$ and not on the *actual fluctuating* velocities $v_1$ and $v_2$. The velocity fluctuations can be expanded in Fourier series and if only the leading term is retained then:

$$v_1(t) = \bar{v}_1 + \Delta v_1 \sin\omega t,\ v_2(t) = \bar{v}_2 + \Delta v_2 \sin(\omega t + k\pi)) \tag{3}$$

where: $\omega = 2\pi f$, $f$ is the shedding frequency and $k$ represents the phase shift; it is expected that $k = 0$ when a coherent vortex grows further downstream.

Equation (3) yields a new expression for circulation after integration over one cycle.

$$\Gamma = \frac{(\bar{v}_1^2 - \bar{v}_2^2)}{2} + \frac{(\Delta v_1^2 - \Delta v_2^2)}{4} \pm \frac{1}{f} \tag{4}$$

Note that if $\Delta v_1 = \Delta v_2$ the Fage and Johansen formula is recovered.

Figure 1 shows measurements of the amplitude of velocity fluctuation $\Delta v_2$ and the mean velocity $\bar{v}_1$ around a circular cylinder by Dwyer and McCroskey [6]. The maximum value of $\Delta v_2 = 0.28$ reduces the circulation $\Gamma$ in equation (4) by 0.02. Toebes [7] traversed the near wake 0.6 diameters downstream of the cylinder and found $\Delta v_2 = 0.39$. The second term in equation (4) yields 0.04. This value is still one order of magnitude less than the loss. It is evident in Fig. 1 that the maximum mean velocity around the cylinder is at 65 deg. There is an apparent loss of circulation of 10 percent between $\theta = 65$ and 78 deg due to the flow retardation caused by the adverse pressure gradient.

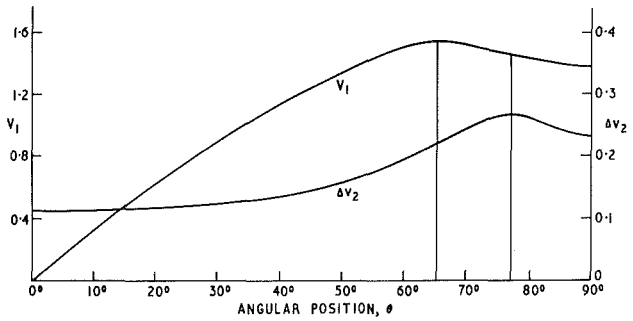


**Fig. 1 Angular distribution of mean and fluctuating velocities around a circular cylinder at $R_e = 1.06 \times 10^5$ (from Dwyer and McCroskey, 1973)**

[1]Reader, Aero Mech. Engrg. Dept., University of Salford, Salford, U.K. Mem. ASME.

Contributed by the Fluids Engineering Division of THE AMERICAN SOCIETY OF MECHANICAL ENGINEERS. Manuscript received by the Fluids Engineering Division December 22, 1987.

4 Michalke, A., "On Spatially Growing Disturbances in an Inviscid Shear Layer," *J. Fluid Mech.*, Vol. 23, 1965, pp. 521-544.
5 Hussain, A. K. M. F., and Hasan, M. A. Z., "Turbulence Suppression in Free Turbulent Shear Flows Under Controlled Excitation, Part 2: Jet Noise Reduction," *J. Fluid Mech.*, Vol. 150, 1985, pp. 159-168.
6 Nallasamy, M., and Hussain, A. K. M. F., "Numerical Study of the Phenomenon of Turbulence Suppression in a Plane Shear Layer," *Turbulent Shear Flows*, Vol. 4, 1984, pp. 169-181.
7 Hussain, Z. D., Ph.D. thesis, University of Houston, 1982.
8 Browand, F. K., and Latigo, B. O., "Growth of the Two Dimensional Mixing Layer From Turbulent and Nonturbulent Boundary Layer," *Phys. Fluids*, Vol. 22, 1979, pp. 1011-1019.
9 Hussain, Z. D., and Husssain, A. K. M. F., "Axisymmetric Mixing Layer: Influence for the Initial and Boundary Conditions," *AIAA J.*, Vol. 17, 1979, pp. 48-55.
10 Nallasamy, M., "Turbulence Suppression at High Amplitudes of Excitation: Numerical and Experimental Study," *Bull. Am. Phys. Soc.*, Vol. 28, 1983, p. 1380.
11 Sato, H., and Saito, H., "Artificial Control of the Laminar-Turbulent Transition of a Two Dimensional Wake by External Sound," *J. Fluid Mech.*, Vol. 84, 1975, pp. 657-672.

## Comment on the Loss of Vorticity in the Near Wake of Bluff Bodies

**M. M. Zdravkovich**[1]

*Fage and his co-workers* [1, 2] *made a remarkable discovery in the 20's that only half of the vorticity generated by bluff bodies remained concentrated in shed vortices. This belated comment reconsiders Fage's method of "loss" calculation by examining nonlinear effects. The ignored effect of three dimensional distortion of vortex filaments before roll up might be another important cause for the "apparent" loss of vorticity.*

### 1 Introduction

Fage and Johansen [1, 2] have noted that less than half of the "*vorticity*" generated at the separation could be found in the fully formed vortices. This large "*loss of vorticity*" was confirmed by subsequent researchers as cited by Cantwell and Coles [3].

Fage and Johansen [1] calculated the *rate of vorticity* shed from each side of the bluff body in unit time by assuming that the width of the vortex sheet is infinitesimally *small* and that the *time-averaged* mean velocities on the outer and inner edges of the shear layer are $\bar{v}_1$ and $\bar{v}_2$, respectively. The elementary circulation $\delta\Gamma$ around a rectangle containing a length $\delta s$ of the vortex sheet is $\delta\Gamma = (\bar{v}_1 - \bar{v}_2)\,\delta s$ and $\delta s/\delta t = \frac{1}{2}(\bar{v}_1 + \bar{v}_2)$ hence

$$\delta\Gamma = (\bar{v}_1^2 - \bar{v}_2^2)\delta t/2 \tag{1}$$

Note that the mean velocity of the vortex sheet as written implies a linear variation of the velocity. This is true neither for the boundary layer nor for the shear layer. The total amount of circulation leaving each separation point during time $T$ is

$$\Gamma = \tfrac{1}{2}(\bar{v}_1^2 - \bar{v}_2^2)T \tag{2}$$

Fage and Johansen [1] measured $\bar{v}_1$ and $\bar{v}_2$ along the separated shear layer up to the rolling up. They found that loss of circulation amounted to 8 percent and was mostly due to the viscous increase in $\bar{v}_2$. At a distance of nine widths behind the plate about 60 percent of the vorticity leaving the edge is passing downstream in the form of large vortices having a definite individuality.

Fage and Johansen [1] inferred that an appreciable dissipation of vorticity occurs at the back of the plate. By counting fluid particles, Nielsen [4] found that only 4 percent of the generated vorticity was entrained into the region close to the rear of the body.

Fage and Johansen [1] further argued that a part of vorticity is dissipated immediately behind the plate, by a *mixture of positive and negative vorticity* from the two edges, and the rest possibly passes downstream as "unattached vortices," which are too small to appreciably affect the measured velocity fluctuations outside the wake.

Abernathy and Kronauer [5] simulated numerically a nonlinear interaction of two inviscid, infinite and uniform vortex sheets, initially a fixed distance apart, and subjected to a sinusoidal perturbation. Only one cluster of vorticity was formed for the spacing ratio 0.28 and contained net 62 percent of the vorticity i.e., +81 percent and −19 percent. It is still not clear how and whether the positive and negative vorticity will anihilate each other in a real viscous flow. The mechanism of mixing positive and negative vorticity has not yet been studied experimentally. In this note we reconsider the other possible mechanisms which could account for the loss of vorticity.

### 2 Reconsideration of the "Loss" Calculation

Fage and Johansen [1] based their calculation on the *time-averaged* vorticies $\bar{v}_1$ and $\bar{v}_2$ and not on the *actual fluctuating* velocities $v_1$ and $v_2$. The velocity fluctuations can be expanded in Fourier series and if only the leading term is retained then:

$$v_1(t) = \bar{v}_1 + \Delta v_1 \sin\omega t,\ v_2(t) = \bar{v}_2 + \Delta v_2 \sin(\omega t + k\pi)) \tag{3}$$

where: $\omega = 2\pi f$, $f$ is the shedding frequency and $k$ represents the phase shift; it is expected that $k = 0$ when a coherent vortex grows further downstream.

Equation (3) yields a new expression for circulation after integration over one cycle.

$$\Gamma = \frac{(\bar{v}_1^2 - \bar{v}_2^2)}{2} + \frac{(\Delta v_1^2 - \Delta v_2^2)}{4} \pm \frac{1}{f} \tag{4}$$

Note that if $\Delta v_1 = \Delta v_2$ the Fage and Johansen formula is recovered.

Figure 1 shows measurements of the amplitude of velocity fluctuation $\Delta v_2$ and the mean velocity $\bar{v}_1$ around a circular cylinder by Dwyer and McCroskey [6]. The maximum value of $\Delta v_2 = 0.28$ reduces the circulation $\Gamma$ in equation (4) by 0.02. Toebes [7] traversed the near wake 0.6 diameters downstream of the cylinder and found $\Delta v_2 = 0.39$. The second term in equation (4) yields 0.04. This value is still one order of magnitude less than the loss. It is evident in Fig. 1 that the maximum mean velocity around the cylinder is at 65 deg. There is an apparent loss of circulation of 10 percent between $\theta = 65$ and 78 deg due to the flow retardation caused by the adverse pressure gradient.

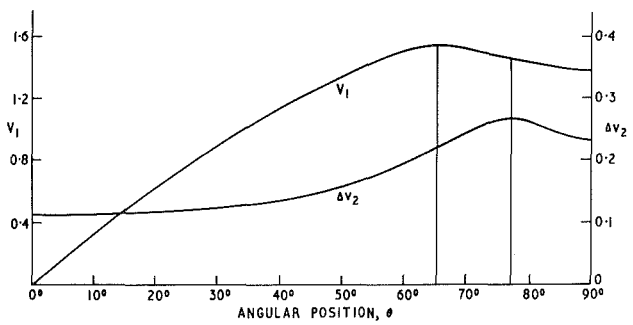


**Fig. 1 Angular distribution of mean and fluctuating velocities around a circular cylinder at $R_e = 1.06 \times 10^5$ (from Dwyer and McCroskey, 1973)**

[1]Reader, Aero Mech. Engrg. Dept., University of Salford, Salford, U.K. Mem. ASME.

Contributed by the Fluids Engineering Division of THE AMERICAN SOCIETY OF MECHANICAL ENGINEERS. Manuscript received by the Fluids Engineering Division December 22, 1987.

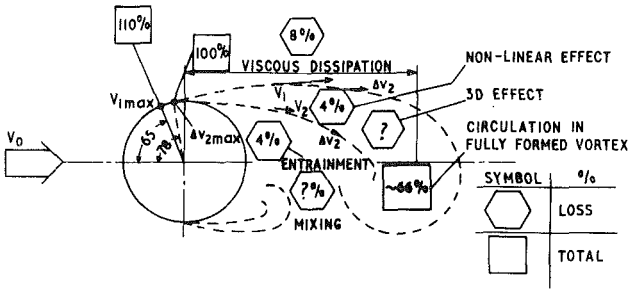


**Fig. 2 Schematic compilation of vorticity losses (applicable only in the upper subcritical range of Reynolds numbers)**

Sears [8] considered circulation production for the fluctuating separation point. He derived an additional term, $v_{sep}v_1$, that was negative. He argued that in flows with fluctuating separation points the circulation calculated by equation (2) would be probably too large. At present there is no experimental data to verify his inference. However, Dywer and McCroskey [6] observed the fluctuating separation and estimated to be in the range $\pm 5$ deg.

Figure 2 shows schematically losses of circulation within the near-wake region. Two question marks appear for the unknown losses due to the mixing of positive and negative vorticity and three-dimensional effects.

## 3 Apparent Loss Due to Three-Dimensional Effects

Turbulent two-dimensional shear layers develop streamwise vortices as shown by Wei and Smith [9] and Cimbala et al. [10]. The slanted orientation of vortex filaments inside the free shear layers produces an apparent deficit in the spanwise vorticity component parallel to the cylinder axis. This unaccounted vorticity loss is depicted in Fig. 2 by (?). It can be inferred that if the "mean" slant angle is in the range 15 to 30 deg the loss would be 4 to 13 percent, respectively. The actual value is unknown at present.

## 4 Conclusion

It appears that the rate of generation of the vorticity by the fluctuating free shear layer is always less than that calculated by using the time-averaged velocities $\bar{v}_1$ and $\bar{v}_2$. One part of the loss of vorticity is "apparent" due to an overestimate of the generation of vorticity in the fluctuating free shear layer. However, this nonlinear effect accounts only for a small amount of vorticity.

The three-dimensional distortion of vortex filaments in the free shear layer causes an apparent deficit of circulation if only the component parallel to the cylinder axis is measured. The mixture of positive and negative vorticity proposed by Fage and Johansen [1, 2] is a long standing puzzle that deserves further research attention. It is hoped that this note will stimulate interest on the topic.

## References

1 Fage, A., and Johansen, F. C., "On the Flow of Air Behind an Inclined Flat Plate of Infinite Span," *Proc. Royal Society A*, Vol. 116, 1927, pp. 170–197.

2 Fage, A., and Johansen, F. C., "The Structure of Vortex Sheets," *Philosophical Magazine*, Royal Society, Series 7, Vol. 5, 1928, pp. 417–441.

3 Cantwell, B., and Coles, D., "An Experimental Study of Entrainment and Transport in the Turbulent Near-Wake of a Circular Cylinder," *Journal Fluid Mechanics*, Vol. 136, 1983, pp. 321–374.

4 Nielsen, K. Th.W., "Vortex Formation in a Two Dimensional Periodic Wake," University of Oxford, PhD thesis, 1970.

5 Abernathy, F. H., and Kronauer, R. E., "The Formation of Vortex Streets," *Journal Fluid Mechanics*, Vol. 13, 1962, pp. 1–20.

6 Dwyer, H. A., and McCroskey, W. J., "Oscillating Flow over a Cylinder at Large Reynolds Number," *Journal Fluid Mechanics*, Vol. 61, 1973, pp. 753–767.

7 Toebes, G. H., "Unsteady Flow and Wake near an Oscillating Cylinder," ASME *Journal of Basic Engineering*, Vol. 91, 1969, pp. 493–502, Discussion, pp. 859–862, Errata p. 862.

8 Sears, W. R., "Unsteady Motion of Airofoils with Boundary Layer Separation," *AIAA Journal*, Vol. 14, 1976, pp. 216–220.

9 Wei, T., and Smith, C. R., "Secondary Vortices in the Wake of Circular Cylinders," *Journal Fluid Mechanics*, Vol. 169, 1986, pp. 573–533.

10 Cimbala, J. M., Nagib, H. M., and Roshko, A., "Large Structures in the Far Wakes of Two-dimensional Bluff Bodies," *Journal Fluid Mechanics*, Vol. 190, 1988, pp. 265–298.